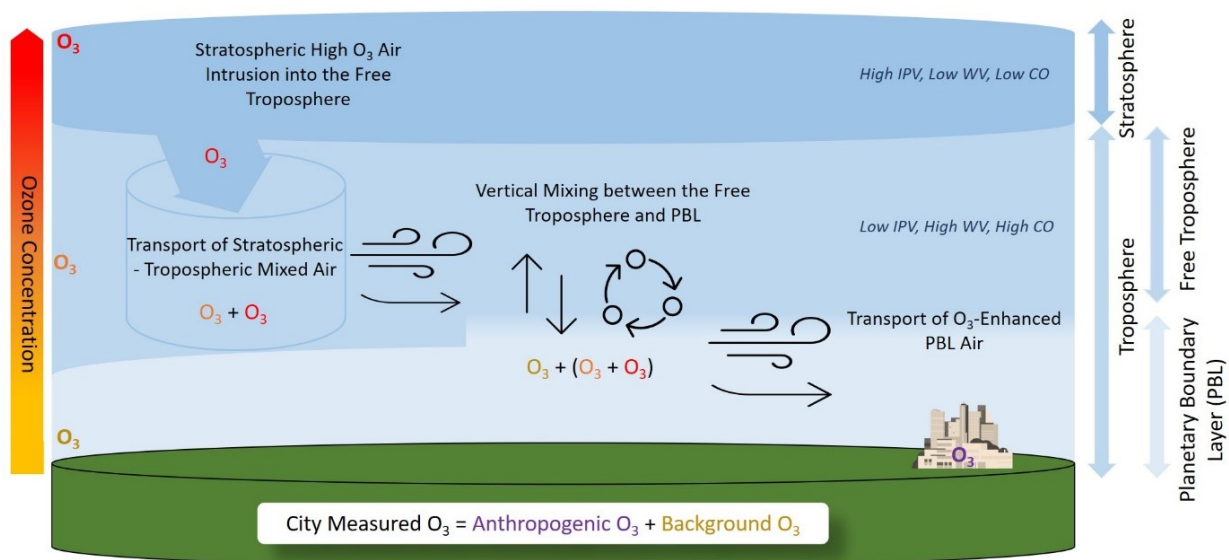


Exceptional Event Demonstration for Ozone Exceedances in Clark County, Nevada – May 28, 2020



Final Report Prepared for

U.S. EPA Region 9
San Francisco, CA

July 2021

This document contains blank pages to accommodate two-sided printing.



Exceptional Event Demonstration for Ozone Exceedances in Clark County, Nevada – May 28, 2020

Prepared by

Steve Brown, PhD
Crystal McClure, PhD
Cari Gostic
Samantha Kramer, PhD
David Miller, PhD
Charles Scarborough
Ningxin Wang, PhD

Sonoma Technology
1450 N. McDowell Blvd., Suite 200
Petaluma, CA 94954
Ph 707.665.9900 | F 707.665.9800
sonomatech.com

Prepared for

Mike Sword
Araceli Pruett

Clark County Department of Environment &
Sustainability
Division of Air Quality
4701 W. Russell Road, Suite 200
Las Vegas, NV 89118
Ph 702.455.3206
www.clarkcountynv.gov

Final Report
STI-920053-7477

July 1, 2021

Contents

Figures	iv
Tables.....	xi
Executive Summary.....	1
1. Overview.....	1-1
1.1 Introduction.....	1-1
1.2 Exceptional Event Rule Summary.....	1-3
1.3 Demonstration Outline.....	1-5
1.4 Conceptual Model.....	1-8
2. Historical and Non-Event Model.....	2-1
2.1 Regional Description.....	2-1
2.2 Overview of Monitoring Network.....	2-3
2.3 Characteristics of Non-Event Historical O ₃ Formation.....	2-6
2.4 Stratospheric Intrusion Event Description	2-13
2.5 Analysis of COVID Restrictions on Ozone.....	2-17
3. Clear Causal Relationship Analyses	3-1
3.1 Comparison of Event Concentrations with Historical Concentrations.....	3-1
3.2 Evidence of Stratospheric-Tropospheric Exchange	3-6
3.2.1 Satellite imagery.....	3-6
3.2.2 Model Results.....	3-15
3.3 Evidence of Stratospheric Air Reaching the Surface.....	3-34
3.3.1 HYSPLIT Trajectory Analysis.....	3-34
3.3.2 Measurements of Tropospheric Mixing	3-44
3.3.3 Model Results of Meteorological Conditions.....	3-56
3.4 Impacts of the Intrusion at the Surface	3-60
3.5 Additional Evidence.....	3-67
3.5.1 Matching Day Analysis	3-67
3.5.2 GAM Statistical Modeling.....	3-73
3.6 Clear Causal Relationship Conclusions.....	3-91
4. Natural Event.....	4-1
5. Not Reasonably Controllable or Preventable	5-1
6. Public Comment.....	6-1
7. Conclusions and Recommendations	7-1
8. References.....	8-1

Figures

Figure 2-1. Regional topography around Clark County, with an inset showing the county boundaries and the air quality monitoring sites analyzed in this report.....2-2

Figure 2-2. Clark County topography, with an inset showing air quality monitoring sites that measure ozone in the Clark County area.....2-3

Figure 2-3. Observed (left) and NOAA GFDL AM4 modeled MDA8 ozone, along with stratospheric ozone tracer anomaly in AM4 relative to monthly means (O3Strat_Anomaly), and the non-anthropogenic emissions AM4 ozone simulation (AM4_USB). Two examples of stratospheric intrusion influenced days in Clark County are shown during the FASTLVOS study (April 23 and May 13, 2017) Adapted from Figure S6 in Zhang et al. (2020).....2-7

Figure 2-4. Time series of 2015-2020 ozone concentrations at the Paul Meyer site. May 28, 2020, is shown in red.2-9

Figure 2-5. Time series of 2015-2020 ozone concentrations at the Walter Johnson site. May 28, 2020, is shown in red.2-10

Figure 2-6. Seasonality of 2015-2020 ozone concentrations from the Paul Meyer site. May 28, 2020, is shown in red.2-11

Figure 2-7. Seasonality of 2015-2020 ozone concentrations from the Walter Johnson site. May 28, 2020, is shown in red.2-12

Figure 2-8. Ozone time series at all monitoring sites. Time series of hourly ozone concentrations at monitoring sites in Clark County for one week before and after the May 28 event are shown. May 28, 2020, is shaded for reference.....2-13

Figure 2-9. Stratospheric intrusion and transport example. Ozone concentration with height is shown on the left, and ozone is colored by each source region to illustrate transport. Tracers for stratospheric and tropospheric air are shown on the right, as well as labels for the different atmospheric layers.....2-15

Figure 2-10. Time series of 2020 and 2019 traffic counts at two stations: US95 south of Las Vegas (top) and at the Nevada-California border west of Las Vegas (bottom). Data were provided by the Nevada Department of Transportation.2-19

Figure 2-11. Annual May distributions of MDA8 ozone at sites with EEs during May 2020. Notches denote 95th confidence interval of the median, boxes are 25th, 50th, and 75th percentiles, and whiskers are 5th and 95th percentiles.2-23

Figure 2-12. Daily time series of 2014-2019 MDA8 ozone distributions and 2020 MDA8 ozone at each site with proposed EE during May 2020. Notches denote 95th confidence interval of the median, boxes are 25th, 50th, and 75th percentiles, and whiskers are 5th and 95th percentile.....2-26

Figure 3-1. Time series of 2020 MDA8 ozone concentrations from the Paul Meyer site. May 28, 2020, is shown in red.3-1

Figure 3-2. Time series of 2020 MDA8 ozone concentrations from the Walter Johnson site. May 28, 2020, is shown in red.....3-2

Figure 3-3. Visible Satellite Imagery from over the area including southern Idaho, California, and Nevada on May 25, 2020. Source: NASA Worldview.....3-7

Figure 3-4. Visible Satellite Imagery from over the area including southern Idaho, California, and Nevada on May 26, 2020. Source: NASA Worldview.....3-8

Figure 3-5. Visible Satellite Imagery from over the area including southern Idaho, California, and Nevada on May 27, 2020. Source: NASA Worldview.....3-9

Figure 3-6. Visible Satellite Imagery from over the area including southern Idaho, California, and Nevada on May 28, 2020. Source: NASA Worldview.....3-10

Figure 3-7. Water vapor imagery from the GOES-East Satellite on May 25, 2020, at 15:50 UTC. Bright blue and white areas indicate the presence of high water vapor or moisture content, whereas dark orange and brown areas indicate little or no moisture present.3-11

Figure 3-8. Water vapor imagery from the GOES-East Satellite on May 26, 2020, at 14:50 UTC. Bright blue and white areas indicate the presence of high water vapor or moisture content, whereas dark orange and brown areas indicate little or no moisture present.3-11

Figure 3-9. Water vapor imagery from the GOES-East Satellite on May 27, 2020, at 08:50 UTC. Bright blue and white areas indicate the presence of high water vapor or moisture content, whereas dark orange and brown areas indicate little or no moisture present.3-12

Figure 3-10. Water vapor imagery from the GOES-East Satellite on May 29, 2020, at 00:20 UTC. Bright blue and white areas indicate the presence of high water vapor or moisture content, whereas dark orange and brown areas indicate little or no moisture present.3-12

Figure 3-11. Maps of satellite-estimated total column ozone from May 24 to May 28 from the OMPS instrument on the Suomi NPP satellite. Data source: NASA Worldview.....3-13

Figure 3-12. Maps of satellite-estimated total column ozone from May 25 at 06:00 UTC from Modern-Era Retrospective analysis for Research and Applications, Version 2 (MERRA-2). The approximate area of the SOI is shown by the circle.....3-14

Figure 3-13. Maps of satellite-estimated total column ozone from May 25 at 15:00 UTC from Modern-Era Retrospective analysis for Research and Applications, Version 2 (MERRA-2).3-15

Figure 3-14. GFS-modeled IPV at 06:00 UTC on May 25 at the 350 hPa geopotential height, plotted with Unidata’s IDV. The region of elevated IPV, where stratosphere-to-troposphere exchange occurred, is boxed in white.....3-16

Figure 3-15. Mixing ratio contour map at 350 hPa geopotential height based on GFS model simulations for 06:00 UTC on May 25. Each contour above 0.1 g/kg represents 0.1 g/kg increments. The region of relatively low water vapor mixing ratios intersecting with back trajectories from Clark County is circled in red and aligns with the region of elevated IPV shown in Figure 3-14.3-17

Figure 3-16. RAQMS-modeled ozone at the 310 K isentrope level at 06:00 UTC on May 25. The model was initialized at 12:00 UTC on May 24. The region with suspected stratosphere-to-troposphere mixing, and corresponding elevated ozone levels, is circled in red.....3-18

Figure 3-17. WACCM-modeled ozone at the 500 mb level on May 25 at 06:00 UTC. The region with the stratosphere-to-troposphere mixing, and corresponding elevated ozone levels, is circled in red..... 3-18

Figure 3-18. WACCM-modeled latitudinal cross-section of ozone along the 42.9-degrees N latitude line on May 25 at 12:00 UTC. This cross section intersects the proposed source of stratospheric ozone for the May 28 exceedance event. The extent of the cross section is shown as a red line on the map to the right. Las Vegas is shown as a blue star..... 3-20

Figure 3-19. Reference map for cross sections shown in Figures 3-20, 3-21, 3-24, and 3-25. Each red line aligns with a numbered subplot in each figure and represents the extent of the cross section shown in the plot. The order of numbered reference lines aligns with the path of air transport from the source region to Clark County, according to HYSPLIT trajectories shown in Section 3.3.1. The approximate latitudes of the proposed source region (labeled “Source”) and Clark County (labeled “Event”) are shown as gray lines. The map on the left shows initial rapid southward motion of air. The map on the right shows slower northward movement of air back towards Clark County. Las Vegas is shown as a blue star. 3-21

Figure 3-20. WACCM-modeled cross-sections of southward movement of air between May 25 at 18:00 UTC through May 26 at 12:00 UTC. The extent of the cross section for each plot is presented on the left map in Figure 3-19 as a red reference line labeled by the number in the upper-left corner of the plot. The black boxes in plots 3 and 4 highlight the progression of the elevated layer of ozone resulting from the tropospheric fold visible in plots 1 and 2. The surface pressure at some elevated altitude portions of the domain is between 700-800 mb..... 3-22

Figure 3-21. WACCM-modeled cross-sections of ozone at 12-hour increments for May 27 at 00:00 UTC through May 28 at 12:00 UTC. The extent of the cross section for each plot is presented in the right map of Figure 3-19 as a red reference line labeled by the number in the upper-left corner of the plot. The black box in each plot highlights the northward progression of an elevated layer of ozone in time and space. The surface pressure at some elevated altitude portions of the domain is between 700-800 mb. 3-23

Figure 3-22. WACCM-modeled latitudinal cross-section of ozone on the event date, May 29 at 00:00 UTC (May 28 at 18:00 PST) over Clark County. A deep layer of elevated ozone between 1000-600 mb is boxed in black. The extent of the cross section is represented by the red line in the map to the right. Las Vegas is shown as a blue star..... 3-24

Figure 3-23. WACCM-modeled latitudinal cross-section of the stratospheric ozone tracer along the 42.9 degrees N latitude line on May 25 at 12:00 UTC. This cross section intersects the proposed source of stratospheric ozone for the May 28 exceedance event. The extent of the cross section is shown as a red line on the map to the right. Las Vegas is shown as a blue star. 3-24

Figure 3-24. WACCM-modeled cross-sections of southward movement of the stratospheric ozone tracer between May 25 at 18:00 UTC through May 26 at 12:00 UTC. The extent of the cross section for each plot is presented in Figure 3-19 as a red reference line labeled by the number in the upper-left corner of the plot. The black boxes highlight the progression of the elevated layer of stratospheric ozone resulting from the source region in Figure 3-23..... 3-25

Figure 3-25. WACCM-modeled cross-sections of northward movement of the stratospheric ozone tracer between May 27 at 00:00 UTC through May 28 at 12:00 UTC. The extent of the cross section for each plot is presented on the map in Figure 3-19 as a red reference line labeled by the number in the upper-left corner of the plot. The black boxes highlight the progression of the stratospheric ozone resulting from the source region visible in Figure 3-23. 3-26

Figure 3-26. WACCM-modeled latitudinal cross-section of stratospheric ozone on the event date, May 29 at 00:00 UTC (May 28 at 18:00 PST) over Clark County. The extent of the cross section is represented by the red line in the map to the right. Las Vegas is shown as a blue star..... 3-27

Figure 3-27. MERRA-2 mean May ozone concentrations at the 488 hPa level based on data from 2014 – 2020 (top). MERRA-2 ozone concentrations at the 488 hPa level at 06:00 UTC (bottom left) and six hours later at 12:00 UTC (bottom right) on May 25. The red oval represents the approximate area of stratospheric intrusion. 3-28

Figure 3-28. MERRA-2 mean May ozone concentrations at the 288 hPa level based on data from 2014 – 2020 (top). MERRA-2 ozone concentrations at the 288 hPa level at 06:00 UTC (bottom left) and six hours later at 12:00 UTC (bottom right) on May 25. The red oval represents the approximate area of stratospheric intrusion. 3-29

Figure 3-29. RAQMS-modeled CO at the 310 K isentrope level at 06:00 UTC on May 25. The model was initialized at 12:00 UTC on May 24. The region with the stratosphere-to-troposphere mixing, and corresponding reduced CO levels, is circled in purple. 3-30

Figure 3-30. WACCM-modeled CO at the 500 mb level on May 25 at 6:00 UTC. 3-31

Figure 3-31. WACCM-modeled CO at the 500 mb level on May 29 at 0:00 UTC (the event date– May 28 at 16:00 PST). The purple circle shows the region of reduced CO over Clark County..... 3-31

Figure 3-32. RAQMS-modeled CO at the 310 K isentrope level at 00:00 UTC on May 29 (the event date–May 28 at 16:00 PST). The model was initialized at 12:00 UTC on May 28. The region circled in purple encompasses the southern end of a low-CO extension and Clark County..... 3-32

Figure 3-33. MERRA-2 mean May CO concentrations at the 288 hPa level based on data from 2014 – 2020 (top). MERRA-2 CO concentrations at the 288 hPa level at 06:00 UTC (bottom left) and six hours later at 12:00 UTC (bottom right) on May 25. The red oval represents the approximate area of stratospheric intrusion. 3-33

Figure 3-34. MERRA-2 mean May CO concentrations near the surface at the 985 hPa level based on data from 2014 – 2020 (left). MERRA-2 CO concentrations at the 985 hPa level at 00:00 UTC (right) on May 29 (4:00 p.m. local standard time on May 28). The red circle represents the Las Vegas area. 3-34

Figure 3-35. 96-hour HYSPLIT back trajectories from the Las Vegas Valley, ending on May 29, 2020. NAM 12 km back trajectories are shown for 3000 m (red) above ground level. Date labels show the position in the trajectory at 00:00 UTC on each date. 3-37

Figure 3-36. 72-hour HYSPLIT back trajectory matrix from Las Vegas Valley, ending on May 29, 2020. NAM 12 km back trajectories are shown for 2000 m above ground level. The approximate area of the SOI is shown by the gray circle..... 3-39

Figure 3-37. 72-hour HYSPLIT back trajectories frequency from Las Vegas Valley, ending on May 29, 2020. NAM 12 km back trajectories are shown for 3000 m above ground level. The colors within the frequency plot indicate the percent of trajectories that pass through a grid square..... 3-41

Figure 3-38. 96-hour HYSPLIT forward trajectories from the stratospheric intrusion source region initiated on May 25, 2020, at 12:00 UTC. NAM 12 km forward trajectories were initiated at 5000 m above ground level..... 3-43

Figure 3-39. An example skew-T diagram with labelled features. Red circle denotes deep mixed layer. Orange box denotes relatively dry layer of air. The approximate (cold-point temperature) tropopause is denoted by the dashed purple line. Dry and moist adiabats are drawn as green and blue lines at a range of initial surface temperatures..... 3-44

Figure 3-40 Skew-T diagrams for 12:00 UTC (left) on April 22, 2017, and 00:00 UTC (right) April 23, 2017, at Grand Junction, Colorado. Orange boxes denote the very dry layer. The red circle denotes the mixed layer. Green arrows indicate the intrusion of very dry air to the surface. The figures were collected directly from EPA’s “Guidance on the Preparation of Exceptional Events Demonstrations for Stratospheric Ozone Intrusions.” 3-46

Figure 3-41. The locations of four National Weather Service offices in the western United States. SLC, FGZ, and TUS are located along the trajectory of air from the region of stratosphere-to-troposphere exchange to Clark County. VEF is located in Las Vegas, near the sites that measured ozone exceedances on May 28. Clark County is shaded in yellow. 3-47

Figure 3-42. Skew-T soundings launched from the SLC National Weather Service office on May 26 and 27, 2020, at 0:00 UTC (May 25 and 26 at 4:00 p.m. local time). Dry layers of air are boxed and labeled in orange..... 3-48

Figure 3-43. Skew-T soundings launched from the FGZ National Weather Service office on May 26 and 27, 2020, at 0:00 UTC (May 25 and 26 at 4:00 p.m. local time). Dry layers of air are boxed and labeled in orange..... 3-50

Figure 3-44. Skew-T soundings launched from the TUS National Weather Service office on May 26 and 27, 2020, at 0:00 UTC (May 25 and 26 at 4:00 p.m. local time). Dry layers of air are boxed and labeled in orange. 3-51

Figure 3-45. Skew-T soundings launched from the VEF National Weather Service office on May 28 at 00:00 UTC, May 28 at 12:00 UTC, and May 29, 2020, at 0:00 UTC (4:00 p.m. on May 27, 4:00 a.m. on May 28, and 4:00 p.m. on May 28 local time). Dry layers of air are boxed and labeled in orange. A layer of well-mixed air is circled in red..... 3-53

Figure 3-46. 48-hour HYSPLIT back trajectories from Boulder (40.01 degrees N, 105.27 degrees W), ending on May 26, 2020, at 18:00 UTC. NAM 12 km back trajectories are shown for 2005 m (red), 3005 m (blue), and 4005 m (blue) above ground level. 3-55

Figure 3-47. Vertical profile of ozone captured at NOAA’s Chemical Sciences Laboratory in Boulder, CO on May 26, 2020, between 10:00 and 20:00 MST (May 26 at 16:00 UTC to May

27 at 2:00 UTC). Data was collected by the TOPAZ lidar. The left y-axis shows altitude above sea level. The right y-axis shows altitude above ground level..... 3-56

Figure 3-48. Daily upper-level meteorological maps for the three days leading up to the EE and during the May 28 EE..... 3-57

Figure 3-49. Daily surface meteorological maps for the three days leading up to the EE and during the May 28 EE..... 3-58

Figure 3-50. PBL height contour map based on the NAM model for May 26, 2020, at 16:00 PST. The gray lines denote PBL heights above 2 km altitude in 1 km increments..... 3-59

Figure 3-51. PBL height contour map based on the NAM model for May 28, 2020, at 16:00 PST. The gray lines denote PBL heights above 2 km altitude in 1 km increments..... 3-60

Figure 3-52. (Top plot) Diurnal profile of temperature (green) and absolute humidity (blue) at Jerome Mack, including temperature and absolute humidity values on May 28 and the 5-year May averages (dotted lines). (Bottom plot) Diurnal profile of ozone at Jerome Mack on May 28. Shaded ribbons represent the five-year 5th-95th percentile range. 3-61

Figure 3-53. Diurnal profile of ozone concentrations (red) at the Paul Meyer site on May 28 and the 5-year seasonal average ozone (dotted lines). Shaded ribbons represent the five-year 5th-95th percentile range. NO and NO₂ data are not available at Paul Meyer. 3-62

Figure 3-54. Diurnal profile of ozone concentrations (red) at the Walter Johnson site on May 28 and the 5-year seasonal average ozone (dotted lines). Shaded ribbons represent the five-year 5th-95th percentile range. NO and NO₂ data are not available at Walter Johnson..... 3-63

Figure 3-55. Diurnal profile of ozone concentrations (red), nitrogen dioxide (NO₂) concentrations (green), and nitric oxide (NO) concentrations (blue) at the Jerome Mack reference site in Clark County, on May 28 and the seasonal averages (dotted lines). Shaded ribbons represent the 5th-95th percentile range. NO₂ data is available from 2017-2020, and NO and ozone data is available from 2015-2020. 3-64

Figure 3-56. Diurnal profile of ozone concentrations (red) and nitrogen dioxide (NO₂) concentrations (green) at the Joe Neal site in Clark County on May 28 and the seasonal averages (dotted lines). Shaded ribbons represent the 5th-95th percentile range. NO₂ data and ozone data is available from 2015-2020. 3-65

Figure 3-57. Observed MDA8 ozone at stations in southern California, southern Nevada, western Arizona, and southwestern Utah..... 3-66

Figure 3-58. Daily ozone AQI for the three days before the May 28 event and the day of the event..... 3-67

Figure 3-59. Clusters for 2014-2020 back trajectories. Seven unique clusters were identified for the twice daily (18 and 22 UTC) back-trajectories for 2014-2020 initiated in the middle of the Las Vegas Valley. The percentage of trajectories per cluster is shown next to the cluster number. The height of each cluster is shown below the map..... 3-75

Figure 3-60. EE vs. non-EE residuals. Non-EEs (non-EE in blue) and EEs (EE in orange) residuals are shown for each site modeled in Clark County. The notches for each box represent the 95th confidence interval. This figure illustrates the information in Table 3-12. 3-80

Figure 3-61. Daily GAM residuals for 2014-2020 vs GAM Fit (Predicted) MDA8 Ozone values. 2018 and 2020 exceptional events residuals are shown in red and blue..... 3-83

Figure 3-62. Histogram of GAM residuals at all modeled Clark County monitoring sites. The red line indicates the mean and the green dashed line indicates the median. The blue line provides the density distribution. 3-84

Figure 3-63. GAM cluster residual results for 18:00 UTC. The cluster is determined by grouping 24-hour back trajectories from Las Vegas based on their path. Clusters were created by using back trajectory results from Clark County between 2014 and 2020 were used (removed EE days)..... 3-85

Figure 3-64. GAM cluster residual results for 22:00 UTC. The cluster is determined by grouping 24-hour back trajectories from Las Vegas based on their path. Clusters were created by using back trajectory results from Clark County between 2014 and 2020 were used (removed EE days)..... 3-86

Figure 3-65. Observed MDA8 ozone vs. GAM fit ozone by year. The relationship between observed MDA8 ozone and GAM fit ozone at all eight modeled monitoring sites in Clark County is broken out by year with linear regression and fit statistics shown (slope, intercept, and r^2). EE days are not included in the regression equations..... 3-87

Figure 3-66. April-May Interannual GAM Response. April-May residuals per year (2014-2020) are plotted for all eight modeled monitoring sites in Clark County. May 6, 9, and 28 potential EE days are included. 3-88

Figure 3-67. GAM MDA8 Fit versus Observed MDA8 ozone for EE affected sites on May 28, 2020. Black circles indicate data not associated with the 2018 or 2020 EE days, red circles indicate 2020 EE days, blue circles indicate 2018 EE days, and purple circles indicate 2014-2016 EE days. May 28 is shown as a red triangle. The black line is linear regression of the data and statistics (equation and R^2 value) are shown in the top of each sub-figure..... 3-89

Figure 3-68. GAM time series showing observed MDA8 ozone for two weeks before and after the May 28 EE (solid lines). The GAM MDA8 ozone fit value is also shown for two weeks before and after May 28 (dotted line)..... 3-91

Tables

Table 1-1. May 28, 2020, EE information. All monitoring sites in Clark County that exceeded the 2015 NAAQS standard during May 28, 2020, are listed along with EPA Air Quality System (AQS) Site Codes, location information, and MDA8 ozone concentrations.1-2

Table 1-2. Proposed Clark County 2018 EEs. For each site and date combination where the 2015 NAAQS standard was exceeded, the MDA8 ozone concentration is shown in parts per billion (ppb). Blank cells indicate that there was no exceedance on that site/date combination.....1-3

Table 1-3. Proposed Clark County 2020 EEs. For each site and date combination where the 2015 NAAQS standard was exceeded, the MDA8 ozone concentration is shown in ppb. Blank cells indicate that there was no exceedance on that site/date combination.1-3

Table 1-4. Tier 1 and 2 requirements for evaluating stratospheric intrusion impacts on ozone exceedances.1-5

Table 1-5. Locations of Tier 1 and 2 analyses within this report.....1-6

Table 2-1. Clark County monitoring site data. The available date ranges of all parameters and monitoring sites used in this report are shown for Clark County, Nevada.....2-5

Table 2-2. Transport mechanisms during a stratospheric ozone intrusion (as displayed in Figure 2-9) and evidence needed to determine transport.....2-16

Table 3-1. Six-year percentile ozone. The May 28 EE ozone concentration at each site is calculated as a percentile of the last five years with and without other 2018 and 2020 EEs included in the historical record.....3-2

Table 3-2. Ozone season (May-September) non-event comparison. May 28, 2020, MDA8 ozone concentrations for each affected site are shown in the top row. Five-year (2015-2019) average MDA8 ozone statistics for May-September are shown for each affected site around Clark County to compare with the event ozone concentrations.3-4

Table 3-3. Six-year ozone-season percentile ozone. The May 28 EE ozone concentration at each site is calculated as a percentile of the last five years' ozone season (May-September) with and without other 2018 and 2020 EEs included in the historical record.....3-4

Table 3-4. Site-specific ozone design values for the Paul Meyer monitoring site. The top five highest ozone concentrations for 2018-2020 at Paul Meyer are shown, and proposed EE days in 2018 and 2020 are included.3-5

Table 3-5. Site-specific ozone design values for the Walter Johnson monitoring site. The top five highest ozone concentrations for 2018-2020 at Walter Johnson are shown, and proposed EE days in 2018 and 2020 are included.....3-5

Table 3-6. Two-week non-event comparison. May 28, 2020, MDA8 ozone concentrations for each affected site are shown in the top row. Five-year (2015-2019) average MDA8 ozone statistics for May 21 through June 4 are shown for each affected site around Clark County to compare with the event ozone concentrations.3-6

Table 3-7. HYSPLIT run configurations for each analysis type, including meteorology data set, time period of run, starting location(s), trajectory time length, starting height(s), starting time(s), vertical motion methodology, and top of model height. 3-36

Table 3-8. Local meteorological parameters and their data sources..... 3-69

Table 3-9. Percentile rank of meteorological parameters on May 28, 2020, compared to the 30-day period surrounding May 28 over seven years (May 13 through June 12, 2014-2020)..... 3-70

Table 3-10. Top ten matching meteorological days to May 28, 2020. WJ and PM refer to monitoring sites, Walter Johnson and Paul Meyer, respectively. Average MDA8 ozone concentration of meteorologically similar days is shown plus-or-minus one standard deviation rounded to the nearest ppb..... 3-72

Table 3-11. GAM variable results. F-values per parameter used in the GAM model are shown for each site. Units and data source for each parameter in the GAM model are shown on the right of the table. 95th quantile, R², and normalized mean square residual information is shown at the bottom of the table..... 3-77

Table 3-12. Overall 2014-2020 GAM median residuals and 95% confidence interval range in square brackets for each site modeled. Sample size is shown in parentheses below the residual statistics. For sample sizes less than ten, we include a range of residuals in square brackets instead of the 95% confidence interval. Residual results are split by non-EE days and the 2018 & 2020 EE days. R² for each site is also shown along with the positive 95th quantile result..... 3-79

Table 3-13. GAM high ozone, non-smoke case study results. Median GAM residuals for ten days in 2014-2020 are shown where most monitoring sites had MDA8 ozone concentrations of 60 ppb or greater. Sites used to calculate the MDA8 and GAM residual median/range are listed in the Clark County AQS Site Number column by site number..... 3-82

Table 3-14. May 28 GAM results and residuals for each site. The GAM residual is the difference between observed MDA8 ozone and the GAM Prediction. We also estimate the minimum predicted fire influence based on the positive 95th quantile and GAM prediction value. 3-90

Table 3-15. Results for each tier analysis of the May 28, 2020, EE. 3-93

Executive Summary

On May 28, 2020, Clark County, Nevada, experienced an atypical, area-wide episode of elevated ambient ozone; during this episode, the 2015 8-hr ozone National Ambient Air Quality Standards (NAAQS) threshold (0.070 ppm) was exceeded at the Walter Johnson and Paul Meyer monitoring sites. The exceedances at both sites could lead to an ozone nonattainment designation for the Clark County area. Air trajectory analysis and air quality modeling suggest that this ozone exceedance was influenced by a Stratospheric Ozone Intrusion (SOI) over Idaho and Utah that transported ozone-rich air to Clark County. The U.S. EPA Exceptional Event Rule (U.S. Environmental Protection Agency, 2016a) allows air agencies to omit air quality data from the design value calculation if it can be demonstrated that the measurement in question was caused by an exceptional event. This report describes analyses that help to establish a clear causal relationship between the SOI and the May 28, 2020, ozone exceedance at the Walter Johnson and Paul Meyer sites.

The analyses conducted provides evidence supportive of SOI impacts on ozone concentrations in Clark County. Analyses show that (1) prior to May 28, meteorological modeling provides evidence that there was an SOI event upwind of Clark County signified by an area of stratosphere-troposphere exchange over Idaho and Utah; (2) ozone-rich stratospheric air was transported from the SOI to the lower troposphere and surface of the Clark County area; (3) the SOI and subsequent transport of dry stratospheric air impacted the typical diurnal profiles of ground-level meteorological measurements, including relative and absolute humidity, in the Clark County area on May 28; and (4) meteorological regression modeling and similar meteorological day analysis show that ozone observations on May 28 were unusual in the historical record given the meteorological conditions. Sources of evidence used in these analyses include (1) air quality monitor data to show that supporting pollutant trends at the surface were influenced by upwind effects from the SOI; (2) air trajectory analysis to show transport from the SOI to the Clark County area; (3) satellite imagery and meteorological model results; (4) meteorological regression modeling; and (5) meteorologically similar day analysis.

The EPA “Guidance on the Preparation of Exceptional Events Demonstration for Stratospheric Ozone Intrusions” (U.S. Environmental Protection Agency, 2018) describes a two-tier approach to evaluating an SOI event and then developing evidence for the EE demonstration; depending on the complexity of the event, increasingly involved information may be required to demonstrate a causal relationship between an SOI event and an exceedance. This report documents the results of analyses conducted to address Tier 1 and Tier 2 exceptional event demonstration requirements.

These analyses show that ozone-laden air was transported from Idaho and Utah over the days leading up to May 28 to the Clark County area. Combined with additional evidence, such as meteorological regression modeling and meteorologically similar day analysis, our results provide key evidence to support SOI impacts on ozone concentrations in Clark County on May 28, 2020.

1. Overview

1.1 Introduction

Stratospheric Ozone Intrusions (SOIs) occur when ozone-enriched, stratospheric air descends into the troposphere and injects ozone (O_3) at altitudes where ozone concentrations are usually lower. SOIs can directly affect surface-level ozone when a tropopause fold (carrying ozone-enriched stratospheric air) extends down to the surface. However, because tropopause folds do not typically extend below around 600 hPa (4.5 km above ground level [agl]) in the mid-latitudes, this effect usually only occurs at high altitude sites. Alternatively, a tropopause fold (or other stratospheric-tropospheric mixing) can occur at high altitudes, and then ozone can be directly transported to the surface downwind of the event. The mixing of ozone-enriched air can be enhanced where the boundary layer (i.e., the lowest well-mixed atmospheric layer that reaches the surface) is very deep (4-5 km) on hot, dry days. In desert regions such as Clark County, Nevada, an upwind SOI can efficiently be mixed down to the surface during hot spring and summer days, which can enhance ozone concentrations. Such an SOI event occurred upwind of Clark County on May 24-25, 2020, and then affected ozone concentrations on May 28. On May 28, two of the 14 ozone monitoring locations around Clark County recorded an exceedance of the 2015 National Ambient Air Quality Standard (NAAQS) for 8-hour ozone (0.070 ppm).

Typically, ozone concentrations in the stratosphere are around 5-10 parts per million (ppm). Depending on the amount of dilution after the SOI event, surface-level ozone concentrations can be significantly enhanced above background tropospheric levels (~0.040-0.050 ppm). Even in areas with urban emissions, such as Las Vegas, the addition of ozone from an upwind SOI event can enhance ozone concentrations above usual levels, potentially driving concentrations above the ozone standard. SOIs in the western U.S. typically occur in spring and are well-documented to affect ozone concentrations in Clark County, providing up to 18-22 ppb of ozone enhancement in May and June (Langford, 2014; Langford and Senff, 2019). We can identify and track the movement of air from an SOI event because stratospheric air (1) is typically depleted in both anthropogenic compounds (i.e., particulate matter [PM], carbon monoxide [CO], and nitrogen oxides [NO_x]) and water vapor compared with tropospheric air, and (2) has enhanced isentropic potential vorticity (IPV). According to guidance from the U.S. Environmental Protection Agency (EPA), exceptional events (EEs) such as SOIs that affect ozone concentrations can be subject to exclusion from calculations of NAAQS attainment if a clear causal relationship can be established between a specific event and the monitoring exceedance (U.S. Environmental Protection Agency, 2018).

For the May 28, 2020, case in Clark County, we describe the clear causal relationship between the event causing the exceedance (an SOI over Idaho and Utah) and the downwind effects on the monitoring sites in Clark County that recorded an exceedance of the maximum daily 8-hour ozone average (MDA8). The evidence in this report provides a Tier 2 analysis required by EPA's Exceptional

Event Guidance for more complex SOI events: comparison with non-event ozone concentrations, analysis of meteorological transport, satellite and model analysis of stratospheric tracers, transport analysis from the SOI to the surface, measurements of column ozone at a high-altitude site, meteorologically similar day analyses, and the effect of the SOI on surface ozone (and other tracer) concentrations. Additionally, we provide Generalized Additive Model (GAM) statistical results to help quantify the effect of the SOI on this EE. The SOI that affected ozone concentrations in Clark County could not be reasonably controlled or prevented because SOIs are considered natural events.

Table 1-1 lists the sites affected during the May 28 event, as well as their locations and MDA8 ozone concentrations.

Table 1-1. May 28, 2020, EE information. All monitoring sites in Clark County that exceeded the 2015 NAAQS standard during May 28, 2020, are listed along with EPA Air Quality System (AQS) Site Codes, location information, and MDA8 ozone concentrations.

AQS Site Code	Site Name	Latitude (degrees N)	Longitude (degrees W)	MDA8 O ₃ Concentration (ppb)
320030043	Paul Meyer	36.106	-115.253	76
320030071	Walter Johnson	36.170	-115.263	71

Concurrent with this document, Clark County is submitting documentation for other ozone EEs in 2018 and 2020 due to wildfires and stratospheric intrusions. These events are mentioned throughout this report and are referred to as “proposed 2018 and 2020 EEs,” recognizing that discussion with EPA is still pending. All proposed EEs for Clark County in 2018 and 2020 are listed in **Tables 1-2 and 1-3**. Wherever possible, we calculated statistics to provide context both including and excluding the proposed EEs from 2018 and 2020.

Table 1-2. Proposed Clark County 2018 EEs. For each site and date combination where the 2015 NAAQS standard was exceeded, the MDA8 ozone concentration is shown in parts per billion (ppb). Blank cells indicate that there was no exceedance on that site/date combination.

Date	Paul Meyer	Walter Johnson	Green Valley	Jerome Mack	Joe Neal	Palo Verde	Jean	Indian Springs	Apex	Boulder City
6/19/2018	72	72	77	75						
6/20/2018	71	74			72					
6/23/2018	72	76	75	72	72	71	77	73		
6/27/2018	75	76	78	76	72	72	81	78	74	72
7/14/2018	72		78	78						
7/15/2018		71	73	73	78					
7/16/2018	75	79	71	73	80	75				
7/17/2018	74	77				74				
7/25/2018	71	72	72							
7/26/2018	72	75	77	77					71	
7/27/2018	72	74			76					
7/30/2018			73	72						
7/31/2018		73			73					
8/6/2018	79	77	74	71	76	72			74	
8/7/2018	73	74	72	71	74				71	

Table 1-3. Proposed Clark County 2020 EEs. For each site and date combination where the 2015 NAAQS standard was exceeded, the MDA8 ozone concentration is shown in ppb. Blank cells indicate that there was no exceedance on that site/date combination.

Date	Walter Johnson	Paul Meyer	Joe Neal	Jerome Mack	Green Valley	Boulder City	Jean	Indian Springs	Apex
5/6/2020	78	77	76	73	72		75		76
5/9/2020	71	74							
5/28/2020	71	76							
6/22/2020	73	74	78						
6/26/2020		73							
8/3/2020	82	78	81		72	72	73	71	
8/7/2020	71		72					72	
8/18/2020	82	79	78						
8/19/2020	74	74	73		71				
8/20/2020			71						
8/21/2020		71							
9/2/2020	75	73							
9/26/2020	71		75						

1.2 Exceptional Event Rule Summary

The EPA “Guidance on the Preparation of Exceptional Events Demonstration for Stratospheric Ozone Intrusions” (U.S. Environmental Protection Agency, 2018) describes a two-tier approach to evaluating

an SOI event and then developing evidence for the EE demonstration. A summary of event requirements for both tiers is listed in [Table 1-4](#). From the EPA 2018 SOI Guidance:

- Tier 1 analyses can be used for events when ground ozone concentrations are much higher than typical observations, with conditions unfavorable to photochemical ozone production, and with synoptic meteorological conditions conducive to stratospheric intrusion being the cause.
- Tier 2 analyses are appropriate for cases when both local photochemical ozone production and stratospheric ozone contributions are present, or for events where the observed ozone is within range of typical seasonal values of that location. Tier 2 demonstrations involve more supporting analytical documentation than Tier 1 demonstrations.

In this demonstration, we conduct the Tier 2 analysis (which is cumulative with Tier 1) because local photochemical ozone production existed simultaneously with the SOI contribution.

Table 1-4. Tier 1 and 2 requirements for evaluating stratospheric intrusion impacts on ozone exceedances.

Tier	Elements of SOI Event
1	<ul style="list-style-type: none"> • Stratospheric intrusion events that cause obvious ozone impacts during periods when: <ul style="list-style-type: none"> – ozone concentrations are typically low, and – meteorological patterns are suggestive of potential transport from the stratosphere. • Meteorological analyses suggest intrusion was recent, nearby, and expansive: <ul style="list-style-type: none"> – associated with a frontal passage, and – with elevated ozone observed across a large region. • Ozone concentrations are clearly distinguishable from usual conditions. • Occurred outside the period in which high ozone from local and/or regional production is typically observed. • Occurred when and where local photochemical production was minimal: <ul style="list-style-type: none"> – at night, – associated with cold air advection, high wind speeds, and/or – strong dispersion conditions.
2	<ul style="list-style-type: none"> • The relationship between the stratospheric intrusion and influenced ozone concentrations is complex and not fully elucidated with Tier 1 elements. • Resulted from long-distance, multi-day transport requiring detailed analyses. • The event-influenced concentrations were in the range of typical exceedances (i.e., close to the area’s design value). • Occurred in season when ozone exceedances are historically common. • Occurred in association with other processes and sources of ozone or on days where meteorological conditions were conducive to local ozone formation.

1.3 Demonstration Outline

This demonstration shows that stratospheric air entered the free troposphere (FT), was mixed down to the surface, and subsequently caused an ozone exceedance at the surface. We use the recommended analyses listed throughout the EPA 2018 SOI guidance. [Table 1-5](#) summarizes the

required and recommended analyses for both a Tier 1 and Tier 2 SOI analyses and shows the corresponding sections for each analysis in this report.

Table 1-5. Locations of Tier 1 and 2 analyses within this report.

Type of Analysis	Tier 1 + Tier 2	Section of This Report (Analysis Type)
Conceptual Model	What conditions generally lead to high ozone in the area?	Section 2.3 (characteristics of non-event historical O ₃ formation)
Historical Comparison	<ul style="list-style-type: none"> • ≥ 5 years of peak daily ozone data with other high event days flagged. • Table with percentile ranks of days. • Historical diurnal profile comparison (Tier 2). 	Section 3.1 (comparison of event with historical data)
Event overview	<ul style="list-style-type: none"> • Spatial and temporal depictions of ozone during the event. • Description of surface and upper air meteorological conditions during the event. • Begin to establish the complex relationship between the intrusion and eventual impact at surface (Tier 2). 	Section 2.4 (stratospheric intrusion event description)
Establish stratospheric intrusion	Several of the following are likely needed: <ul style="list-style-type: none"> • Water vapor imagery • Total column ozone • Meteorological evidence 	Sections 3.2.1 (total column ozone and water vapor); Section 3.2.2 (model results of ozone, CO, water vapor, & meteorological conditions)
Establish stratospheric air reached surface	Several of the following are likely needed: <ul style="list-style-type: none"> • LIDAR, rawinsonde data • Meteorological evidence • Modeled parameter cross sections • Trajectory models 	Section 3.2.2 (Model parameter cross sections); Section 3.3.1 (HYSPLIT trajectories); Sections 3.3.2 (LIDAR measurements of the ozone vertical profile); Section 3.3.3 (Meteorological analysis)
Impacts at the surface	Several of the following are likely needed: <ul style="list-style-type: none"> • Coincidence between high ozone and meteorological/parameter conditions characteristic of stratospheric intrusions • Statistical model evidence of impacts • Summary narrative 	Section 3.4 (ozone & RH, ozone & NO _x diurnal patterns, surface ozone concentration time series); Section 3.5.1 (Meteorologically similar matching day analysis); Section 3.5.2 (GAM statistical analysis); Section 3.6 (summary narrative)

In Chapter 2 of this report, we establish a narrative conceptual model of the EE with a description of the monitoring network, the event causing the exceedance, and transport from the event that led to the exceedance at the affected monitors. Section 2.1 and 2.2 provides detailed information of the region and the existing ozone monitors. Section 2.3 summarizes the processes that led to high ozone concentrations at the monitor on non-event days and the ozone seasonality. In Section 2.4, we introduce the meteorology that caused the stratospheric ozone intrusion and provide a brief narrative for how stratospheric air was transported into the free troposphere and ultimately mixed down through the planet boundary layer (PBL) to the surface monitors.

In Section 3 of this report, we establish the clear causal relationship between the event and the monitored ozone exceedance. As a first step, we provide a comparison of the exceedance concentrations with historical data in Section 3.1. In Section 3.2, we provide evidence of stratospheric-tropospheric exchange using satellite imagery and meteorological model results. Section 3.3 shows evidence of stratospheric air reaching the surface using trajectory analysis, light detection and ranging (LIDAR) ozone measurements, and meteorological observations. We then demonstrate the event impact at the surface in Section 3.4. Additionally, we developed a statistical GAM to estimate the contribution of stratospheric ozone to the monitored ozone concentrations in Section 3.5.

Following the EPA's SOI event guidance, we performed both Tier 1 and Tier 2 analyses to show the clear causal relationship between the stratospheric intrusion event which occurred over Idaho and Utah and the exceedance event in Clark County, Nevada, on May 28, 2020. Focusing on the characterization of the meteorology, transport, and air quality on the days leading up to the event, we conducted the following specific analyses (results from these analyses are presented in both Section 2 and 3):

- Developed time series plots that show the May 28 ozone concentrations in historical context at each affected monitoring site for both 2020 and the past five years.
- Compiled maps of ozone and water vapor in the area from satellite data.
- Retrieved total column ozone from the Ozone Mapping and Profile Suite (OMPS) instrument aboard the Suomi National Polar-orbiting Partnership (NPP) satellite and Modern-Era Retrospective analysis for Research and Applications, Version 2 (MERRA-2) product.
- Provided evidence of a stratospheric intrusion event over Idaho and Utah using model results of IPV, relative humidity (RH), and potential vorticity (PV) at 350 hPa using the Global Forecast System (GFS).
- Provided model results and cross sections of ozone and CO concentrations using the Realtime Air Quality Modeling System (RAQMS).
- Provided model results of ozone at 500 hPa height using the National Center for Atmospheric Research (NCAR) Whole Atmosphere Community Climate Model (WACCM).

- Provided surface and upper-level (500 hPa) meteorological maps using the North American Surface Analysis.
- Provided boundary layer depth analysis on the EE day using North American Mesoscale (NAM) data and the University Corporation for Atmospheric Research (UCAR) Integrated Data Viewer (IDV).
- Showed the transport patterns of stratospheric ozone from the intrusion location to the Clark County region via the Hybrid Single-Particle Lagrangian Integrated Trajectory (HYSPLIT) model.
- Performed statistical analysis to compare event ozone concentrations to non-event concentrations.
- Developed plots to show diurnal patterns of ozone and supporting pollutants such as RH and NO_x.
- Assessed vertical transport of stratospheric ozone using Tunable Optical Profiler for Aerosol and Ozone (TOPAZ) LIDAR measurements from the National Oceanic and Atmospheric Administration's (NOAA) Chemical Sciences Laboratory site in Boulder, CO.
- Created a GAM model of MDA8 ozone concentrations to assess the enhancement of ozone concentrations at the impacted monitors due to the transported stratospheric ozone.

1.4 Conceptual Model

The conceptual model for the exceptional event that led to the ozone exceedances at the Walter Johnson and Paul Meyer monitoring sites on May 28, 2020, is outlined in Table 1-5. We provide the analysis techniques performed and evidence for each Tier. This establishes a weight of evidence for the clear causal relationship between a stratospheric intrusion over Idaho and Utah and the May 28 exceptional ozone event. We assert that stratospheric ozone was transported into the upper troposphere over Idaho and Utah, and subsequently reached Clark County, where it provided a small, detectable contribution—along with local photochemistry and other regional sources—to two Clark County monitoring site ozone exceedances on May 28. In support of this assertion, the key points of evidence for the conceptual model are summarized below.

1. The May 28 ozone exceedance occurred during a typical ozone season, but event concentrations at the two exceedance sites were significantly higher than non-event concentrations. Ozone concentrations at the exceedance sites showed high percentile rank when compared with the past six years and ozone seasons.
2. Multiple atmospheric models (GFS, WACCM, and RAQMS) provide consistent evidence from isentropic potential vorticity, water vapor, and CO concentrations for a stratospheric intrusion event that injected ozone-rich stratospheric air into the upper troposphere over southern

Idaho and northern Utah on May 25 from 0:00 to 12:00 UTC. Time series of mid-tropospheric ozone profile simulations from May 25 through 27 indicate a continuous stratospheric-tropospheric ozone tongue was rapidly (within 24 hours) transported to western Arizona and descended into a deep boundary layer.

3. Although the stratospheric ozone contribution was diluted and partially lost during boundary layer transport to Clark County due to chemical and dry deposition ozone sinks, the WACCM model stratospheric ozone contribution indicates a persistent ozone feature along the boundary layer transport path, and a small (around 5-10 ppb) positive detection of stratospheric ozone contribution at the surface in Clark County on May 28.
4. Back and forward trajectories from the exceedance sites, at near-surface altitude, and the time of maximum ozone concentration, show consistent transport patterns from the free troposphere coinciding with the SOI source and modeled ozone tongue to the boundary layer in Clark County on May 28. The deep mixed layer observed upwind on the preceding days and in Clark County on the event day provide evidence for sufficient vertical mixing between the mid-troposphere and the surface.
5. Meteorological conditions on May 28 did not favor enhanced local ozone production when compared with meteorologically similar ozone season days. Average MDA8 ozone across similar days was well below the ozone NAAQS and >10 ppb lower than the May 28 exceedance.
6. GAM model predictions of MDA8 ozone on May 28 are all well below the 70 ppb ozone NAAQS for each EE-affected site. Using the GAM residuals (observed MDA8 ozone minus GAM-predicted MDA8 ozone) to estimate the effect of the SOI on Clark County, we find a contribution of 10 to 13 ppb ozone from an atypical source; in this case, likely the stratospheric intrusion over Idaho and Utah.
7. The arrival of dry, SOI influenced air to Clark County coincided with abnormally lower daytime surface absolute humidity on May 28 in Clark County. NO and NO₂ concentrations were within average levels on May 28 in Clark County, suggesting that local photochemical ozone production was unlikely the only source of the high ozone exceedance event.

2. Historical and Non-Event Model

2.1 Regional Description

Clark County is located in the southern portion of Nevada and borders California and Arizona. Clark County includes the City of Las Vegas, which has a population of approximately 2 million and is one of the fastest growing metropolitan areas in the United States (U.S. Census Bureau, 2010). Las Vegas is located in a 1,600 km² desert valley basin at 500 to 900 m above sea level (Langford et al., 2015). It is surrounded by the Spring Mountains to the west (3,000 m elevation) and the Sheep Mountain Range to the north (2,500 m elevation), and three mountain ranges to the south. The valley floor slopes downward from west to east, which influences surface wind, temperature, precipitation, and runoff patterns. The Cajon Pass and I-15 corridor to the west is an important atmospheric transport pathway from the Los Angeles Basin into the Las Vegas Valley (Langford et al., 2015). [Figures 2-1 and 2-2](#) show the topography of Clark County and the surrounding areas.

The Las Vegas Valley climatology features abundant sunshine and hot summertime temperatures, with average summer month high temperatures of 34-40°C. Because of the mountain barriers to moisture inflow, the region experiences dry conditions year-round (~107 mm annual precipitation, 22% of which occurs during the summer monsoon season in July through September). The urban heat island effect in Las Vegas during the summer leads to large temperature gradients within the valley, with generally cooler temperatures on the eastern side. During the summer season, monsoon moisture brings high humidity and thunderstorms to the region, typically in July and August (National Weather Service Forecast Office, 2020). Winds in the Las Vegas basin tend to be out of the southwest (from Los Angeles) during the spring and summer; winds in the fall and winter tend to be out of the northwest, with air transported between the neighboring mountain ranges and along the valley.

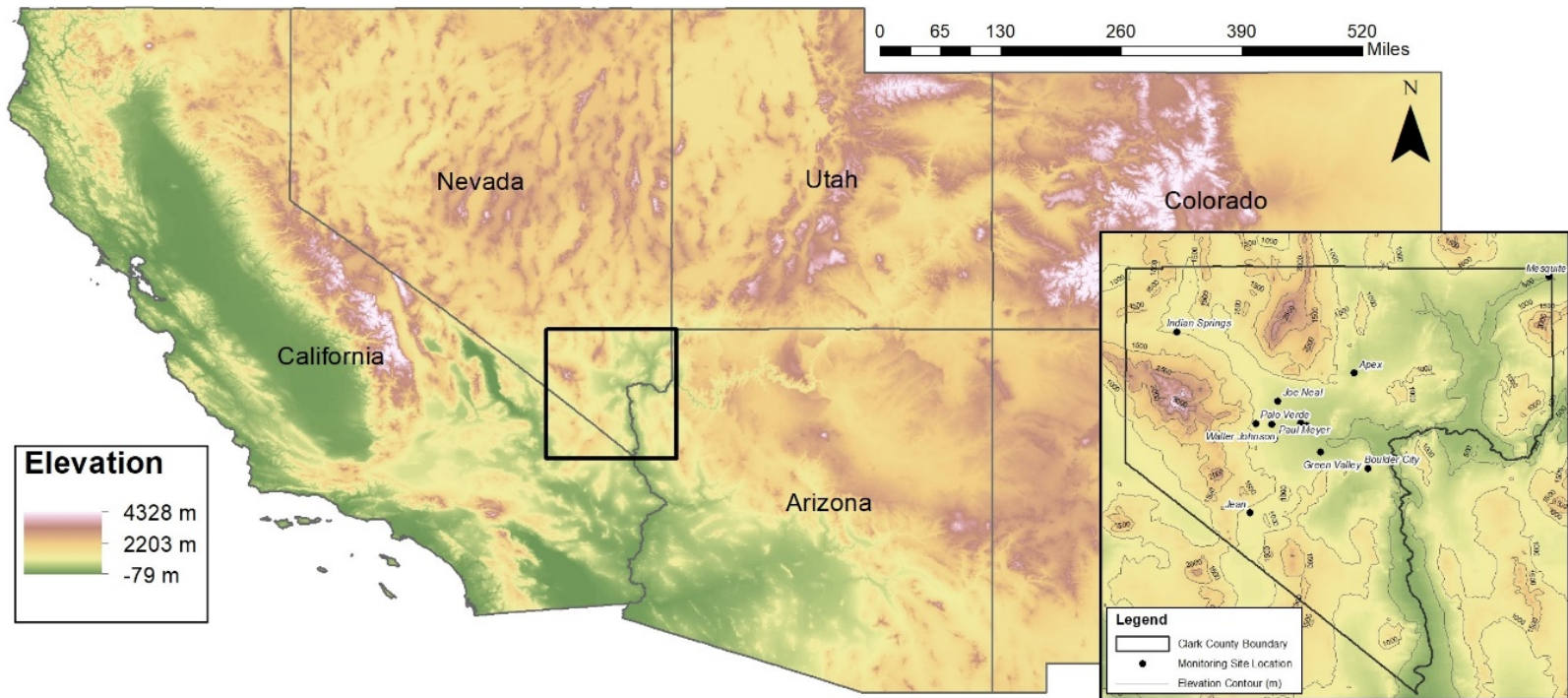


Figure 2-1. Regional topography around Clark County, with an inset showing the county boundaries and the air quality monitoring sites analyzed in this report.

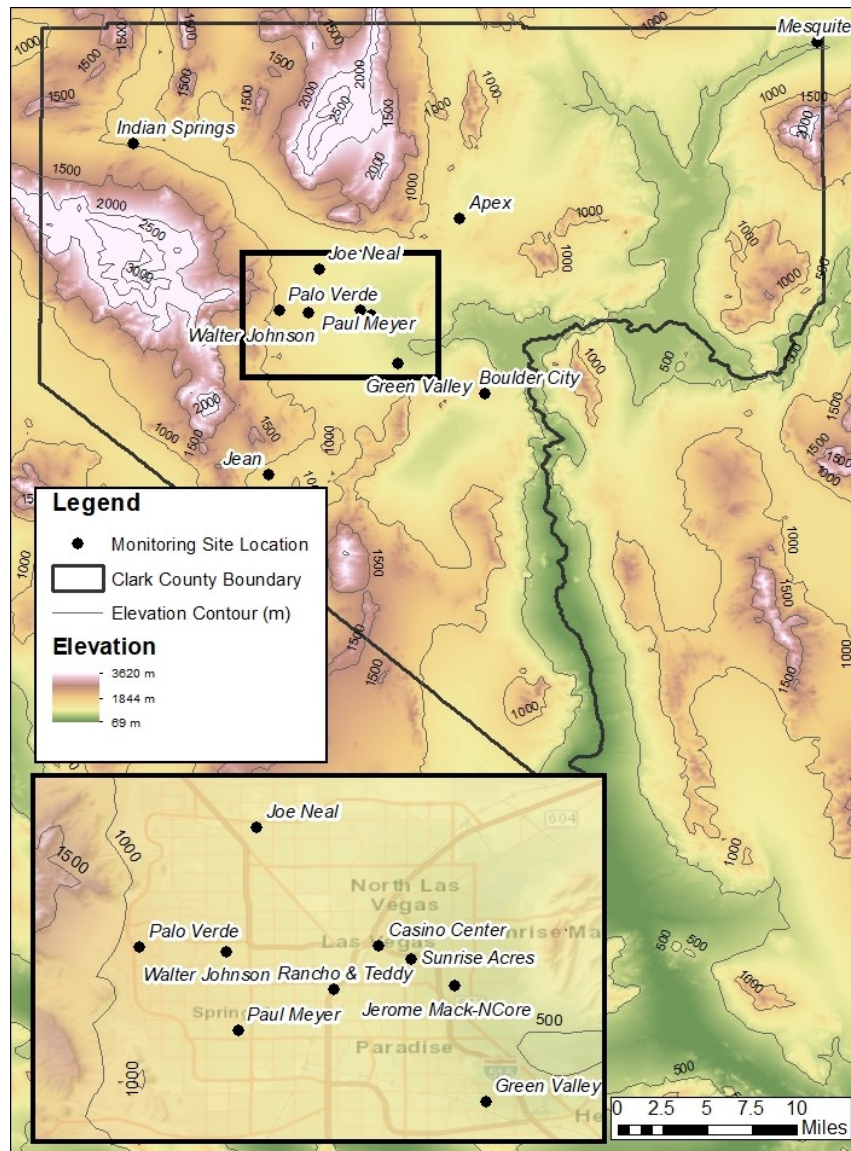


Figure 2-2. Clark County topography, with an inset showing air quality monitoring sites that measure ozone in the Clark County area.

2.2 Overview of Monitoring Network

The Clark County Department of Environment and Sustainability, Division of Air Quality (DAQ), operated 14 ambient air monitoring sites in the region during 2020 (shown in Figure 2-2). These sites measure hourly ozone, particulate matter with a diameter less than 2.5 micrometers (PM_{2.5}), particulate matter with a diameter less than 10 micrometers (PM₁₀), NO_x, total nonmethane organic compounds (TNMOC), and CO concentrations along with meteorological parameters. Table 2-1 presents the monitoring data coverage for all the monitoring sites used in this report across time

and space for criteria pollutants, surface meteorological parameters (barometric pressure, temperature, wind speed, and direction), and mixing height. We examined ozone and other criteria pollutants at 11 sites around Clark County to investigate the high ozone event observed on May 28, and Table 1-1 shows the two monitoring sites that were investigated for NAAQS ozone exceedances due to a stratospheric ozone intrusion. DAQ's ambient air monitoring network meets the monitoring requirements for criteria pollutants pursuant to Title 40, Part 58, of the Code of Federal Regulations (CFR), Appendix D (Code of Federal Regulations, 1997). Data are quality-assured in accordance with 40 CFR 58 and submitted to the EPA's AQS. The spatial distribution of the monitoring sites characterizes the regional air quality in Las Vegas, as well as air quality upwind and downwind of the urban valley region (Figure 2-2). The Jean monitoring site along the I-15 corridor is generally upwind such that it captures atmospheric transport into the region and is least impacted by local sources.

Table 2-1. Clark County monitoring site data. The available date ranges of all parameters and monitoring sites used in this report are shown for Clark County, Nevada.

Site	AQS Sitecode	O ₃	PM _{2.5}	CO	NO	NO ₂	TNMOC	Temp.	Wind Speed	Wind Direction	Barom. Pressure	Mixing Height
Apex	320030022	2014-2020						2014-2020	2014-2020	2014-2020		
Boulder City	320030601	2014-2020									2014-2016	
Casino Center	320031502							2014-2020	2016-2020	2016-2020		
Green Valley	320030298	2015-2020	2014-2020	2020				2016-2020	2014-2020	2014-2020	2014-2016	
Indian Springs	320037772	2014-2020										
Jean	320031019	2014-2020	2014-2020					2014-2020	2014-2020	2014-2020	2014-2016	
Jerome Mack	320030540	2014-2020	2014-2020	2015-2020 ^{1,2}	2015-2020	2015-2020	2020	2014-2020	2014-2020	2014-2020	2014-2020	2020
Joe Neal	320030075	2020	2018-2020	2019-2020		2015-2020		2014-2020	2014-2020	2014-2020	2014-2016	
Mesquite	320030023	2014-2020						2014-2020	2014-2020	2014-2020		
Palo Verde	320030073	2014-2020	2020					2014-2020	2014-2020	2014-2020	2014-2016	
Paul Meyer	320030043	2014-2020	2017-2020					2014-2020	2014-2020	2014-2020	2014-2016	
RT	320031501							2015-2020	2015-2020	2015-2020	2014-2016	
Sunrise Acres	320030561			2020				2014-2020	2014-2020	2014-2020	2014-2016	
Walter Johnson	320030071	2014-2020	2020					2015-2020	2015-2020	2015-2020	2014-2016	

¹ CO data invalid at Jerome Mack on Sep. 2, 2020

² CO data invalid at Jerome Mack Apr. 28, 2020 – May 20, 2020

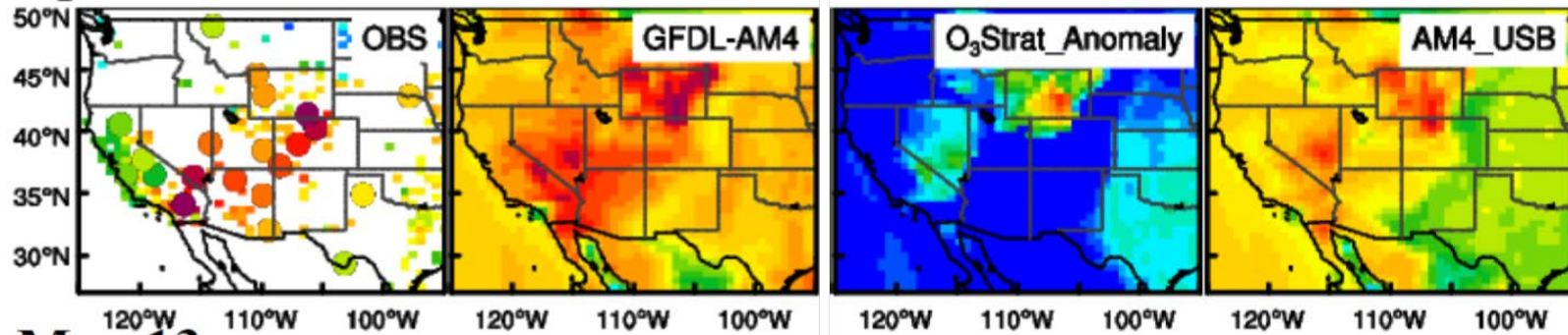
2.3 Characteristics of Non-Event Historical O₃ Formation

During the ozone season (April–September) in Clark County, ozone concentrations are typically influenced by local formation, transport into the region, and on occasion by EEs such as wildfires and stratospheric intrusions. Transport from upwind source regions (e.g., the Los Angeles Basin, Mojave Desert, Asia) occurs with southwesterly winds, and southerly transport dominates the later portion of the season due to the summer monsoon (Langford et al., 2015; Zhang et al., 2020). Local precursor emissions in Clark County include mobile NO_x and volatile organic compounds (VOCs) sources, natural-gas fueled power generation NO_x sources, and biogenic VOC emissions. Based on 2017 Las Vegas emission inventories, on a typical ozone season weekday there are 98 tons of NO_x emissions per day and 238 tons of VOC emissions per day (Clark County Department of Environment and Sustainability, 2020). On-road mobile sources comprise 40% of NO_x emissions and total mobile emissions comprise 88% of total NO_x emissions during the ozone season. In contrast, 52% of VOC emissions originate from biogenic sources within Clark County. Local emissions and/or precursors transported into the region contribute to ozone formation within Clark County (Langford et al., 2015; Clark County Department of Air Quality, 2019).

Stratospheric ozone intrusion events over the western U.S. have impacted Clark County when stratospheric ozone mixes with regional pollutants and local photochemical ozone leading to exceedance events (Zhang et al., 2020). The 2017 Fires, Asian, and Stratospheric Transport–Las Vegas Ozone Study (FAST-LVOS) provides evidence for April, May and June stratospheric intrusion events impacting ozone in Clark County (Zhang et al., 2020). [Figure 2-3](#) depicts contributions of stratospheric ozone (stratospheric O₃ tracer (O3Strat)) and non-anthropogenic ozone to MDA8 surface O₃ concentrations across the western U.S. from the NOAA GFDL AM4 model on two exemplary SOI events in April and May 2017. AM4 model results generally agree well with observations, with reduced ozone biases compared with AM3. O3Strat tracks ozone of stratospheric origin and its anomaly can be used qualitatively because it is subject to tropospheric chemical and depositional losses. Based on the FAST-LVOS study, Clark County typically experiences episodes with elevated O3Strat of 20–40 ppbv above April–June mean O3Strat ozone baseline and larger non-anthropogenic ozone contributions (Zhang et al., 2020). The exceedance event examples in [Figure 2-3](#) show 5 and 15 ppb O3Strat anomalies along with ~60 ppb ozone contributed from non-anthropogenic sources. Overall, stratospheric ozone intrusions can play a large role in ozone exceedances during April through June in the Clark County area.

Typical SOI events in Clark County occur under similar meteorological conditions as those on May 28, 2020. The LVOS study ozone exceedances occurred during periods with south-southwest winds and dry air following descending air behind cold fronts (Langford, 2014), similar to the conditions observed with the May 28 EE. These meteorological conditions are typical for late spring ozone exceedances and well-documented in the LVOS and FAST-LVOS study periods.

April 23



May 13

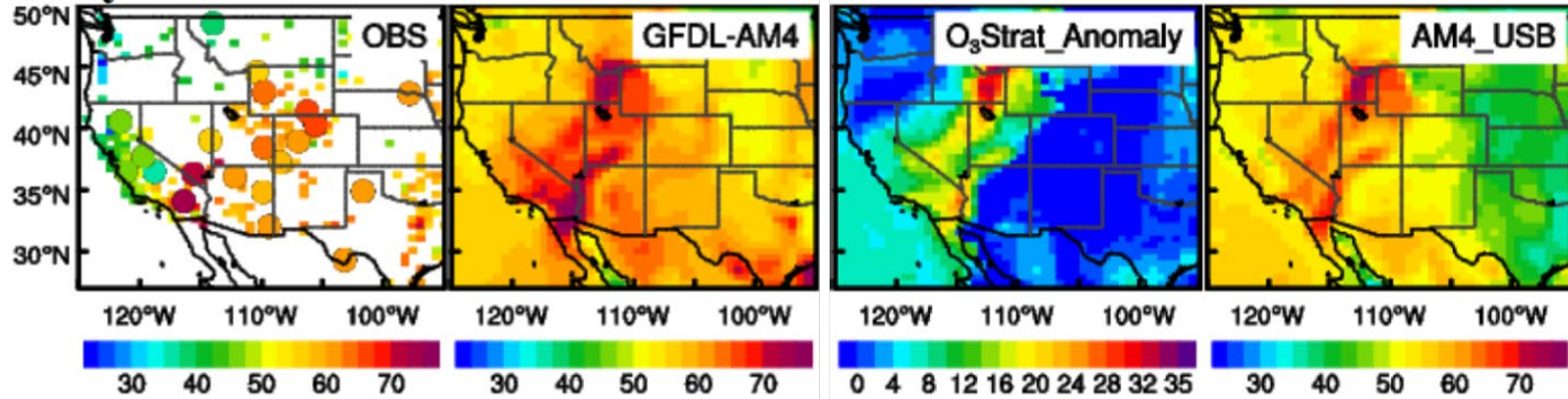


Figure 2-3. Observed (left) and NOAA GFDL AM4 modeled MDA8 ozone, along with stratospheric ozone tracer anomaly in AM4 relative to monthly means (O₃Strat_Anomaly), and the non-anthropogenic emissions AM4 ozone simulation (AM4_USB). Two examples of stratospheric intrusion influenced days in Clark County are shown during the FASTLVOS study (April 23 and May 13, 2017) Adapted from Figure S6 in Zhang et al. (2020)

In this demonstration, we discuss the impacts of a stratospheric intrusion event on ozone concentrations in Clark County on May 28, 2020. In order to fully discern the effect of the stratospheric intrusion on ozone concentrations in Clark County on this date, we examine the historical ozone record for all affected sites (Table 1-1). *Non-event days* refer to all days other than the May 28 event. Because percentile rankings are sensitive to including the relatively large number of potential EE days during 2018 and 2020, we also provide statistics *excluding potential EE days* (i.e., without including the 2018 and 2020 potential EE days as defined in Tables 1-2 and 1-3 in Section 1). The 8-hour ozone design value (DV) is the three-year running average of the fourth-highest MDA8 ozone concentration (U.S. Environmental Protection Agency, 2015). Within Clark County, Las Vegas is classified as an EPA Region 9 marginal nonattainment region, with a 73 ppb ozone DV for 2017-2019 (U.S. Environmental Protection Agency, 2020). Ozone EE days are identified as days with significant wildfire or stratospheric intrusion influence in addition to an MDA8 concentration greater than 70 ppb. By this criterion, we identified 15 possible EE days in 2018 and 13 possible EE days in 2020, and no EE days in 2019.

The May 28, 2020, EE occurred early in the ozone season under hot, dry air conditions with a deep mixed layer and surface level trough of low pressure over Clark County. These meteorological conditions, which are often associated with a typical high ozone day (non-event conceptual model), favor enhanced vertical mixing of free tropospheric air into the boundary layer. Compared with a non-event conceptual model of local precursor emissions contributing to ozone formation at ground level under similar conditions, the May 28 conditions indicate transport of free tropospheric air via upper-level winds from the north.

Figures 2-4 through 2-7 depict the six-year historical record and seasonality of MDA8 ozone concentrations at each EE-affected monitoring site, along with the 99th percentile and NAAQS standard ozone concentrations. May 28 ranks in the top 1% for daily maximum ozone concentration in the six-year historical record at the Paul Meyer monitoring site.

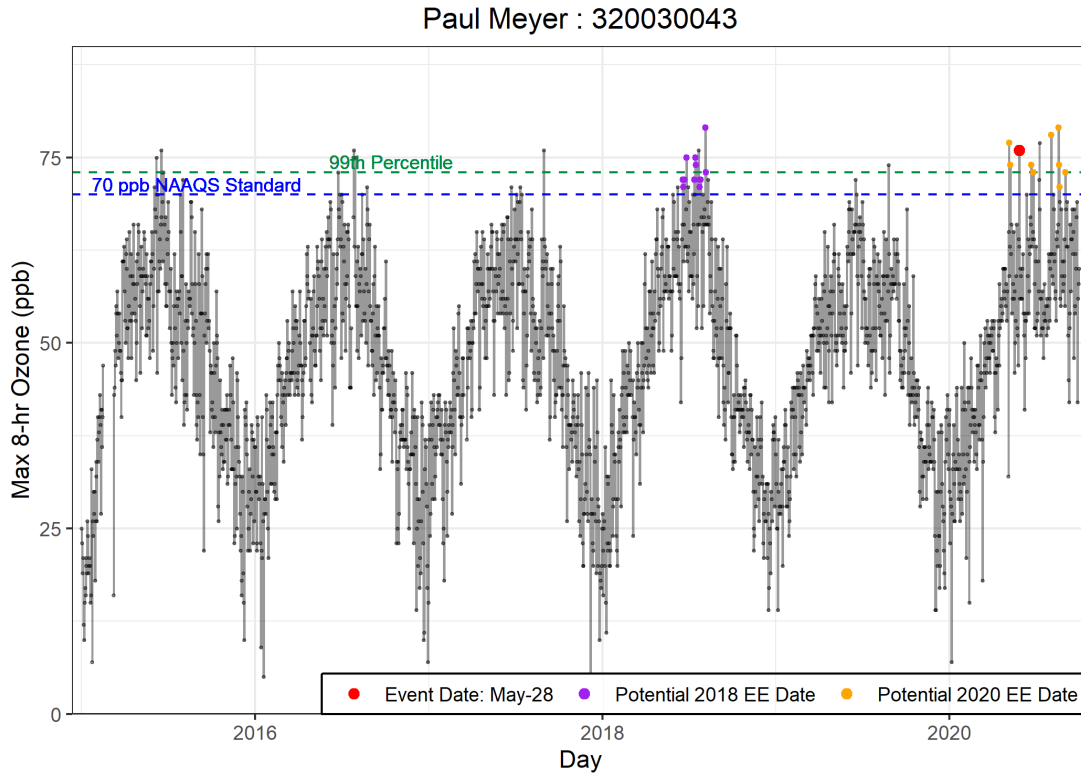


Figure 2-4. Time series of 2015-2020 ozone concentrations at the Paul Meyer site. May 28, 2020, is shown in red.

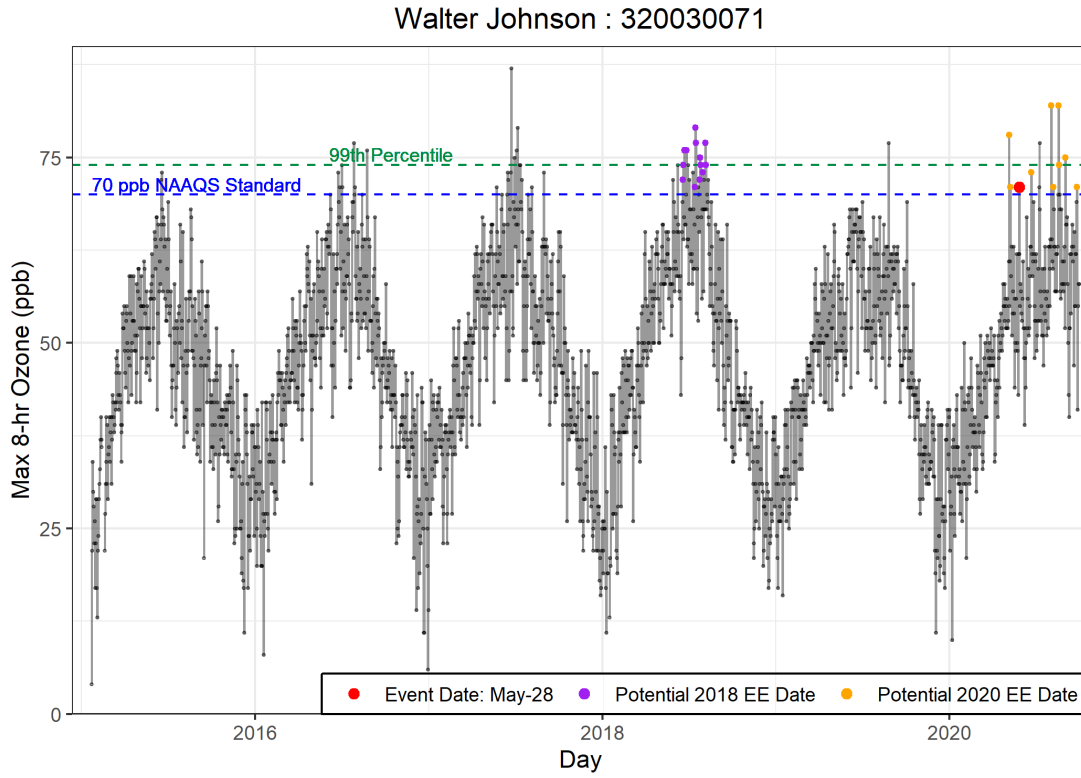


Figure 2-5. Time series of 2015-2020 ozone concentrations at the Walter Johnson site. May 28, 2020, is shown in red.

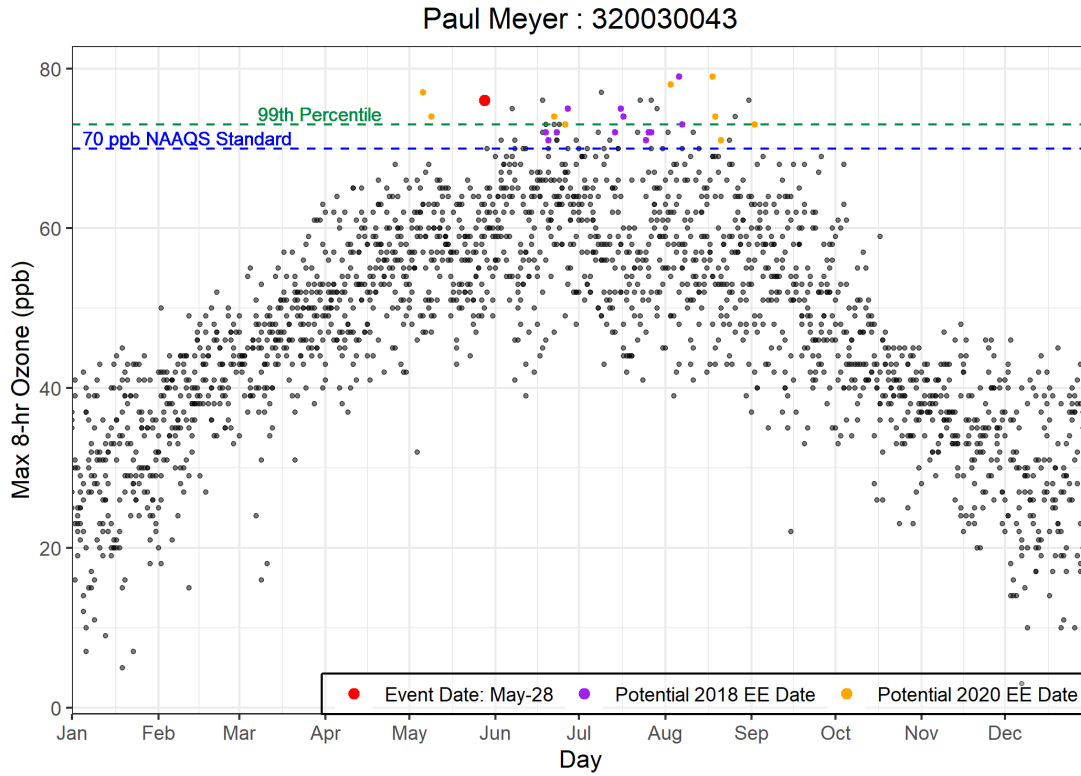


Figure 2-6. Seasonality of 2015-2020 ozone concentrations from the Paul Meyer site. May 28, 2020, is shown in red.

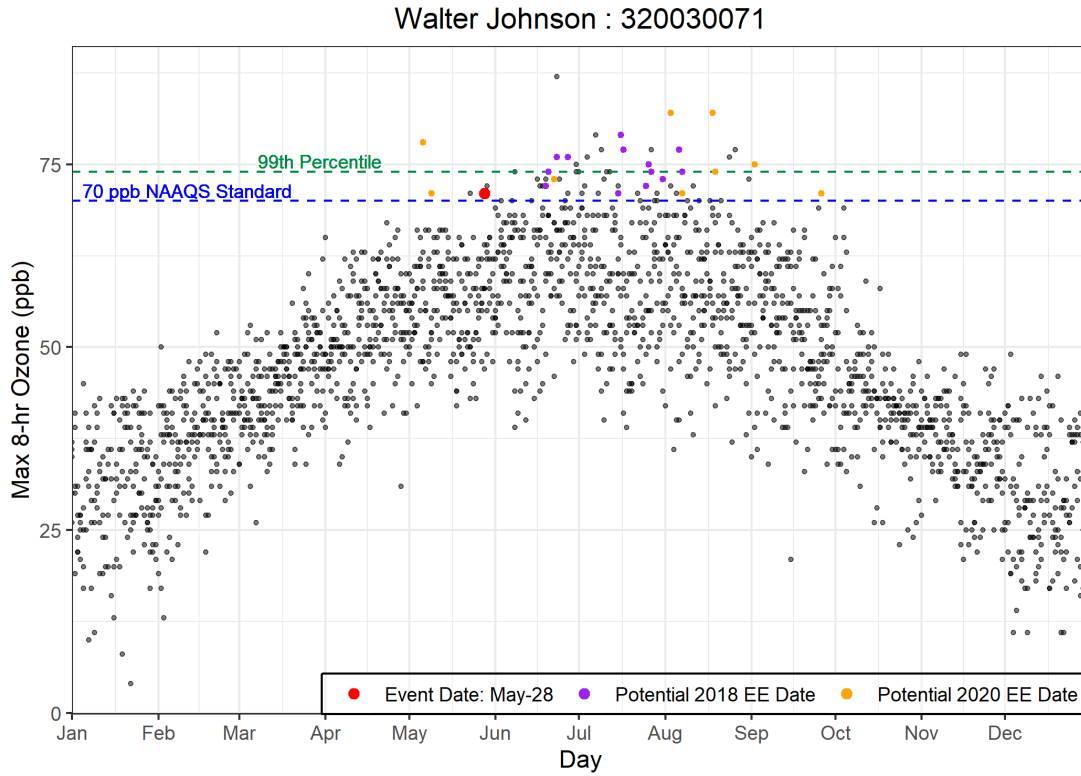


Figure 2-7. Seasonality of 2015-2020 ozone concentrations from the Walter Johnson site. May 28, 2020, is shown in red.

Figure 2-8 depicts a two-week ozone diurnal cycle of 1-hour ozone, beginning one week before the May 28 event and ending one week after. On May 28, daily maximum 1-hour ozone concentrations were the highest at the two EE-affected monitoring sites during this two-week period.

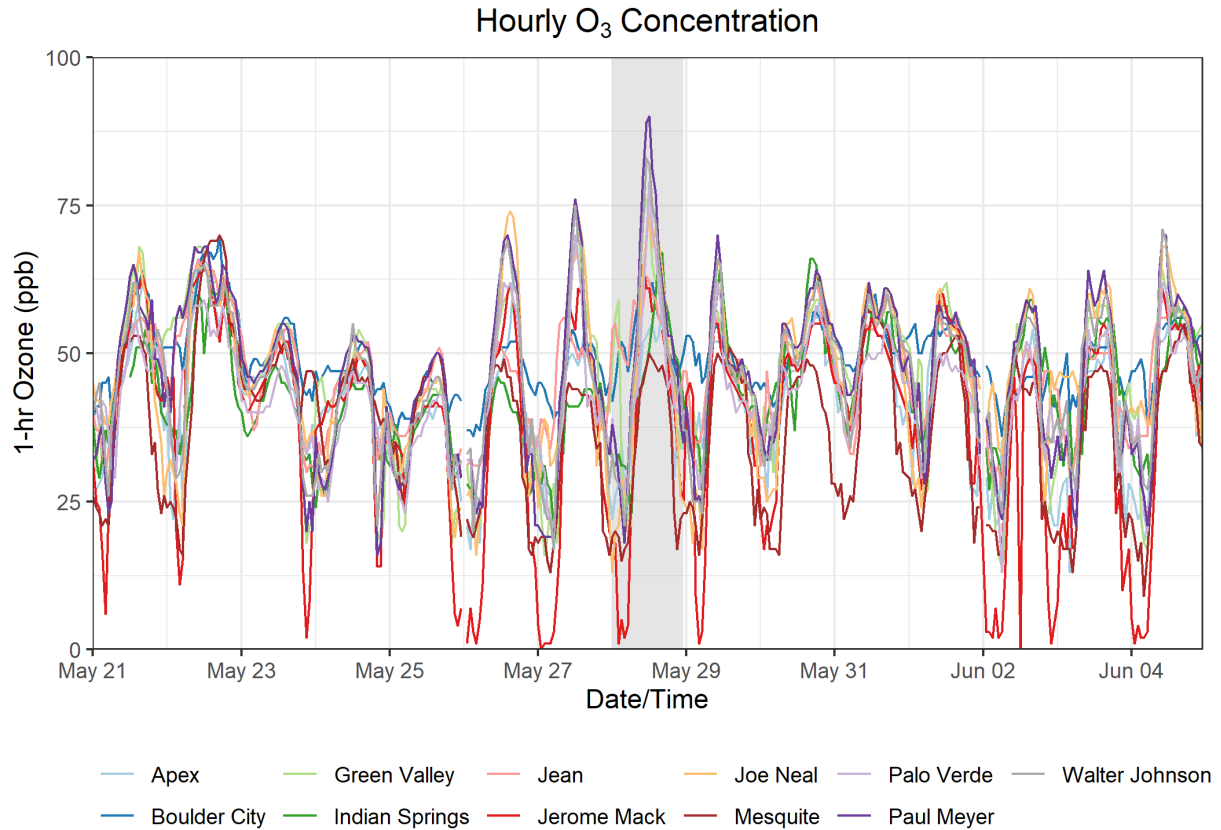


Figure 2-8. Ozone time series at all monitoring sites. Time series of hourly ozone concentrations at monitoring sites in Clark County for one week before and after the May 28 event are shown. May 28, 2020, is shaded for reference.

2.4 Stratospheric Intrusion Event Description

Figure 2-9 shows a basic model of stratospheric-tropospheric mixing and transport of ozone-rich air downwind to an area like Clark County. The basic narrative for these events starts with a stratospheric intrusion of high ozone air into the troposphere, then transport and mixing of the stratospheric-tropospheric air into the free troposphere and PBL, which is eventually mixed to the surface. In this narrative, the city-measured ozone concentration—a combination of anthropogenic and background ozone—can thus be enhanced by the transport of stratospheric ozone into the area. On photochemically active days, the addition of even small quantities of stratospheric ozone can cause ozone concentrations to exceed the NAAQS standards. In order to trace stratospheric air, we

can look for the key parameters identified in Figure 2-9. Stratospheric air usually has high ozone concentrations, high IPV, low concentrations of water vapor, and low CO concentrations, while tropospheric air has lower ozone concentrations, low IPV, and may exhibit higher concentrations of water vapor and CO. First, we identify where stratospheric intrusion occurred, as indicated by the above parameters, then show that the stratospheric-tropospheric air mass was transported and mixed to the surface. [Table 2-2](#) identifies the analyses needed to confirm each step of the stratospheric intrusion and transport. Each piece of evidence described in the table is shown in Section 3 and is consistent with the EPA SOI demonstration requirement shown in Table 1-4.

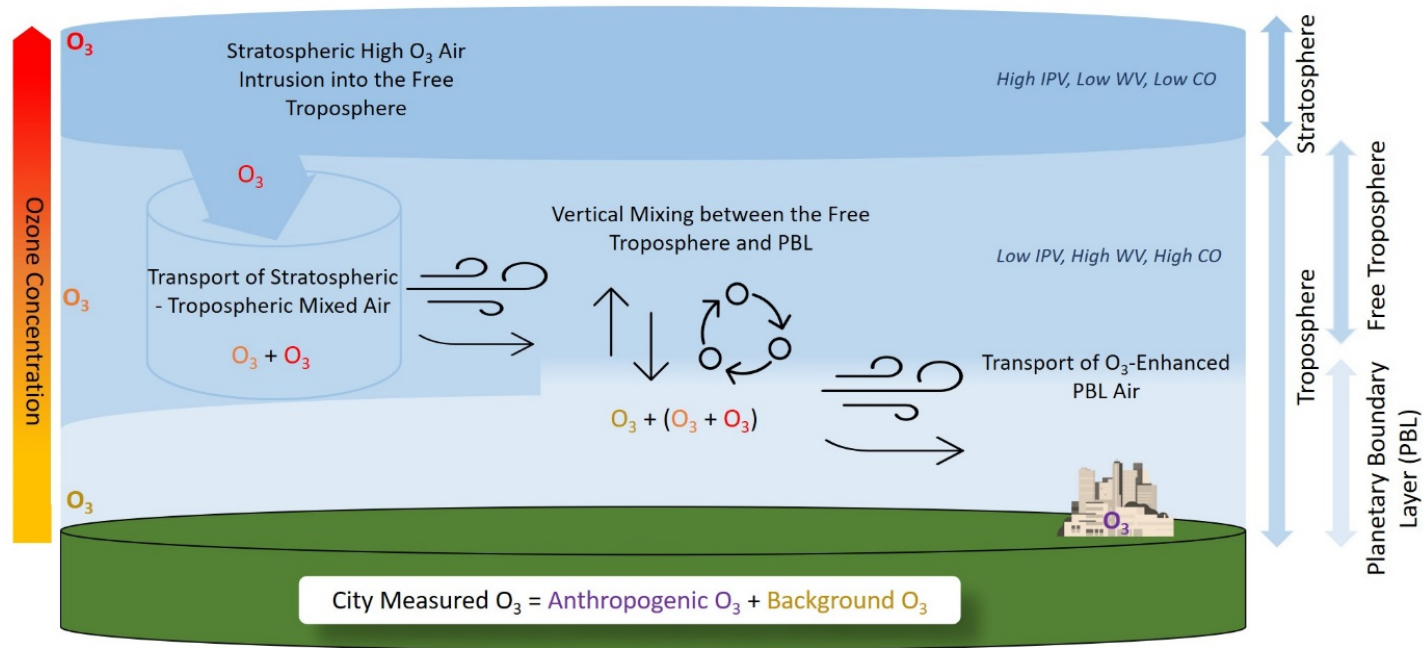


Figure 2-9. Stratospheric intrusion and transport example. Ozone concentration with height is shown on the left, and ozone is colored by each source region to illustrate transport. Tracers for stratospheric and tropospheric air are shown on the right, as well as labels for the different atmospheric layers.

Table 2-2. Transport mechanisms during a stratospheric ozone intrusion (as displayed in Figure 2-9) and evidence needed to determine transport.

Transport of Stratospheric Air	Evidence of Transport
Stratospheric High Ozone Air Intrusion into the Free Troposphere	Potential Vorticity Plots, High Ozone, Low Carbon Monoxide, Low Water Vapor
Transport of Stratospheric–Tropospheric Mixed Air	Upper-Level Meteorology Maps, HYSPLIT Modeling
Vertical Mixing between the Free Troposphere and PBL	Meteorology Maps, Skew-T Diagrams, PBL Height Maps
Transport of Ozone-Enhanced PBL Air	Surface-Level Meteorology Maps, HYSPLIT Modeling, Measured Ozone, Water Vapor, and NO _x

In this report, we describe evidence of a stratospheric intrusion upwind of Clark County influencing already high ozone levels expected under the non-event conceptual model for May 28, 2020. We detail evidence for (1) stratospheric intrusion into the free troposphere, (2) transport of ozone-rich air in the free troposphere, (3) vertical mixing between the free troposphere and PBL, and (4) mixing into the PBL and surface in Clark County. The meteorological conditions on May 28 (explained in Sections 2.3 and 3.3.3) suggest that local and regional ozone production from surface pollutant precursors should be relatively high (statistical [GAM] modeling also predicted MDA8 ozone concentrations to be in the mid-60s ppb on May 28). Thus, additional ozone entrained into the PBL from the stratosphere could increase surface concentrations over the 70 ppb NAAQS standard. The key differences between the observed SOI event-related concentration(s) and a typical non-SOI event ozone exceedance are detailed in Section 3.1.

Back trajectories from Clark County (Section 3.3.1) demonstrate that air was transported from the free troposphere over Idaho, Utah, Oregon, and Washington. We identified this source region for a possible stratospheric intrusion based on evidence for the exchange of stratospheric and tropospheric air. Specifically, there is evidence for this exchange based on IPV, water vapor mass mixing ratio at 350 hPa pressure level, enhanced ozone, and depleted CO levels in the upper troposphere. Values of water vapor below 0.3 g/kg, CO at or below 100 ppb, and ozone concentrations greater than 40–60 ppb in the mid-troposphere, can be indicative of stratospheric influence. IPV is a proxy for atmospheric rotation and is an important indicator for detecting stratospheric intrusion events. Stratospheric air has values of greater than 1 potential vorticity unit (PVU), which are much greater than the IPV of tropospheric air; values remain above 1 even after stratospheric air enters the troposphere. In the source region on May 25 at 6:00 UTC, we see stratospheric air in the upper troposphere with modeled IPV greater than 1 and water vapor mixing ratio less than 0.3 g/kg (Section 3.2.2). High modeled ozone and low modeled CO concentrations are

seen in the source region near the tropopause at this same time and location (Section 3.2.2). The combination of high IPV and ozone concentrations, as well as low water vapor and CO concentrations, provides evidence for a stratospheric intrusion into the free troposphere over Idaho and Utah at ~200-300 hPa level at ~6:00 UTC on May 25, 2020.

Meteorological conditions promoted transport from the source region through the free troposphere to the mixed layer and surface at Clark County. Forward trajectories indicate air was transported from southern Idaho at elevated heights across Utah and eastern Nevada and intersected with the Clark County area at 1000-3000 m agl (Section 3.3.1). Radiosonde profiles (skew-T diagrams) in Salt Lake City, Utah along this transport path observed upper-level dry air layers (Section 3.3.2). Additionally, ozone vertical profile data from Boulder, CO provide evidence of enhanced ozone concentrations in the mid-troposphere during the same time period and from the same source region (Section 3.3.2). Upper level (500 hPa) and surface weather maps at 7:00 PST on May 25 through 28, 2020, (Section 3.3.3) indicate that source region air masses were transported southward along the western edge of an upper-level trough. Surface high pressure along the transport path north of Clark County promoted subsidence of free tropospheric air towards the deep mixed layers over the region (Section 3.3.2). On May 27 and 28, surface low pressure beneath the upper-level ridge over Clark County induced vertical mixing between the free troposphere and the planetary boundary layer. The skew-T diagram on May 28 at 16:00 PST shows the air temperature profile follows the dry adiabatic lapse rate, indicating a well-mixed, dry layer from the surface up to 550 hPa, corresponding to a mixing height of ~5 km. This deep, well-mixed layer over Clark County indicates the potential transport and mixing of ozone to the surface (Section 3.3.3).

The combination of a stratospheric intrusion source region—based on IPV, water vapor, ozone, and CO data—along with trajectories, upper-level and surface weather maps, radiosonde temperature profiles, and modeled mixing heights, provide evidence that the air mass over Clark County on May 28, 2020, had contributions from a region of enhanced upper tropospheric ozone of stratospheric origin. We cannot rule out contributions from enhanced local photochemical ozone production due to surface precursor emissions in Clark County or upwind. However, statistical GAM modeling results provide a way to estimate ozone enhancements from outside sources (e.g., an SOI) and show that there was a significant atypical enhancement of ozone concentrations on May 28 (i.e., MDA8 concentrations are predicted to be less than the NAAQS without outside sources). Further detailed meteorology, satellite imagery, and model simulation-based evidence are presented in detail in Section 3.

2.5 Analysis of COVID Restrictions on Ozone

Mobile emission sources decreased throughout the U.S. during the mobility restrictions for the COVID-19 pandemic beginning in mid-March 2020. Because decreases in NO_x emissions from these mobile sources could result in higher ozone concentrations, we evaluate the potential contribution and sensitivity of the COVID shutdown effects on ozone concentrations and MDA8 ozone on EE days.

Ozone production has non-linear dependence on precursor emissions of NO_x and VOCs and meteorological conditions. Changes in precursors also can shift photochemical regimes. Thus, the effects of COVID-induced NO_x emission changes on ozone are complex and uncertain (Kroll et al., 2020). Recent studies have found variable ozone responses during lockdowns across countries ranging from -2 to +10% (Venter et al., 2020). Parker et al. (2020) found spatially disparate effects of higher ozone concentrations downwind of Los Angeles and lower concentrations in the western Los Angeles Basin. To evaluate the potential influence of COVID shutdown precursor emission decreases on increases in MDA8 ozone, we compared May 2020 ozone to the historical climatology and compared the GAM residuals during May 2020 with those for the same historical record.

Based on 2017 Las Vegas emission inventories, on-road mobile sources comprise 40% of NO_x emissions, and total mobile (vehicle + aviation) emissions comprise 88% of total NO_x emissions for typical ozone season weekdays (Clark County Department of Environment and Sustainability, 2020). In contrast, only 11% of VOC emissions originate from on-road mobile sources. The effects of decreased mobility due to COVID restrictions has a significant effect on total NO_x emissions, but minimal effect on VOC emissions. To determine the time period for these effects, we compared 2020 daily traffic count data from the Nevada Department of Transportation with data from 2019 at 10 monitoring sites (two examples in [Figure 2-10](#)). On-road traffic activity was significantly reduced from mid-March through early-June 2020 in Clark County compared with 2019. Although aviation activity remained lower than pre-pandemic levels for a longer duration of 2020, commercial aviation represents only 12% of NO_x emissions in Clark County. Thus, the reduced aviation activity had a minimal influence on precursors available for ozone formation from mid-June 2020 onwards. Here we focus on May 2020, the first month of 2020 with EE days.

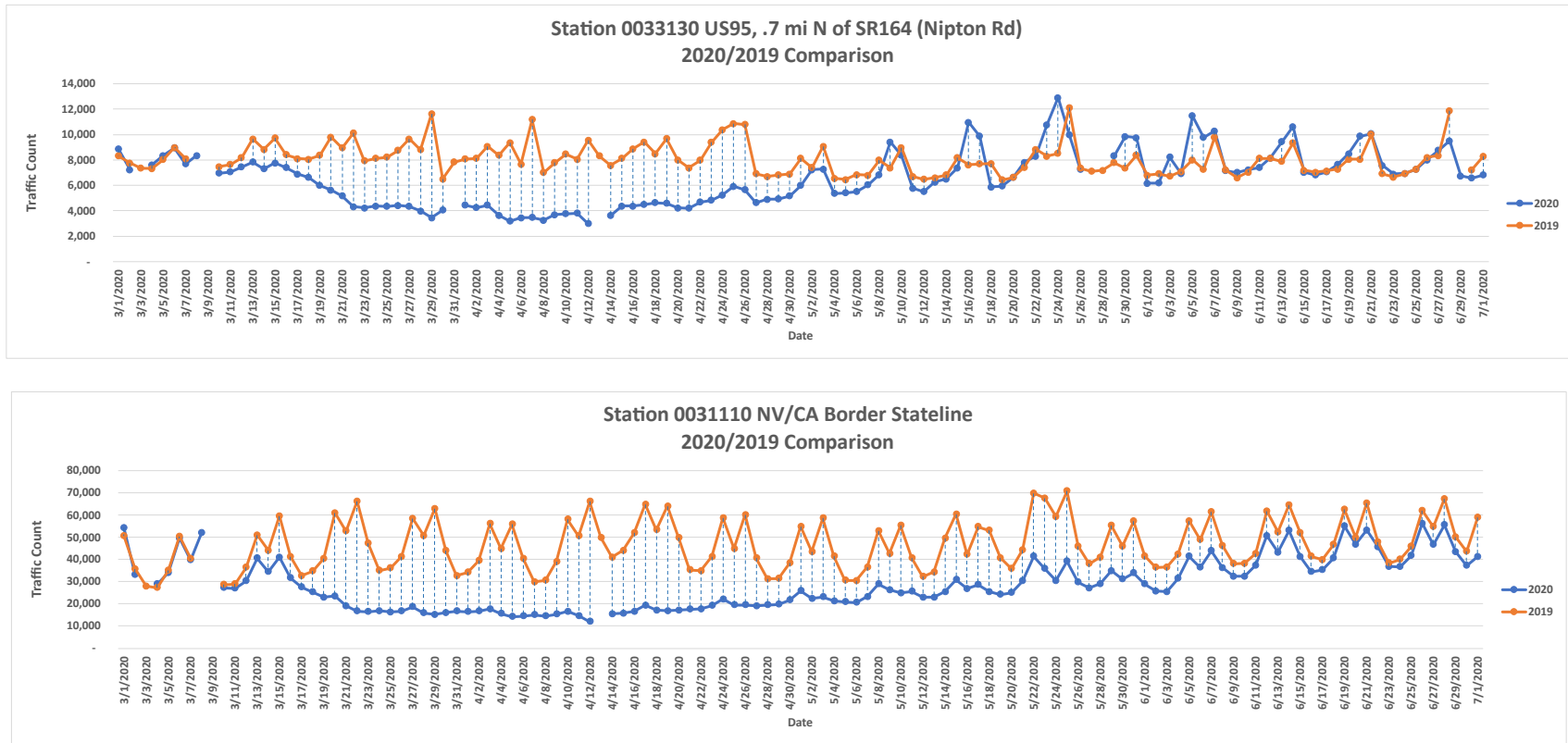


Figure 2-10. Time series of 2020 and 2019 traffic counts at two stations: US95 south of Las Vegas (top) and at the Nevada-California border west of Las Vegas (bottom). Data were provided by the Nevada Department of Transportation.

Two sub-analyses for the ozone comparison to historical climatology were performed. First, we compared the distribution of daily MDA8 ozone during May 2020 with values during each May in the previous five years. Across all EE sites, we found median 2020 MDA8 ozone was not statistically different than any of the previous five years. This is illustrated by the overlap in the 95th confidence intervals of the monthly medians of previous years and the monthly median for 2020 (Figure 2-11). Furthermore, monthly median MDA8 ozone during May 2020 was not particularly high (much less than 65 ppb) at all sites despite the EE days. This indicates that the EE day exceedances were extreme episodes that did not affect the monthly median. Thus, the observations do not suggest a month-long high ozone effect due to COVID emission precursor changes. Second, we compared the historical distribution of daily MDA8 ozone during May with the observations during May 2020 (Figure 2-12). Across all EE sites, MDA8 ozone on the exceedance days for a given site rank above the confidence interval of the historical daily median MDA8 ozone. Based on these sub-analyses, we conclude that although precursor NO_x emissions decreased during May 2020 due to COVID restrictions, MDA8 ozone concentrations were not statistically higher than previous years, and the EE days cannot be attributed to a consistent month-long increase in ozone concentrations due to the COVID shutdown.

To evaluate the GAM model residuals during the COVID shutdown period, Figure 3-66 provides a more in-depth look at April to May 2020, which were the most heavily affected months. The 95th confidence interval of the median GAM MDA8 residuals (shown by the notches in the box plots) overlap between 2020 and most other years (except 2015 and 2016). The May 2020 median residual with EE days (1.5 ppb) is lower than the typical GAM model uncertainty given by the range of confidence intervals for median residuals at comparable ozone concentrations (+2.9 to 5.3 ppb, Table 3-12). The median GAM residuals during May 2020 were within the typical GAM model error during the previous 5 years.

In summary, although mobile source precursor emissions of NO_x decreased during April and May 2020 due to COVID shutdown restrictions, we did not observe statistically higher ozone concentrations, nor a higher residual in the GAM model, during May 2020. We find consistent evidence across analyses that the EE day ozone concentrations cannot be attributed to an increase in ozone concentrations associated with COVID shutdown periods.

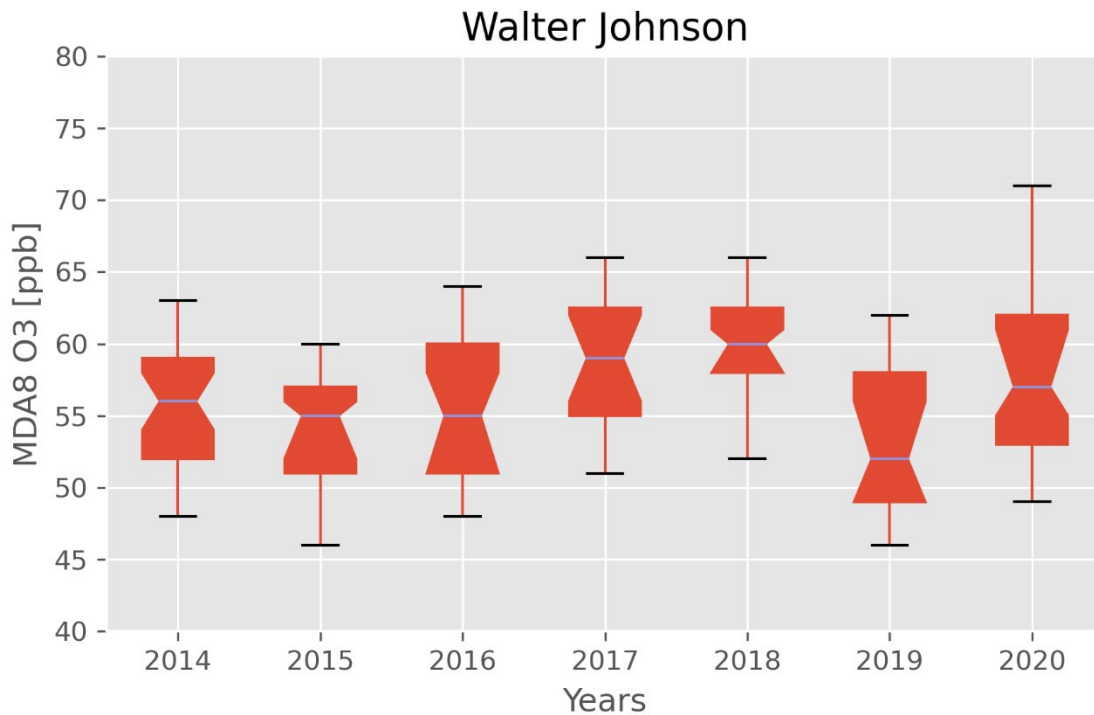
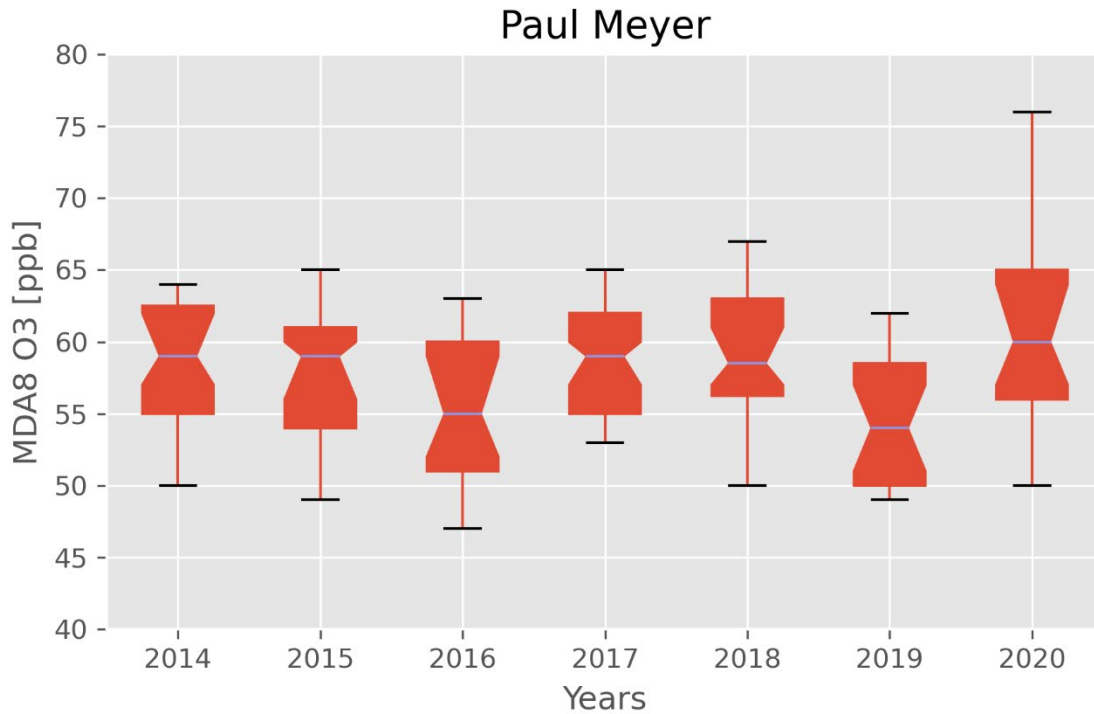


Figure 2-11. Annual May distributions of MDA8 ozone at sites with EEs during May 2020. Notches denote 95th confidence interval of the median, boxes are 25th, 50th, and 75th percentiles, and whiskers are 5th and 95th percentiles.

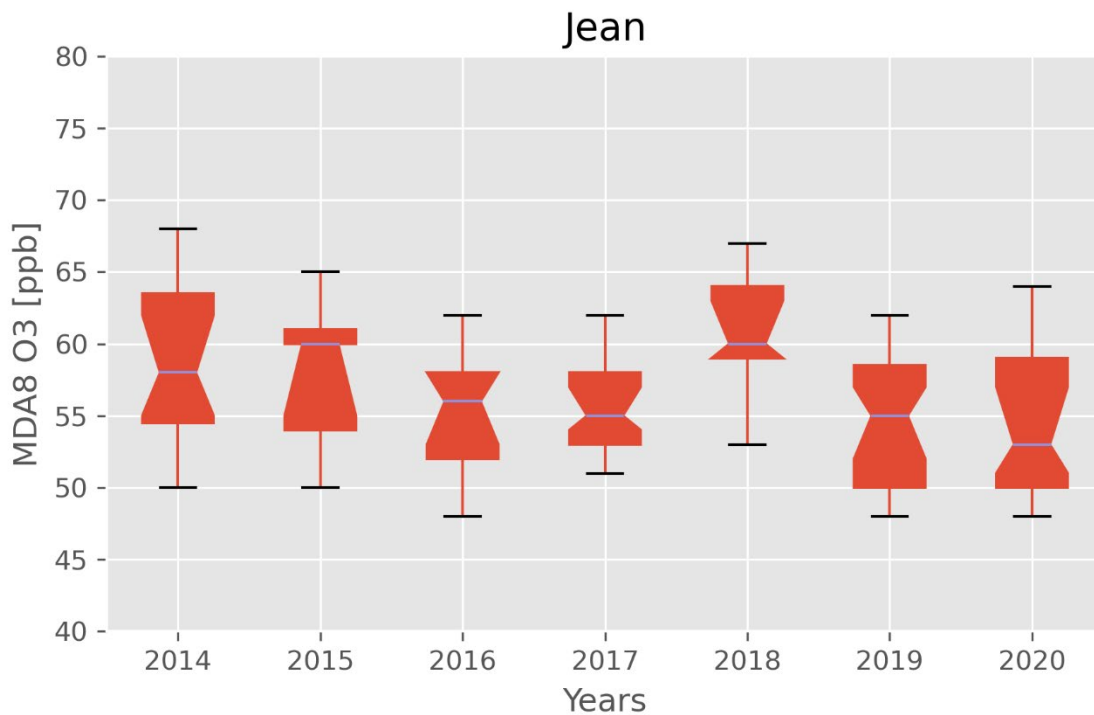
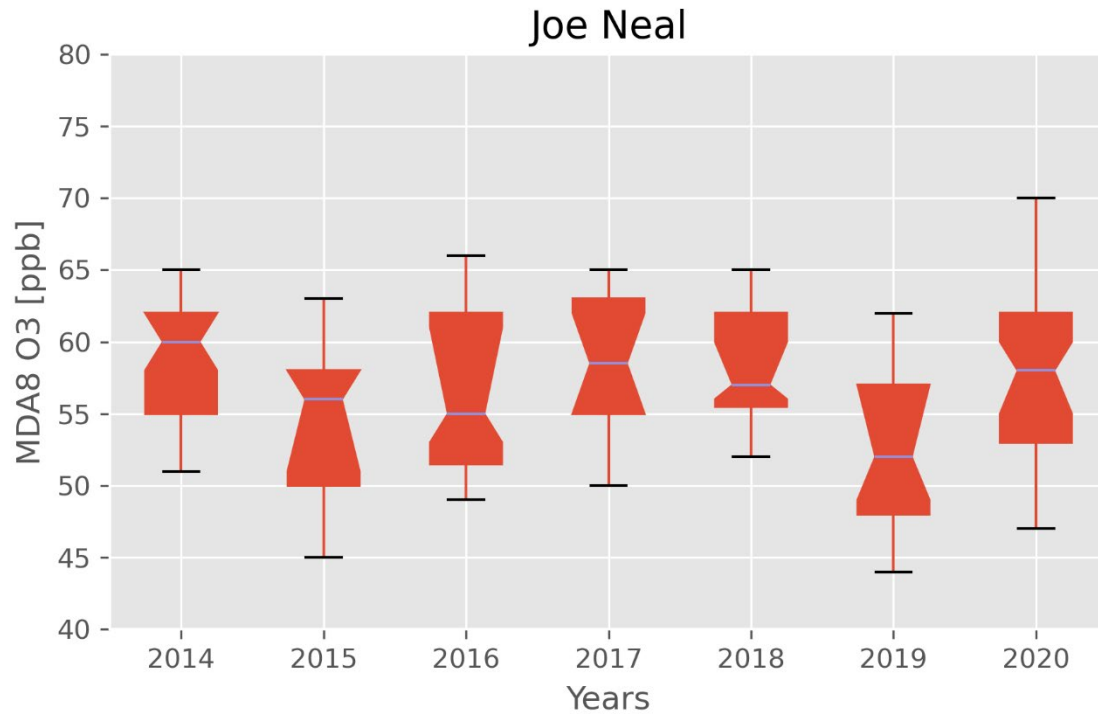


Figure 2-11 (cont.) Annual May distributions of MDA8 ozone at sites with EEs during May 2020. Notches denote 95th confidence interval of the median, boxes are 25th, 50th, and 75th percentiles, and whiskers are 5th and 95th percentiles.

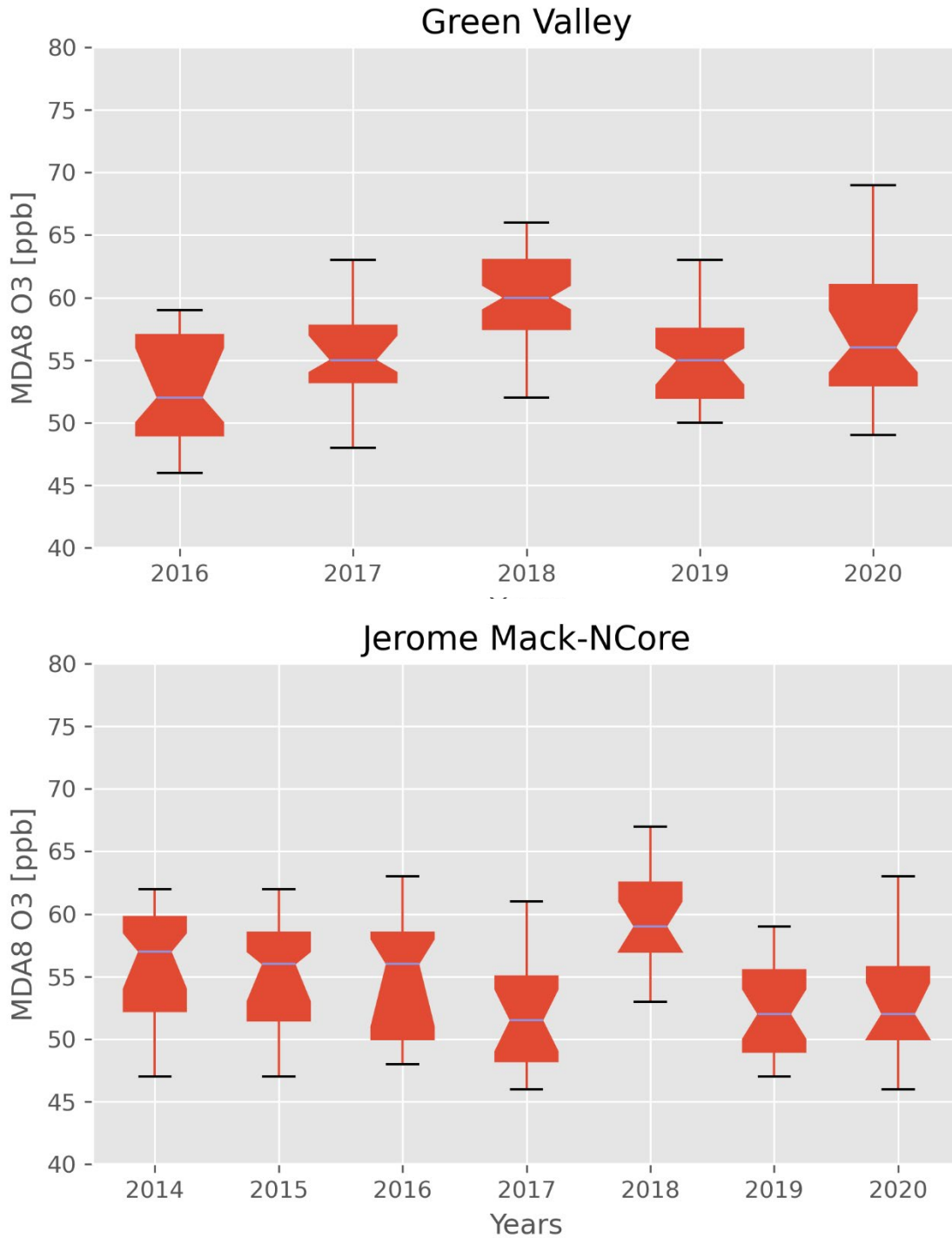


Figure 2-11 (cont.) Annual May distributions of MDA8 ozone at sites with EEs during May 2020. Notches denote 95th confidence interval of the median, boxes are 25th, 50th, and 75th percentiles, and whiskers are 5th and 95th percentiles.

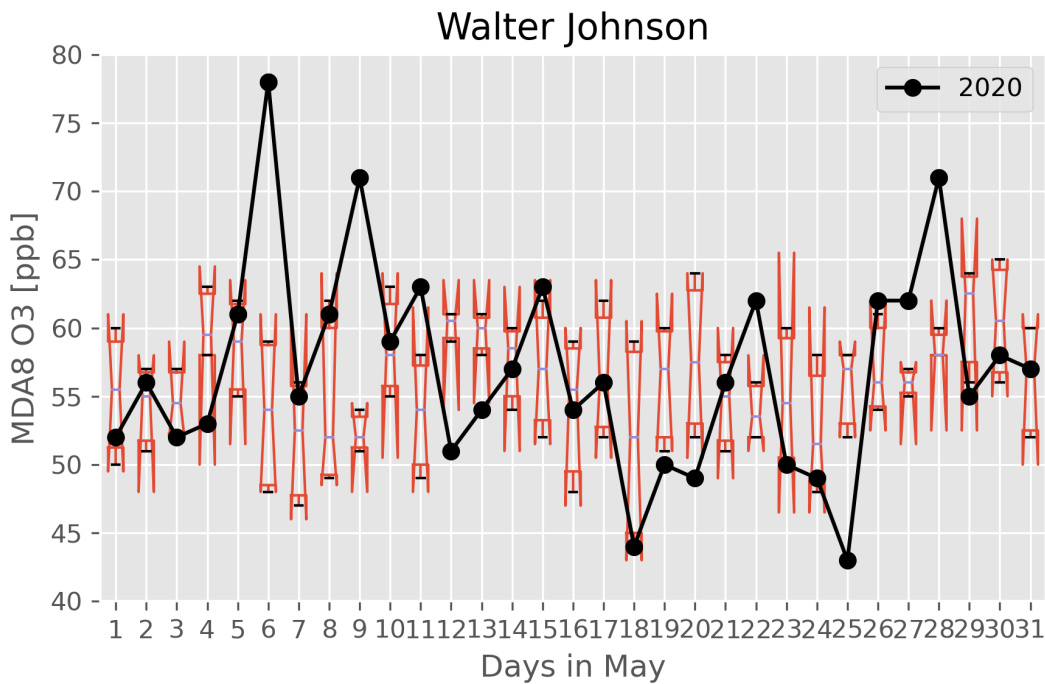
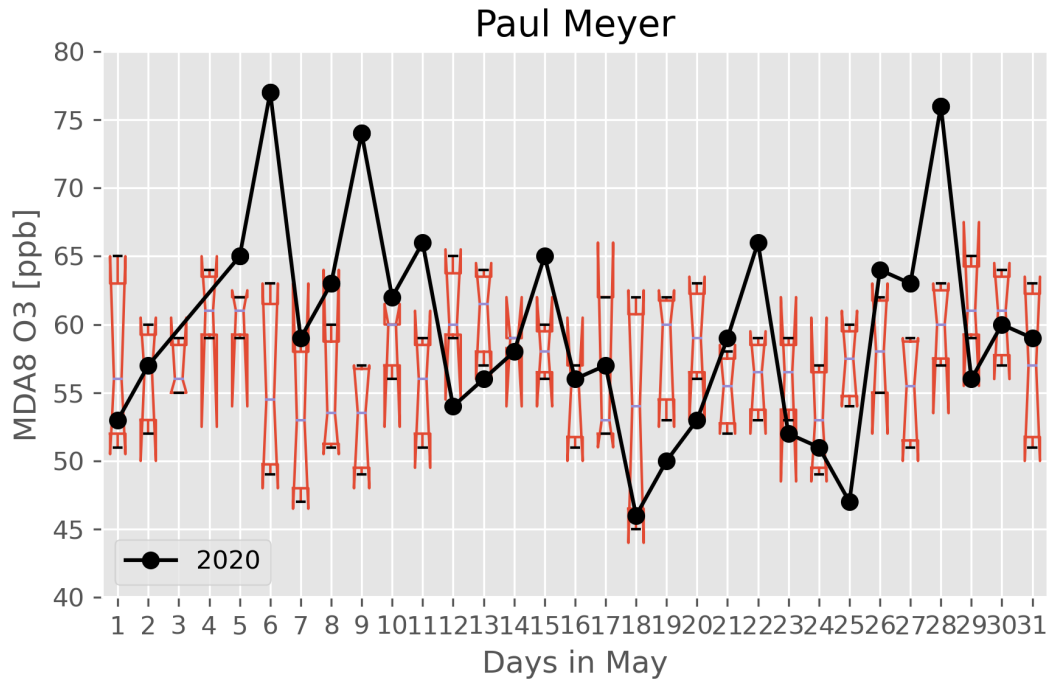


Figure 2-12. Daily time series of 2014-2019 MDA8 ozone distributions and 2020 MDA8 ozone at each site with proposed EE during May 2020. Notches denote 95th confidence interval of the median, boxes are 25th, 50th, and 75th percentiles, and whiskers are 5th and 95th percentile.

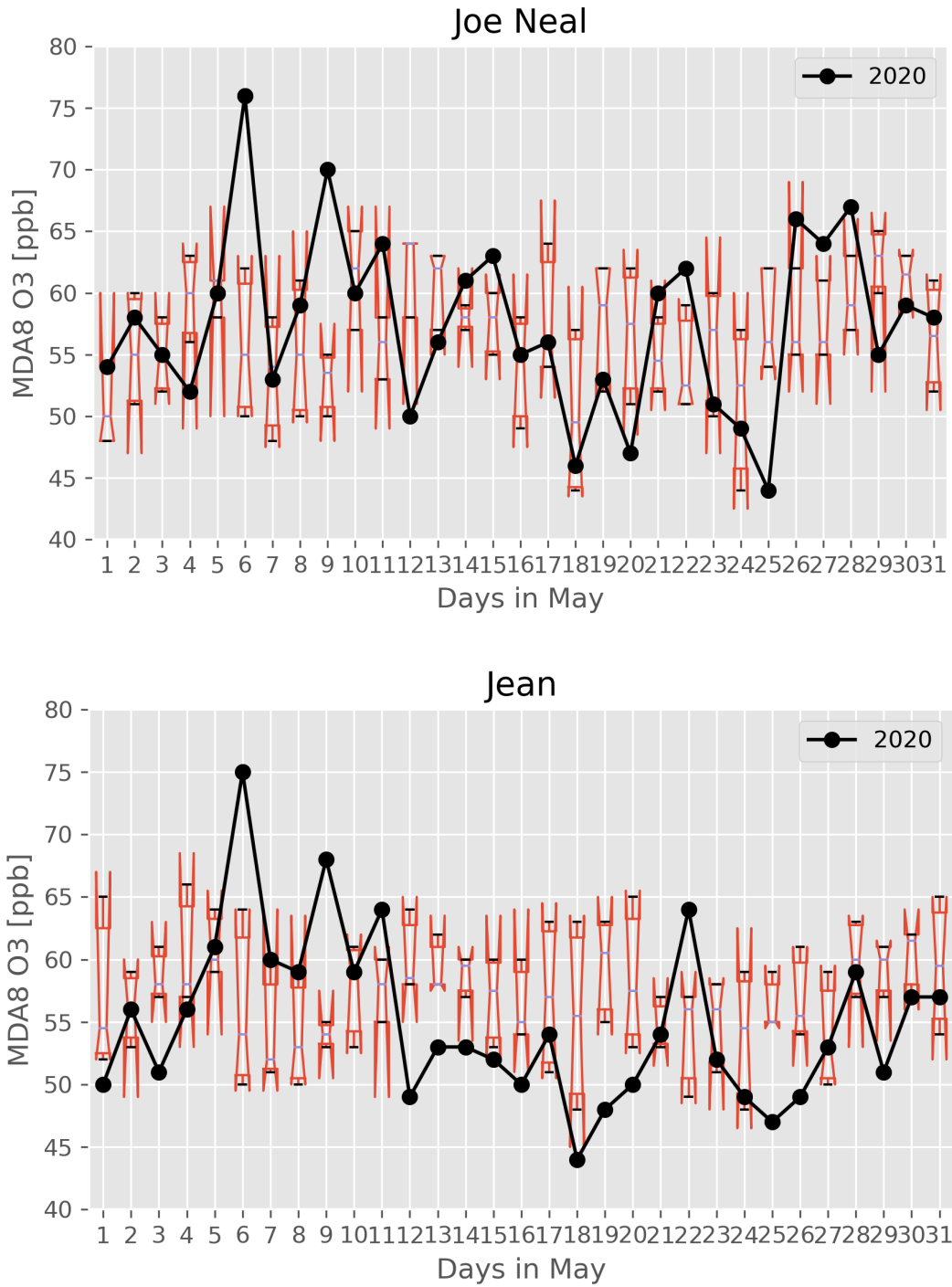


Figure 2-12 (cont.) Daily time series of 2014-2019 MDA8 ozone distributions and 2020 MDA8 ozone at each site with proposed EE during May 2020. Notches denote 95th confidence interval of the median, boxes are 25th, 50th, and 75th percentiles, and whiskers are 5th and 95th percentile.

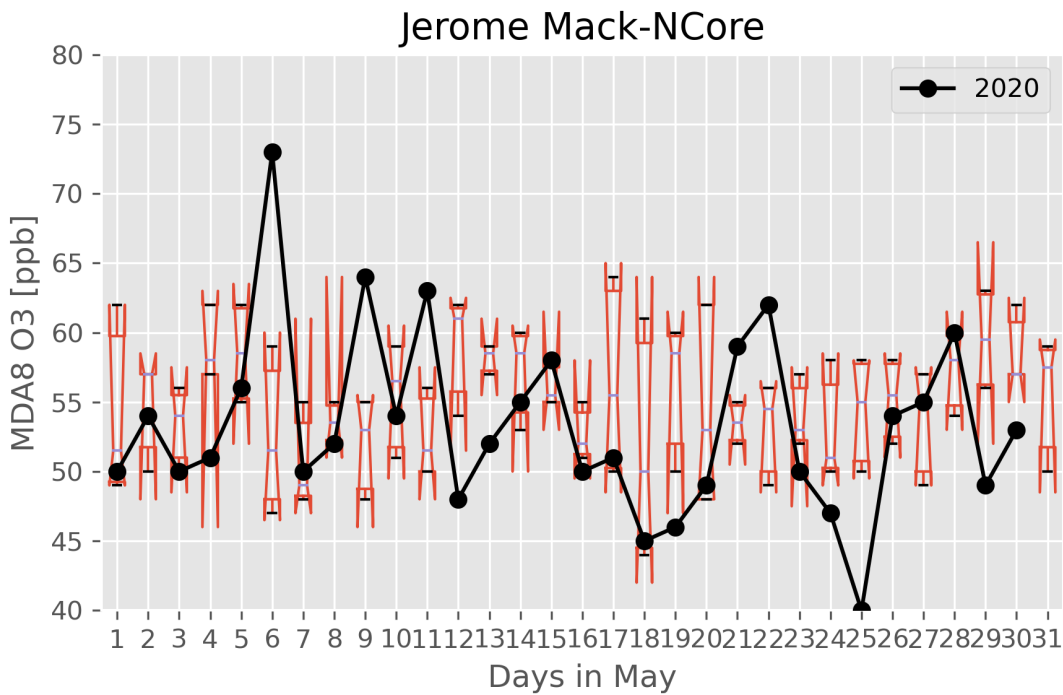
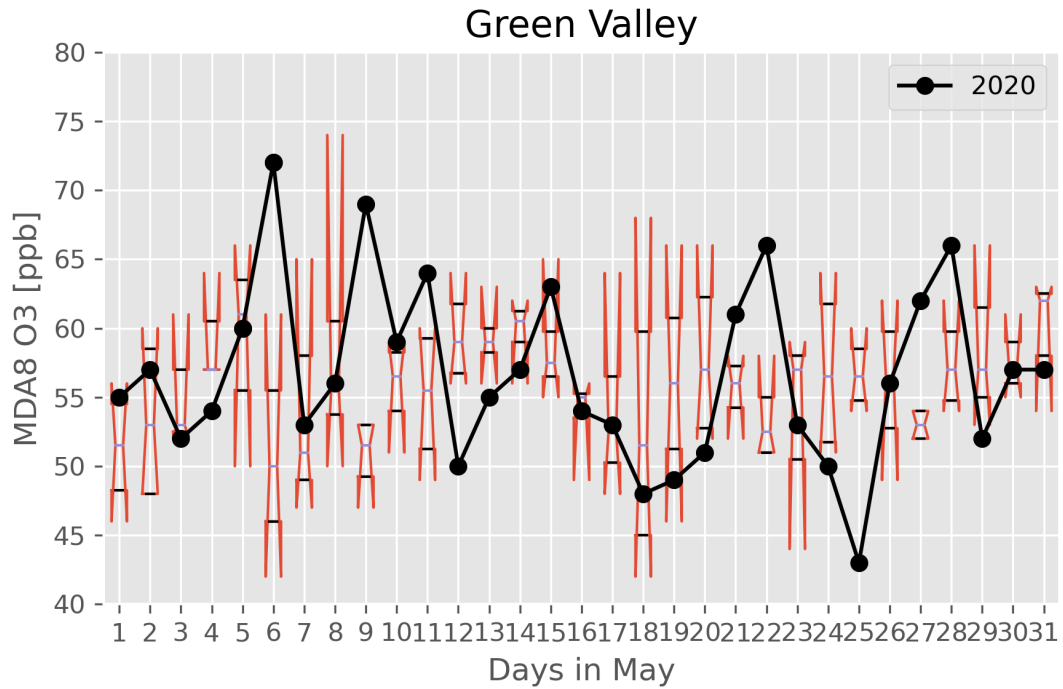


Figure 2-12 (cont.) Daily time series of 2014-2019 MDA8 ozone distributions and 2020 MDA8 ozone at each site with proposed EE during May 2020. Notches denote 95th confidence interval of the median, boxes are 25th, 50th, and 75th percentiles, and whiskers are 5th and 95th percentile.

3. Clear Causal Relationship Analyses

3.1 Comparison of Event Concentrations with Historical Concentrations

To address the Tier 1 EE criterion of comparison with historical ozone concentrations, we compared the May 28 EE ozone concentrations at each site with the 2020 ozone record, focusing mainly on the ozone season when highest ozone concentrations occur. **Figures 3-1 and 3-2** depict the 2020 daily maximum ozone record at each monitoring site, along with the 99th percentile over the previous six years and NAAQS criteria ozone concentrations. During 2020, May 28 ranks in the top 1% for daily maximum ozone concentration at the Paul Meyer monitoring site. For the Las Vegas Valley sites that were affected by the EE (the Paul Meyer and Walter Johnson sites), the May 28 EE was in the top 3% of MDA8 ozone concentrations in the past five years (**Table 3-1**). When compared with daily ozone rankings on May 28 over the six-year ozone record (Figures 2-5 and 2-6), the 2020 rankings indicate that May 28, 2020, was an extreme ozone event.

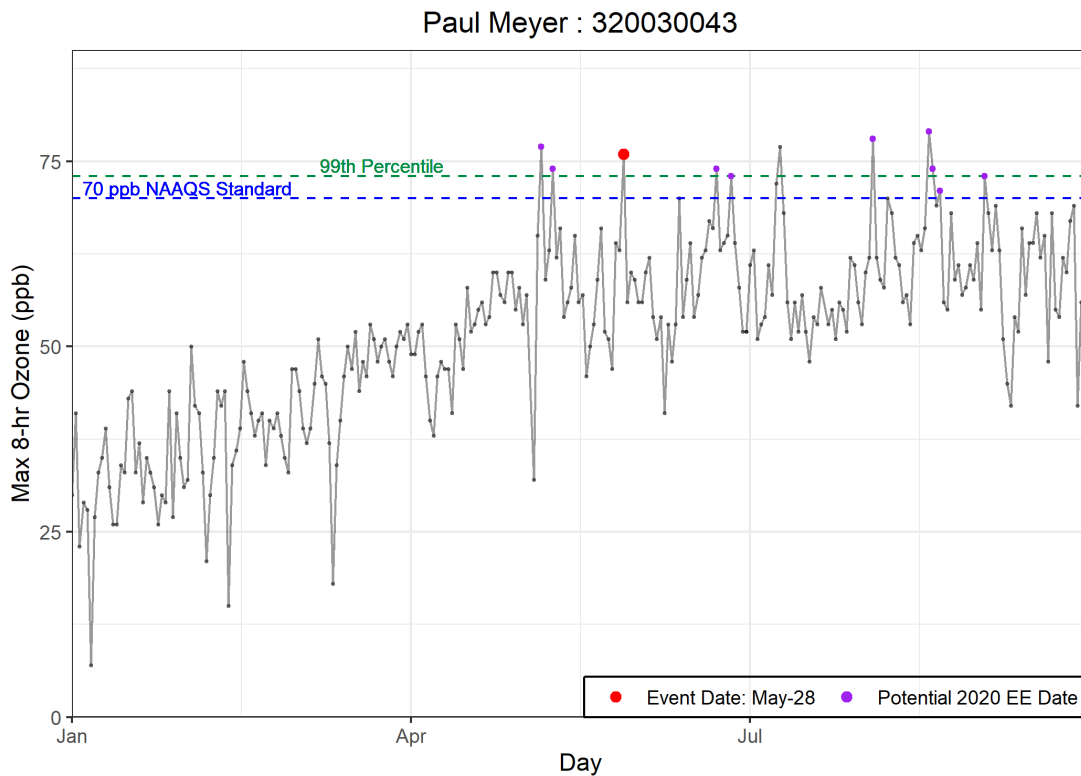


Figure 3-1. Time series of 2020 MDA8 ozone concentrations from the Paul Meyer site. May 28, 2020, is shown in red.

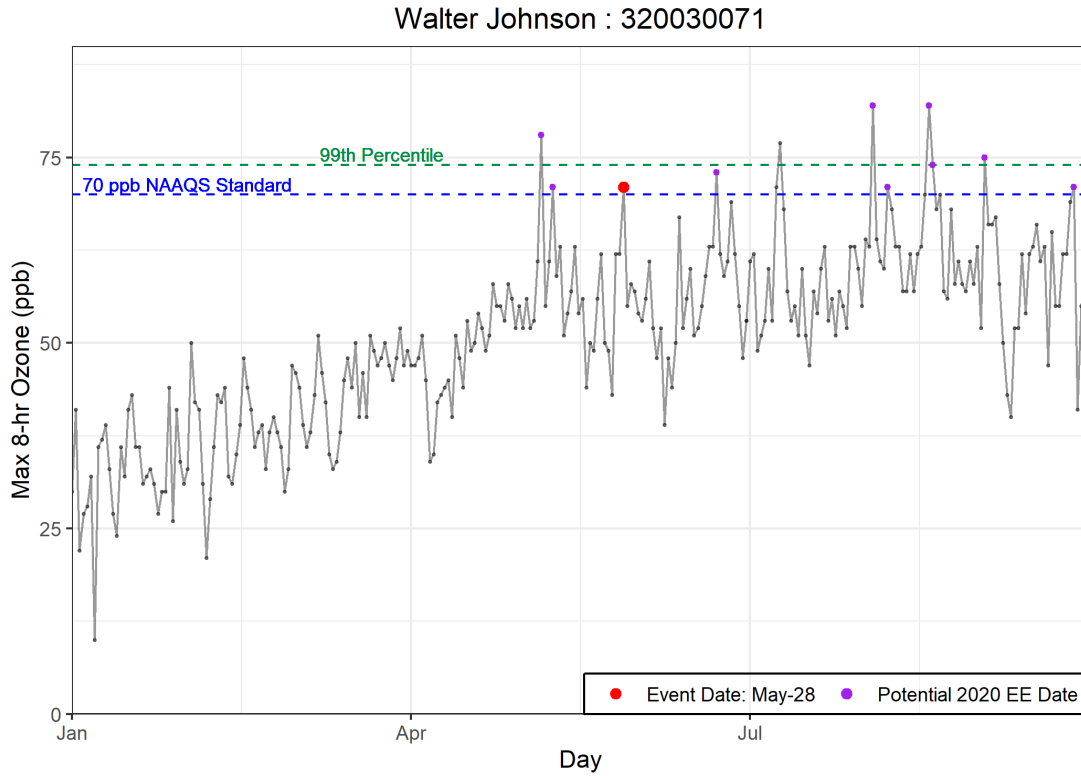


Figure 3-2. Time series of 2020 MDA8 ozone concentrations from the Walter Johnson site. May 28, 2020, is shown in red.

Table 3-1. Six-year percentile ozone. The May 28 EE ozone concentration at each site is calculated as a percentile of the last five years with and without other 2018 and 2020 EEs included in the historical record.

AQS Site Code	Site Name	6-Year Percentile	6-Year Percentile w/o EE Dates
320030071	Walter Johnson	97.9	98.7
320030043	Paul Meyer	99.8	100.

The May 28, 2020, ozone exceedance occurred during the typical ozone season, but MDA8 ozone concentrations on May 28 were the second highest compared with daily ozone concentrations excluding potential EE days (Figures 3-1 and 3-2). **Table 3-2** provides historical ozone season monitoring site statistics for each EE-affected site on May 28. The statistics shown are for May through September 2015-2019; we do not exclude the dates with proposed 2018 EE ozone concentrations. The MDA8 ozone concentrations on May 28 were more than 10 ppb above the mean and median ozone concentrations for the historical ozone season at all EE-affected sites. Additionally, MDA8 ozone concentrations were 3 and 8 ppb above the 95th percentile of non-event day historical ozone concentrations at EE-affected sites. Because May 28 is during the normal ozone

season, but MDA8 ozone concentrations at both EE-affected sites could not be clearly distinguished from the 95th percentile ozone concentration during the non-event historical ozone season, further analysis (Tier 2) is required.

To address the Tier 2 EE criterion to determine whether the May 28, 2020, exceedance event is exceptional, we compare event ozone concentrations with non-event concentrations via percentile and rank-order analysis. Table 3-1 shows May 28 concentrations as a percentile in comparison with the last six years of data (with and without the other proposed 2018 and 2020 EE days). For all monitoring sites that show a NAAQS standard exceedance on May 28, the exceedances are greater than the 97th percentile when compared to the last six years of data, even with all other proposed 2018 and 2020 EE days included. Without the other EE days included, the percentiles are slightly higher (>98th percentile). To confirm that the calculated percentiles are not biased by non-ozone season data, [Table 3-3](#) shows the May 28 percentile ranks for all monitoring sites around Clark County in comparison with the last six years of ozone season (May to September) data. The May 28 ozone concentration percentile over the last six ozone seasons (with all proposed 2018 and 2020 EE days included) ranks above the 95th percentile at all EE-affected sites. When the other possible EE days are excluded, the percentile rank of ozone season concentrations increases to >97th percentile. Although not all of the sites ranked above the 99th percentile of ozone season concentrations on May 28, this analysis confirms that the May 28 EE included unusually high concentrations of ozone when compared with ozone concentrations across the last six years and the last six ozone seasons.

Table 3-2. Ozone season (May-September) non-event comparison. May 28, 2020, MDA8 ozone concentrations for each affected site are shown in the top row. Five-year (2015-2019) average MDA8 ozone statistics for May-September are shown for each affected site around Clark County to compare with the event ozone concentrations.

	Paul Meyer 320030043	Walter Johnson 320030071
May. 28	76	71
Mean	59	58
Median	59	58
Mode	59	62
St. Dev	6	6
Minimum	44	43
95 %ile	68	68
99 %ile	71	71
Maximum	76	72
Range	32	29
Count	96	96

Table 3-3. Six-year ozone-season percentile ozone. The May 28 EE ozone concentration at each site is calculated as a percentile of the last five years' ozone season (May-September) with and without other 2018 and 2020 EEs included in the historical record.

AQS Site Code	Site Name	6-Year Percentile	6-Year Percentile w/o EE Dates
320030071	Walter Johnson	95.2	97.1
320030043	Paul Meyer	99.5	99.9

We also compared the rank-ordered concentrations at each site for 2020. As shown in Figures 2-4 and 2-5, ozone concentrations across 2020 were not atypically low, which might bias our rank-ordered analysis for May 28. **Tables 3-4 and 3-5** show the rank-ordered ozone concentrations for 2018 through 2020 and the design values for 2020, with the proposed 2018 and 2020 EEs included. Based on the concentration rankings, May 28 shows the fifth highest ozone concentration of 2020 at the Paul Meyer monitoring site with the inclusion of all other proposed EE events. Without the inclusion of other proposed EE events, May 28 shows the second highest ozone concentration during 2020 at both Paul Meyer and Walter Johnson.

Table 3-4. Site-specific ozone design values for the Paul Meyer monitoring site. The top five highest ozone concentrations for 2018-2020 at Paul Meyer are shown, and proposed EE days in 2018 and 2020 are included.

Paul Meyer Rank	2018	2019	2020
Highest	79	74	79
Second Highest	76	72	78
Third Highest	75	70	77
Fourth Highest	75	69	77
Fifth Highest	74	69	76
Design Value		73	

Table 3-5. Site-specific ozone design values for the Walter Johnson monitoring site. The top five highest ozone concentrations for 2018-2020 at Walter Johnson are shown, and proposed EE days in 2018 and 2020 are included.

Walter Johnson Rank	2018	2019	2020
Highest	79	77	82
Second Highest	77	69	82
Third Highest	77	69	78
Fourth Highest	76	68	77
Fifth Highest	76	68	75
Design Value		73	

For further comparison with non-event ozone concentrations, [Table 3-6](#) shows five-year (2015-2019, proposed 2018 EE events included) MDA8 ozone statistics for one week before and after May 28. This two-week window analysis shows that each affected monitoring site had MDA8 ozone concentrations on May 28 that were greater than 10 ppb above the mean or median, and 3 and 8 ppb above the 95th percentile of ozone concentrations in the last five years.

The percentile, rank-ordered analyses and the two-week window analysis indicate that all affected monitoring sites on May 28 showed atypically high ozone concentrations compared with non-event concentrations. This conclusion supports Tier 1 and 2 criteria, suggesting that May 28 was an EE in Clark County.

Table 3-6. Two-week non-event comparison. May 28, 2020, MDA8 ozone concentrations for each affected site are shown in the top row. Five-year (2015-2019) average MDA8 ozone statistics for May 21 through June 4 are shown for each affected site around Clark County to compare with the event ozone concentrations.

	Paul Meyer 320030043	Walter Johnson 320030071
May. 28	76	71
Mean	59	58
Median	59	58
Mode	59	62
St. Dev	6	6
Minimum	44	43
95 %ile	68	68
99 %ile	71	71
Maximum	76	72
Range	32	29
Count	96	96

3.2 Evidence of Stratospheric-Tropospheric Exchange

3.2.1 Satellite imagery

Satellite retrievals can help identify signatures of a stratospheric intrusion event, such as ozone-rich and extremely dry air. We examined maps of true color visible imagery from the Moderate Resolution Imaging Spectroradiometer (MODIS) instruments onboard the Terra satellite, water vapor imagery from Geostationary Operational Environmental Satellite (GOES)-East, and total column ozone from the OMPS Nadir-Mapper (NM) instrument onboard the Suomi NPP satellite and from Modern-Era Retrospective analysis for Research and Applications, Version 2 (MERRA-2). These maps provide evidence to support the transport of ozone-rich stratospheric air over southern Idaho on May 25 from 00:00 UTC to 12:00 UTC to Clark County, Nevada on May 28.

Visible satellite imagery can be used to identify areas of very dry and cloudless air that are indicative of a stratospheric intrusion event. True color visible satellite imagery from the MODIS instrument onboard the Terra satellite shows a lack of extensive cloud cover over Clark County from May 25 to May 28 (Figures 3-3 through 3-6). On May 25, southern Idaho was almost entirely devoid of cloud

cover, which is a characteristic of dry stratospheric air. By May 28, most of the southwestern United States, including Clark County, was almost completely clear.

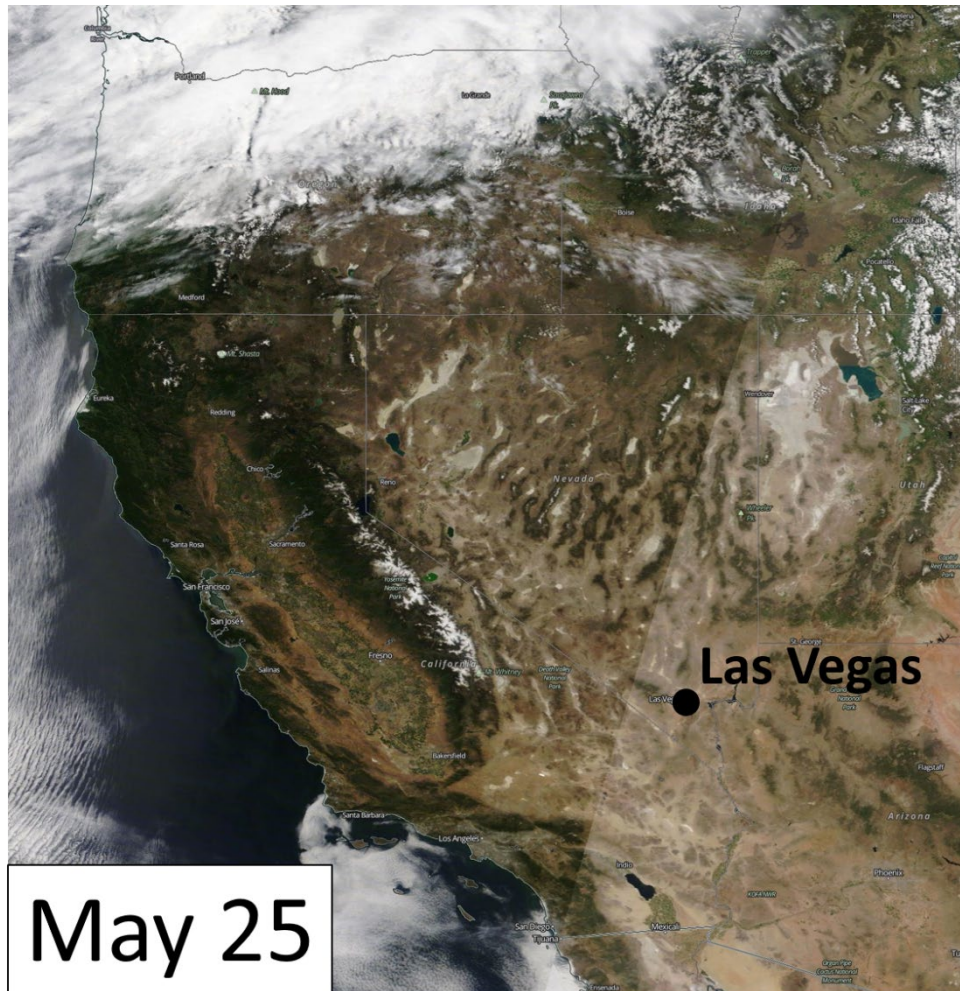


Figure 3-3. Visible Satellite Imagery from over the area including southern Idaho, California, and Nevada on May 25, 2020. Source: NASA Worldview

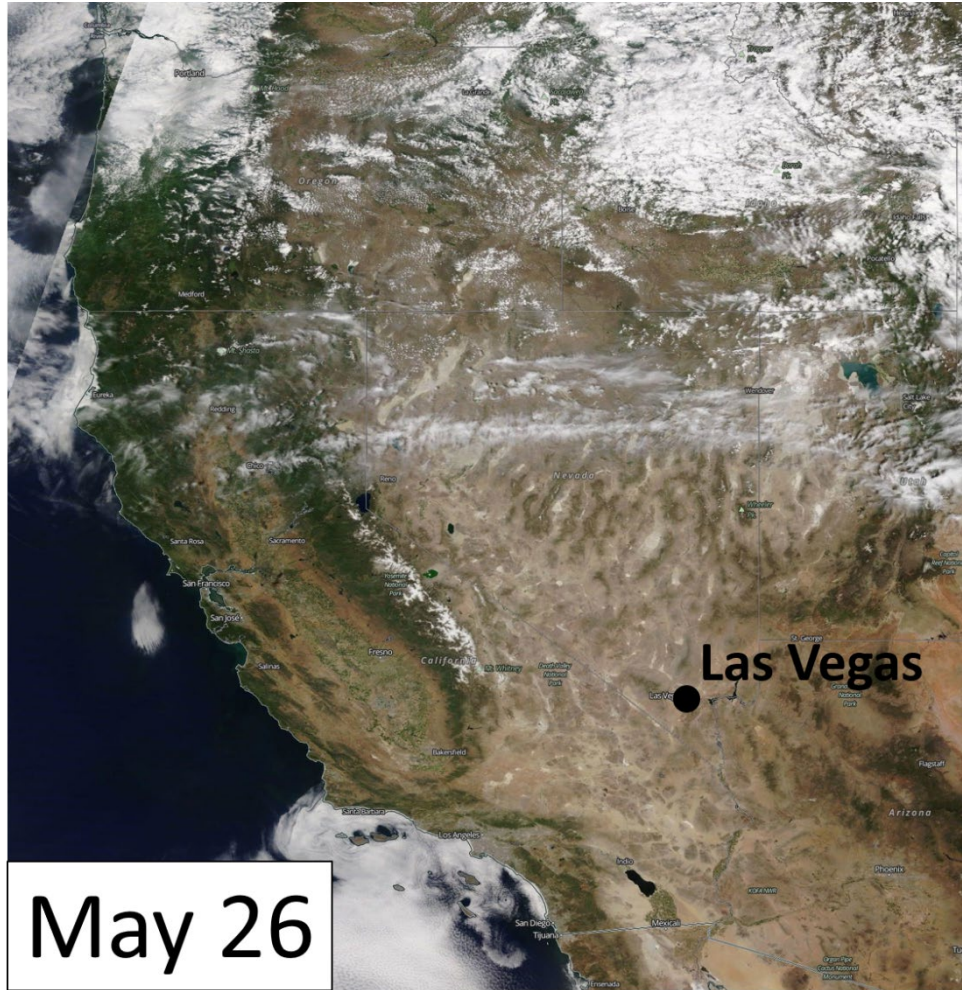


Figure 3-4. Visible Satellite Imagery from over the area including southern Idaho, California, and Nevada on May 26, 2020. Source: NASA Worldview



Figure 3-5. Visible Satellite Imagery from over the area including southern Idaho, California, and Nevada on May 27, 2020. Source: NASA Worldview



Figure 3-6. Visible Satellite Imagery from over the area including southern Idaho, California, and Nevada on May 28, 2020. Source: NASA Worldview

The stratosphere’s lack of water vapor relative to that of the troposphere is a key characteristic when tracing stratospheric air. Because stratospheric intrusion events will lead to the drying of tropospheric air, satellite imagery of total column water vapor can be used to highlight areas of dry and potentially stratospheric air. Water vapor imagery from the GOES-East satellite shows an area of dry air—as indicated by increasingly darker shades of brown—near the area of potential stratospheric intrusion on May 25 at 15:50 UTC (**Figures 3-7 through 3-10**). The maps show that by May 29 at 00:20 UTC, the atmosphere to the south of Clark County was somewhat dry. The maps are consistent with Figures 3-3 through 3-6, which also show an extensive area of dry air, relatively low cloud cover, and clear atmosphere over southern Idaho at the approximate time of stratospheric intrusion.

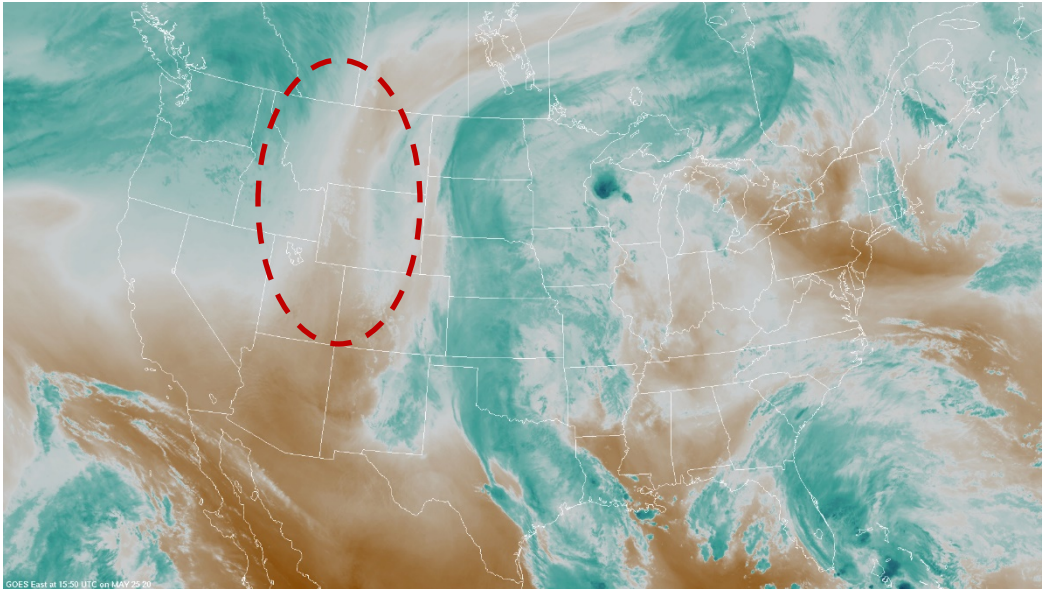


Figure 3-7. Water vapor imagery from the GOES-East Satellite on May 25, 2020, at 15:50 UTC. Bright blue and white areas indicate the presence of high water vapor or moisture content, whereas dark orange and brown areas indicate little or no moisture present.

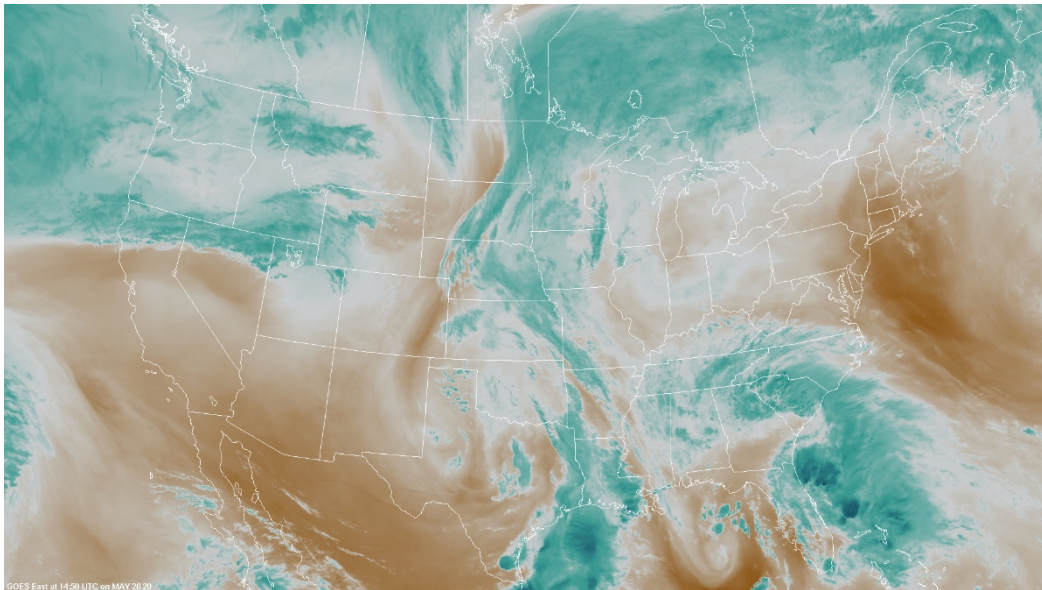


Figure 3-8. Water vapor imagery from the GOES-East Satellite on May 26, 2020, at 14:50 UTC. Bright blue and white areas indicate the presence of high water vapor or moisture content, whereas dark orange and brown areas indicate little or no moisture present.

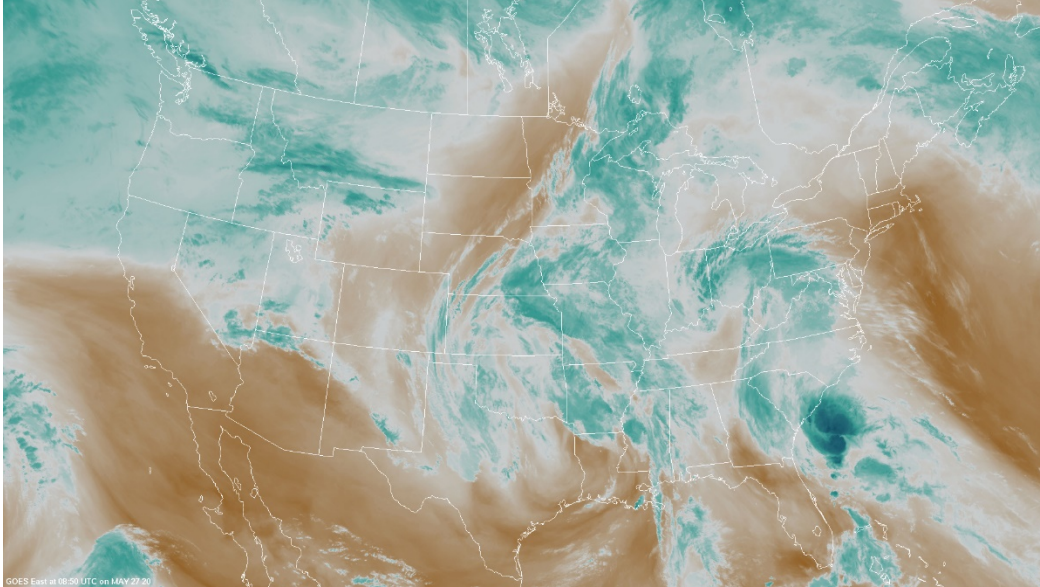


Figure 3-9. Water vapor imagery from the GOES-East Satellite on May 27, 2020, at 08:50 UTC. Bright blue and white areas indicate the presence of high water vapor or moisture content, whereas dark orange and brown areas indicate little or no moisture present.

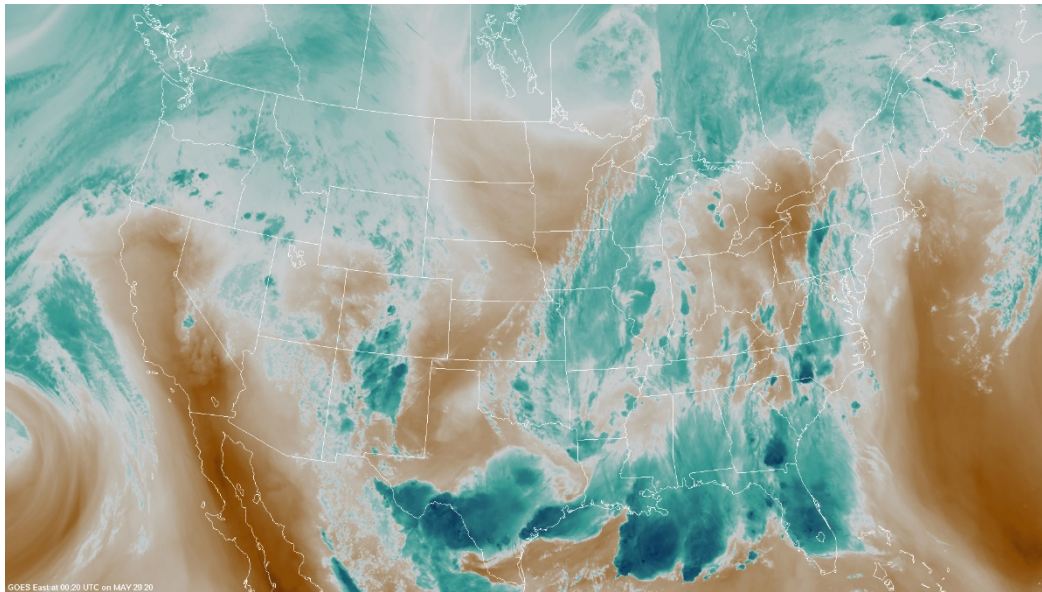


Figure 3-10. Water vapor imagery from the GOES-East Satellite on May 29, 2020, at 00:20 UTC. Bright blue and white areas indicate the presence of high water vapor or moisture content, whereas dark orange and brown areas indicate little or no moisture present.

Satellite retrievals of total column ozone are useful in identifying areas with high ozone concentrations that may be associated with stratospheric intrusion events. Maps of total column ozone from OMPS from May 24 to May 28 are shown in [Figure 3-11](#). On May 24, total column ozone

concentrations were enhanced—shown by shades of yellow and orange—over Montana, Idaho, and Utah from approximately 340 Dobson Units (DU) to 355 DU. In local standard time, the afternoon of May 24 (when the OMPS satellite images were taken) corresponds with the early morning of May 25 in UTC time. This means that the May 24 image in Figure 3-11 matches the May 25 image in Figure 3-7. Total column ozone in Montana and Idaho remained slightly elevated until May 28 (the event date). Additionally, we examined maps of total column ozone from MERRA-2 for May 25 at 00:60 UTC and 15:00 UTC (Figure 3-12 through 3-13). The maps show that total column ozone was elevated over the Mountain West region of the United States. This band of high ozone was transported eastward from 06:00 UTC to 15:00 UTC. These maps provide evidence that total column ozone was elevated in the area of the possible stratospheric intrusion.

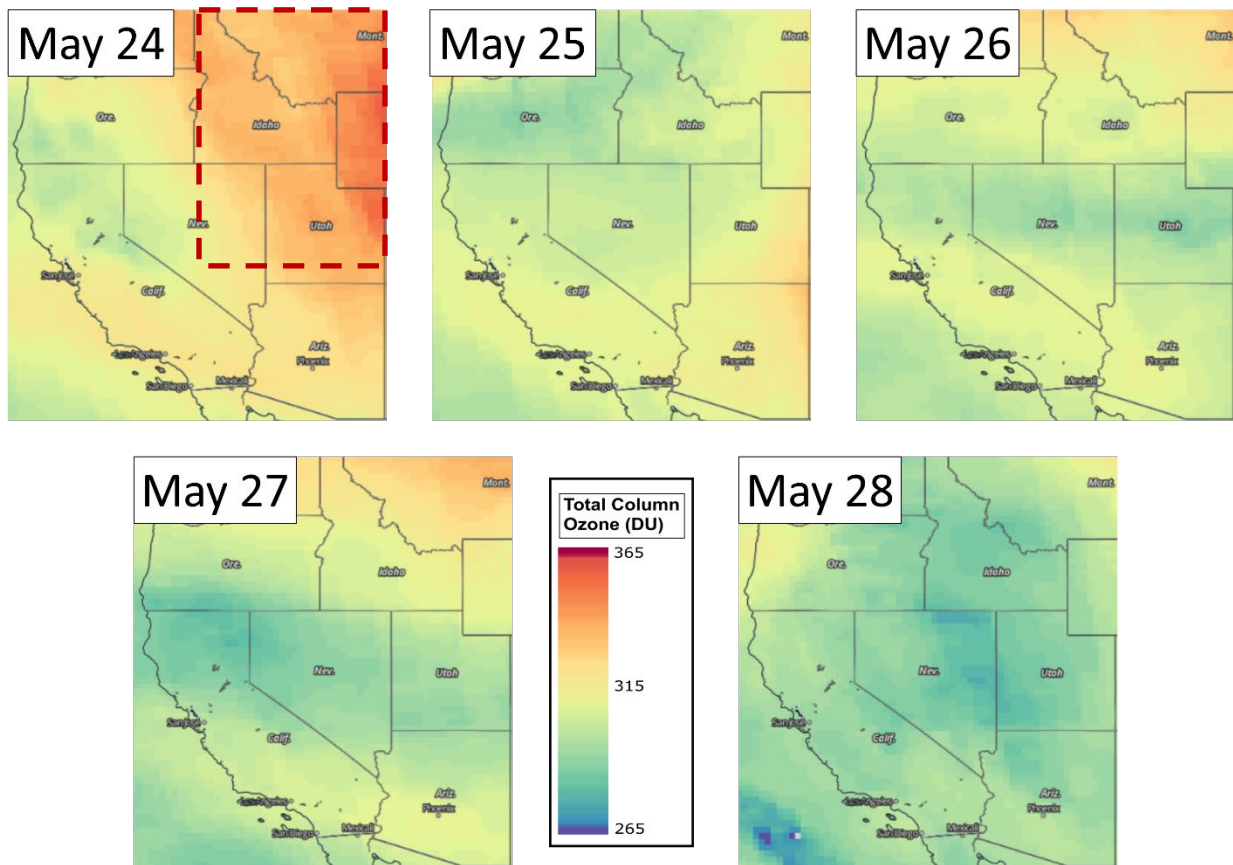
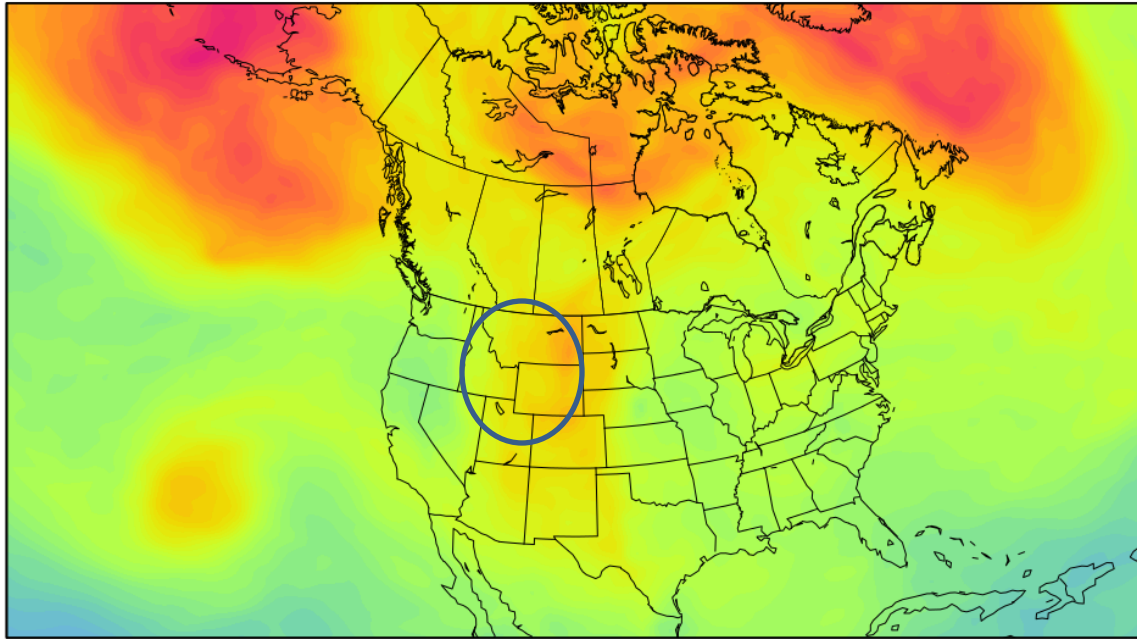


Figure 3-11. Maps of satellite-estimated total column ozone from May 24 to May 28 from the OMPS instrument on the Suomi NPP satellite. Data source: NASA Worldview.



Modern-Era Retrospective Analysis for Research and Applications, Version 2 (MERRA-2)

Total Ozone [Dobson Units]



Mon 05/25/2020 06Z

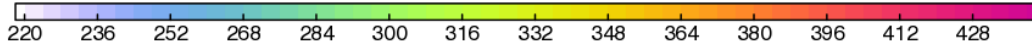


Figure 3-12. Maps of satellite-estimated total column ozone from May 25 at 06:00 UTC from Modern-Era Retrospective analysis for Research and Applications, Version 2 (MERRA-2). The approximate area of the SOI is shown by the circle.



Modern-Era Retrospective Analysis for Research and Applications, Version 2 (MERRA-2)

Total Ozone [Dobson Units]

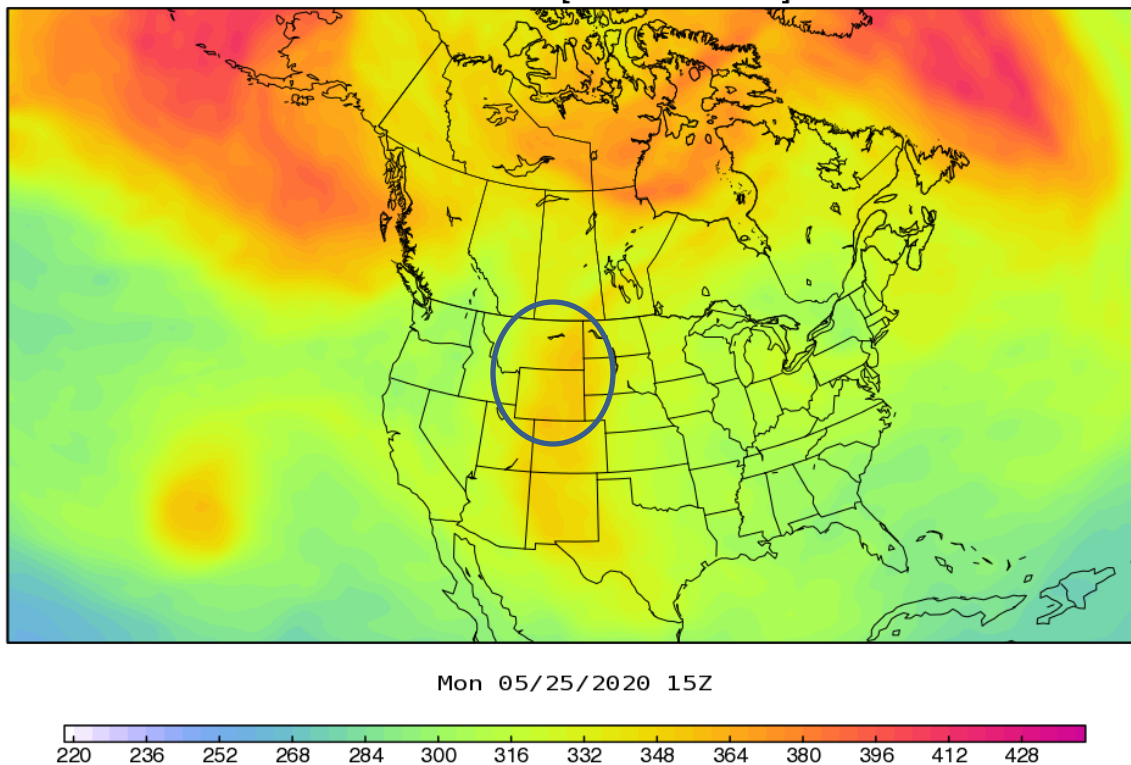


Figure 3-13. Maps of satellite-estimated total column ozone from May 25 at 15:00 UTC from Modern-Era Retrospective analysis for Research and Applications, Version 2 (MERRA-2).

3.2.2 Model Results

Modeled analysis of IPV, ozone, and CO can provide supporting evidence of the stratosphere-to-troposphere mixing north of Clark County that likely contributed to the ozone exceedance on May 28. Stratospheric air is characterized by high IPV, low moisture, high concentrations of ozone, and low concentrations of CO compared to tropospheric air. Therefore, these three measurements can act as tracers for the penetration of stratospheric air into the troposphere. The RAQMS, GFS, and WACCM are utilized in this section to provide evidence of stratosphere-to-troposphere exchange through the examination of IPV, ozone, and CO levels. Animations to accompany the images in this section are provided in [Appendix A](#).

The region of stratosphere-to-troposphere exchange, an external source of ozone in Clark County on May 28, was located over Idaho and Utah on May 25 (00:00 UTC to 12:00 UTC). [Figure 3-14](#) shows the GFS model analysis of IPV at the 350 mb level at 06:00 UTC on May 25. The area with IPV greater than 1 over Idaho indicates a stratosphere-to-troposphere exchange. The white box in [Figure 3-14](#)

encompasses the source region of air crossing Clark County on May 28, which does not include the high IPV region over Montana and Wyoming (see HYPPLIT trajectories in section 3.3.1).

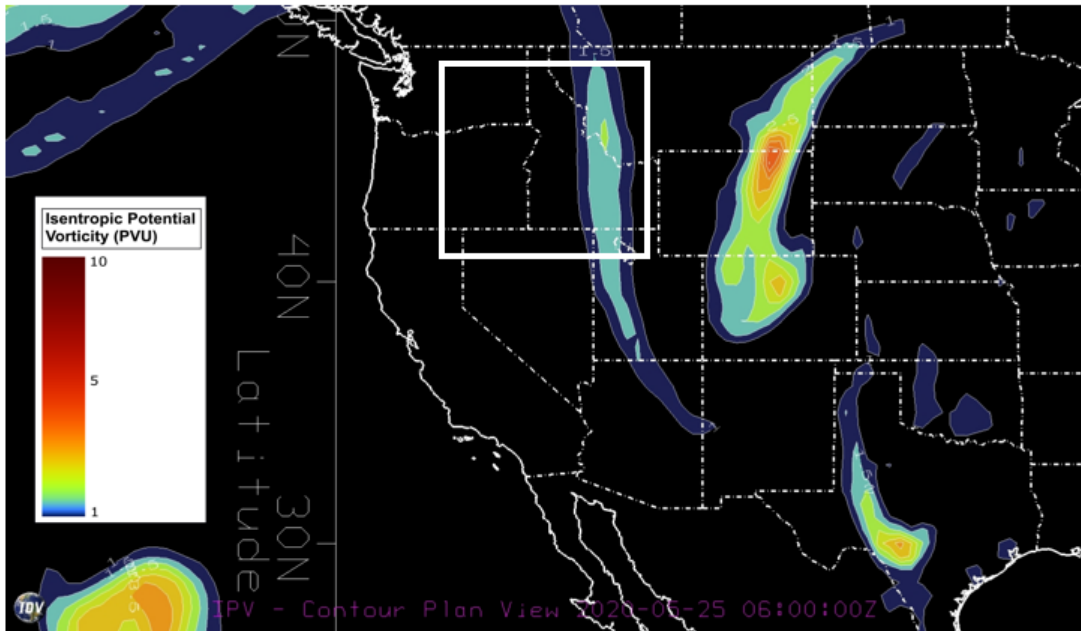


Figure 3-14. GFS-modeled IPV at 06:00 UTC on May 25 at the 350 hPa geopotential height, plotted with Unidata’s IDV. The region of elevated IPV, where stratosphere-to-troposphere exchange occurred, is boxed in white.

Figure 3-15 shows the GFS model analysis of water vapor mixing ratio at 350 mb at 06:00 UTC on May 25. Stratospheric air is typically very dry, so regions near stratospheric-tropospheric exchange are often marked by low measurements of water vapor in the troposphere. Lower modeled water vapor mixing ratios relative to surrounding regions and collocated with the area of high IPV over Idaho and Utah provide consistent evidence for a stratospheric intrusion.

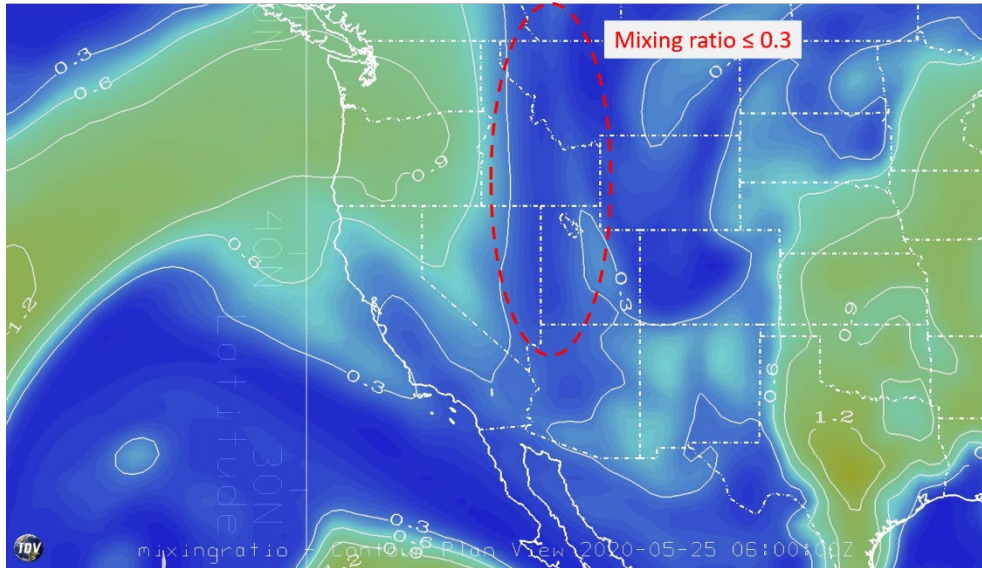


Figure 3-15. Mixing ratio contour map at 350 hPa geopotential height based on GFS model simulations for 06:00 UTC on May 25. Each contour above 0.1 g/kg represents 0.1 g/kg increments. The region of relatively low water vapor mixing ratios intersecting with back trajectories from Clark County is circled in red and aligns with the region of elevated IPV shown in Figure 3-14.

Stratospheric air is characterized by high ozone concentrations, as ozone is produced naturally and efficiently in the stratosphere. The mid-troposphere, on the other hand, typically has much lower ozone concentrations, so elevated layers of mid-tropospheric ozone could be indicative of stratospheric exchange. **Figure 3-16** shows the modeled ozone concentration from RAQMS. A region of elevated tropospheric ozone can be seen over Idaho and Utah at the 600 mb level (circled in purple), at 06:00 UTC on May 25.

The WACCM model analysis of ozone on May 25 at 06:00 UTC aligns with the RAQMS, providing additional evidence of stratosphere-to-troposphere mixing north of Clark County. **Figure 3-17** shows modeled ozone in the mid-troposphere at the 500 mb level. At this height, a similar area of elevated ozone, circled in red, is visible near 115 degrees west longitude in Idaho.

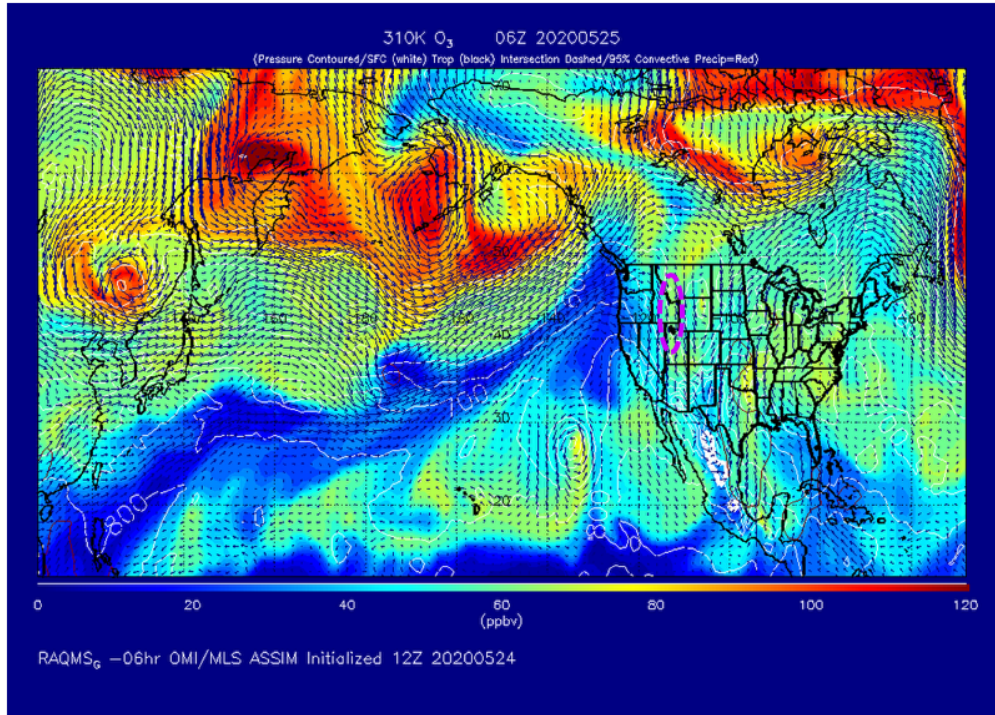


Figure 3-16. RAQMS-modeled ozone at the 310 K isentropic level at 06:00 UTC on May 25. The model was initialized at 12:00 UTC on May 24. The region with suspected stratosphere-to-troposphere mixing, and corresponding elevated ozone levels, is circled in red.

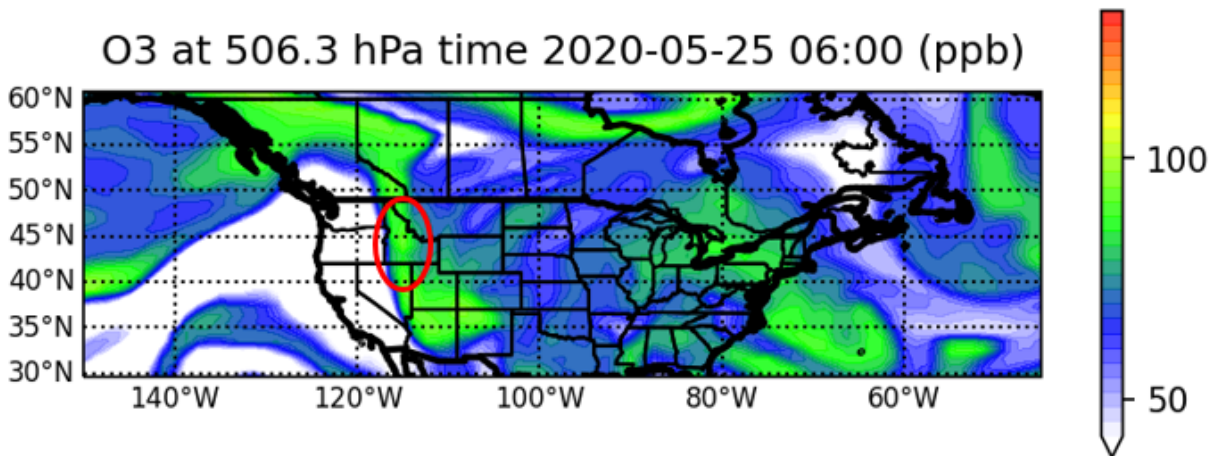


Figure 3-17. WACCM-modeled ozone at the 500 mb level on May 25 at 06:00 UTC. The region with the stratosphere-to-troposphere mixing, and corresponding elevated ozone levels, is circled in red.

Figure 3-18 shows the WACCM-modeled latitudinal cross section of ozone over the source region on May 25 at 12:00 UTC. A tropospheric fold is visible over eastern Idaho, lending further evidence to the existence of a stratospheric intrusion in this region. The maps shown in **Figure 3-19** provide WACCM-modeled latitudinal cross section reference locations and extent for the time series displayed in **Figures 3-20 and 3-21**. These cross sections track the general timing of the HYSPLIT trajectories and air transport between the source region and Clark County (36-degrees north and 115-degrees west) on the days leading up to the event date. HYSPLIT trajectories, discussed in detail in Section 3.3.1, show rapid air parcel transport from the source region southward (within 24 hours), bypassing Las Vegas to the east, and then swinging back northward to Clark County. The maps (**Figure 3-19**) show the approximate latitudes of the suspected source region (labeled “Source”) and north-south progression of air ordered from 1 to 8 leading up to the event date (labeled “Event”). Rapid southward movement from the source region is shown in the left map. Slower northward movement back towards Clark County is shown to the right. The ordered reference lines align with the labels on each cross section presented in **Figures 3-20 and 3-21**.

Modeled ozone is presented in **Figure 3-20** in a southward progression between May 25 at 18:00 to May 26 at 12:00 UTC at selected latitudes that align with HYSPLIT trajectories shown in Section 3.3.1. Cross sections at 40.1-degrees and 38.2-degrees north latitude are both presented at 18:00 UTC because HYSPLIT trajectories show air moving rapidly southward from the source region near this time. The tropospheric fold is visible at both of these latitudes at 18:00 UTC, confirming the north-south extent of this ozone feature. The tropospheric fold results in a layer of higher ozone concentrations between 500–800 mb that can be tracked along the HYSPLIT trajectory in the days leading up to the event date. This feature is highlighted by a black box in all plots in **Figures 3-20 and 3-21**. Between 00:00 UTC and 12:00 UTC on May 26, this elevated layer of ozone is transported further south to 35.3 and 32.5 degrees, respectively.

Figure 3-21 and **Figure 3-22** show the progression of this ozone feature (highlighted by a black box) as the ozone-rich air mass curves back northward towards Clark County between May 27 and the event date (May 29 00:00 UTC/May 28 16:00 PST). On May 27 at 00:00 UTC, the modeled ozone enhancement of stratospheric origin is a thin layer at ~600 mb, immediately below a layer of low ozone in the free troposphere (**Figure 3-21**). Based on the skew-T data and PBL height modeling (detailed in sections 3.3.2 and 3.3.3), 600 mb is within the deep daytime mixed layer over the region. During the 36 to 48 hours from May 27 at 00:00 UTC to the morning of the May 28 event date, the elevated ozone of stratospheric origin was transported and mixed within the boundary layer, at which point the feature was difficult to track and distinguish from local photochemical or regional background ozone. To discern the stratospheric source appointment at the surface, we examined the stratospheric ozone tracer (O3S) in the WACCM model. **Figures 3-23 through 3-26** depict the O3S tracer time series and correspond to the WACCM latitudinal cross sections of total ozone concentration. The modeled O3S cross section profiles indicate a persistent feature in the boundary layer along the transport path to Clark County. Due to the expected chemical and dry deposition losses of a stratospheric ozone contribution during multi-day boundary layer transport, the O3S values decrease over time leading up to the event day. On the morning of the event (12:00

UTC/04:00 PST on May 28), the O3S tracer shows value around 10-15 immediately upwind of Clark County within the boundary layer. On the afternoon of May 28 (after morning/early afternoon boundary layer expansion and mixing), the WACCM model predicts a non-zero stratospheric ozone contribution of 5-10 ppb in the boundary layer and up to 6 ppb at the surface in Clark County (Figure 3-26). This positive detection of stratospheric influence is within the range of SOI episodes detected previously. Chouza et al. (2020) report comparable values for the stratospheric ozone tracer in the WACCM model near Clark County downwind of the Los Angeles Basin, with a typical interquartile range including exceptional SOI event days during late spring 2019 and 2020 that overlaps with 6 ppb. Furthermore, the total ozone bias in WACCM is typically +20% or less near the surface (Chouza et al., 2020). Overall, the WACCM model results provide evidence for a small but detectable stratospheric ozone influence on May 28, 2020, in Clark County.

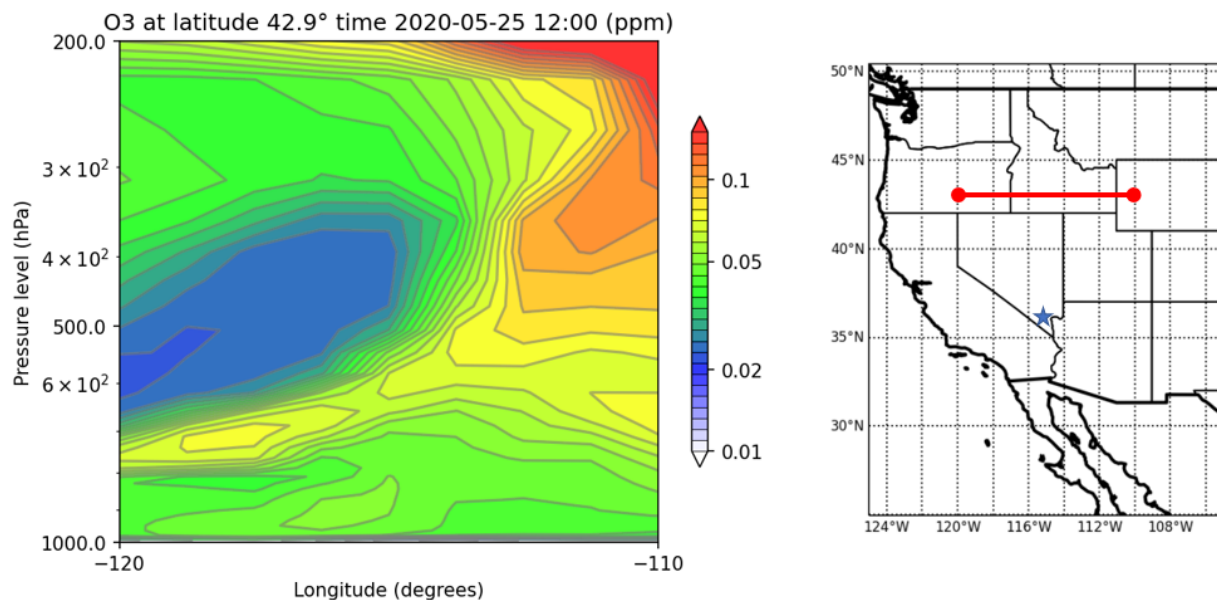


Figure 3-18. WACCM-modeled latitudinal cross-section of ozone along the 42.9-degree N latitude line on May 25 at 12:00 UTC. This cross section intersects the proposed source of stratospheric ozone for the May 28 exceedance event. The extent of the cross section is shown as a red line on the map to the right. Las Vegas is shown as a blue star.

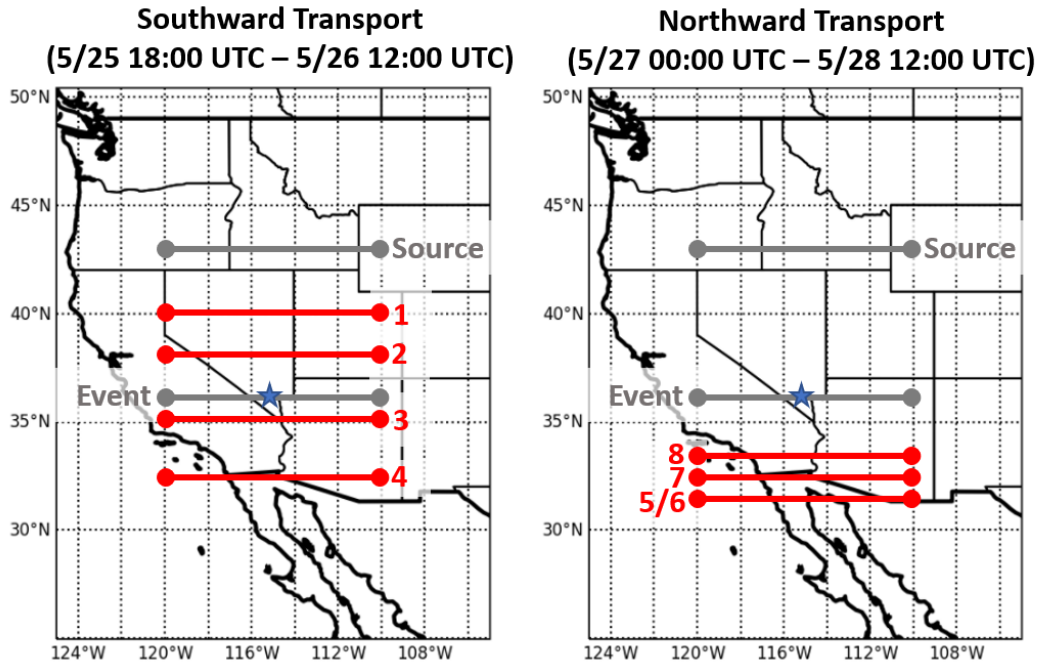


Figure 3-19. Reference map for cross sections shown in Figures 3-20, 3-21, 3-24, and 3-25. Each red line aligns with a numbered subplot in each figure and represents the extent of the cross section shown in the plot. The order of numbered reference lines aligns with the path of air transport from the source region to Clark County, according to HYSPLIT trajectories shown in Section 3.3.1. The approximate latitudes of the proposed source region (labeled “Source”) and Clark County (labeled “Event”) are shown as gray lines. The map on the left shows initial rapid southward motion of air. The map on the right shows slower northward movement of air back towards Clark County. Las Vegas is shown as a blue star.

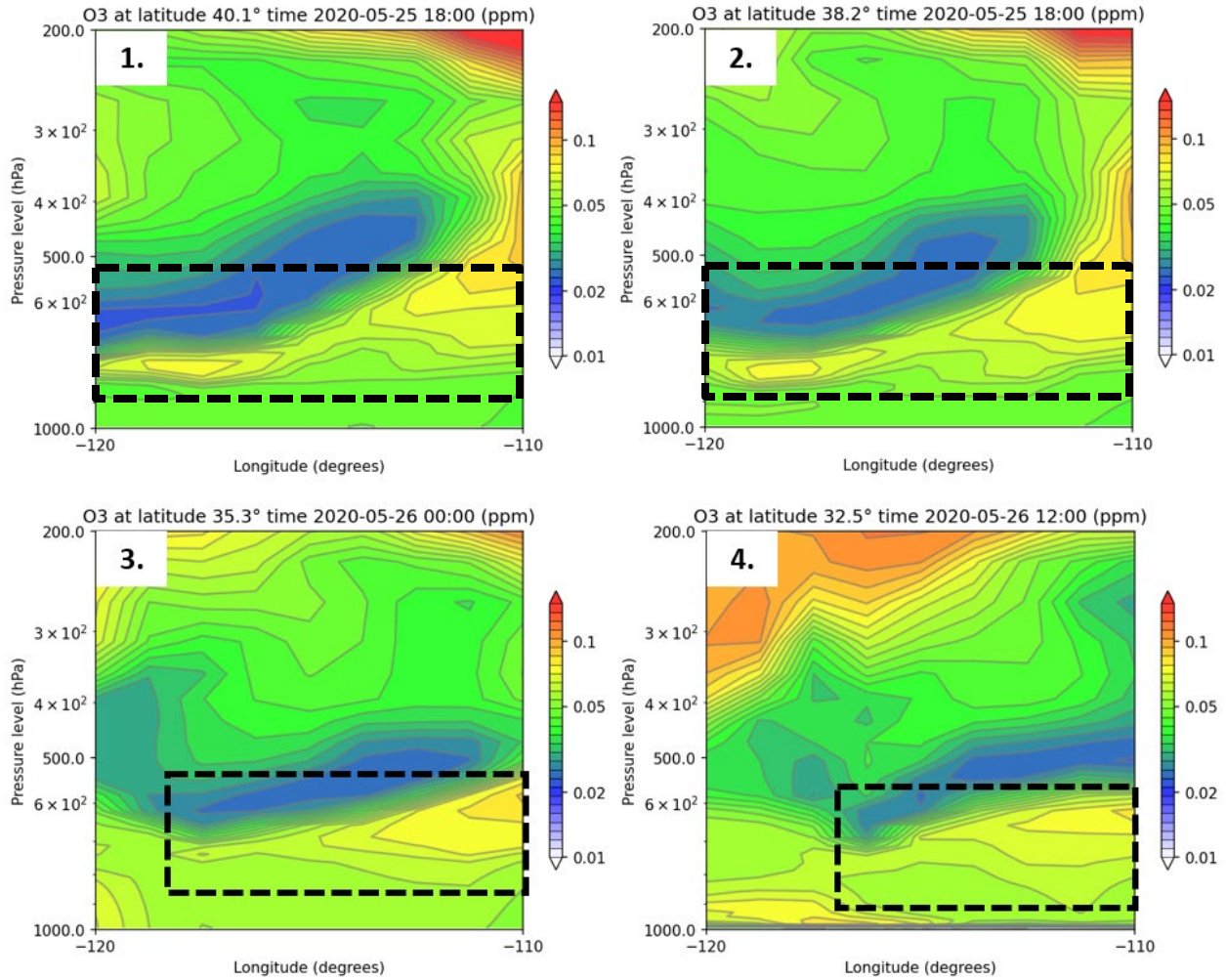


Figure 3-20. WACCM-modeled cross-sections of southward movement of air between May 25 at 18:00 UTC through May 26 at 12:00 UTC. The extent of the cross section for each plot is presented on the left map in Figure 3-19 as a red reference line labeled by the number in the upper-left corner of the plot. The black boxes in plots 3 and 4 highlight the progression of the elevated layer of ozone resulting from the tropospheric fold visible in plots 1 and 2. The surface pressure at some elevated altitude portions of the domain is between 700-800 mb.

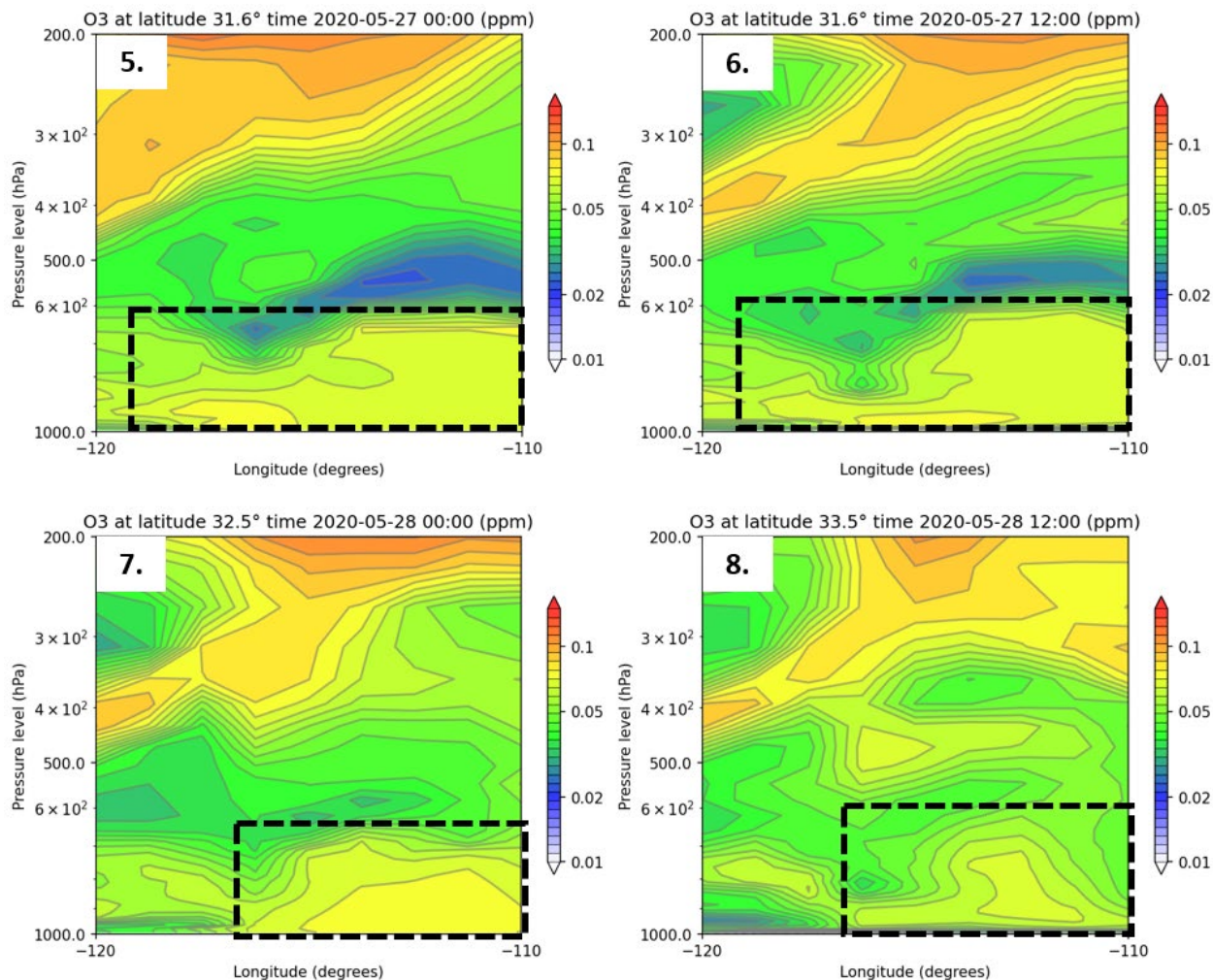


Figure 3-21. WACCM-modeled cross-sections of ozone at 12-hour increments for May 27 at 00:00 UTC through May 28 at 12:00 UTC. The extent of the cross section for each plot is presented in the right map of Figure 3-19 as a red reference line labeled by the number in the upper-left corner of the plot. The black box in each plot highlights the northward progression of an elevated layer of ozone in time and space. The surface pressure at some elevated altitude portions of the domain is between 700-800 mb.

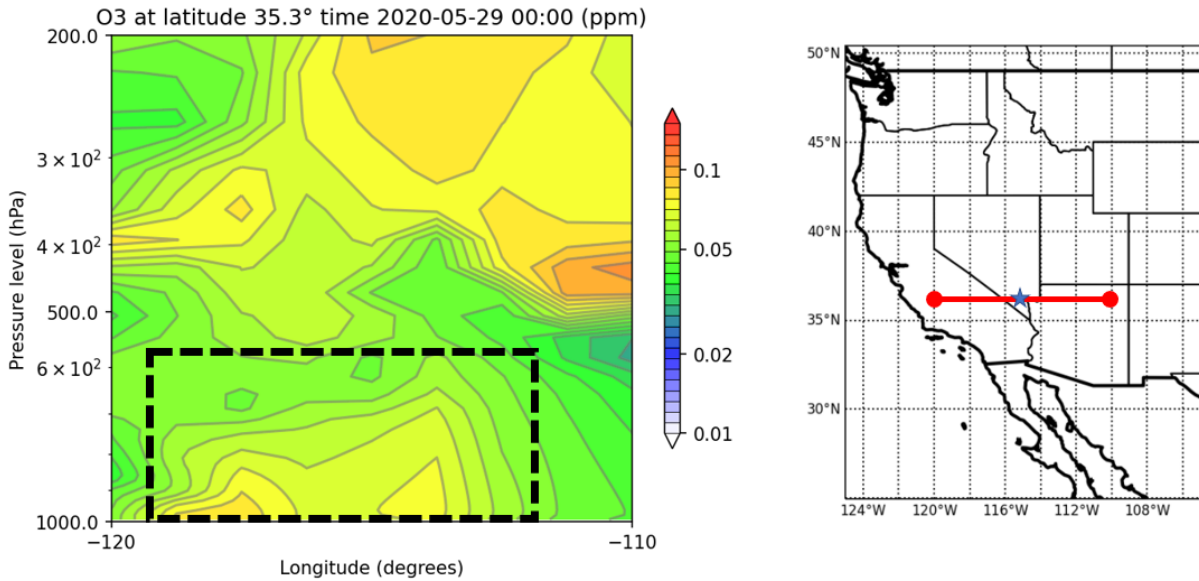


Figure 3-22. WACCM-modeled latitudinal cross-section of ozone on the event date, May 29 at 00:00 UTC (May 28 at 18:00 PST) over Clark County. A deep layer of elevated ozone between 1000-600 mb is boxed in black. The extent of the cross section is represented by the red line in the map to the right. Las Vegas is shown as a blue star.

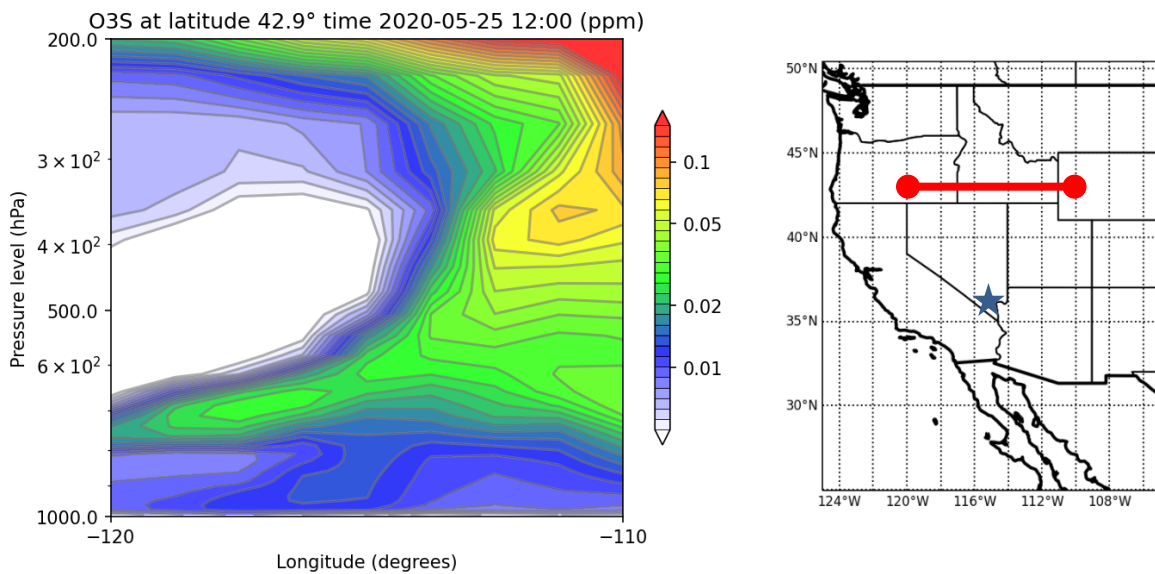


Figure 3-23. WACCM-modeled latitudinal cross-section of the stratospheric ozone tracer along the 42.9 degrees N latitude line on May 25 at 12:00 UTC. This cross section intersects the proposed source of stratospheric ozone for the May 28 exceedance event. The extent of the cross section is shown as a red line on the map to the right. Las Vegas is shown as a blue star.

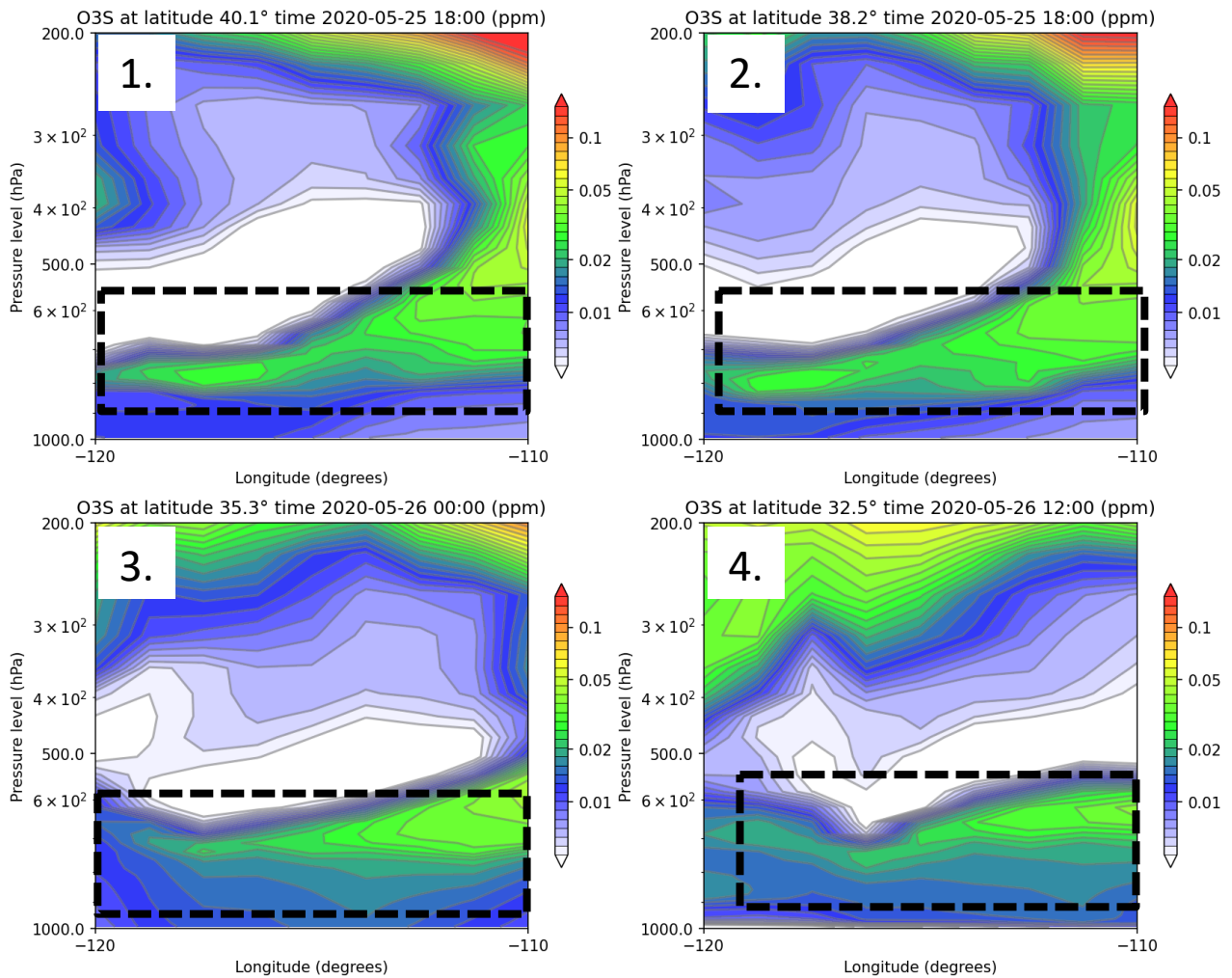


Figure 3-24. WACCM-modeled cross-sections of southward movement of the stratospheric ozone tracer between May 25 at 18:00 UTC through May 26 at 12:00 UTC. The extent of the cross section for each plot is presented in Figure 3-19 as a red reference line labeled by the number in the upper-left corner of the plot. The black boxes highlight the progression of the elevated layer of stratospheric ozone resulting from the source region in Figure 3-23.

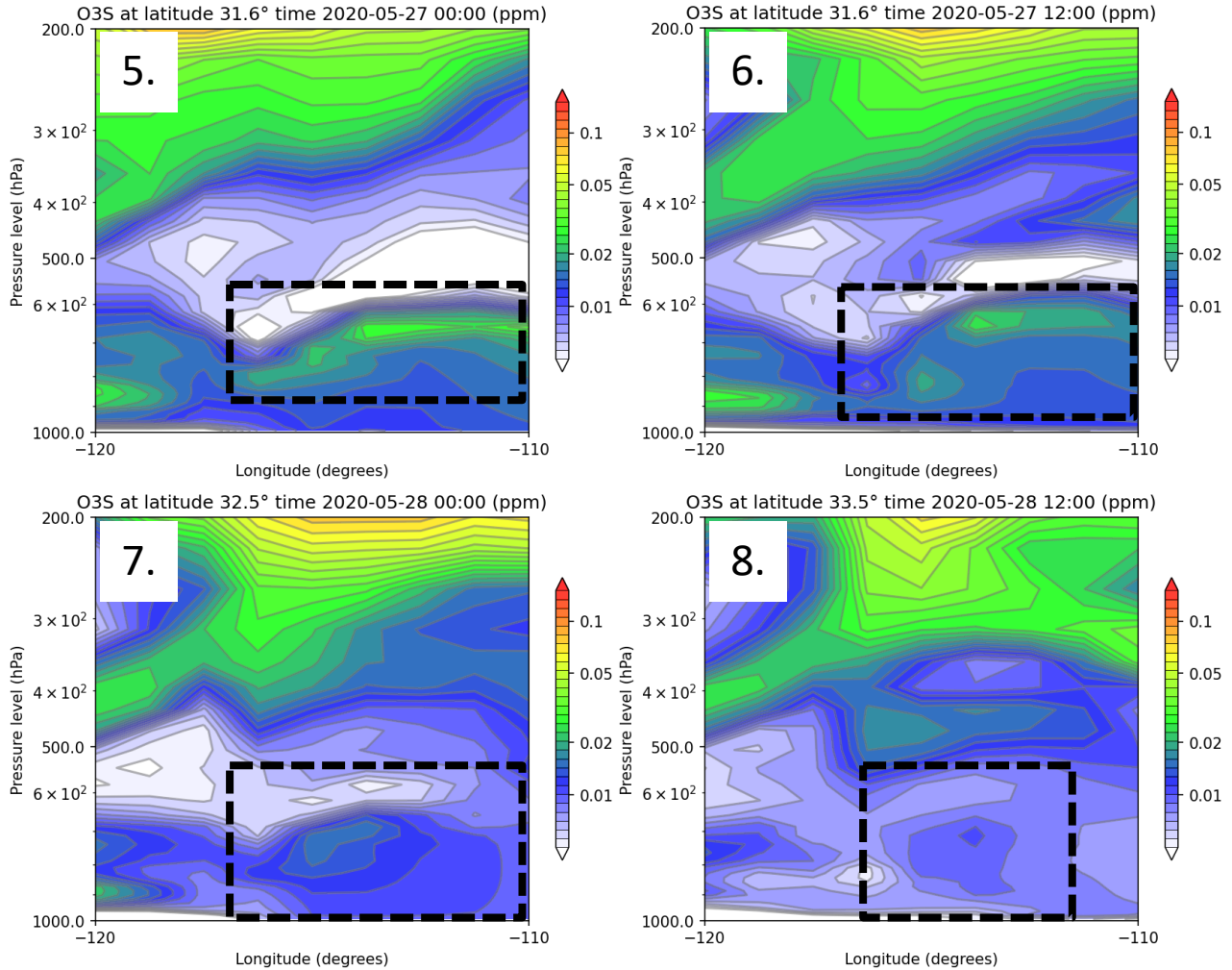


Figure 3-25. WACCM-modeled cross-sections of northward movement of the stratospheric ozone tracer between May 27 at 00:00 UTC through May 28 at 12:00 UTC. The extent of the cross section for each plot is presented on the map in Figure 3-19 as a red reference line labeled by the number in the upper-left corner of the plot. The black boxes highlight the progression of the stratospheric ozone resulting from the source region visible in Figure 3-23.

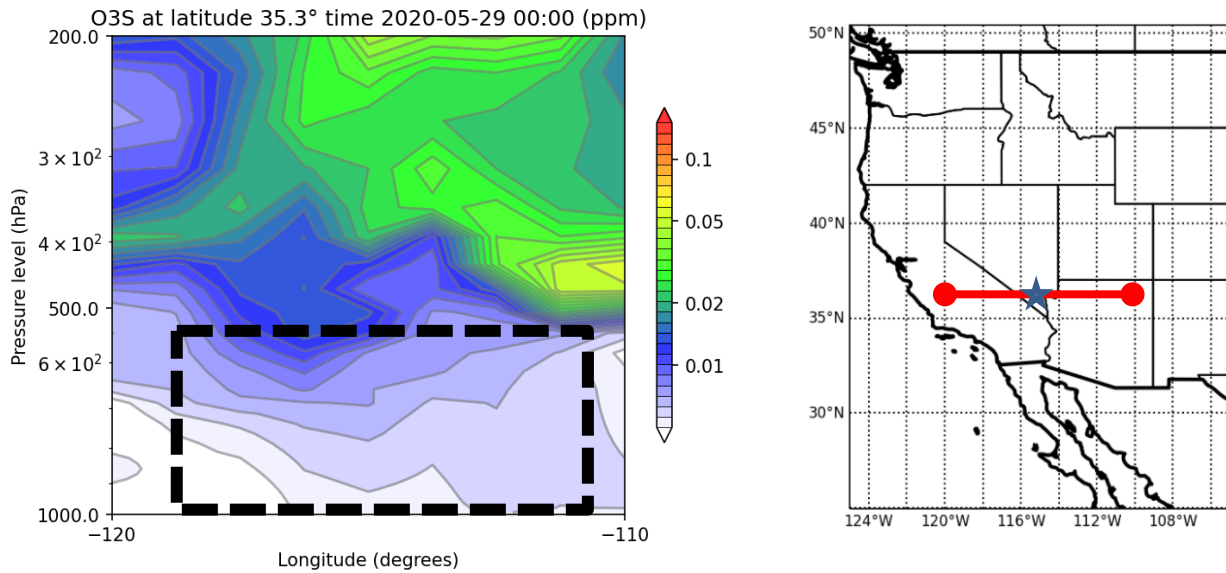


Figure 3-26. WACCM-modeled latitudinal cross-section of stratospheric ozone on the event date, May 29 at 00:00 UTC (May 28 at 18:00 PST) over Clark County. The extent of the cross section is represented by the red line in the map to the right. Las Vegas is shown as a blue star.

Figures 3-27 and 3-28 show MERRA-2 modeled ozone concentrations for the May mean (2014 – 2020), and at 06:00 and 12:00 UTC on May 25 over the western United States at 488 hPa and 288 hPa, respectively. During the hours of the stratospheric intrusion that led to the May 28 ozone exceedance in Las Vegas, ozone concentrations over Idaho in the upper troposphere were well above the May average. On May 25 at 06:00 UTC and 12:00 UTC at 488 hPa and 288 hPa, ozone concentrations at the area of stratospheric intrusion were well above the mean May ozone concentrations over the same area. Figures 3-27 and 3-28 are consistent with Figures 3-16 and 3-17, which also show elevated ozone in the upper troposphere over the area of stratospheric intrusion.

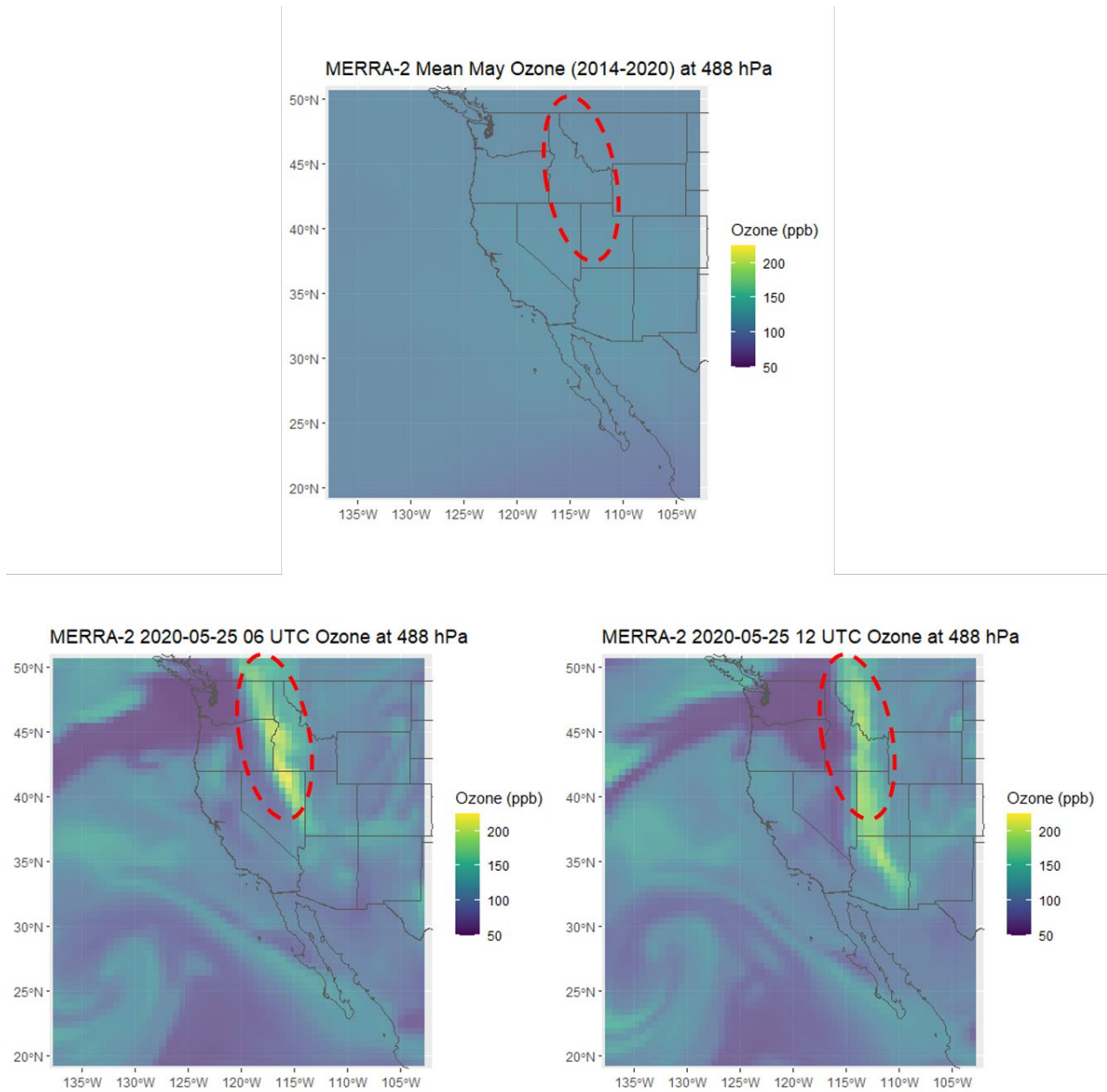


Figure 3-27. MERRA-2 mean May ozone concentrations at the 488 hPa level based on data from 2014 – 2020 (top). MERRA-2 ozone concentrations at the 488 hPa level at 06:00 UTC (bottom left) and six hours later at 12:00 UTC (bottom right) on May 25. The red oval represents the approximate area of stratospheric intrusion.

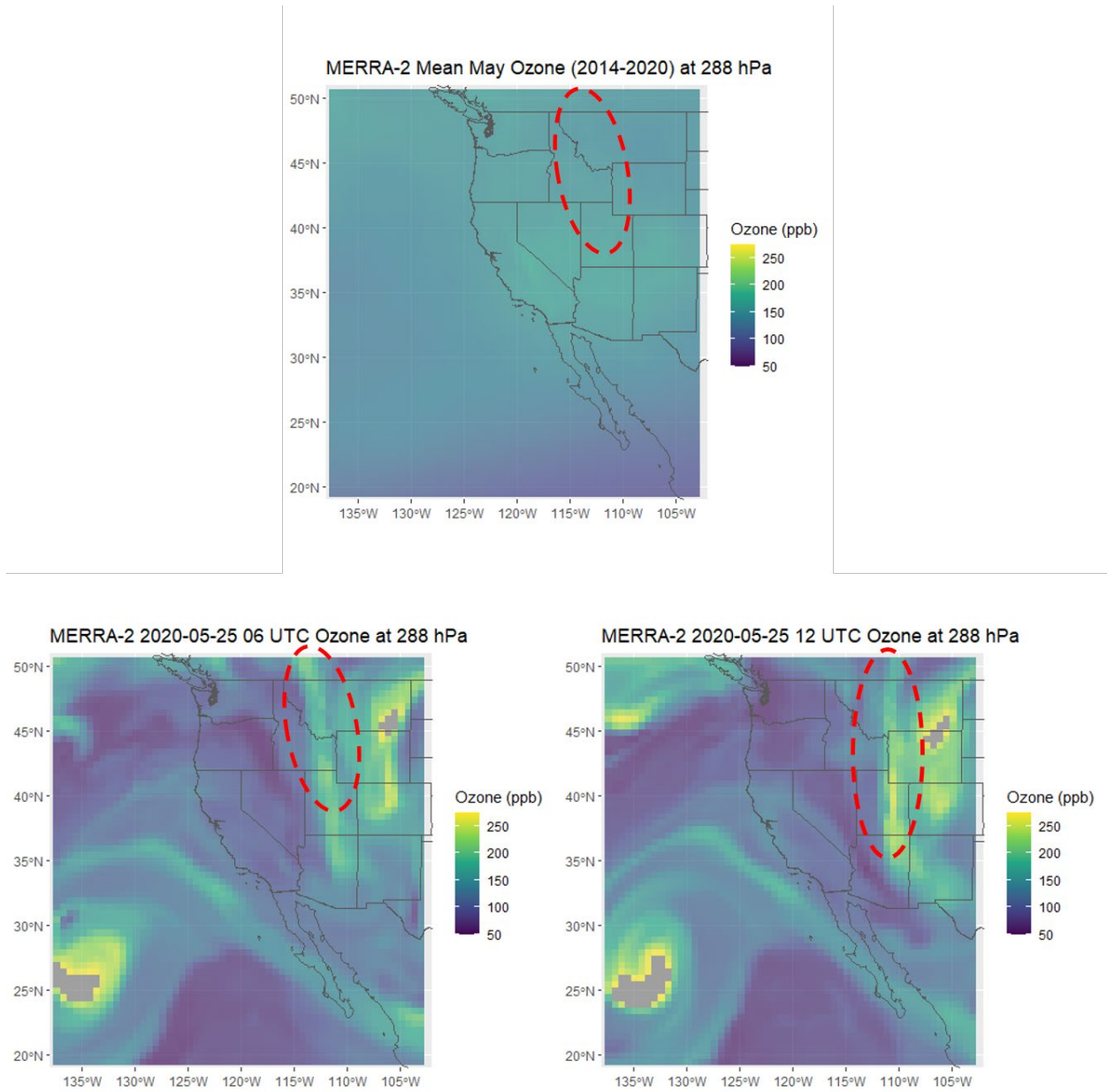


Figure 3-28. MERRA-2 mean May ozone concentrations at the 288 hPa level based on data from 2014 – 2020 (top). MERRA-2 ozone concentrations at the 288 hPa level at 06:00 UTC (bottom left) and six hours later at 12:00 UTC (bottom right) on May 25. The red oval represents the approximate area of stratospheric intrusion.

Stratospheric air is characterized by low CO concentrations. Therefore, an instance of stratosphere-to-troposphere mixing can be indicated by the presence of low concentrations of CO in the troposphere. **Figure 3-29** shows the modeled CO concentration from RAQMS on May 25 at 6:00 UTC. There is relatively low CO over the region of stratosphere-to-troposphere mixing in Idaho

and Utah (circled in purple), at the eastern end of a regional minimum off the western coast. Similarly, the WACCM-modeled CO concentrations (Figure 3-30) show a minimum in CO concentrations off the western coast, though the extent of these reduced concentrations does not span as far east.

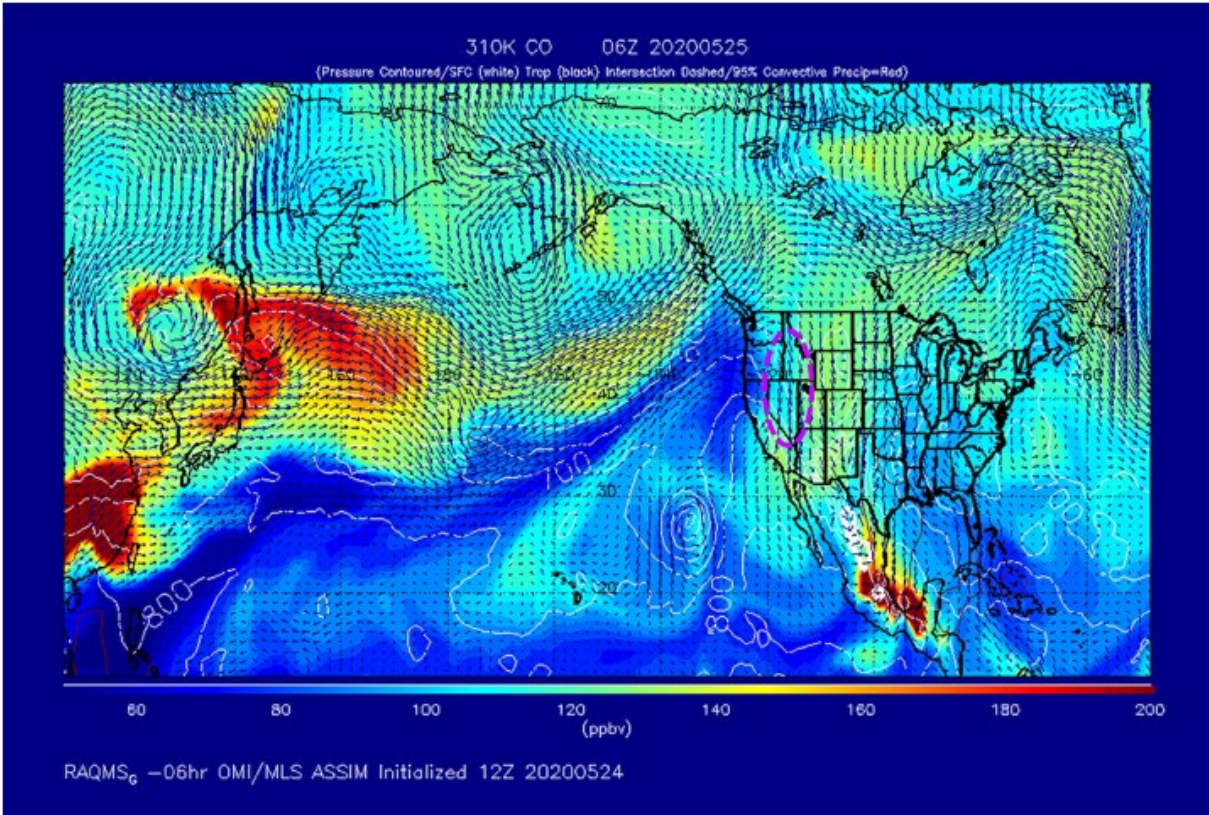


Figure 3-29. RAQMS-modeled CO at the 310 K isentropic level at 06:00 UTC on May 25. The model was initialized at 12:00 UTC on May 24. The region with the stratosphere-to-troposphere mixing, and corresponding reduced CO levels, is circled in purple.

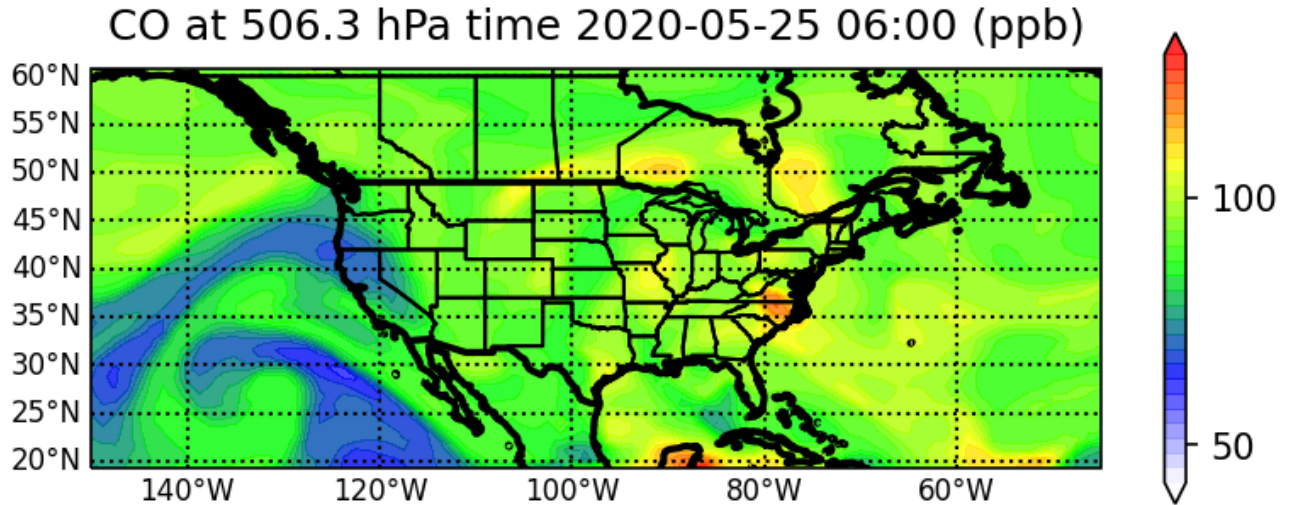


Figure 3-30. WACCM-modeled CO at the 500 mb level on May 25 at 6:00 UTC.

Modeled CO from WACCM and RAQMS are seen in Figures 3-31 and 3-32. Each of these maps show reduced CO concentrations at the 500 hPa level extending southward over Nevada (circled in purple) on the event date, May 29 at 00:00 UTC (May 28 at 16:00 PST). Low CO concentrations over Clark County on the EE date are consistent with SOI influence.

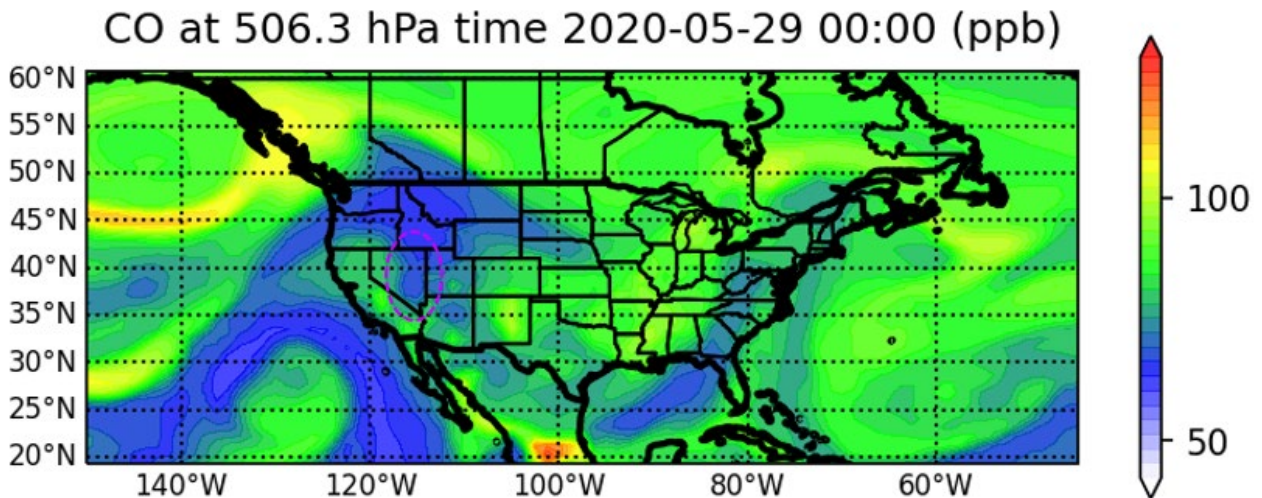


Figure 3-31. WACCM-modeled CO at the 500 mb level on May 29 at 0:00 UTC (the event date–May 28 at 16:00 PST). The purple circle shows the region of reduced CO over Clark County.

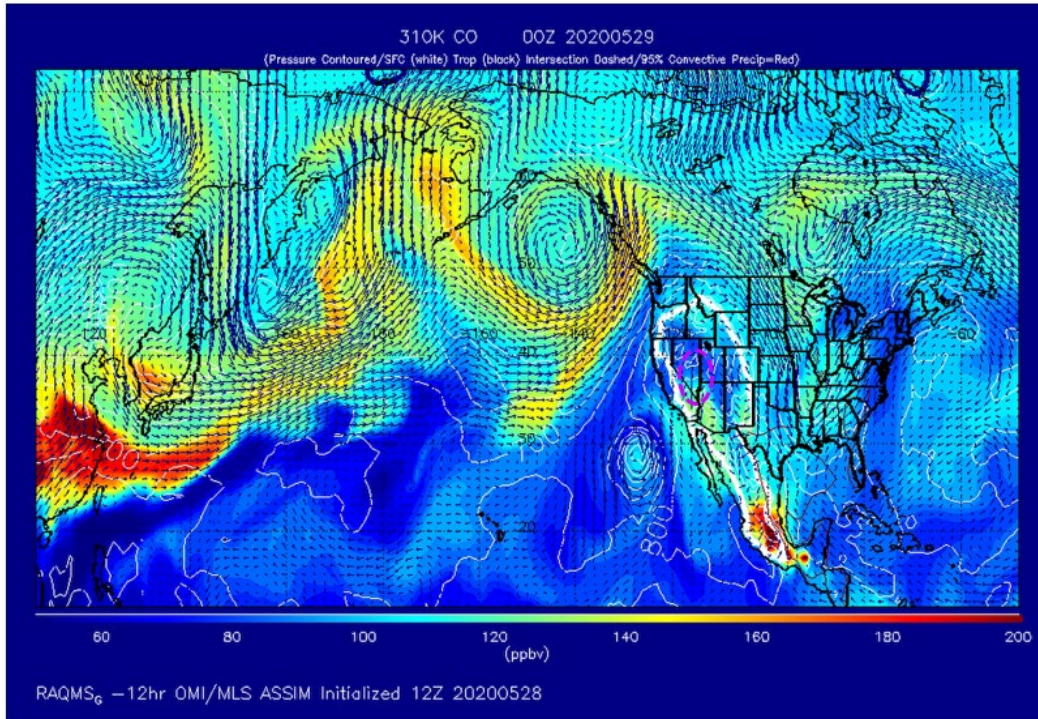


Figure 3-32. RAQMS-modeled CO at the 310 K isentrope level at 00:00 UTC on May 29 (the event date—May 28 at 16:00 PST). The model was initialized at 12:00 UTC on May 28. The region circled in purple encompasses the southern end of a low-CO extension and Clark County.

Figure 3-33 shows MERRA-2 modeled CO concentrations for the May mean (2014 – 2020) and at 06:00 and 12:00 UTC on May 25 over the western United States at 288 hPa. During the hours of the stratospheric intrusion that led to the May 28 ozone exceedance in Las Vegas, CO concentrations over Idaho, Montana, Wyoming, and Utah at the 288 hPa level were lower than average. This area of low CO concentrations aloft is consistent with modeled CO in the upper troposphere shown in Figures 3-27 and 3-28. Near the surface at the 985 hPa level on the event date, May 28, CO concentrations over the Las Vegas area were average to slightly below average (**Figure 3-34**) as indicated by darker shades of blue and purple.

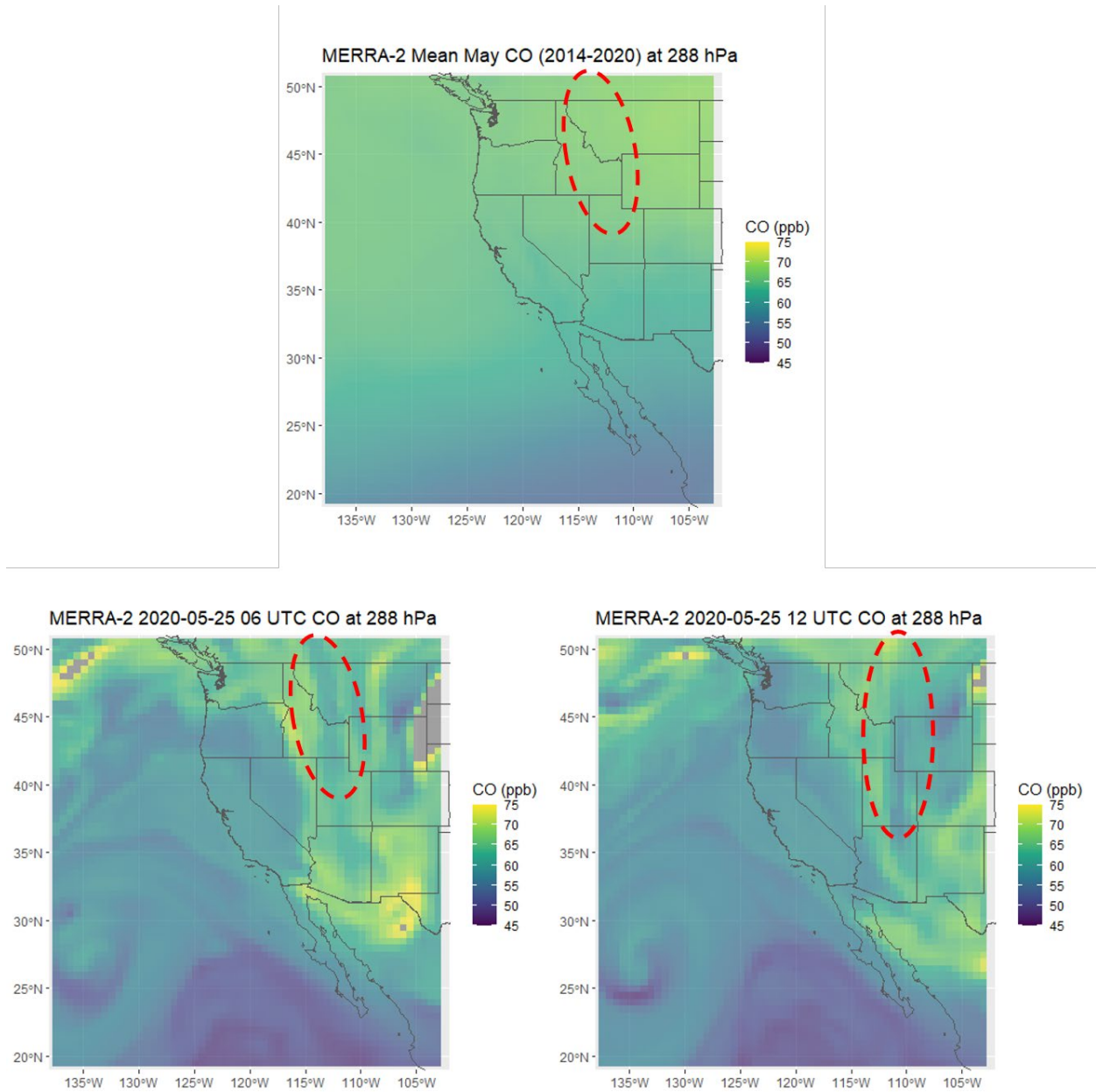


Figure 3-33. MERRA-2 mean May CO concentrations at the 288 hPa level based on data from 2014 – 2020 (top). MERRA-2 CO concentrations at the 288 hPa level at 06:00 UTC (bottom left) and six hours later at 12:00 UTC (bottom right) on May 25. The red oval represents the approximate area of stratospheric intrusion.

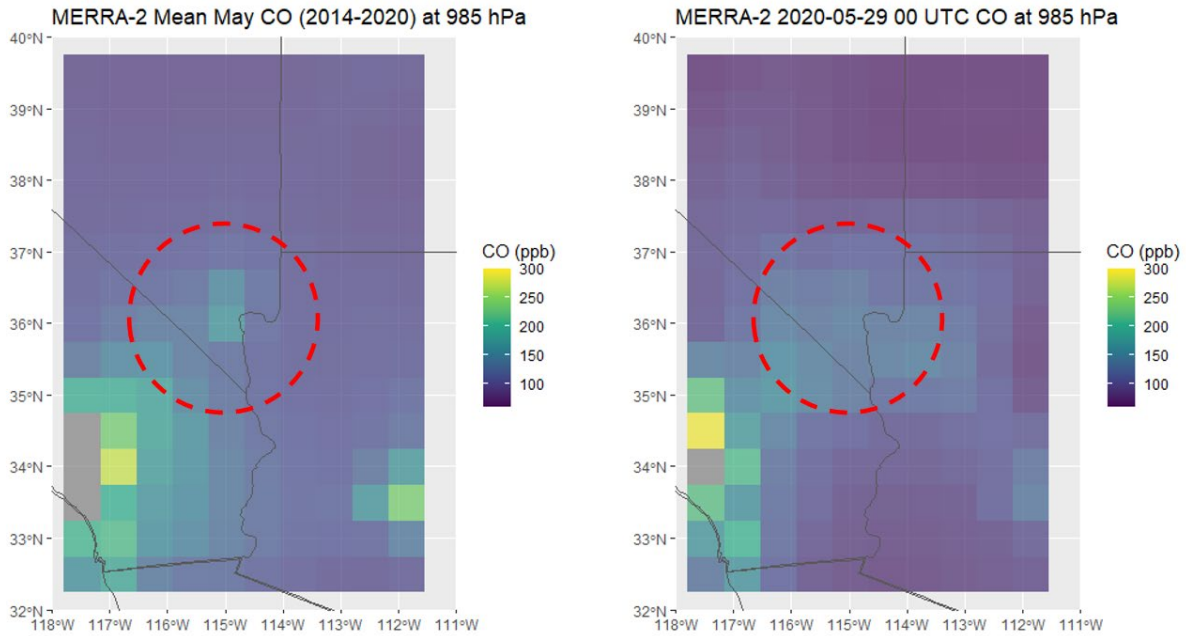


Figure 3-34. MERRA-2 mean May CO concentrations near the surface at the 985 hPa level based on data from 2014 – 2020 (left). MERRA-2 CO concentrations at the 985 hPa level at 00:00 UTC (right) on May 29 (4:00 p.m. local standard time on May 28). The red circle represents the Las Vegas area.

Modeled values of IPV, ozone, and CO all show that stratosphere-to-troposphere mixing occurred over Idaho on May 25 at approximately 06:00 UTC. This region saw relatively high IPV, elevated ozone throughout the upper- and mid-troposphere, and reduced CO levels in the upper troposphere, which are all markers of stratospheric air. Further, a series of modeled ozone in mid-troposphere from May 25 through the event date on May 28 show transport of air from the source region over Idaho southward into the mid-troposphere and then down to the surface level. The modeled CO provides supporting evidence of this transport pattern with very low mid-tropospheric CO values over Clark County on the EE date. The timeline for the transport of this stratospheric air to Clark County aligns with the modeled HYSPLIT trajectories presented in Section 3.3.1 and with the overall conceptual model presented in Section 1.4.

3.3 Evidence of Stratospheric Air Reaching the Surface

3.3.1 HYSPLIT Trajectory Analysis

HYSPLIT trajectories were run to demonstrate the transport of air from a stratospheric intrusion to Clark County. These trajectories show that air was transported from the stratospheric intrusion, generally located over Idaho and Utah, to the Clark County area in the days prior to the event and on May 28, 2020. Combined with satellite observations and modeled analyses described in

Sections 3.2.1 and 3.2.2, these trajectories provide evidence that stratospheric ozone was transported to Las Vegas, Nevada.

NOAA's online HYSPLIT model tool was used for the trajectory modeling (<http://ready.arl.noaa.gov/HYSPLIT.php>). HYSPLIT is a commonly used model that calculates the path of a single air parcel from a specific location and height above the ground over a period of time; this path is the modeled trajectory. HYSPLIT trajectories can be used as evidence that high-ozone stratospheric air was transported to an air quality monitor. This type of analysis is important for meeting both Tier 1 and 2 requirements.

The model options used for this study are summarized in [Table 3-7](#). The meteorological data from the NAM 12 km resolution model were used (ready.noaa.gov/archives.php). These data are high in spatial resolution, readily available for HYSPLIT modeling over the desired lengths of time, and expected to capture fine-scale meteorological variability. The backward trajectory start time was selected to be in the evening at 05:00 UTC (i.e., 22:00 PST). Additionally, the backward trajectory matrix analysis was initiated in the evening (05:00 UTC or 22:00 PST). The reason for the late start time was due to the low wind speeds during the afternoon of May 28 causing highly variable trajectories between different start times and meteorological data used. Throughout the late afternoon on May 28, the trajectories were consistent and allowed us to model the entire day on May 28. A backward trajectory length of 96 hours was selected to assess whether stratospheric air from the current day or from the previous three days may have been transported over a long distance to the monitoring sites. The trajectory was initiated at 3,000 m above ground level to capture transport to the mixed boundary layer, as stratospheric ozone may be transported aloft and influence concentrations at the surface through vertical mixing. Three backward trajectory approaches available in the HYSPLIT model were used in this analysis, including site-specific trajectories, trajectory matrix, and trajectory frequency. Site-specific back trajectories were run to show direct transport from the SOI to the affected site(s). This analysis is useful in linking air quality and meteorological impacts at a single location (i.e., an air quality monitor) to an SOI. Matrix back trajectories were run to show the general air parcel transport patterns from the Las Vegas area to the SOI. Similarly, matrix forward trajectories were run to show air parcel transport patterns from the SOI region to the Las Vegas area. Matrix trajectories are useful in analyzing air transport over areas larger than a single air quality site. Trajectory frequency analysis shows the frequency with which multiple trajectories initiated over multiple hours pass over a grid cell on a map. Trajectory frequencies are useful in estimating the temporal and spatial patterns of air transport from a source region to a specific air quality monitor. Additionally, a forward trajectory matrix was run for the area over southern Idaho to examine transport patterns in the direction of Clark County.

Table 3-7. HYSPLIT run configurations for each analysis type, including meteorology data set, time period of run, starting location(s), trajectory time length, starting height(s), starting time(s), vertical motion methodology, and top of model height.

HYSPLIT Parameters	Back Trajectory Analysis – Matrix	Backward Trajectory Analysis – Frequency	Forward Trajectory Analysis – Matrix	Backward Trajectory Analysis – High Resolution
Meteorology	12-km NAM	12-km NAM	12-km NAM	12-km NAM
Time Period	May 25–May 29, 2020	May 25–May 29, 2020	May 25–May 29, 2020	May 25–May 29, 2020
Starting Location	Evenly spaced grid covering Las Vegas, Nevada	36.1381 N, 115.2582 W	Evenly spaced grid covering southern Idaho	36.1381 N, 115.2582 W
Trajectory Time Length	96 hours	96 hours	96 hours	96 hours
Starting Heights (agl)	2000 m	3000 m	5000 m	3000
Starting Times	05:00 UTC	05:00 UTC	12:00 UTC	05:00 UTC
Vertical Motion Method	Model Vertical Velocity	Model Vertical Velocity	Model Vertical Velocity	Model Vertical Velocity
Top of Model	10,000 m	10,000 m	10,000 m	10,000 m

Site-specific backward trajectories were calculated from the Las Vegas Valley (36.1381° N, 115.2581° W) on May 29 (May 28 in PST). We chose to model all trajectories for sites within the Las Vegas metropolitan area using the Las Vegas Valley location. The hour of 05:00 UTC (i.e., 22:00 PST on May 28) was chosen as the model starting time. The NAM-based backward trajectories from the Las Vegas Valley are shown in [Figure 3-35](#). The trajectory follows a path from the Las Vegas Valley to the area of stratospheric intrusion over southern Idaho and Utah with a very high starting altitude and descent into the Clark County area.

NOAA HYSPLIT MODEL Backward trajectory ending at 0500 UTC 29 May 20 NAM Meteorological Data

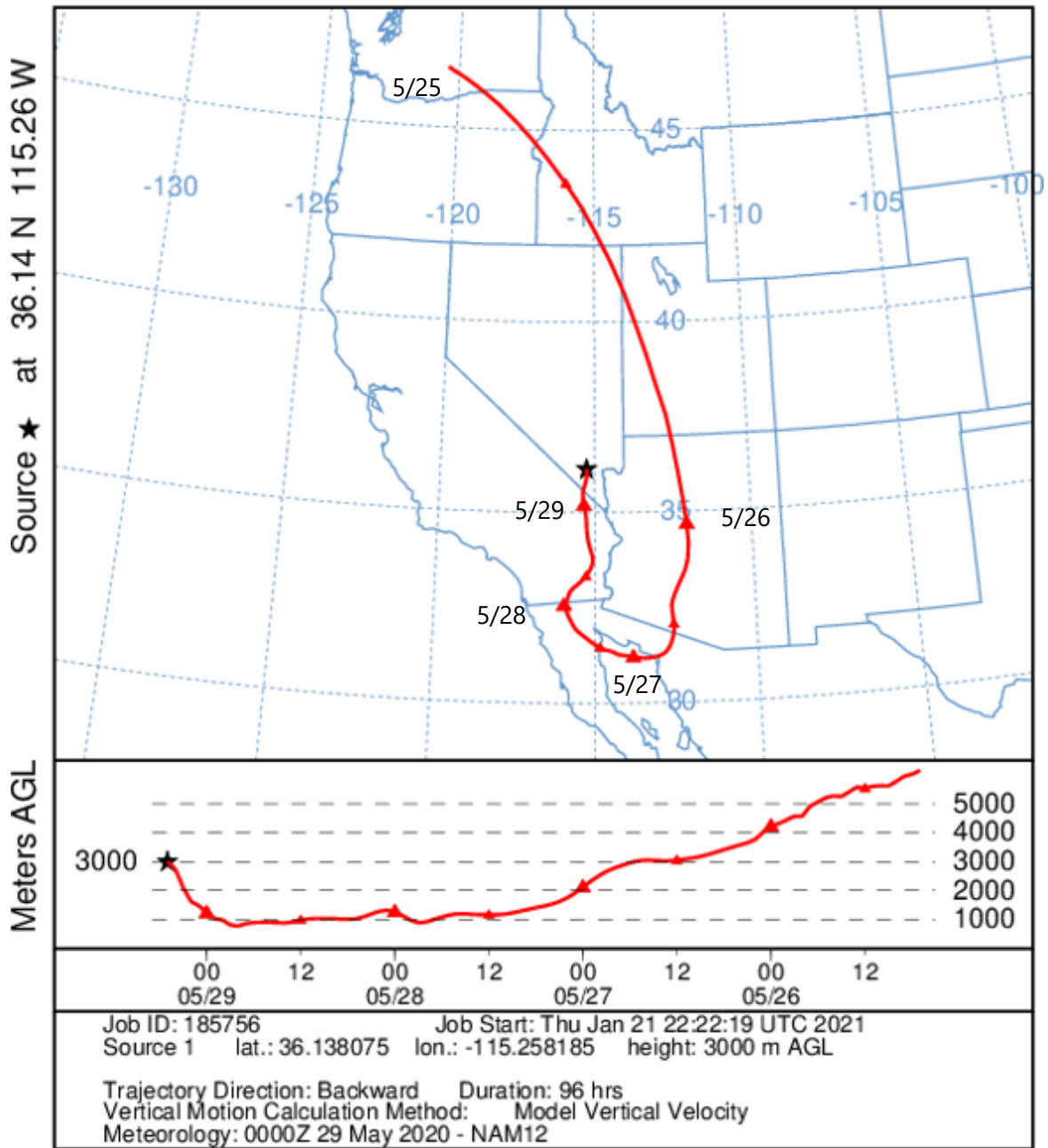


Figure 3-35. 96-hour HYSPLIT back trajectories from the Las Vegas Valley, ending on May 29, 2020. NAM 12 km back trajectories are shown for 3000 m (red) above ground level. Date labels show the position in the trajectory at 00:00 UTC on each date.

To identify variations in meteorological patterns of transported air to Las Vegas, we generated a HYSPLIT trajectory matrix. For this approach, trajectories are run in an evenly spaced grid of source locations. **Figure 3-36** shows a 96-hour backward trajectory matrix with source locations encompassing Clark County. The backward trajectories were initiated from the evening at 05:00 UTC on May 29, 2020 (i.e., 22:00 PST on May 28), at a starting height of 2000 m agl. As shown in the plot, the transported air intersects Las Vegas on May 29. Consistent with the trajectory depicted in Figure 3-35, air originating partly over southern Idaho traveled south through Utah and western Arizona to intersect with Clark County at 2000 m agl on the EE date.

NOAA HYSPLIT MODEL Backward trajectories ending at 0500 UTC 29 May 20 NAM Meteorological Data

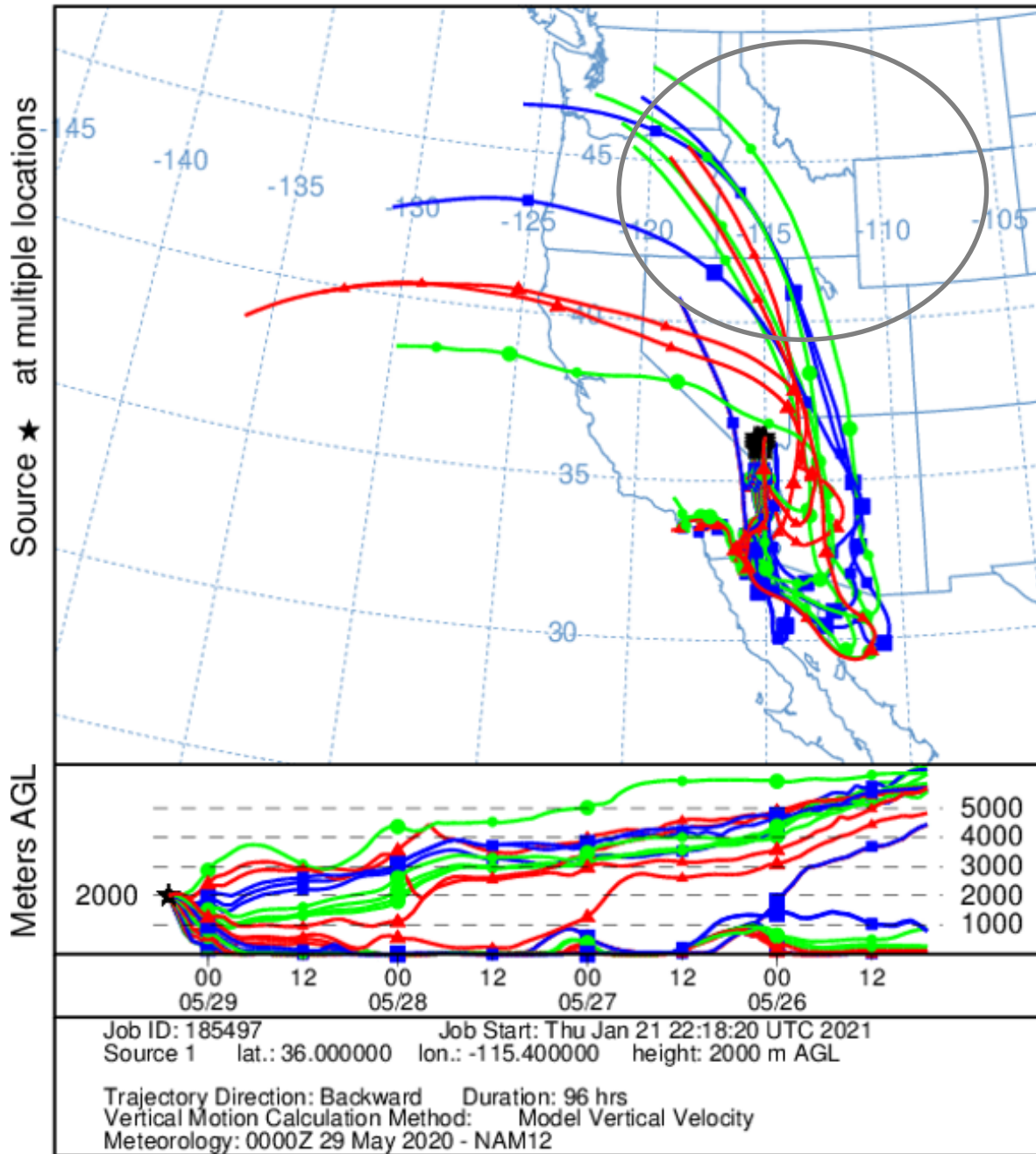


Figure 3-36. 72-hour HYSPLIT back trajectory matrix from Las Vegas Valley, ending on May 29, 2020. NAM 12 km back trajectories are shown for 2000 m above ground level. The approximate area of the SOI is shown by the gray circle.

The third trajectory approach used in this analysis was HYSPLIT trajectory frequency. In this option, a trajectory from a single location and height starts every three hours. Using a continuous 0.25-degree grid, the frequency of trajectories passing through each grid cell is totaled and then normalized by the total number of trajectories. [Figure 3-37](#) shows 96-hour backward trajectory frequency plots starting from the Las Vegas Valley at 3000 m agl at 05:00 UTC on May 29, 2020 (i.e., 22:00 PST on May 28). The trajectory frequency plot yields similar results to those from the back trajectory matrix; transported air impacting the Las Vegas Valley on May 28, 2020, partly came from the southern Idaho and Utah area.

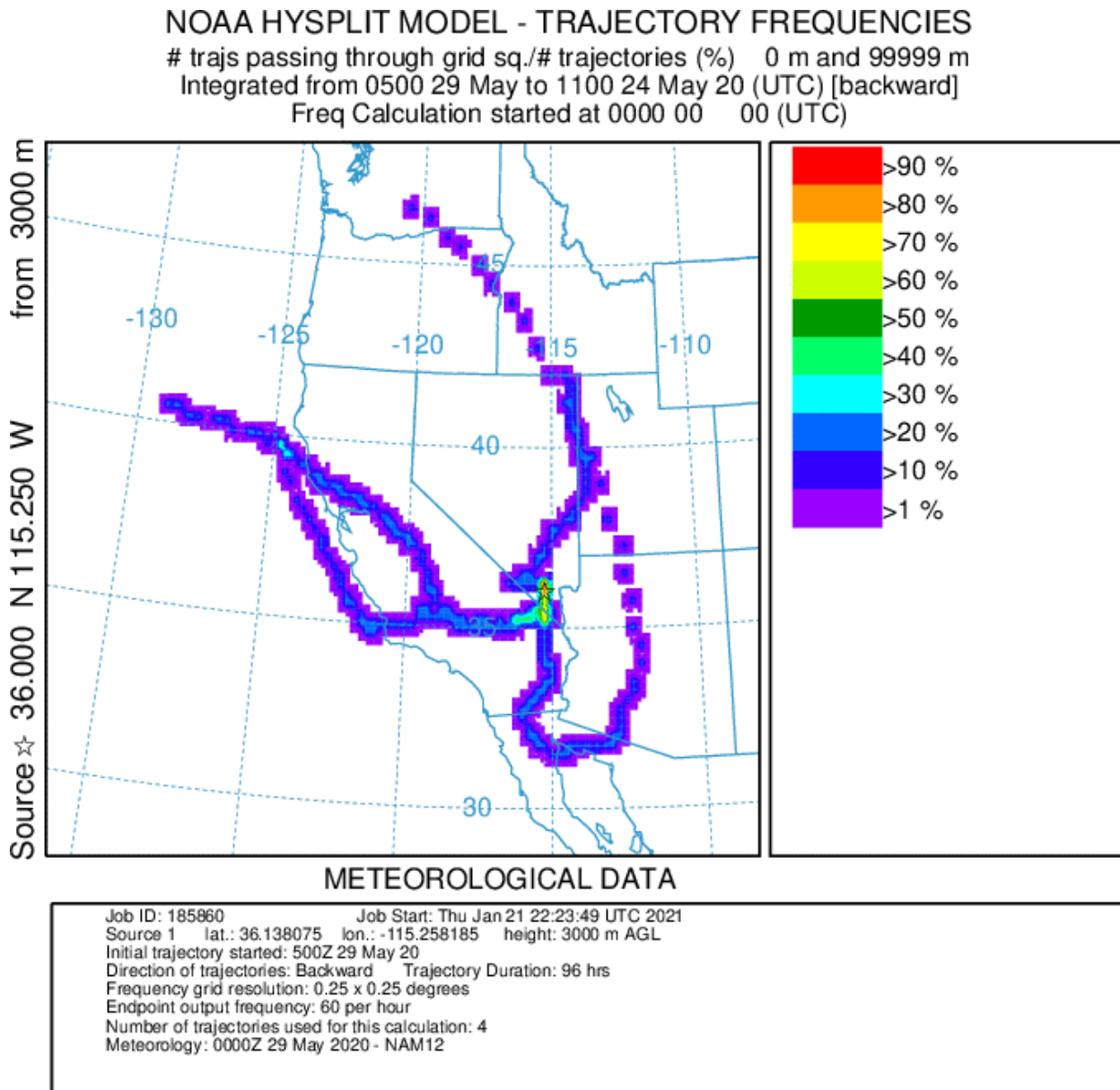


Figure 3-37. 72-hour HYSPLIT back trajectories frequency from Las Vegas Valley, ending on May 29, 2020. NAM 12 km back trajectories are shown for 3000 m above ground level. The colors within the frequency plot indicate the percent of trajectories that pass through a grid square.

Forward trajectories were run from the approximate area of the stratospheric intrusion starting at a height of 5000 m agl at 12:00 UTC on May 25 ([Figure 3-38](#)). These trajectories show the transport of air from the approximate area of the stratospheric intrusion toward Clark County. Trajectories become more uncertain as modeled time increases, but these trajectories show the same quick southward transport east of Clark County, then air circling back northward toward western Arizona and Clark County. This shows the same transport pattern as [Figures 3-35](#) and [3-36](#) even though the

end of the trajectories does not specifically enter Clark County by the event date. The back trajectories initiated in Figures 3-35 and 3-36 would be more accurate for nearer to the event date than this forward trajectory. These forward trajectories, combined with the back trajectories shown above, further support the transport of stratospheric air from southern Idaho to Clark County, Nevada.

NOAA HYSPLIT MODEL Forward trajectories starting at 1200 UTC 25 May 20 NAM Meteorological Data

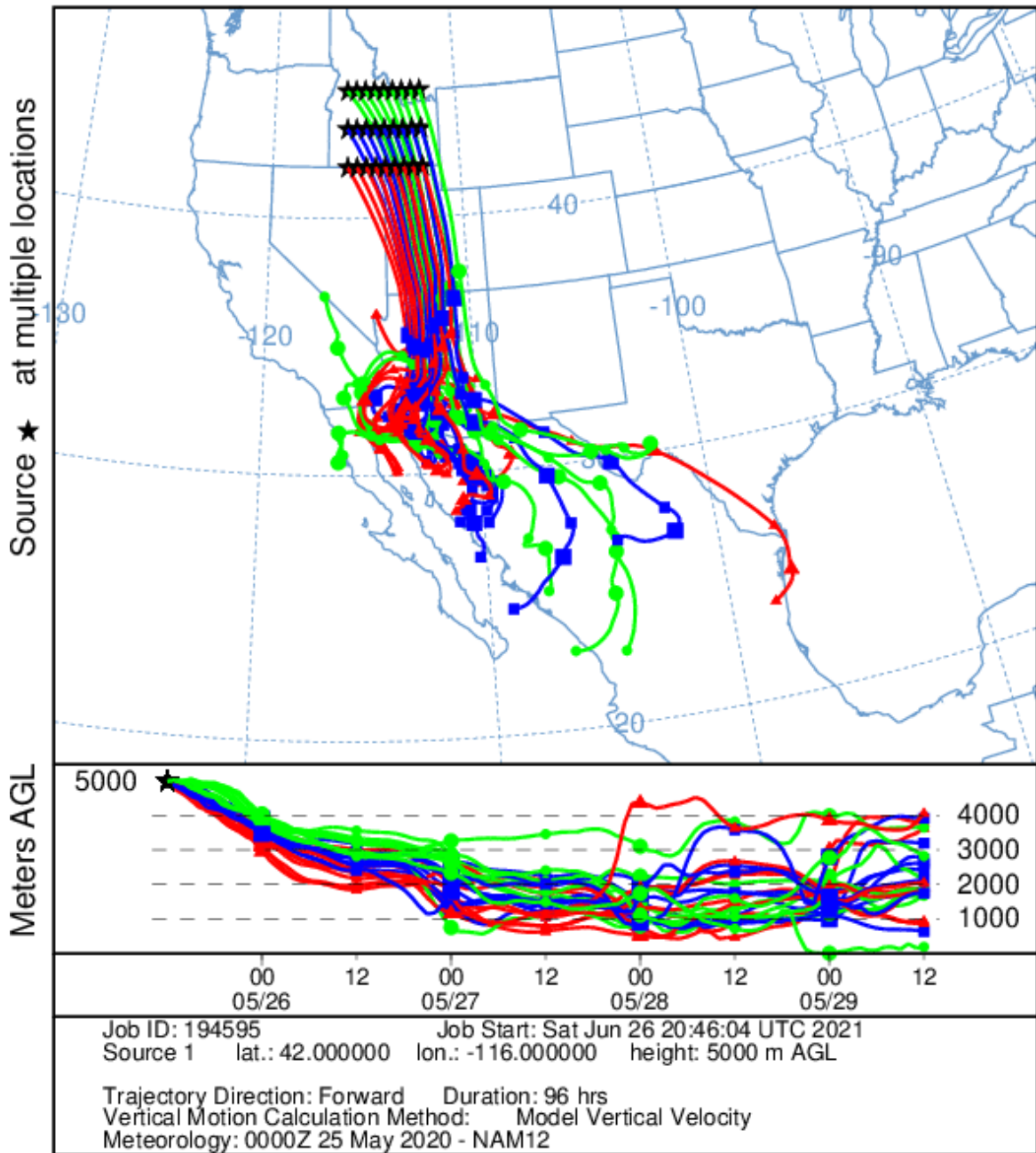


Figure 3-38. 96-hour HYSPLIT forward trajectories from the stratospheric intrusion source region initiated on May 25, 2020, at 12:00 UTC. NAM 12 km forward trajectories were initiated at 5000 m above ground level.

3.3.2 Measurements of Tropospheric Mixing

Atmospheric soundings in the form of skew-T diagrams can provide an initial view into the extent of vertical mixing between the stratosphere and the troposphere. Some indications of stratospheric intrusion revealed by a sequence of these atmospheric soundings include the transport of dry, stratospheric air to lower elevations, a lowering of the tropopause, and favorable conditions for mixing between the surface and higher altitudes. An example of a skew-T diagram, shown in **Figure 3-39**, shows the change in air temperature (T) and dewpoint temperature (T_d) as a function of altitude and corresponding pressure level. Drier air is indicated by a separation between T and T_d (e.g. orange-boxed region). The tropopause is indicated by temperatures reaching a minimum before increasing with height and represents the boundary between the troposphere and the stratosphere. The air temperature profile follows the dry adiabatic lapse rate (green curve), indicating a well-mixed, dry layer from the surface up to 500 hPa. Dry adiabats identify the slope at which the temperature lapse rate is absolutely or conditionally unstable. Moist adiabats are drawn in blue and identify the slope at which the temperature lapse rate indicates conditionally unstable or absolutely stable air.

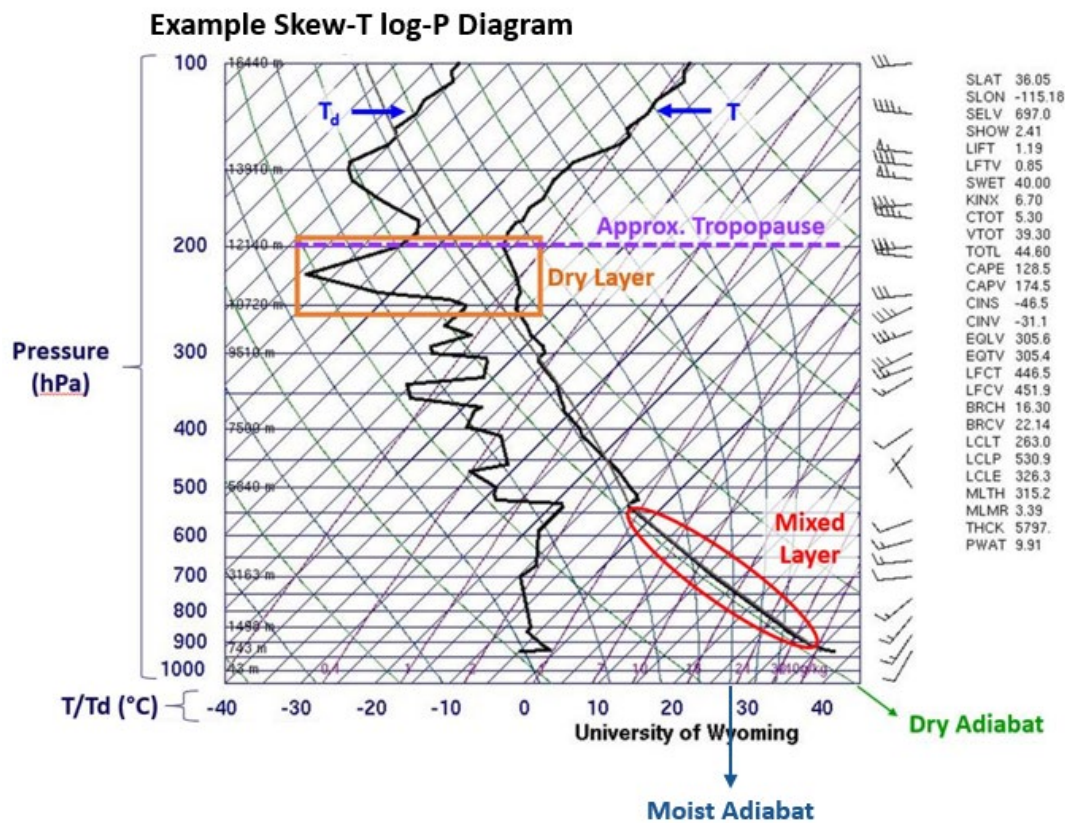


Figure 3-39. An example skew-T diagram with labelled features. Red circle denotes deep mixed layer. Orange box denotes relatively dry layer of air. The approximate (cold-point temperature) tropopause is denoted by the dashed purple line. Dry and moist adiabats are drawn as green and blue lines at a range of initial surface temperatures.

Our analysis of atmospheric soundings during the May 28 event period was guided by an example included in the EPA SOI Guidance that displayed skew-T diagrams from a documented stratospheric intrusion over Grand Junction, Colorado, in 2017. This example included two skew-T diagrams, shown in [Figure 3-40](#) of this report, with particular characteristics that suggest viable tropospheric mixing to facilitate vertical transport of ozone injected into the mid-troposphere to the surface. The two skew-T diagrams are characterized primarily by the large, very dry layer at a height greater than approximately 5 km above mean sea level, or 3.5 km above ground level. A temperature inversion, observed from the 00:00 UTC sounding, likely prevented the dry air above from mixing down into the lower troposphere. During the 12:00 UTC sounding 12 hours after the 00:00 UTC sounding and 12 hours before the exceedances occurred, it is clear from the widening of the gap between the dewpoint temperature profile and the temperature profile that dry air mixed into the lower troposphere. The base of the very dry mixed layer also moved down into the atmosphere by about 500 m. Further, the temperature lapse rate of the lower troposphere was approximately dry-adiabatic, indicating that the lower PBL was well-mixed. These skew-Ts provide an example of an SOI above an area and being mixed down into the boundary layer. In the Grand Junction example, the SOI affected surface ozone concentrations and caused an exceedance of the ozone NAAQS.

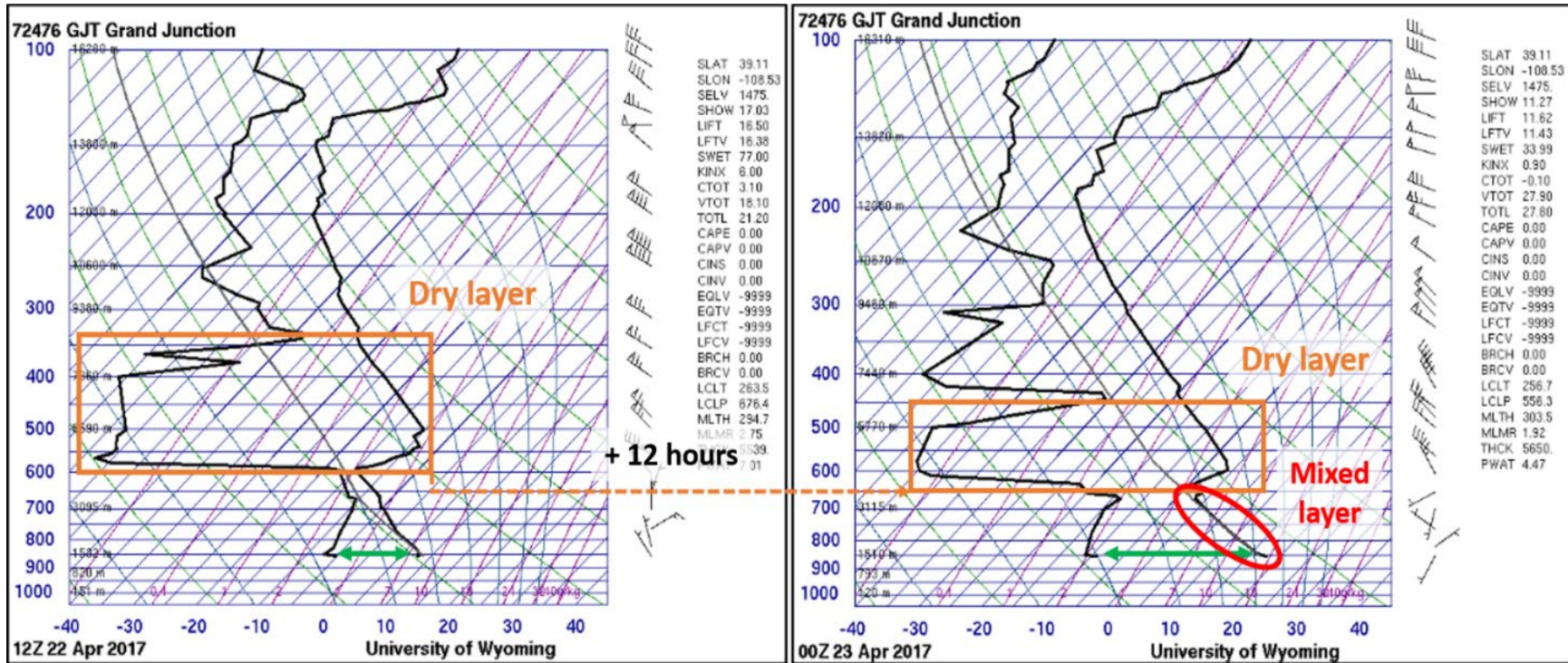


Figure 3-40 Skew-T diagrams for 12:00 UTC (left) on April 22, 2017, and 00:00 UTC (right) April 23, 2017, at Grand Junction, Colorado. Orange boxes denote the very dry layer. The red circle denotes the mixed layer. Green arrows indicate the intrusion of very dry air to the surface. The figures were collected directly from EPA's "Guidance on the Preparation of Exceptional Events Demonstrations for Stratospheric Ozone Intrusions."

We examined skew-T diagrams from four National Weather Service forecasting offices in the western United States: Salt Lake City, Utah (SLC), Flagstaff, Arizona (FGZ), Tucson, Arizona (TUS), and Las Vegas, Nevada (VEF), which were along the trajectories shown in Section 3.3.1. The approximate location of each office is shown in **Figure 3-41** along with the location of Clark County (shaded in yellow).



Figure 3-41. The locations of four National Weather Service offices in the western United States. SLC, FGZ, and TUS are located along the trajectory of air from the region of stratosphere-to-troposphere exchange to Clark County. VEF is located in Las Vegas, near the sites that measured ozone exceedances on May 28. Clark County is shaded in yellow.

Based on the HYSPLIT trajectories presented in Section 3.3.1, SLC lies along several pathways between the SOI source region and Clark County during the days leading up to the ozone exceedance on May 28. Skew-T soundings from SLC on May 26 and May 27 at 00:00 UTC are shown in **Figure 3-42**, according to the timelines presented in Figures 3-35 and 3-36. Over this 24-hour period, a layer of very dry air persists in the mid-to-upper troposphere (boxed in orange). This indicates that dry, stratospheric air was injected into the troposphere over Idaho and transported across this region, consistent with the HYSPLIT trajectories.

The HYSPLIT matrix presented in Figure 3-36 shows air passing through Arizona on its eventual trajectory towards Clark County. Skew-T soundings from FGZ on May 26 and May 27 at 00:00 UTC are shown in [Figure 3-43](#). Dry air has descended into the mid-troposphere, and this significant dry layer persists throughout this 24-hour period (boxed in orange). As air is transported further south, the soundings over TUS on May 26 and 27 at 00:00 UTC also exhibit this mid-troposphere dry layer ([Figure 3-44](#)). In the layer from the surface to 650 hPa (circled in red) in both soundings, the temperature lapse rate follows a dry adiabatic lapse rate. This condition, where the slope of the temperature lapse rate parallels the dry adiabatic lapse rate (green curve), is characteristic of a well-mixed layer. A deep mixing layer can be seen over Flagstaff and Tucson during this period, providing a mechanism for air in the mid-troposphere to mix downwards to lower altitudes.

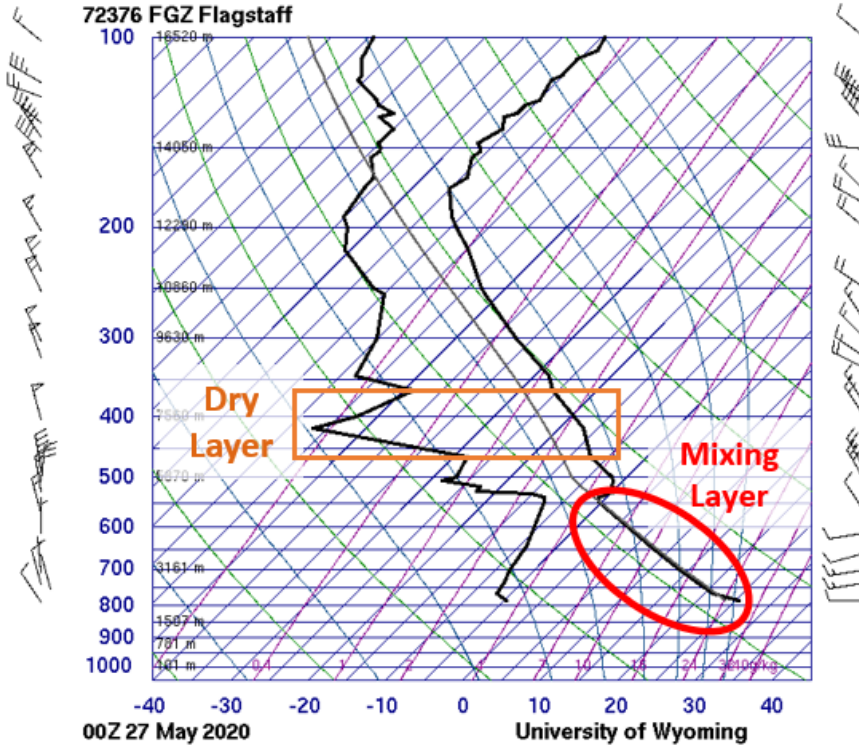
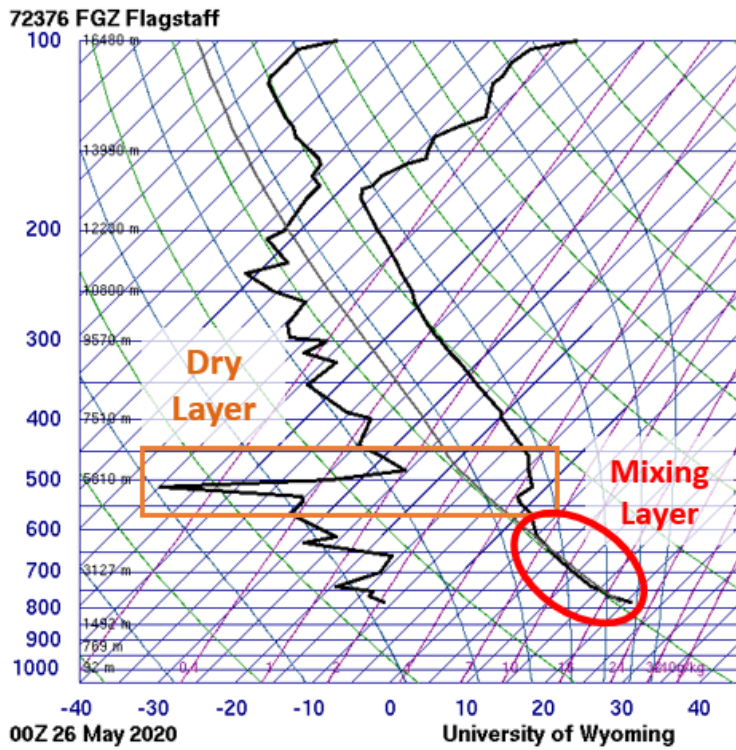


Figure 3-43. Skew-T soundings launched from the FGZ National Weather Service office on May 26 and 27, 2020, at 0:00 UTC (May 25 and 26 at 4:00 p.m. local time). Dry layers of air are boxed and labeled in orange.

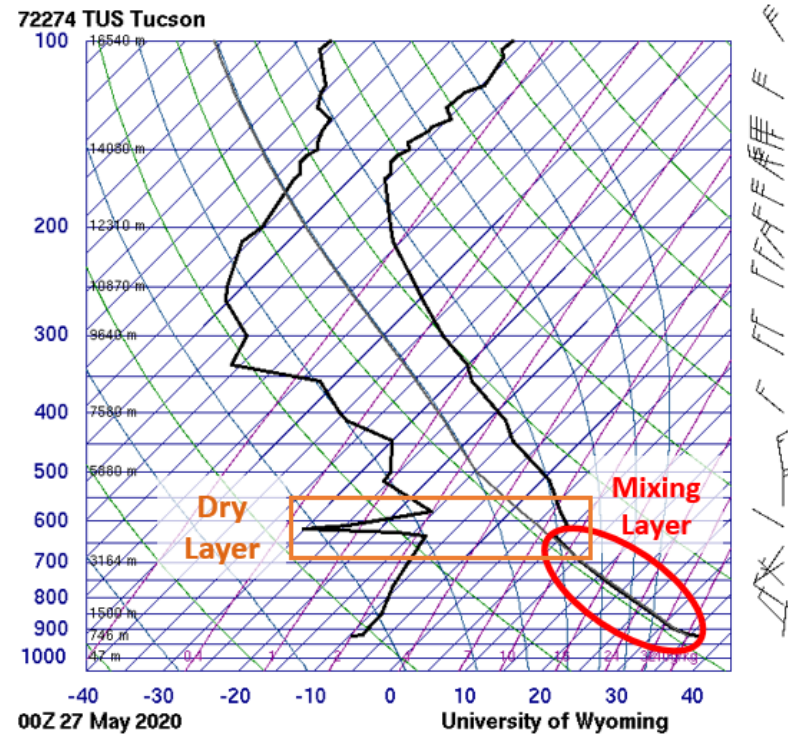
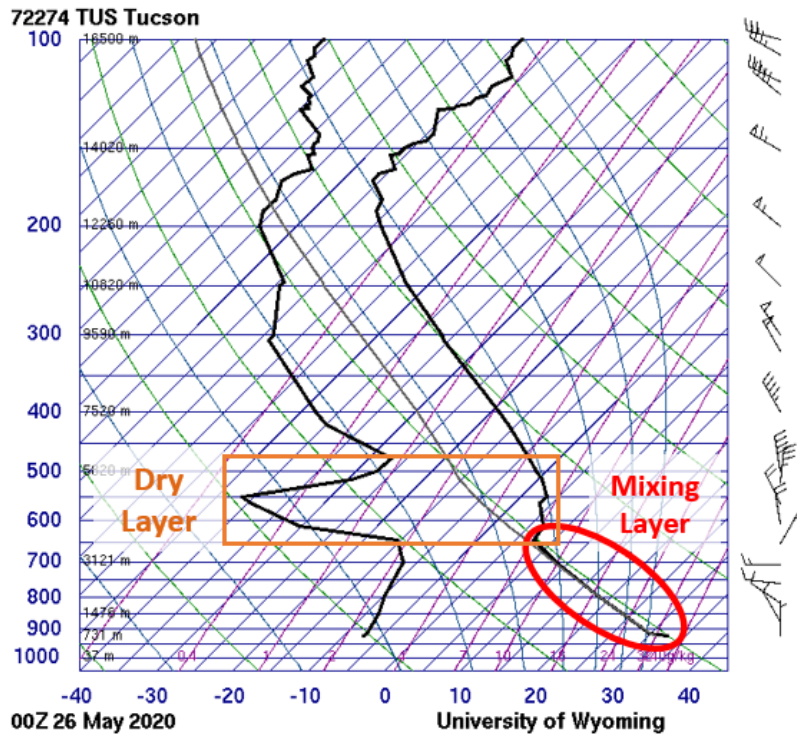


Figure 3-44. Skew-T soundings launched from the TUS National Weather Service office on May 26 and 27, 2020, at 0:00 UTC (May 25 and 26 at 4:00 p.m. local time). Dry layers of air are boxed and labeled in orange.

Figure 3-45 shows the skew-T diagram for soundings launched from Las Vegas between 0:00 UTC on May 28 and 0:00 UTC on May 29 (May 27 16:00 PST to May 28 16:00 PST). The May 29 sounding is the observation closest to the exceedance event. On May 28, a very large dry layer near 500 hPa (just above the mixing layer) can be seen boxed in orange. The comparison of the temperature lapse rate against the dry adiabatic lapse rate (green) reveals conditions that are well-suited for vertical mixing throughout the mid-to-lower troposphere, up to the 500 hPa level (circled in red). This suggests that air entrained from higher altitudes into these layers could be mixed toward the surface. These soundings provide supporting evidence to the hypothesis that dry, stratospheric air entrained into the free troposphere over Idaho was transported southward across Utah and Arizona, and then back northward to Clark County between May 25 and 28 as shown in the modeled HYSPLIT trajectories in Section 3.3.1.

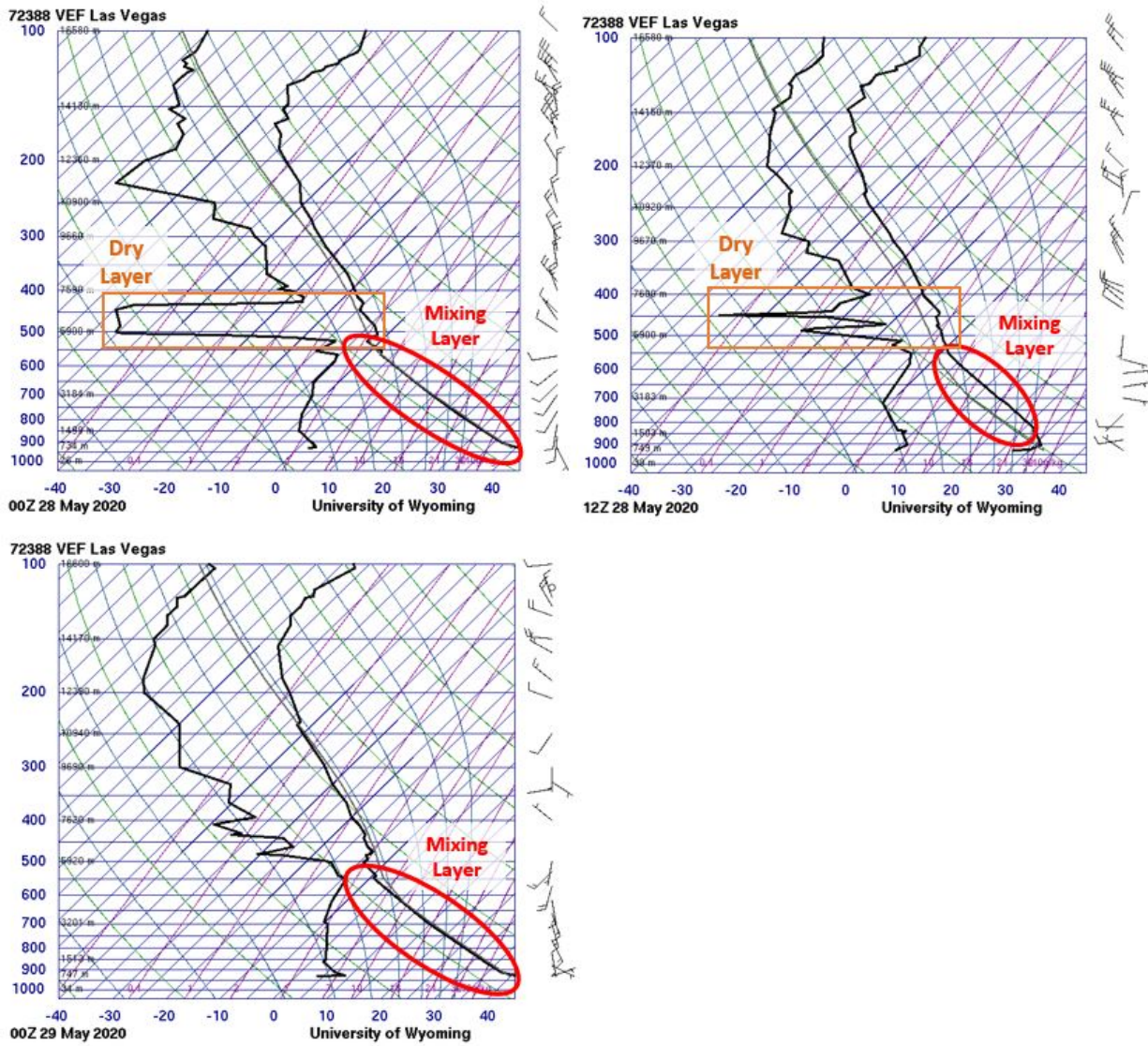


Figure 3-45. Skew-T soundings launched from the VEF National Weather Service office on May 28 at 00:00 UTC, May 28 at 12:00 UTC, and May 29, 2020, at 0:00 UTC (4:00 p.m. on May 27, 4:00 a.m. on May 28, and 4:00 p.m. on May 28 local time). Dry layers of air are boxed and labeled in orange. A layer of well-mixed air is circled in red.

Vertical profiles of ozone are available from NOAA's Chemical Sciences Laboratory site at Boulder, CO. The Chemical Science Laboratory collects routine vertical measurements of ozone via the TOPAZ lidar. HYSPLIT back-trajectories initialized on May 26 at 18:00 UTC from Boulder ([Figure 3-46](#)) show that the air mass passed directly through the region of stratosphere-to-troposphere exchange over Idaho the day before, as identified in Section 3.2. [Figure 3-47](#) shows the TOPAZ ozone profile from May 26, 2020. Starting at 11:00 MST (18:00 UTC), a layer of ozone is observed between 6 and 8 km above sea level (asl) that is above 100 ppb in concentration. Over the next few hours, the elevation of this enhanced ozone feature decreases and concentrations between 70 and 80 ppb are seen as low as 5 km asl. This vertical profile of ozone provides evidence to support the hypothesis that stratospheric air was injected into the mid-troposphere over Idaho and transported southward in the days leading up to the exceedance event in Clark County.

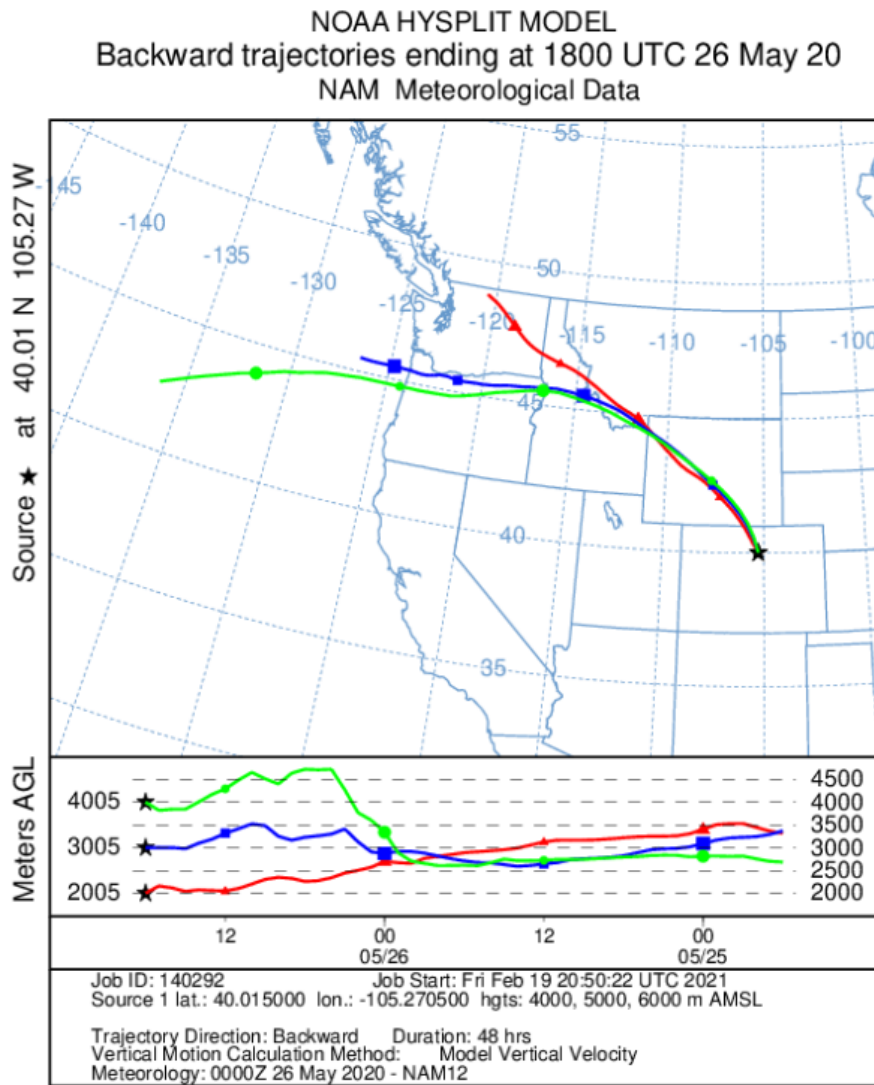


Figure 3-46. 48-hour HYSPLIT back trajectories from Boulder (40.01 degrees N, 105.27 degrees W), ending on May 26, 2020, at 18:00 UTC. NAM 12 km back trajectories are shown for 205 m (red), 305 m (blue), and 4005 m (blue) above ground level.

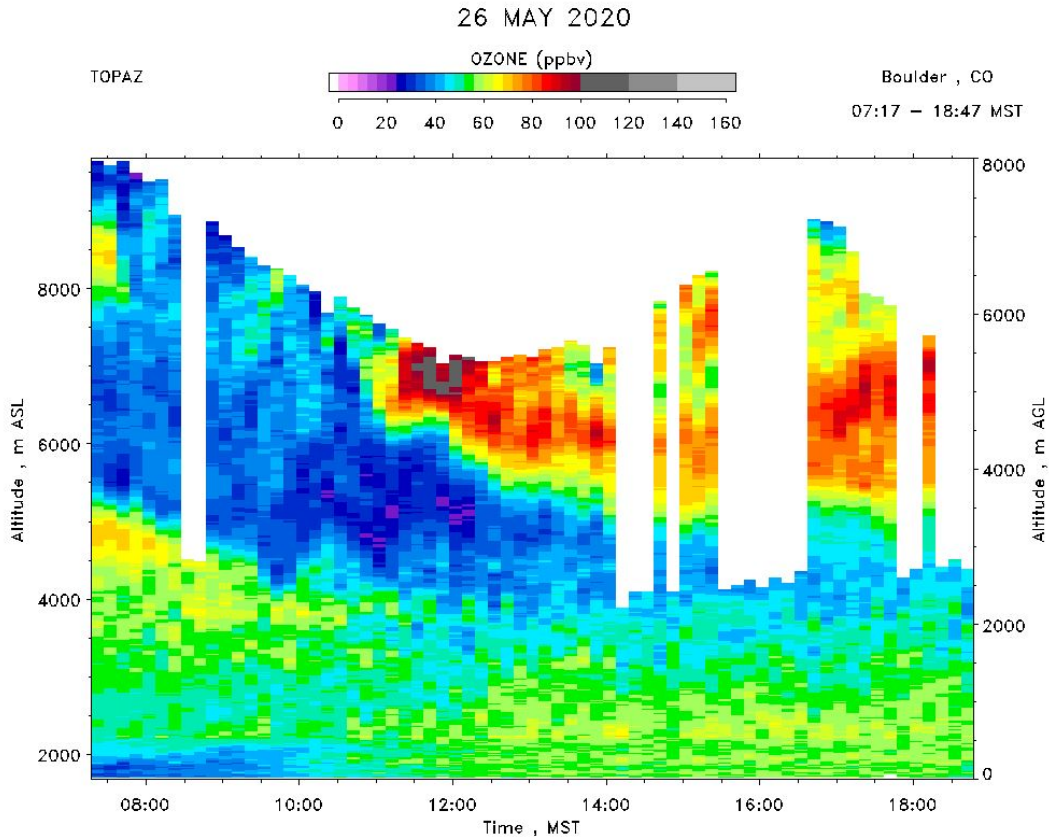


Figure 3-47. Vertical profile of ozone captured at NOAA's Chemical Sciences Laboratory in Boulder, CO on May 26, 2020, between 10:00 and 20:00 MST (May 26 at 16:00 UTC to May 27 at 2:00 UTC). Data was collected by the TOPAZ lidar. The left y-axis shows altitude above sea level. The right y-axis shows altitude above ground level.

The combination of the skew-T diagrams, vertical profiles of ozone, and trajectories to and from area with the SOI to Clark County provide evidence for the free tropospheric transport of ozone enhancements towards the deep mixed layer and the surface at Clark County on May 28, 2020.

3.3.3 Model Results of Meteorological Conditions

The upper-level wind direction indicates stratospheric air originating over Idaho moved south along the west side of an upper-level trough, identified by the "v" shape of the brown height contours (**Figure 3-48**). The high pressure over southern California on May 26 and May 27 induced clockwise upper-level flow southward. On May 28, Clark County, Nevada, was within an upper-level ridge, identified by the upside-down "v" shape of the brown height contours, associated with high pressure and air flow from the south. On May 28, there is evidence of an omega-block, in which two low pressure centers occur to the east and west of a high-pressure ridge. This is associated with warm temperatures and mild, stagnant wind conditions in the upper atmosphere.

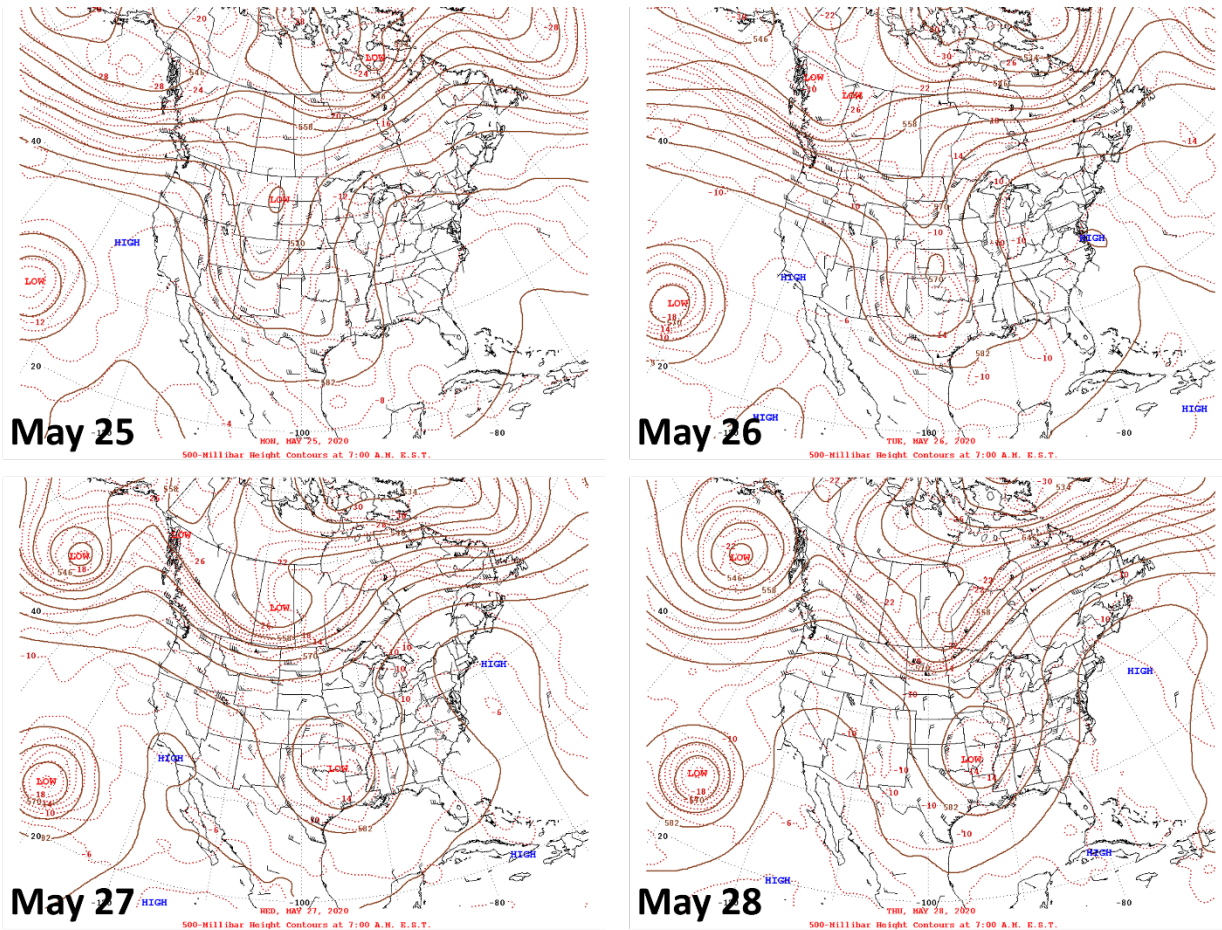


Figure 3-48. Daily upper-level meteorological maps for the three days leading up to the EE and during the May 28 EE.

The corridor of surface high pressure from Idaho to New Mexico on May 25 and May 26 implies fair weather with slow winds (**Figure 3-49**). The surface low pressure over Clark County, Nevada on May 26, May 27, and May 28 provided conditions favorable for vertical mixing. In addition, the high surface temperature and stagnant wind conditions are associated with buoyant surface air that further facilitated vertical mixing within the boundary layer over Clark County, Nevada.

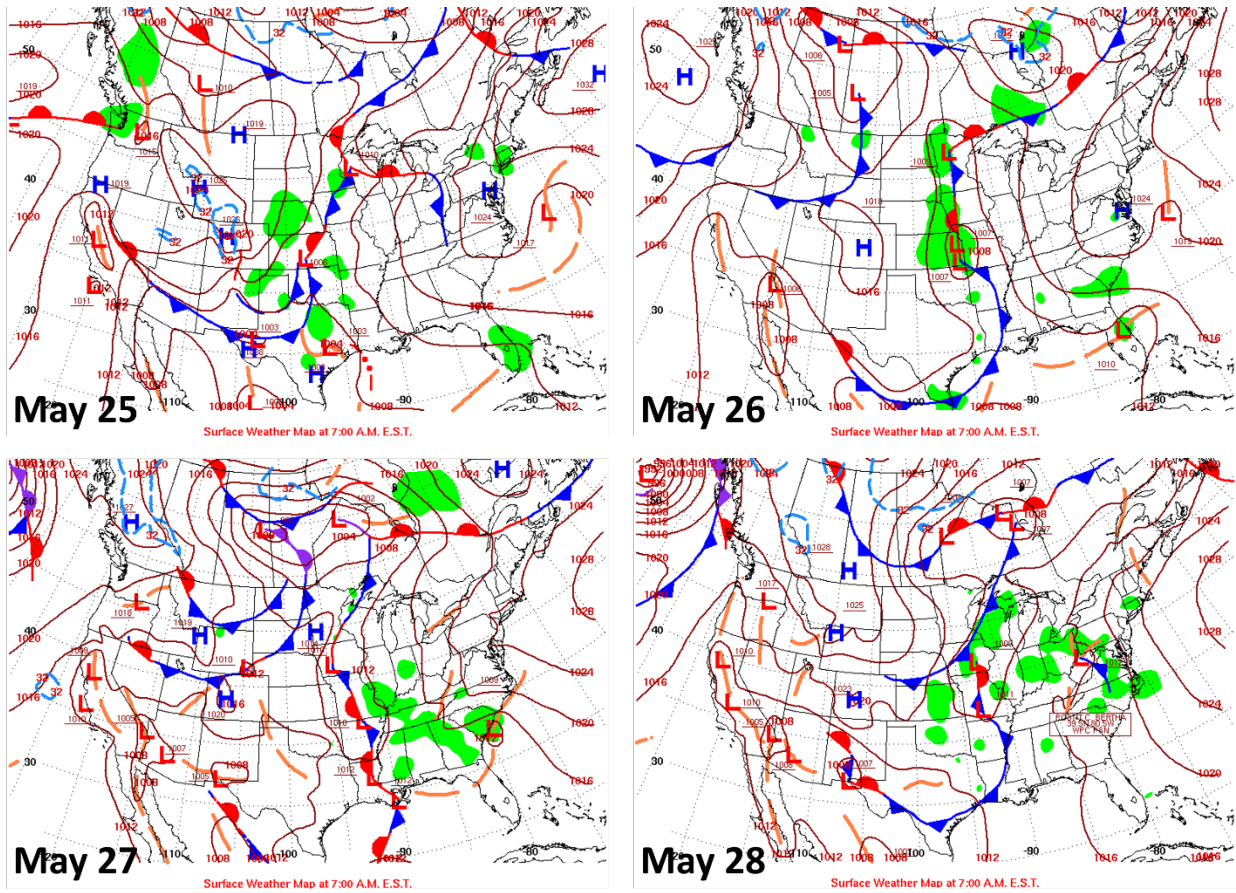


Figure 3-49. Daily surface meteorological maps for the three days leading up to the EE and during the May 28 EE.

The planetary boundary layer denotes the atmospheric layer closest to the surface, and the height of the planetary boundary layer conveys to what vertical extent the surface air characteristics prevail. On the afternoon of May 26, the planetary boundary layer heights were 3-4 km across southern California and western Arizona, indicating a deep, well-mixed layer southeast of Clark County, Nevada (Figure 3-50). These model results are consistent with the skew-T mixed layers heights at Flagstaff and Tuscan (Figures 3-43 and 3-44). On May 28, the planetary boundary layer height for the southern region of Clark County, Nevada, reached 5 km in altitude, consistent with the skew-T 650 hPa mixed layer (Figure 3-51). This observation shows the presence of a very deep, well-mixed layer of air over Clark County, Nevada, on May 28.

Ozone-rich stratospheric air originating over Idaho moved southward along the western edge of an upper-level ridge on May 25 and May 26 into Arizona. An upper-level omega-block in the region led to persistent upper-level high pressure over Clark County, Nevada, on May 28. The surface low-pressure system and high temperature indicates conditions favoring vertical mixing within the planetary boundary layer and buoyant air from the surface. Although photochemical production

likely occurred on May 28, this analysis provides evidence that meteorological conditions were favorable for vertical mixing of ozone to the surface on May 28 in the Las Vegas area.

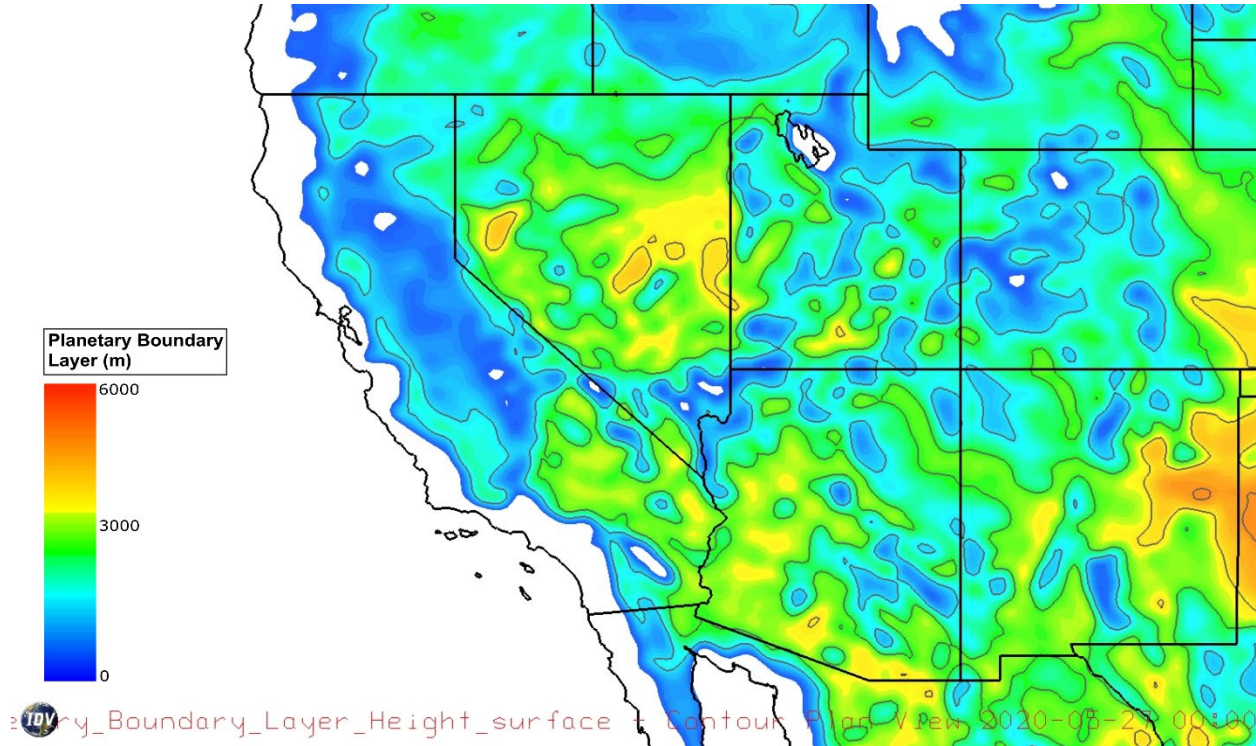


Figure 3-50. PBL height contour map based on the NAM model for May 26, 2020, at 16:00 PST. The gray lines denote PBL heights above 2 km altitude in 1 km increments.

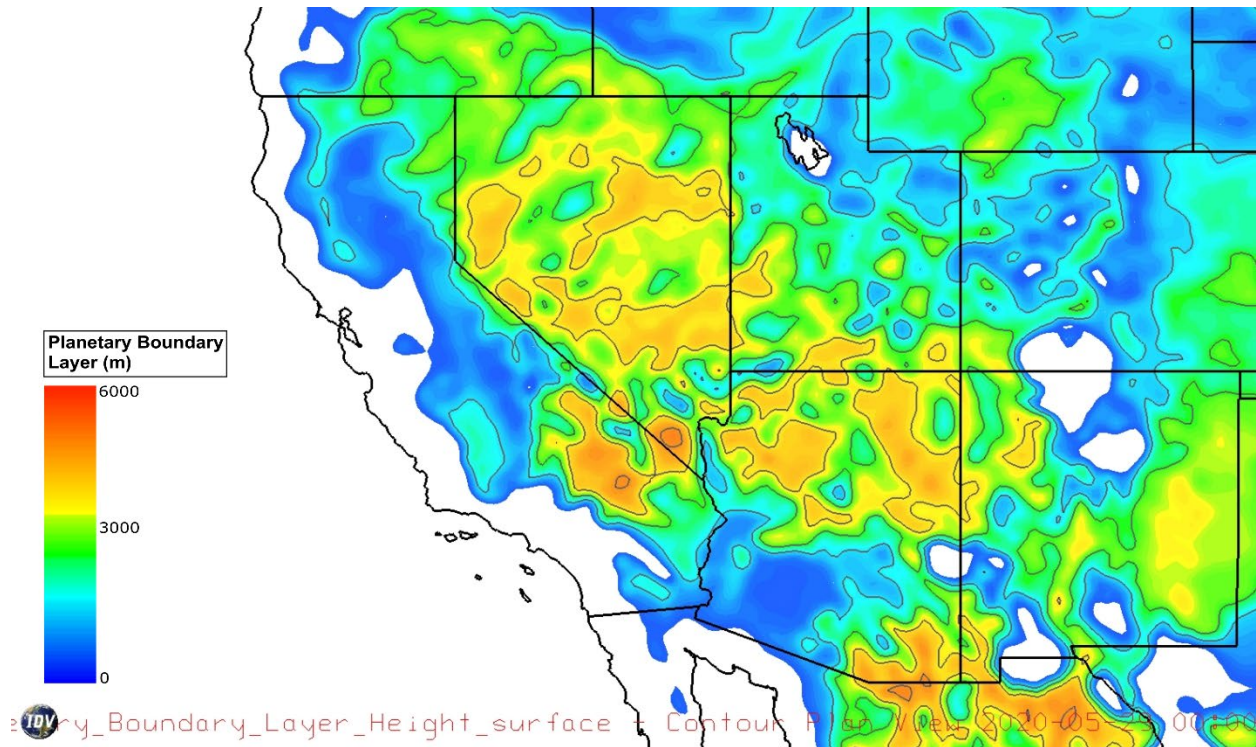


Figure 3-51. PBL height contour map based on the NAM model for May 28, 2020, at 16:00 PST. The gray lines denote PBL heights above 2 km altitude in 1 km increments.

3.4 Impacts of the Intrusion at the Surface

As stated in Sections 3.2.1, 3.2.2, and 3.3.2, stratospheric air is characterized by high ozone content and low water vapor content relative to tropospheric air. Therefore, stratospheric intrusion and subsequent transport of stratospheric air to the surface should cause surface ozone and absolute humidity concentrations to have characteristics similar to stratospheric air.

Figure 3-52 shows observations from May 28 and a typical diurnal profile of ozone concentrations, temperature, and absolute humidity observed at the Jerome Mack station for May 2015-2019. Absolute humidity has a relatively constant diurnal profile in May, hovering between 5 to 7 grams per cubic meter with a slight dip in the afternoon. The diurnal profile of ozone concentrations in May shows a trough in the early morning, followed by a peak throughout the afternoon, and a gradual decrease into the evening. Temperature shows a similar diurnal profile to ozone, reaching a maximum in the late afternoon and a minimum in the early morning. Temperature on May 28 was very high compared to the 5-year May average, maintaining a magnitude above the 95th percentile throughout the day. Absolute humidity, rather than relative humidity, is displayed in Figure 3-52 to decouple the measurement of humidity from temperature. From mid-morning through midnight, on May 28, absolute humidity values were lower than the five-year May average and reached magnitudes below the 5th percentile of May observations for most of the afternoon. Absolute

humidity values on May 28 were below 1 gram per cubic meter for much of the afternoon. During the late morning on May 28, ozone concentrations were briefly higher than the highest 95th percentile of May observations and also higher than the 5-year May average (the Jerome Mack monitoring site did not record a NAAQS exceedance on May 28). The extremely low absolute humidity values and high ozone concentrations provide evidence that stratospheric air reached the lower troposphere in Las Vegas on May 28.

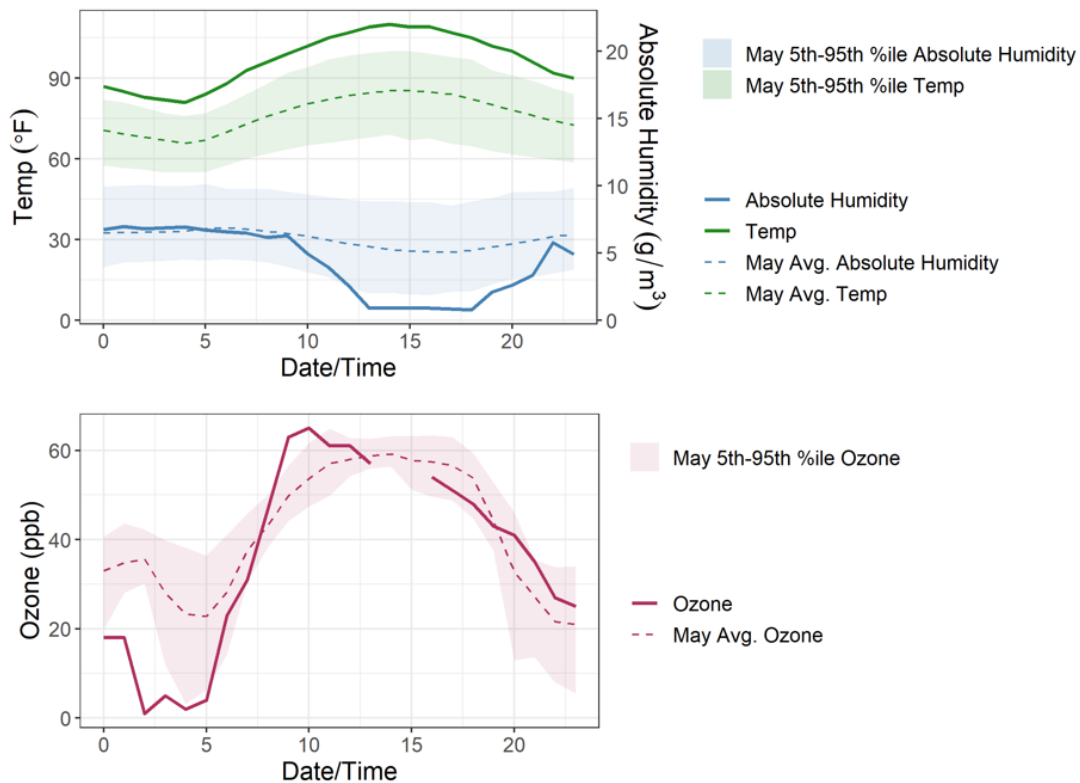


Figure 3-52. (Top plot) Diurnal profile of temperature (green) and absolute humidity (blue) at Jerome Mack, including temperature and absolute humidity values on May 28 and the 5-year May averages (dotted lines). (Bottom plot) Diurnal profile of ozone at Jerome Mack on May 28. Shaded ribbons represent the five-year 5th-95th percentile range.

Figures 3-53 through 3-56 show observations from May 28 and a typical diurnal profile of ozone concentrations from the Paul Meyer and Walter Johnson stations. Nitric oxide (NO) and nitrogen dioxide (NO₂) observations are available only from two non-exceedance sites in Clark County: Jerome Mack and Joe Neal. Plots for these two sites are included in this section to provide a reference for regional NO and NO₂ concentrations in Clark County on the day of the event, though these sites should not serve as a direct proxy for concentrations at either event site due to local variation. NO₂ concentrations in May usually reach a peak in the early to mid-morning and gradually decrease throughout the day, followed by a gradual increase in the later evening. The diurnal profile of NO is similar to NO₂ but does not have a distinct increase into the late evening. NO_x (NO + NO₂) is an

important ingredient (in addition to volatile organic compounds [VOCs] and sunlight) in the creation of ozone in the troposphere. To determine whether the May 28 event was predominately due to photochemical processes at the surface, we examine whether NO_x was abnormally high during this event.

During the afternoon on May 28, ozone concentrations at Paul Meyer and Walter Johnson were higher than the seasonal 95th percentile concentrations. Jerome Mack and Joe Neal monitoring sites also showed abnormally high ozone concentrations on May 28, though magnitudes remained over the NAAQS for a shorter period than at either exceedance site. During this time, NO and NO₂ concentrations were approximately average relative to seasonal average at both monitoring sites. The average NO and NO₂ concentrations at Jerome Mack and Joe Neal during the May 28 event provide evidence that photochemistry alone was not likely responsible for the EE in Clark County on May 28.

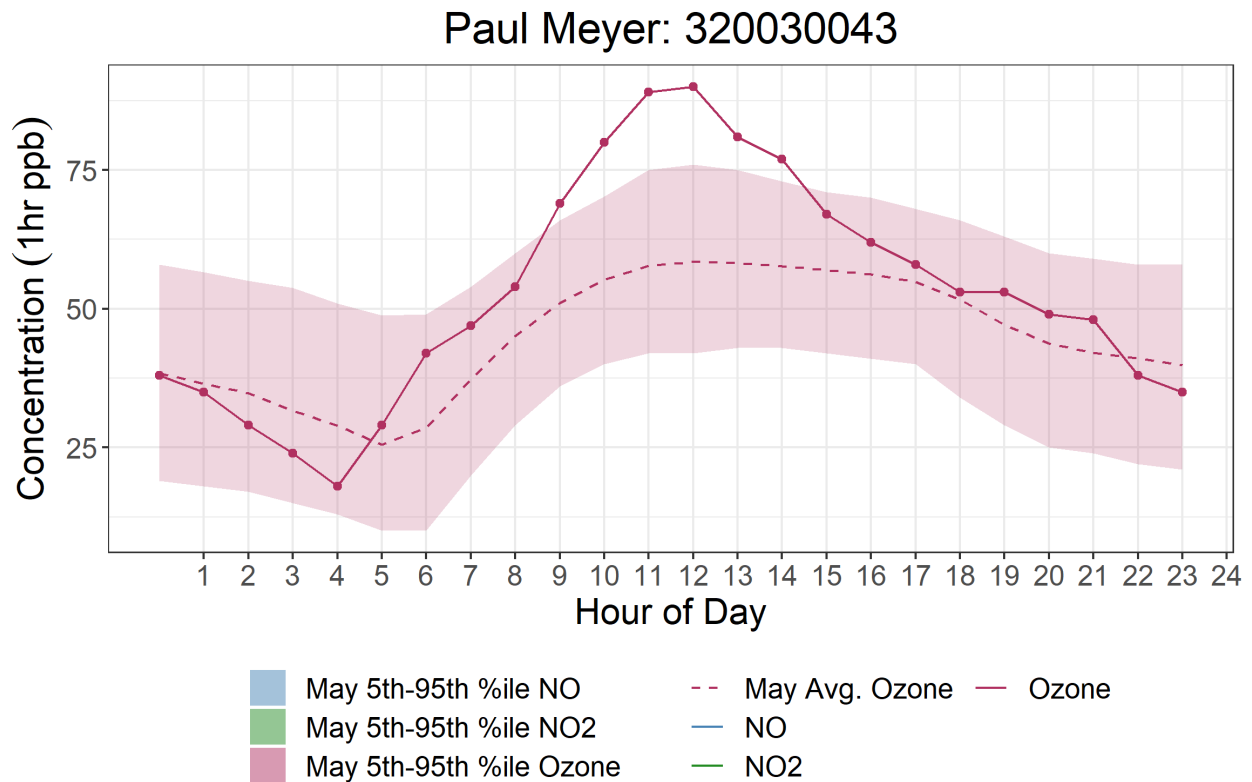


Figure 3-53. Diurnal profile of ozone concentrations (red) at the Paul Meyer site on May 28 and the 5-year seasonal average ozone (dotted lines). Shaded ribbons represent the five-year 5th-95th percentile range. NO and NO₂ data are not available at Paul Meyer.

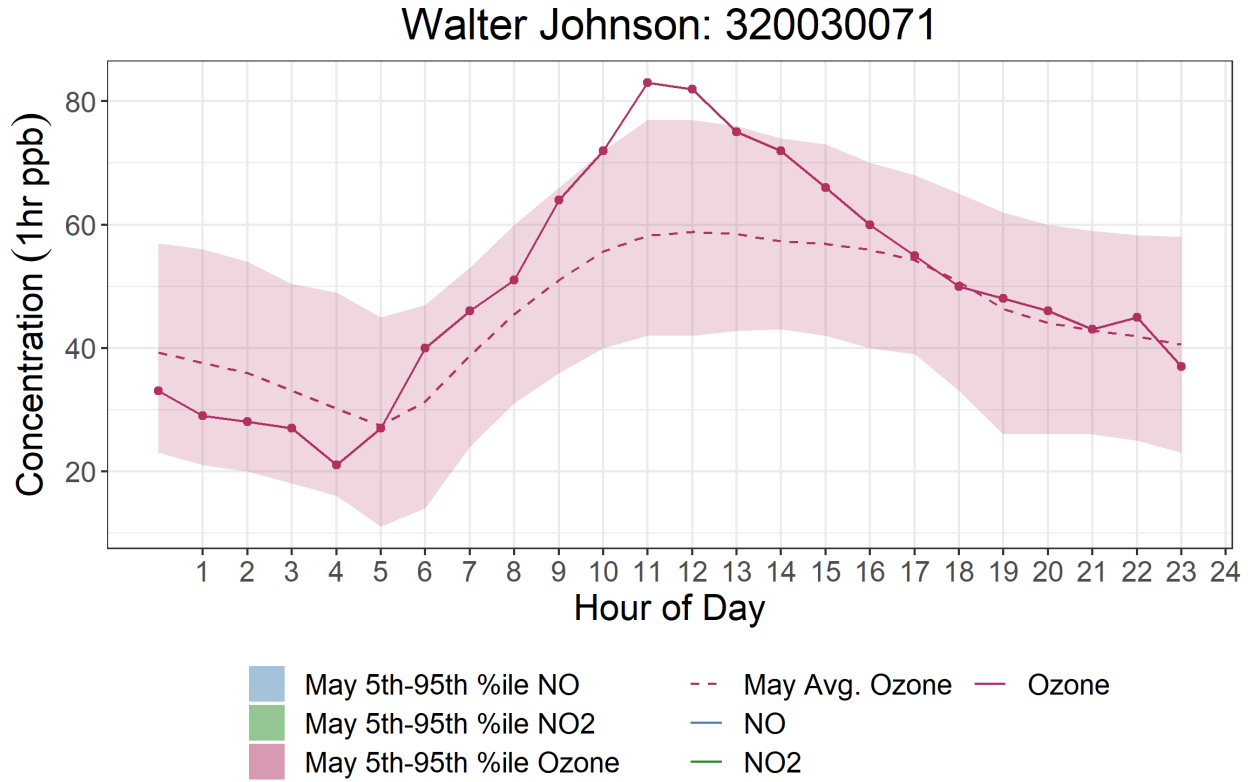


Figure 3-54. Diurnal profile of ozone concentrations (red) at the Walter Johnson site on May 28 and the 5-year seasonal average ozone (dotted lines). Shaded ribbons represent the five-year 5th-95th percentile range. NO and NO₂ data are not available at Walter Johnson.

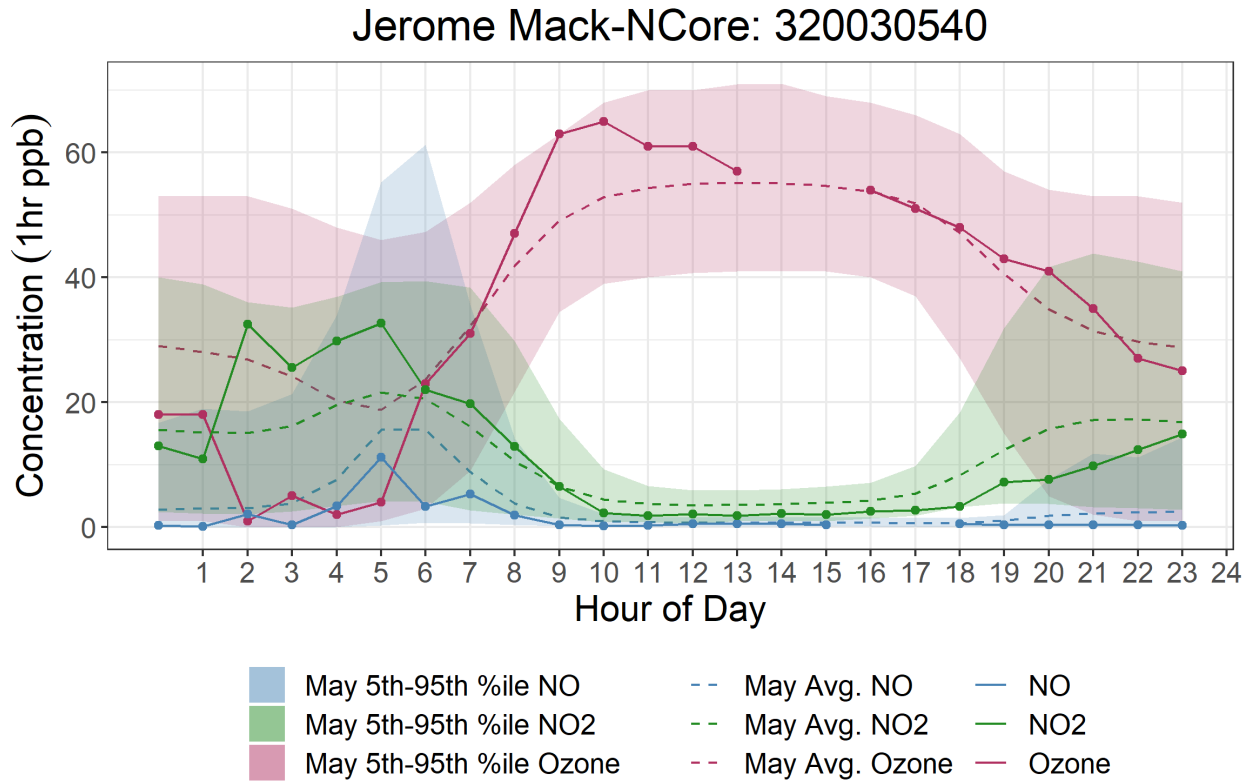


Figure 3-55. Diurnal profile of ozone concentrations (red), nitrogen dioxide (NO₂) concentrations (green), and nitric oxide (NO) concentrations (blue) at the Jerome Mack reference site in Clark County, on May 28 and the seasonal averages (dotted lines). Shaded ribbons represent the 5th-95th percentile range. NO₂ data is available from 2017-2020, and NO and ozone data is available from 2015-2020.

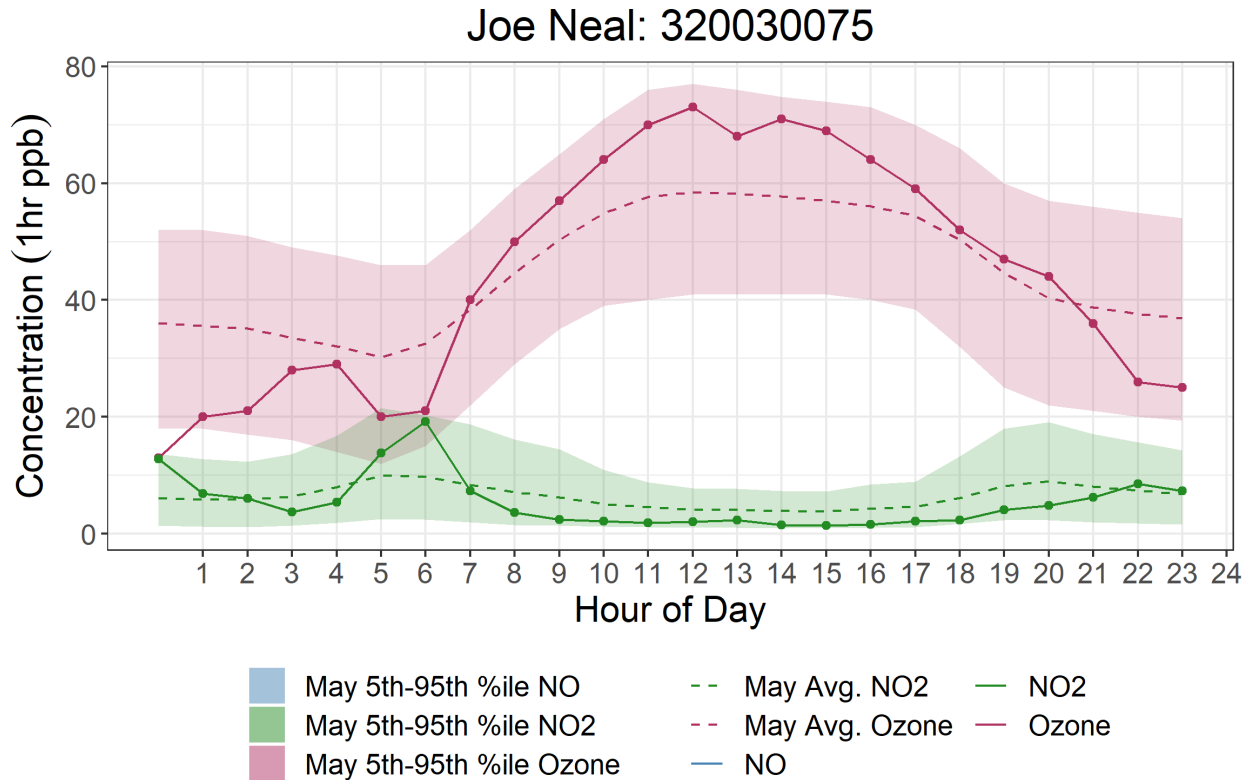


Figure 3-56. Diurnal profile of ozone concentrations (red) and nitrogen dioxide (NO₂) concentrations (green) at the Joe Neal site in Clark County on May 28 and the seasonal averages (dotted lines). Shaded ribbons represent the 5th-95th percentile range. NO₂ data and ozone data is available from 2015-2020.

A map of observed MDA8 ozone concentrations shows elevated ozone levels throughout southern California to the east of Los Angeles, in the Central Valley, and a subset of southern Nevada sites within the Clark County border (Figure 3-57). Stations with recorded NAAQS ozone exceedances are colored orange or red. Three stations located in southern California reached MDA8 ozone concentrations between 86–106 ppb. In Clark County, the Paul Meyer and Walter Johnson stations exceeded the 2015 ozone NAAQS of 70 ppb on May 28, 2020. They were surrounded by stations that observed elevated MDA8 ozone concentrations (55 to <71 ppb) but did not exceed the NAAQS. The highest observed value of 76 ppb was recorded at the Paul Meyer station. The Jean and Indian Springs stations often act as indicators of background ozone concentrations because they are not within the Las Vegas metropolitan area. Although the Indian Springs and Jean stations did not exceed NAAQS on May 28, both stations reached a moderate concentration of approximately 60 ppb. Based on the trajectories shown in Section 3.3.1, we found that on the May 28 event, air arrived from the south. Non-urban sites to the south and west of Clark County also show high MDA8 ozone concentrations on May 28. Regionally high ozone concentrations, along with enhanced background ozone recorded at non-urban sites around Clark County, as well as the Indian Springs and Jean

stations, provide more evidence that suggests stratospheric ozone enhanced surface ozone on May 28, 2020.

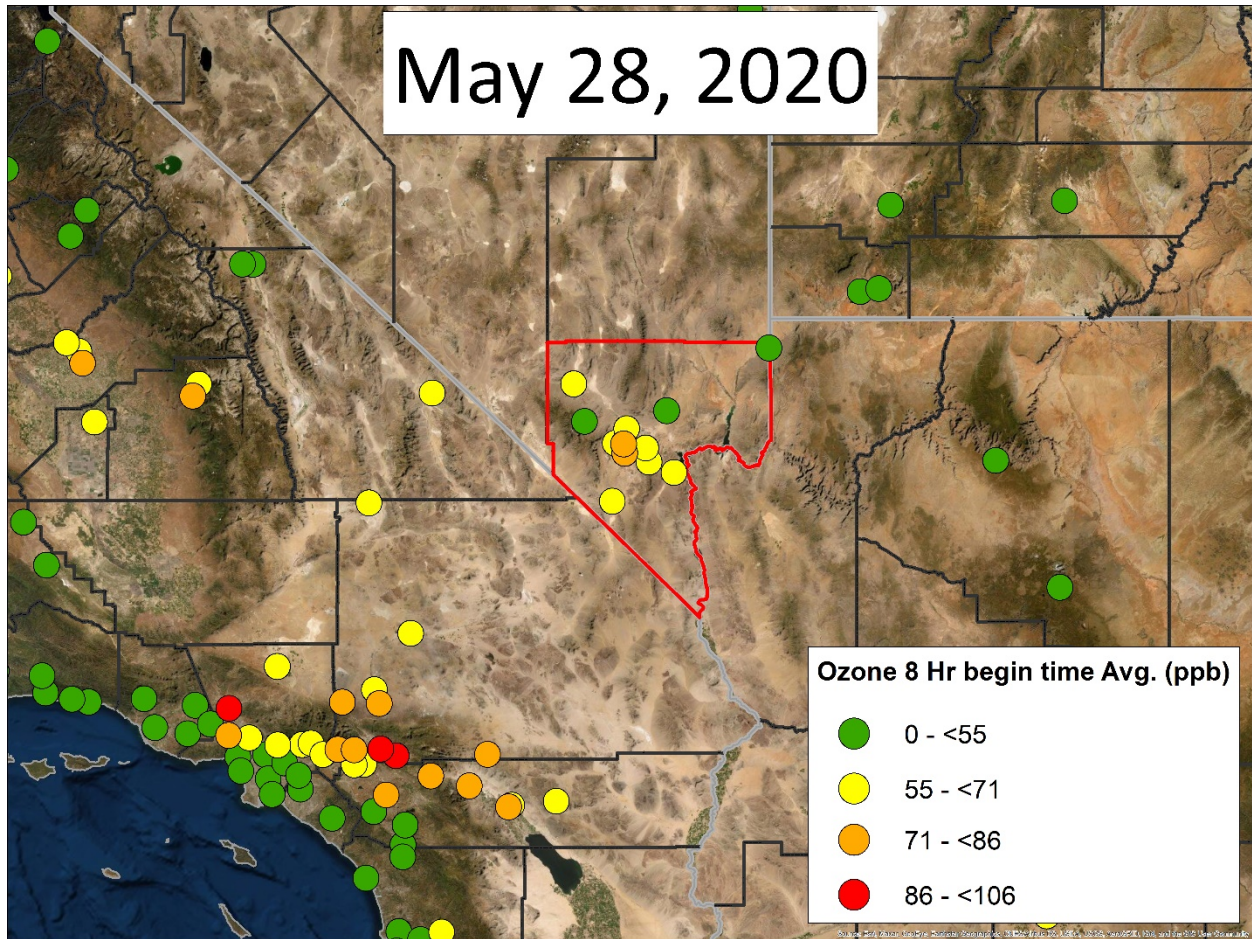


Figure 3-57. Observed MDA8 ozone at stations in southern California, southern Nevada, western Arizona, and southwestern Utah.

We also produced maps of daily ozone Air Quality Index (AQI) for the three days leading up to the May 28 event and the day of the event. These maps show moderate and unhealthy ground-level AQI values (indicated by yellow, orange, and red area) across the western United States, with unhealthy levels expanding between May 25 and May 28 (**Figure 3-58**). Again, regionally high ozone/AQI can be indicative of stratospheric ozone influence. Based on low water vapor, regionally high ozone, and typical concentrations of NO_x , ozone concentrations on May 28 were enhanced by an upwind SOI event and not purely due to photochemical production or transport from the Los Angeles basin.

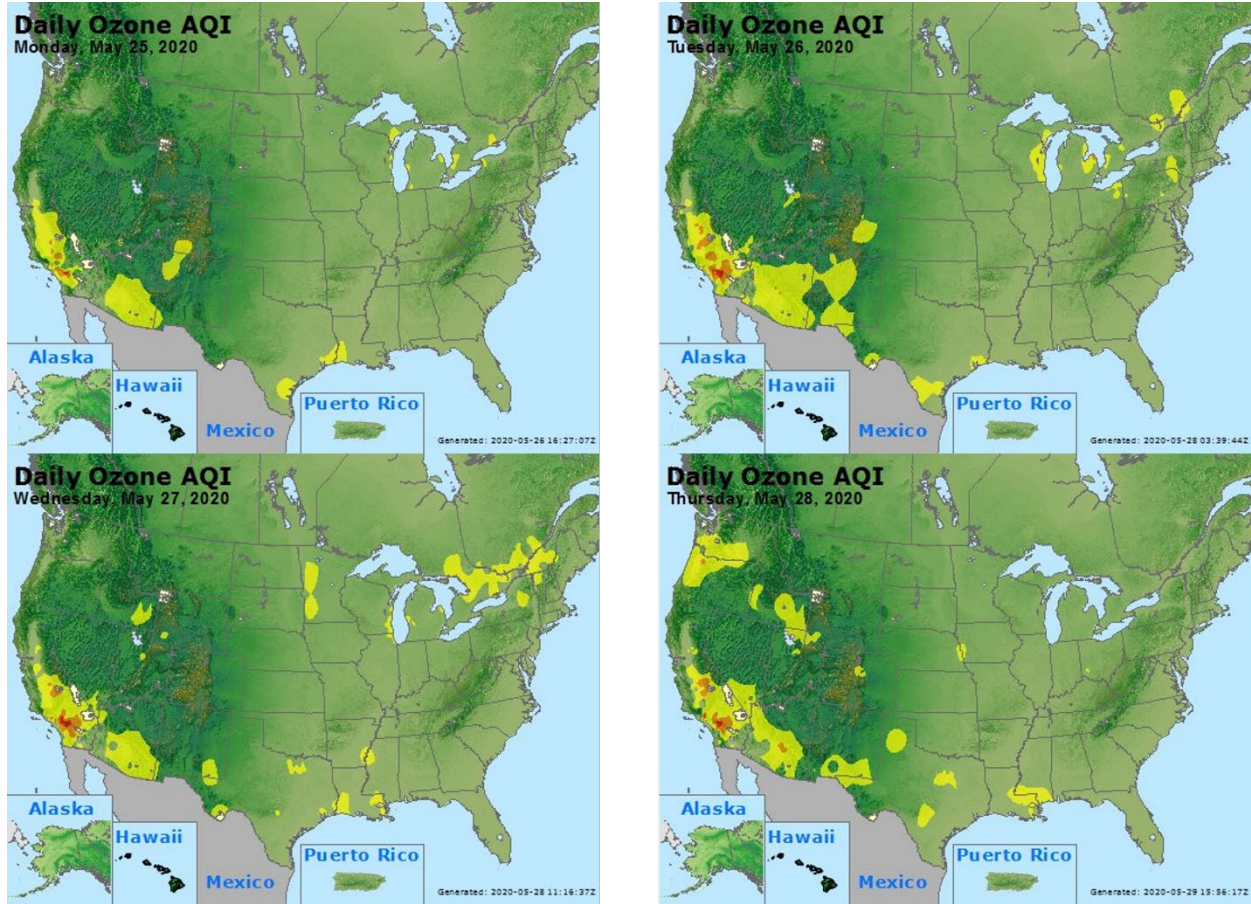


Figure 3-58. Daily ozone AQI for the three days before the May 28 event and the day of the event.

3.5 Additional Evidence

3.5.1 Matching Day Analysis

Ozone production and transport strongly depend on regional and local meteorological conditions. A comparison of ozone concentrations on suspected EE days with non-event days that share similar meteorology can help identify periods when ozone production was affected by an atypical source. Given that similar meteorological days are likely to have similar ozone concentrations, noticeable differences in levels of ozone between the event date and meteorologically similar days can lend evidence to a clear causal relationship between wildfire smoke and elevated ozone concentration.

Identify Meteorologically Similar Days

In order to identify the best matching meteorological days, both synoptic and local conditions were examined from ozone-season days (April 1 through September 30) between 2014 and 2020. Excluded from this set are days with suspected EEs in the 2018 and 2020 seasons, as well as dates within five days of the event date to ensure that lingering effects of smoke transport or stratospheric intrusion did not appear in the data.

To best represent similar air transport, twice daily HYSPLIT trajectories (initiated at 18:00 and 22:00 UTC) from Clark County for 2014-2020 were clustered by total spatial variance. The calculation, based on the difference between each point along a trajectory, provides seven distinct pathways of airflow into Clark County. The cluster that best represented the trajectory on the EE day was chosen, and ozone-season days within the cluster were then subset for regional meteorological comparison to the EE day.

For the meteorological comparison, a correlation score was assigned to each day from the cluster subset. The National Centers for Environmental Prediction (NCEP) reanalysis data was compiled for the ozone seasons in 2014-2020. Daily average wind speed, geopotential height, relative humidity, and temperature were considered at 1000 mb and 500 mb. At the surface, daily average atmospheric pressure, maximum temperature, and minimum temperature were utilized. Pearson product-moment coefficient of linear correlation (pattern correlation) was calculated between the EE date and each cluster-subset ozone-season day in 2014-2020 for each parameter. The pattern correlation calculates the similarity between two mapped variables at corresponding grid locations within the domain. The statistic was calculated using a regional domain of 30 °N-45 °N latitude and 125° W-105° W longitude. The correlation score for each day was defined as the average pattern correlation of all parameters at each height level. The correlations scores were then ranked by the highest correlation for 1000 mb, surface, and finally 500 mb. Dates within 5 days of the EE were removed from the similar day analysis to ensure the data are mutually exclusive. The 50 dates with the highest rank correlation scores were then chosen as candidate matching days for further analysis.

Local meteorological conditions for the subset of candidate matching days were then compared to conditions on May 28, and filtered to identify five or more days that best matched the event date. Meteorological maps at the surface and 500 mb, and local meteorological data describing temperature, wind, moisture, instability, mixing layer height, and cloud cover, were examined. The data source for each parameter is summarized in [Table 3-8](#).

Table 3-8. Local meteorological parameters and their data sources.

Meteorological Parameter	Data Source
Maximum Daily Temperature	Jerome Mack - NCore Monitoring Site
Average Daily Temperature	Jerome Mack - NCore Monitoring Site
Resultant daily wind direction	Jerome Mack - NCore Monitoring Site (calculated vector average)
Resultant daily wind speed	Jerome Mack - NCore Monitoring Site (calculated vector average)
Average daily wind speed	Jerome Mack - NCore Monitoring Site
Average daily relative humidity (RH)	Jerome Mack - NCore Monitoring Site
Precipitation	Jerome Mack - NCore Monitoring Site
Total daily global horizontal irradiance (GHI)	UNLV Measurement and Instrumentation Data Center (MIDC) in partnership with NREL (https://midcdmz.nrel.gov/apps/daily.pl?site=UNLV&start=20060318&yr=2021&mo=4&dy=29)
4 p.m. local standard time (LST) mixing layer mixing ratio	Upper air soundings from KVEF (http://weather.uwyo.edu/upperair/sounding.html)
4 p.m. LST lifted condensation level (LCL)	Upper air soundings from KVEF (http://weather.uwyo.edu/upperair/sounding.html)
4 p.m. LST convective available potential energy (CAPE)	Upper air soundings from KVEF (http://weather.uwyo.edu/upperair/sounding.html)
4 p.m. LST 1000-500 mb thickness	Upper air soundings from KVEF (http://weather.uwyo.edu/upperair/sounding.html)
Daily surface meteorological map	NOAA's Weather Prediction Center Daily Weather Maps (https://www.wpc.ncep.noaa.gov/dailywxmap/index.html)
Daily 500 mb meteorological map	NOAA's Weather Prediction Center Daily Weather Maps (https://www.wpc.ncep.noaa.gov/dailywxmap/index.html)

Matching Day Analysis

The meteorological conditions on May 28, 2020, were typical for the region at this time of year, except for very high temperatures. [Table 3-9](#) displays the percentile ranking of each examined meteorological parameter at the Jerome Mack- NCore site in the 30-day period surrounding May 28 (May 13 through June 12) across the years 2014 through 2020. All examined meteorological parameters fall within the 10th to 90th percentile except maximum temperature, which is at the 90th percentile. As is typical for Clark County, there was no precipitation.

Table 3-9. Percentile rank of meteorological parameters on May 28, 2020, compared to the 30-day period surrounding May 28 over seven years (May 13 through June 12, 2014-2020).

Date	Max Temp (°F)	Avg Temp (°F)	Resultant Wind Direction (°)	Resultant Wind Speed (mph)	Avg Wind Speed (mph)	Avg RH (%)	Precip (in)	Total GHI (kWh/m ²)	Mixing Layer Mixing Ratio (g/kg)	LCL (mb)	CAPE (J/kg)	500-100mb Thickness (m)
2020-05-28	90	72	NA	29	28	32	NA	29	81	69	87	63

The subset of synoptically similar days identified according to the methodology above was further filtered based on parameters listed in Table 3-8 to match local meteorological conditions. [Table 3-10](#) shows the ten days that best match the meteorological conditions that existed on May 28, 2020, as well as the maximum daily 8-hour ozone concentration at each site that experienced an exceedance on May 28, 2020. Due to the unusually high temperatures on May 28, 2020, most of the identified meteorologically similar days fall in later months of the year (July and August). Two days from 2020 are included in Table 3-10, June 4 and July 11. These two days are particularly valuable comparisons to include in this analysis since they occurred under similar abnormal anthropogenic emissions as the event date, a result of Covid-19 restrictions. Surface and upper-level maps for May 28, 2020, and each date listed in Table 3-10 show highly consistent conditions. All dates show a surface low pressure system and an upper-level region of high pressure over Clark County. Surface and upper-level maps are included in [Appendix B](#).

Table 3-10 shows the average MDA8 ozone concentration across these ten days with an expected range defined by one standard deviation, a conservative estimate given the small sample size. The average MDA8 ozone concentration across these ten days is well below the 70-ppb ozone standard at both of the sites that had an exceedance on May 28, 2020, with the expected ozone concentration ranging from 60 to 61 ppb. Further, the upper end of the provided range at each site also falls below the ozone standard. Neither site had an MDA8 above 70 ppb on any of the meteorologically matching days, including those from 2020 that better match the levels of anthropogenic emissions that existed on May 28, 2020. Therefore, an ozone exceedance on May 28, 2020, was unexpected based on meteorological conditions alone. If meteorological conditions were the sole cause of the ozone exceedance on May 28, 2020, we would expect to see similarly high ozone levels on each of the similar days listed in Table 3-10, especially those with similar temperatures and an even higher GHI. These findings lend weight to the assertion that an external source of ozone contributed to the ozone exceedance on May 28, 2020.

Table 3-10. Top ten matching meteorological days to May 28, 2020. WJ and PM refer to monitoring sites, Walter Johnson and Paul Meyer, respectively. Average MDA8 ozone concentration of meteorologically similar days is shown plus-or-minus one standard deviation rounded to the nearest ppb.

Date	Max Temp (°F)	Avg Temp (°F)	Resultant Wind Direction (°)	Resultant Wind Speed (mph)	Avg Wind Speed (mph)	Avg RH (%)	Precip (in)	Total GHI (kWh/m ²)	Mixing Layer Mixing Ratio (g/kg)	LCL (mb)	CAPE (J/kg)	500-100mb Thickness (m)	MDA8 Ozone Concentration (ppb)	
													PM	WJ
2020-05-28	110	96.71	152.86	2.00	3.59	9.38	0	8.39	6.57	575	337	5886	76	71
2017-07-01	111	97.54	156.49	3.57	4.83	8.04	0	8.7	4.35	519	162	5906	64	68
2017-07-13	109	99.04	166.1	2.07	3.51	17.67	0	8.06	8.33	607	533	5899	65	69
2017-07-28	109	98.42	134.76	3.37	4.12	18.62	0	8.1	7.48	592	147	5902	60	64
2017-08-10	109	97.88	204.77	2.58	3.99	13.75	0	7.84	7.03	588	238	5889	46	46
2018-06-25	110	97.33	136.09	4.05	4.58	12.54	0	8.54	7.27	584	409	5911	63	66
2019-07-05	103	91.92	117.33	2.19	3.67	11.88	0	8.22	5.91	592	91	5831	64	64
2019-07-21	108	96.71	122.07	2.72	3.97	12.46	0	8.42	5.54	554	69	5912	49	52
2019-08-14	111	96.62	178.14	0.51	1.65	11.12	0	7.87	5.81	565	78	5890	59	59
2020 Dates														
2020-06-04	108	96.79	202.09	2.59	4.15	9.58	0	8.58	5.47	557	174	5881	62	61
2020-07-11	113	102.17	215.86	3.50	4.72	9.04	0	7.71	7.71	583	233	5938	56	57
Average MDA8 Ozone Concentration of Meteorologically Similar Days													59 ± 6	60 ± 7

These findings show that an external source of ozone contributed to the ozone exceedance on May 28, 2020. On May 28, normal meteorological conditions other than maximum temperature were present, which fell at the 90th percentile. Our analysis expanded on methods shown in the EPA guidance and a previously concurred EE to identify eight days that are meteorologically similar to May 6, 2020 (Arizona Department of Environmental Quality, 2018). No exceedance occurred on any of these ten days at either monitoring site that experienced an ozone exceedance on May 28, 2020, including on two 2020 dates that occurred under similar, altered anthropogenic emissions due to COVID-19 restrictions. The expected MDA8 ozone concentration at each site is more than 10 ppb below the concentrations measured at each site on May 28, 2020. Based on this evidence, it is unlikely that meteorology alone enhanced photochemical production of ozone enough to cause an exceedance on May 28, 2020.

3.5.2 GAM Statistical Modeling

Generalized additive models (GAM) are a type of statistical model that allows the user to predict a response based on linear and non-linear effects from multiple variables (Wood, 2017). These models tend to provide a more robust prediction than Eulerian photochemical models or simple comparisons of similar events (Simon et al., 2012; Jaffe et al., 2013; U.S. Environmental Protection Agency, 2016). Camalier et al. (2007) successfully used GAM modeling to predict ozone concentrations across the eastern United States using meteorological variables with r^2 values of up to 0.8. Additionally, previous concurred exceptional event demonstrations and associated literature, i.e., Sacramento Metropolitan Air Quality Management District (2011), Alvarado et al. (2015), Louisiana Department of Environmental Quality (2018), Arizona Department of Environmental Quality (2016), and Pernak et al. (2019) used GAM modeling to predict ozone events that exceed the NAAQS standards, some in EE cases. By comparing the GAM-predicted ozone values to the actual measured ozone concentrations (i.e., residuals), we can determine the effect of outside influences, such as wildfires or stratospheric intrusions, on ozone concentrations each day (Jaffe et al., 2004). High, positive residuals suggest a non-typical source of ozone in the area but cannot specifically identify a source. Gong et al. (2017) and McClure and Jaffe (2018) used GAM modeling, in addition to ground and satellite measurements of wildfire pollutants, to estimate the enhancement of ozone during wildfire smoke events. Similar to other concurred EE demonstrations, we used GAM modeling of meteorological and transport variables to estimate the MDA8 ozone concentrations at multiple sites across Clark County for 2014-2020. To estimate the effect of wildfire smoke on ozone concentrations, we can couple the GAM residual results (observed MDA8 ozone–GAM-predicted MDA8 ozone) with the other analyses to confirm that the non-typical enhancement of ozone is due to a stratospheric intrusion on May 28, 2020.

Using the same GAM methodology as prior concurred EE demonstrations and the studies mentioned above, we examined more than 30 meteorological and transport predictor variables, and through testing, compiled the 16 most important variables to estimate MDA8 ozone each day at eight monitoring sites across Clark County, Nevada (Paul Meyer, Walter Johnson, Joe Neal, Green Valley,

Boulder City, Jean, Indian Springs, and Jerome Mack). As suggested by EPA guidance (U.S. Environmental Protection Agency, 2016), we used meteorological variables measured at each station (the previous day's MDA8 ozone, daily min/max temperature, average temperature, temperature range, wind speed, wind direction, or pressure), if available (see Table 2-1). If meteorological variables were not available at a specific site, we supplemented the data with National Centers for Environmental Prediction (NCEP) reanalysis meteorological data to fill any data gaps. We also tested filling data gaps with Jerome Mack meteorological data and found results had no statistical difference. We used sounding data from KVEF (Las Vegas Airport) to provide vertical meteorological components; soundings are released at 00:00 and 12:00 UTC daily. Variables such as temperature, relative humidity, wind speed, and wind direction were averaged over the first 1000 m above the surface to provide near-surface, vertical meteorological parameters. Other sounding variables, such as Convective Available Potential Energy (CAPE), Lifting Condensation Level (LCL) pressure, mixing layer potential temperature, mixed layer mixing ratio, and 500-1,000 hPa thickness provided additional meteorological information about the vertical column above Clark County. We also initiated HYSPLIT GDAS 1°x1° 24-hour back trajectories from downtown Las Vegas (36.173° N, -115.155° W, 500 m agl) at 18:00 and 22:00 UTC (10:00 a.m. and 2:00 p.m. local standard time) each day to provide information on morning and afternoon transport during critical ozone production hours. We clustered the twice-per-day back trajectories from 2014-2020 into seven clusters. **Figure 3-59** shows the clusters, percentage of trajectories per cluster, and heights of each trajectory cluster. We identified a general source region for each cluster: (1) Northwest U.S., (2) Stagnant Las Vegas, (3) Central California, (4) Long-Range Transport, (5) Northern California, (6) Southern California, and (7) Baja Mexico. Within the GAM, we use the cluster value to provide a factor for the distance traveled by each back trajectory. Additionally, day of year (DOY) was used in the GAM to provide information on season and weekly processes. The year (2014, 2015, etc.) was used a factor for the DOY parameter to distinguish interannual variability.

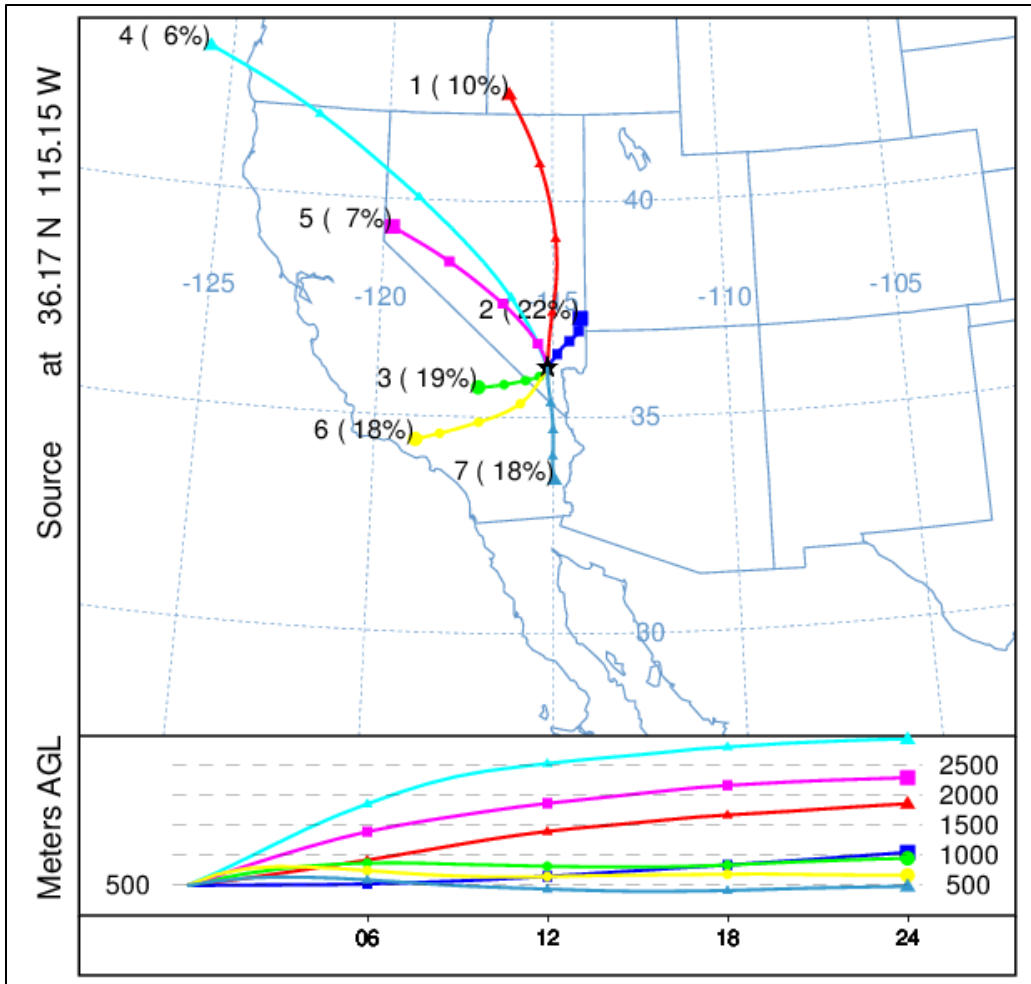


Figure 3-59. Clusters for 2014-2020 back trajectories. Seven unique clusters were identified for the twice daily (18 and 22 UTC) back-trajectories for 2014-2020 initiated in the middle of the Las Vegas Valley. The percentage of trajectories per cluster is shown next to the cluster number. The height of each cluster is shown below the map.

Once all the meteorological and transport variables were compiled, we inserted them into the GAM equation to predict MDA8 ozone:

$$g(MDA8 O_{3,i}) = f_1(V1_i) + f_2(V2_i) + f_3(V3_i) + \dots + residual_i$$

where f_i are fit functions calculated from penalized cubic regression splines of observations (allowing non-linearity in the fit), V_i are the variables, and i is the daily observation. All variables were given a cubic spline basis except for wind direction, which used a cyclic cubic regression spline basis. For DOY and back trajectory distances, we used year factors (i.e., 2014-2020) and cluster factors (i.e., 1-7) to distinguish interannual variability and source region differences. The factors provide a different smooth function for each category (Wood, 2017). For example, the GAM smooth of DOY for 2014 can

be different than 2015, 2016, etc. In order to optimize the GAM, we first must adjust knots or remove any variables that are over-fitting or under-performing. We used the “mgcv” R package to summarize and check each variable for each monitoring site (Wood, 2020). A single GAM equation (using the same variables) was used for each monitoring site for consistency. During the initial optimization process, we removed the proposed 2018 and 2020 EE days from the dataset. We also ran 10 cross-validation tests by randomly splitting data 80/20 between training/testing for each monitoring site to ensure consistent results. All cross-validation tests showed statistically similar results with no large deviations for different data splits. We used data from each site during the April -September ozone seasons for 2014 through 2020, which is consistent with other papers modeling urban ozone (e.g., Pernak et al., 2019; McClure and Jaffe, 2018; Solberg et al., 2019; Solberg et al., 2018) and ozone concentrations during the periods with exceptional events are within the representative range of ozone in the GAM model.

Table 3-11 shows the variables used in the GAM and their F-value. The F-value suggests how important each variable is (higher value = more important) when predicting MDA8 ozone. Any bolded F-values had a statistically significant correlation ($p < 0.05$). R^2 , the positive 95th quantile of residuals, and normalized mean square residual values for each monitoring site are listed at the bottom of the table.

Table 3-11. GAM variable results. F-values per parameter used in the GAM model are shown for each site. Units and data source for each parameter in the GAM model are shown on the right of the table. 95th quantile, R², and normalized mean square residual information is shown at the bottom of the table.

Parameters	Paul Meyer	Walter Johnson	Joe Neal	Green Valley	Jerome Mack	Boulder City	Jean	Indian Springs	Unit	Source
Day of Year (DOY) factored by Year (2014-2020)	8.11	7.09	7.65	11.8	7.94	7.11	8.68	7.53	--	--
Previous Day MDA8 Ozone	37.9	22.7	41.5	18.1	27.9	31.3	105.5	123.8	ppb	Monitor Data
Average Daily Temperature	1.92	2.90	4.80	0.05	1.83	2.13	0.12	1.83	K	Monitor Data/NCEP Reanalysis
Maximum Daily Temperature	1.37	2.74	2.48	0.16	0.38	0.02	1.30	1.52	K	
Temperature Range (TMax - TMin)	4.12	2.13	1.38	1.74	1.77	1.51	0.50	0.54	K	
Average Daily Pressure	5.54	6.42	6.74	4.64	2.94	0.22	2.17	0.24	hPa	
Average Daily Wind Speed	11.1	5.03	7.49	5.02	15.3	0.07	0.49	2.19	knots	
Average Daily Wind Direction	0.47	1.04	0.24	1.35	2.43	0.69	0.11	2.48	deg	
18 UTC HYSPLIT Distance factored by Cluster	1.70	1.82	1.69	0.92	2.52	2.97	1.66	1.03	km	HYSPLIT Back-Trajectories
22 UTC HYSPLIT Distance factored by Cluster	1.03	0.74	1.47	1.47	1.20	1.26	1.19	0.50	km	
00 UTC Convective Available Potential Energy	3.50	0.13	0.37	1.17	1.16	0.57	5.71	6.49	J/kg	Sounding Data
00 UTC Lifting Condensation Level Pressure	1.36	2.78	2.29	2.41	3.76	0.38	1.43	0.38	hPa	
00 UTC Mixing Layer Potential Temperature	0.65	0.79	1.72	0.10	1.23	0.97	1.09	2.53	K	
00 UTC Mixed Layer Mixing Ratio	2.10	2.76	2.85	3.09	3.07	2.42	0.69	1.04	g/kg	
00 UTC 500-1000 hPa Thickness	2.91	0.43	1.70	1.60	1.69	4.11	2.18	1.83	m	
12 UTC 1km Average Relative Humidity	12.4	14.6	17.8	21.3	37.5	26.0	11.1	2.18	%	
95 th Quantile of Positive Residuals (ppb)	10	10	10	10	9	9	9	10		
R ²	0.55	0.58	0.60	0.58	0.61	0.58	0.57	0.55		
Normalized Mean Square Residual	3.6E-06	7.3E-04	6.1E-05	1.3E-04	3.1E-05	1.3E-04	1.2E-04	1.5E-04		

Table 3-12 provides GAM residual and fit results for all sites for ozone season between 2014 and 2020. Overall, the residuals are low for all data points and similarly low for all non-EE days. However, the 2018 and 2020 EE day residuals are significantly higher than the non-EE day results, meaning there are large, atypical influences on these days. **Figure 3-60** shows non-EE vs EE median residuals with the 95th confidence intervals denoted as notches in the boxplots. We show the data in both ways to provide specific values as well as illustrate the difference in non-EE vs EE residuals. Since the 95th confidence intervals for median EE residuals are above and do not overlap with those for non-EE residuals at any site in Clark County, we can state that the median residuals are higher and statistically different ($p < 0.025$). The R^2 for each site ranged between 0.55 and 0.61, suggesting a good fit for each monitoring site and similar to the results in prior studies and EE demonstrations mentioned previously (r^2 range 0.4-0.8). We also provide the positive 95th quantile MDA8 ozone concentration, which is used to estimate a “No Fire” MDA8 ozone value based on the EPA guidance (U.S. Environmental Protection Agency, 2016). We also provide the median residuals (and confidence interval) for all non-EE days with observed MDA8 at or above 60 ppb (this threshold was needed for a sufficient sample size to build a representative distribution and derive the median and 95% confidence interval). It should be noted that four out of the seven years modeled by the GAM were high wildfire years and these values likely include a significant amount of wildfire days. We were not able to systematically remove wildfire influence by subsetting the Clark County ozone data based on HMS smoke, HMS smoke and $PM_{2.5}$ concentrations, and low wildfire years. These methods produced a significant number of false positives and negatives and yielded datasets that were still affected by wildfire smoke. Therefore, these values should be considered an upper estimate of residuals for high ozone days. We see that the median residuals for 2018 and 2020 EE days are significantly higher than those on non-EE high observed ozone days since their confidence intervals do not overlap (or are comparable for Jerome Mack). The non-EE day residuals on days where observed MDA8 was at or above 60 ppb were determined to be normally distributed with a slight positive skew (median skewness = 0.39).

Table 3-12. Overall 2014-2020 GAM median residuals and 95% confidence interval range in square brackets for each site modeled. Sample size is shown in parentheses below the residual statistics. For sample sizes less than ten, we include a range of residuals in square brackets instead of the 95% confidence interval. Residual results are split by non-EE days and the 2018 & 2020 EE days. R² for each site is also shown along with the positive 95th quantile result.

Site Name	All Residuals (ppb)	Non-EE Day Residuals (ppb)	2018 & 2020 EE Day Residuals (ppb)	R ²	Positive 95th Quantile (ppb)	Non-EE Day Residuals when MDA8 ≥ 60 ppb (ppb)
Boulder City	0.22 [-0.04, 0.48] (1,132)	0.22 [-0.04, 0.48] (1,130)	12.05 [10.38-13.72] (2)	0.58	9	4.05 [3.55, 4.55] (200)
Green Valley	0.17 [-0.15, 0.48] (948)	0.10 [-0.21, 0.41] (934)	7.38 [5.40, 9.36] (14)	0.58	10	3.76 [3.28, 4.23] (271)
Indian Springs	0.13 [-0.18, 0.44] (1,014)	0.08 [-0.22, 0.38] (1,010)	12.30 [9.37-17.19] (4)	0.55	10	4.79 [4.26, 5.32] (201)
Jean	0.21 [-0.06, 0.48] (1,149)	0.20 [-0.07, 0.47] (1,146)	12.57 [9.59-13.90] (3)	0.57	9	3.40 [2.94, 3.85] (290)
Jerome Mack	0.09 [-0.19, 0.36] (1,152)	0.05 [-0.22, 0.32] (1,141)	6.83 [4.21, 9.45] (11)	0.61	9	3.83 [3.32, 4.33] (242)
Joe Neal	0.23 [-0.08, 0.54] (1,113)	0.17 [-0.13, 0.47] (1,097)	7.77 [5.79, 9.75] (16)	0.60	10	3.32 [2.92, 3.71] (377)
Paul Meyer	0.21 [-0.08, 0.50] (1,159)	0.10 [-0.19, 0.39] (1,137)	8.11 [6.34, 9.88] (22)	0.55	10	3.58 [3.19, 3.97] (388)
Walter Johnson	0.27 [-0.03, 0.57] (1,163)	0.19 [-0.10, 0.48] (1,141)	7.16 [5.11, 9.21] (22)	0.58	10	3.53 [3.13, 3.93] (379)

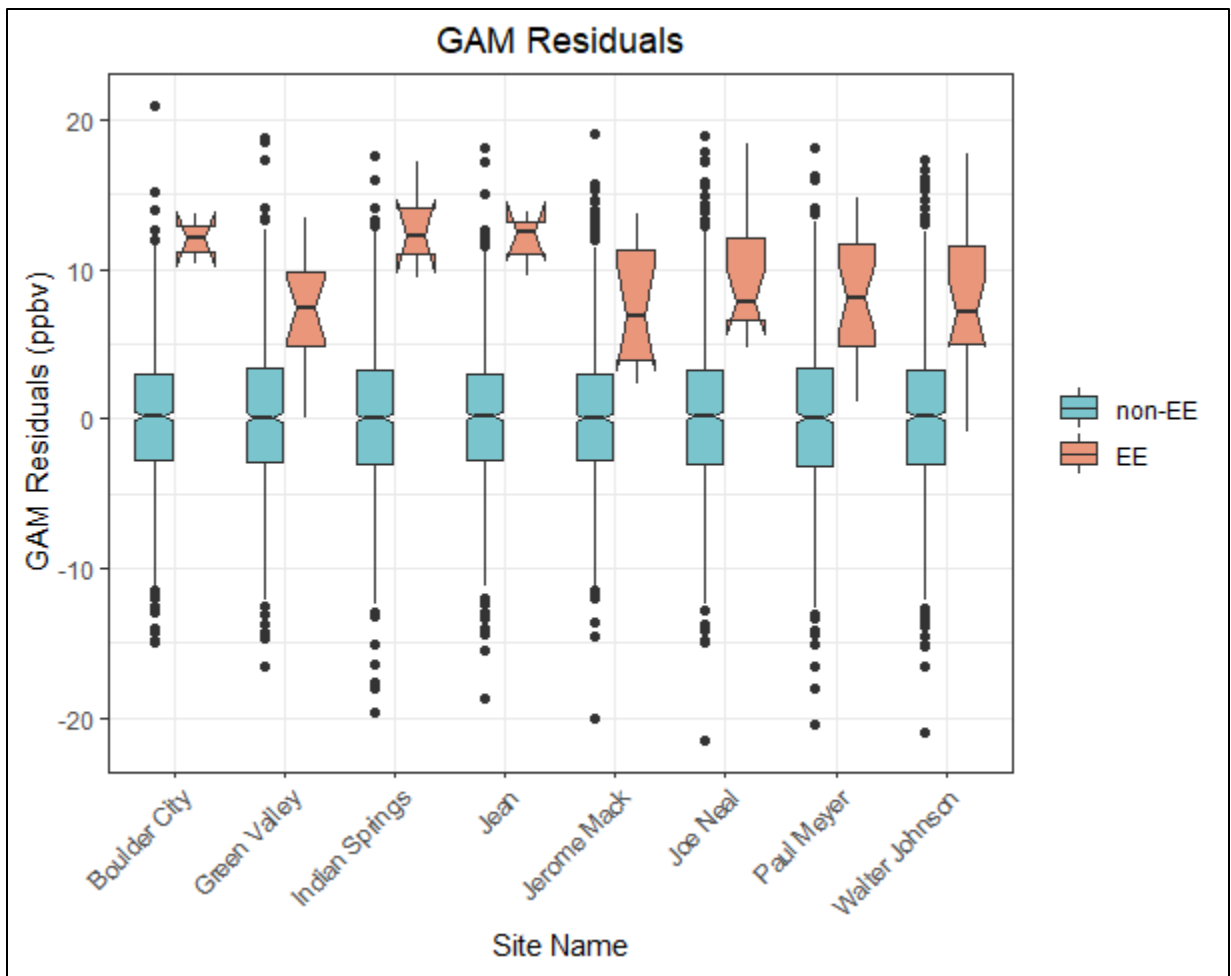


Figure 3-60. EE vs. non-EE residuals. Non-EEs (non-EE in blue) and EEs (EE in orange) residuals are shown for each site modeled in Clark County. The notches for each box represent the 95th confidence interval. This figure illustrates the information in Table 3-12.

Overall, the GAM results show low bias and consistently significantly higher residuals on EE days compared with non-EE days. We also evaluated the GAM performance on verified high ozone, non-smoke days by looking at specific case studies. This was done to assess whether high-ozone days, such as the EE days, have a consistent bias that is not evident in the overall or high ozone day GAM performance. Out of the seven years used in the GAM model, four were high wildfire years in California (2015, 2017, 2018, and 2020). Since summer winds in Clark County are typically out of California (44% of trajectories originate in California according to the cluster analysis [not including transport through California in the Baja Mexico cluster]), wildfire smoke is likely to affect a large portion of summer days and influence ozone concentrations in Clark County. We identified specific case studies where most monitoring sites in Clark County had an MDA8 ozone concentration greater than or equal to 60 ppb and had no wildfire influence; “no wildfire influence” was determined by inspecting HMS smoke plumes and HYSPLIT back trajectories for each day and confirming no smoke

was over, near, or transported to Clark County. We found one to two examples from each year used in the GAM modeling, and required that at least half of the case study days needed to include an exceedance of the ozone NAAQS. [Table 3-13](#) shows the results of these case studies. Most case study days, including NAAQS exceedance days, show positive and negative residuals even when median ozone is greater than or equal to 65 ppb in Clark County, similar to the results for the entire multi-year dataset. GAM residuals on non-EE days when MDA8 is at or above 60 ppb have a median of 3.69 [95% confidence interval: 3.47, 3.88] (see [Table 3-12](#)). The high ozone, non-smoke case study days all show median residuals within or below the confidence interval of the high ozone residuals (from [Table 3-12](#)), meaning that the GAM model is able to accurately predict high ozone, non-smoke days within a reasonable range of error. Two additional factors indicate the GAM has good performance on normal, high ozone days: (1) the median residuals for the case studies are mostly lower than the 95% confidence interval of high ozone residuals (i.e., includes non-EE wildfire days), and (2) the case study days were verified as non-smoke days. Thus, residuals above the 95th confidence interval of the median residuals, such as those on the EE days, are statistically higher than on days with comparable high ozone concentrations, and not biased high because of the high ozone concentrations on these days.

We also evaluate the bias of GAM residuals versus predicted MDA8 ozone concentrations in [Figure 3-61](#). Residuals (i.e., observed ozone minus GAM-predicted MDA8 ozone) should be independent of the GAM-predicted ozone value, meaning that the difference between the actual ozone concentration on a given day and the GAM output should be due to outside influences and not well described by meteorological or seasonal values (i.e., variables used in the GAM prediction). Therefore, in a well-fit model, positive and negative residuals should be evenly distributed across all GAM-predicted ozone concentrations and on average zero. In [Figure 3-61](#), we see daily GAM residuals at all eight monitoring sites in Clark County from 2014-2020, the residuals are evenly distributed across all GAM-predicted ozone concentrations, with no pattern or bias at high or low MDA8 fit concentrations. This evaluation of bias in the model is consistent with established literature and other EE demonstrations (Gong et al., 2018; McVey et al., 2018; Texas Commission on Environmental Quality, 2021; Pernak et al., 2019), and indicate a well-fit model. In [Figure 3-62](#), we also provide a histogram of the residuals at each monitoring site modeled in Clark County. This analysis shows that residuals at each site are distributed normally around a median near zero, and none of the distributions shows significant tails at high or low residuals (median skew = 0.05 with 95% confidence interval [-0.03, 0.12]). This analysis of error in the model and our results are consistent with previously concurred EE demonstrations (Arizona Department of Environmental Quality, 2016) and previous literature (Jaffe et al., 2013; Alvarado et al., 2015; Gong et al., 2017; McClure and Jaffe, 2018; Pernak et al., 2019). [Appendix C](#) provides GAM residual analysis from the concurred ADEQ and submitted TCEQ demonstrations that compare well with our GAM residual results. Based on these analysis methods, bias in the model is low throughout the range of MDA8 prediction values and confirms that the GAM can be used to predict MDA8 ozone concentrations in Clark County.

Table 3-13. GAM high ozone, non-smoke case study results. Median GAM residuals for ten days in 2014-2020 are shown where most monitoring sites had MDA8 ozone concentrations of 60 ppb or greater. Sites used to calculate the MDA8 and GAM residual median/range are listed in the Clark County AQS Site Number column by site number.

Date	Clark County AQS Site Number	Median (Range) of Observed MDA8 Ozone (ppb)	Median (Range) GAM Residual (ppb)
5/17/2014	0601, 0075, 1019, 0540, 0043, 0071	66 (64-71)	1.66 (-0.53-4.28)
6/4/2014	0601, 0075, 0540, 1019, 0043, 0071	69 (66-72)	3.46 (1.70-4.80)
6/3/2015	1019, 0043, 0075, 0540, 7772, 0601, 0071	71 (65-72)	3.01 (-0.34-5.77)
6/20/2015	0601, 0298, 7772, 1019, 0540, 0075, 0043, 0071	65 (63-70)	1.40 (-6.20-5.28)
6/3/2016	0298, 1019, 0075, 0540, 0043, 0071	65 (63-71)	3.89 (1.89-5.26)
7/28/2016	0075, 0071, 0298, 0540, 0043	70 (63-72)	0.24 (-5.95-3.67)
6/17/2017	0601, 0075, 0071, 1019, 0540, 0298, 0043	66 (63-72)	1.85 (-1.94-7.01)
6/4/2018	0601, 0298, 7772, 1019, 0540, 0075, 0043, 0071	65 (60-67)	3.06 (-0.91-3.60)
5/5/2019	0601, 0298, 7772, 1019, 0540, 0075, 0043, 0071	65 (62-67)	1.28 (-2.00-3.42)
5/15/2020	0298, 0043, 0075, 0071	63 (63-65)	1.52 (1.09-3.49)

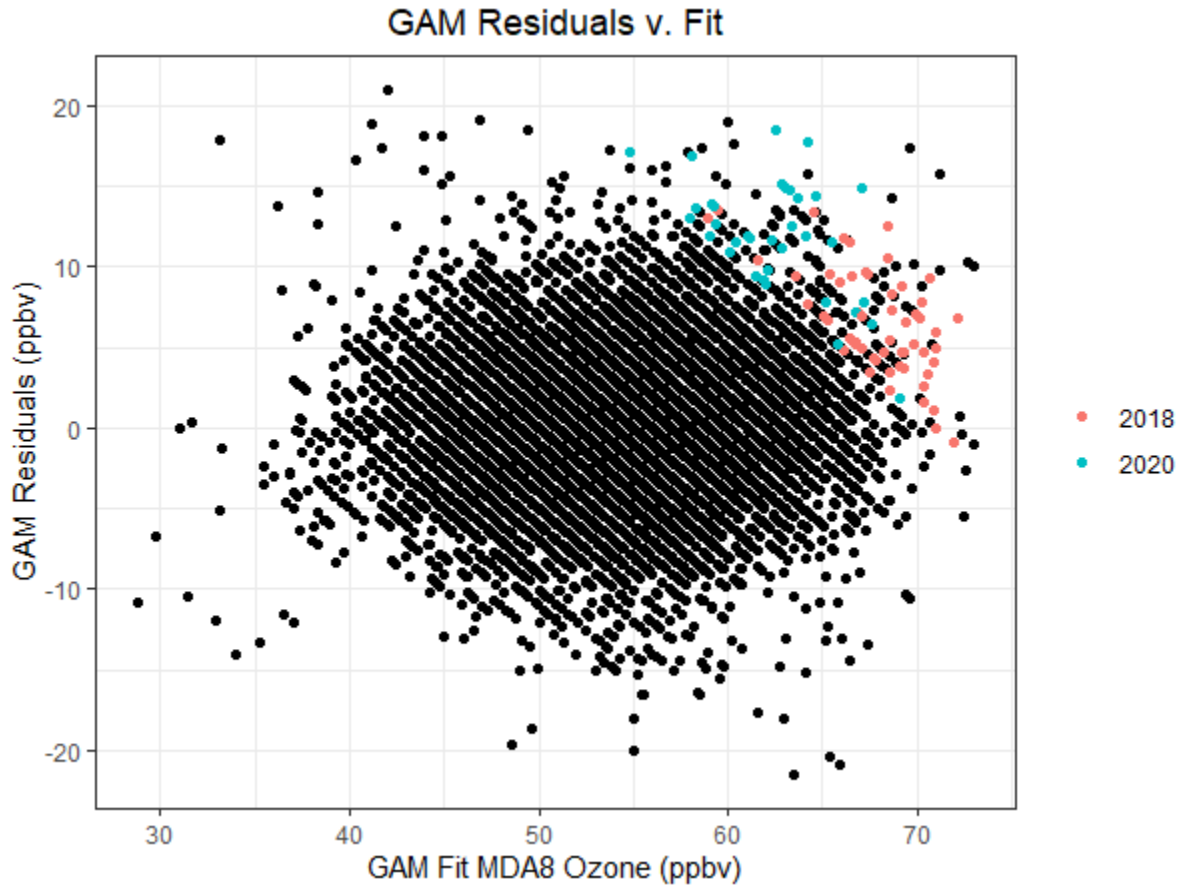


Figure 3-61. Daily GAM residuals for 2014-2020 vs GAM Fit (Predicted) MDA8 Ozone values. 2018 and 2020 exceptional events residuals are shown in red and blue.

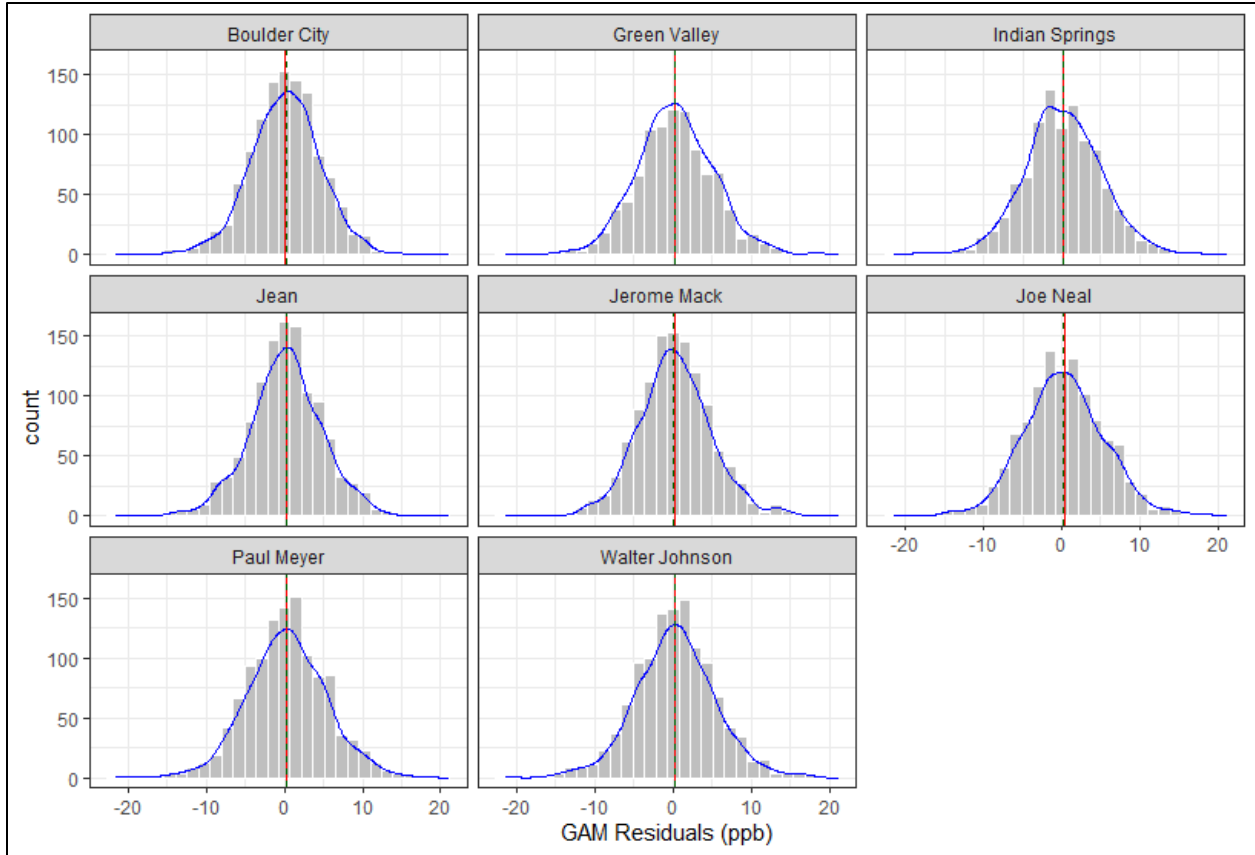


Figure 3-62. Histogram of GAM residuals at all modeled Clark County monitoring sites. The red line indicates the mean and the green dashed line indicates the median. The blue line provides the density distribution.

Within the GAM model, we include HYSPLIT 24-hour distance values, which are factored by cluster, to provide source region and stagnation information into the algorithm. A major upwind pollution source for Las Vegas is the Los Angeles Basin (see the Southern California cluster), which is around 400 km away. Since the GAM model uses source region and distance traveled information to help predict daily MDA8 ozone concentrations, contributions from LA should be accounted for in the algorithm. Based on this, we can assess whether GAM residuals on LA-source region days were significantly different from other source regions. In **Figures 3-63 and 3-64**, we subset the GAM results by removing any potential EE days. From these results, we find that both morning (18:00 UTC) and afternoon (22:00 UTC) trajectory data have similar distributions for all clusters. The notches in the box plots (representing the 95th confidence interval) provide an estimate of statistical difference, and show that the median of residuals is near zero for all clusters. The Northwest U.S. cluster at 18:00 UTC shows slightly negative residuals, while the Long-Range Transport cluster shows slightly positive residuals for both 18:00 and 22:00 UTC. The Southern California cluster shows a median residual of around zero for both 18:00 and 22:00 UTC trajectories, with significant overlap between the 95th confidence intervals of most other clusters (not statistically different). Additionally, the number of data points per cluster (bottom of each figure) corresponds well with transport from California being

dominant for the April through September time frame. Overall, this analysis provides evidence that even when the Los Angeles Basin (Southern California cluster) is upwind of Las Vegas, the GAM model performs well (low median residuals), and the results are statistically similar to most of the other clusters. This implies that when residuals are large, the Los Angeles Basin’s influence is unlikely to be the only contributor to enhancements in MDA8 ozone.

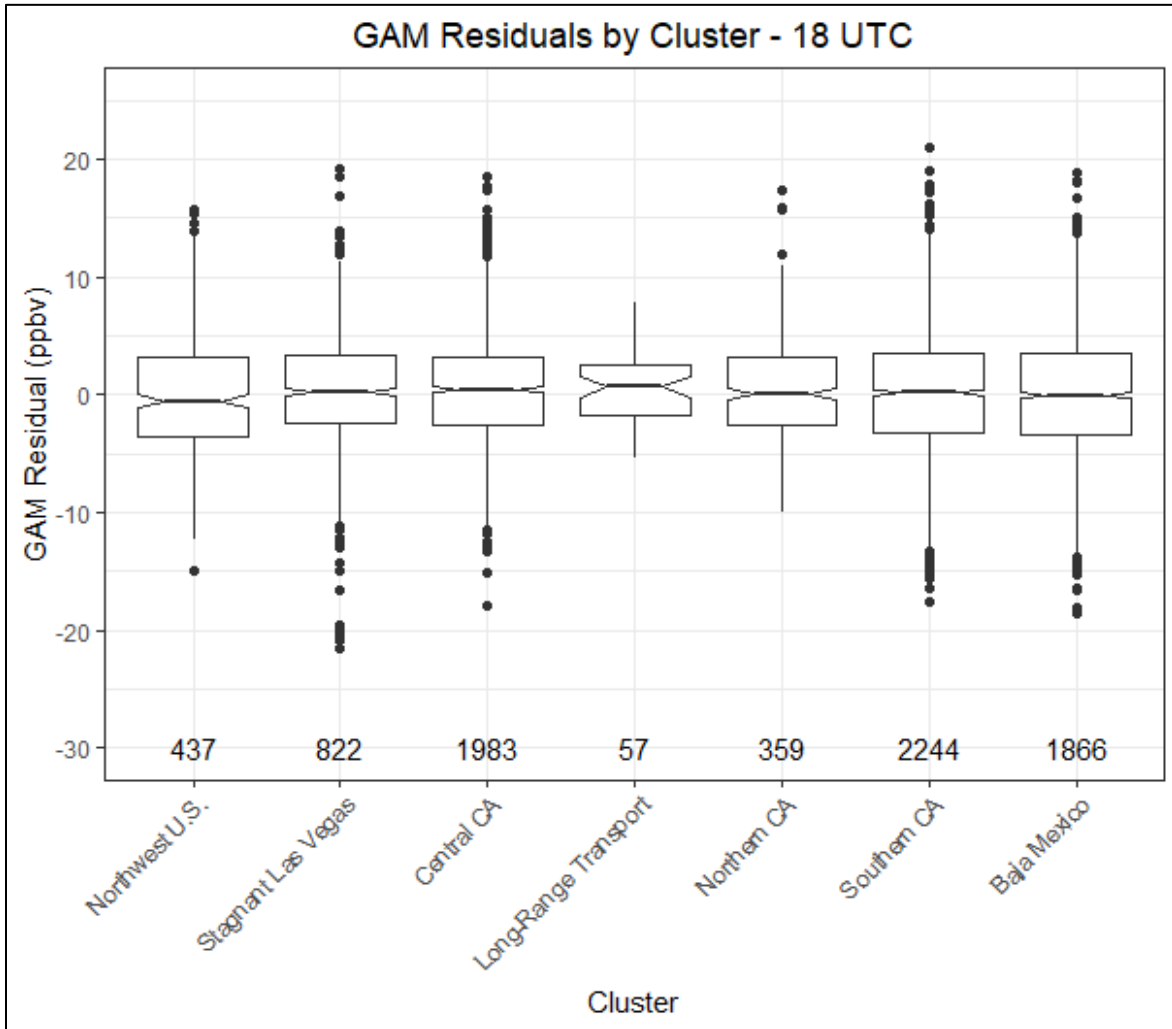


Figure 3-63. GAM cluster residual results for 18:00 UTC. The cluster is determined by grouping 24-hour back trajectories from Las Vegas based on their path. Clusters were created by using back trajectory results from Clark County between 2014 and 2020 were used (removed EE days).

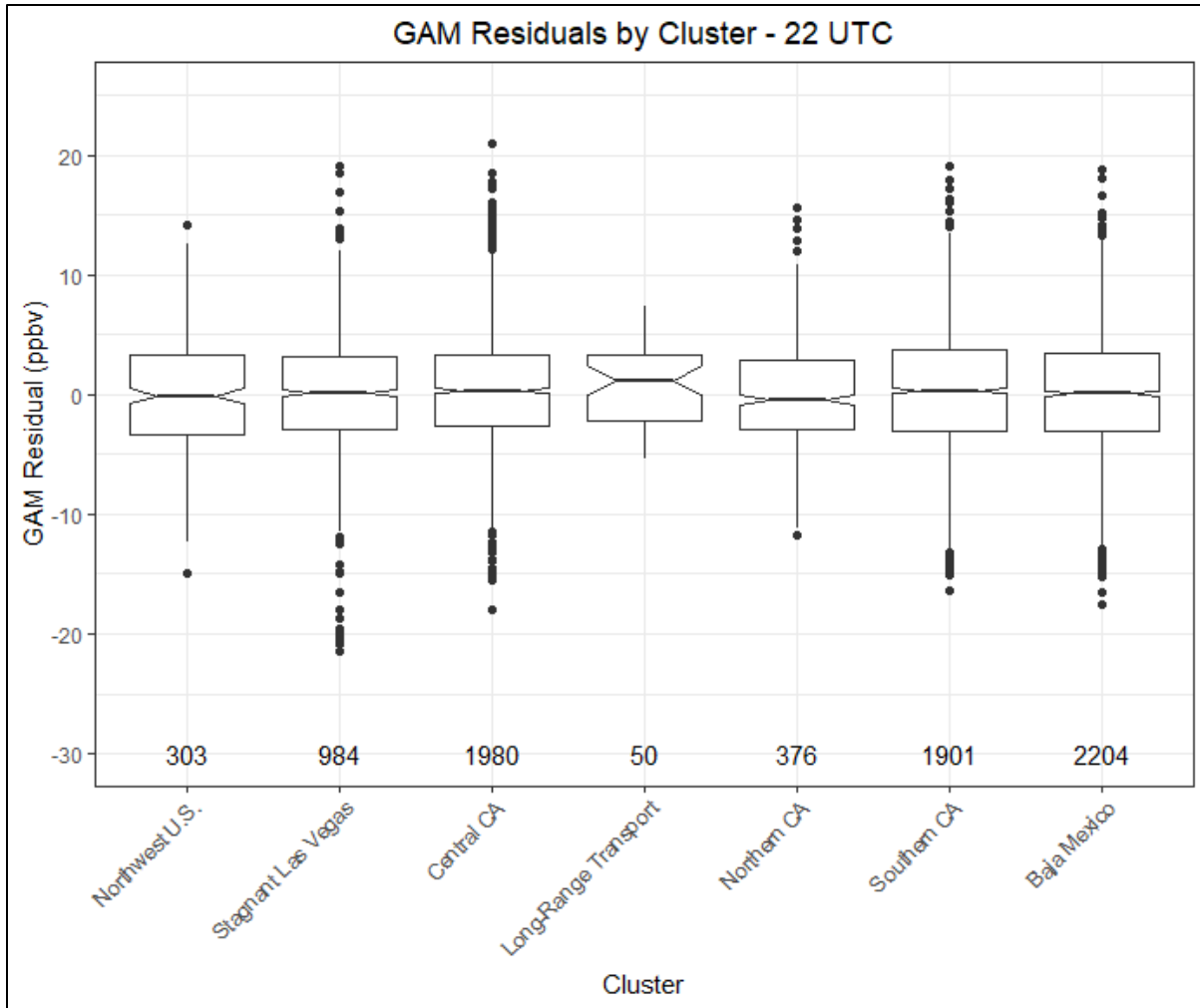


Figure 3-64. GAM cluster residual results for 22:00 UTC. The cluster is determined by grouping 24-hour back trajectories from Las Vegas based on their path. Clusters were created by using back trajectory results from Clark County between 2014 and 2020 were used (removed EE days).

Mobile emissions sources decreased throughout the U.S. after COVID restrictions went into place in March 2020. Based on emission inventories from Las Vegas, on-road emissions make up a significant portion of the NO_x emissions inventory (see Section 2.3 for more details). Based on traffic data from the Nevada Department of Transportation, on-road traffic in Clark County in 2020 was significantly different than 2019 through early to mid-June (depending on the area where traffic volume was measured; see Section 2.5 for more details). **Figure 3-65** provides a scatter plot of MDA8 ozone observed versus GAM fit for all eight monitoring sites, separated by year. The linear regression fit, slope, and intercept do not show large difference between 2020 and other modeled years.

Figure 3-66 provides a more in-depth look at the most heavily affected months due to COVID restrictions and traffic changes (April – May 2020). The 95th confidence interval (shown as a notch in the box plots) show overlap between 2020 and most other years (except 2015 and 2016). The May 6,

9, and 28 EE days are included in the 2020 box. This analysis shows that there was not a statistically different GAM response in 2020 compared with other years; this is confirmed in the COVID analysis section (Section 2.5), where we show that MDA8 ozone during April – May 2020 in Las Vegas was not statistically different from previous years. Overall, ozone in Clark County did not change significantly and, similarly, GAM results were not significantly affected.

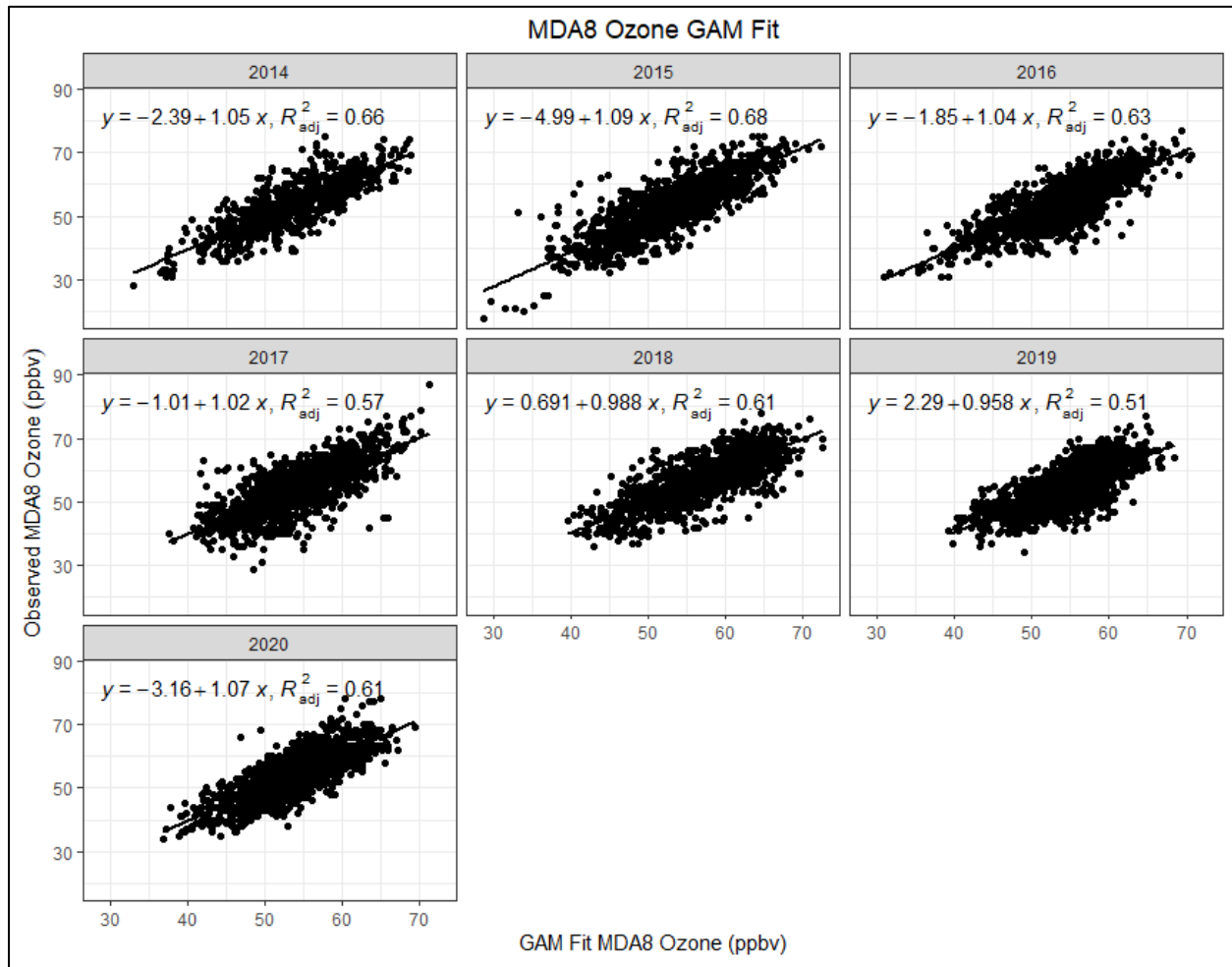


Figure 3-65. Observed MDA8 ozone vs. GAM fit ozone by year. The relationship between observed MDA8 ozone and GAM fit ozone at all eight modeled monitoring sites in Clark County is broken out by year with linear regression and fit statistics shown (slope, intercept, and r^2). EE days are not included in the regression equations.

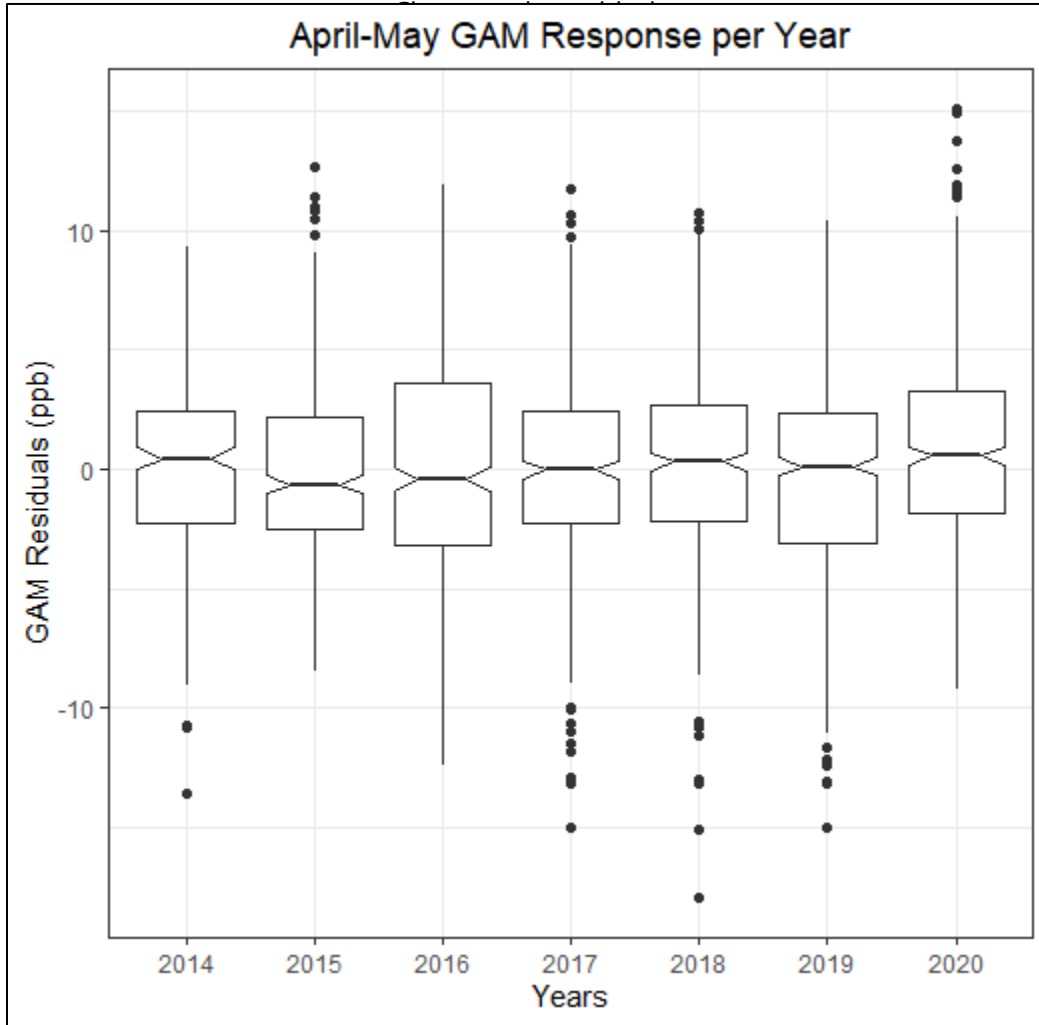


Figure 3-66. April-May Interannual GAM Response. April-May residuals per year (2014-2020) are plotted for all eight modeled monitoring sites in Clark County. May 6, 9, and 28 potential EE days are included.

Figure 3-67 provides the observed MDA8 ozone versus GAM Fit MDA8 from 2014 through 2020 for the sites affected on May 28 (Paul Meyer and Walter Johnson). We marked the possible 2020 (red), 2018 (blue), and other (purple) EE days to show that observed MDA8 ozone on these days is higher than those predicted by the GAM. The other (purple) points are from 2014-2016 suspected wildfire events, as indicated in the EPA AQS record. We also highlight the May 28, 2020, EE day as a large red triangle in each figure. Linear regression statistics (slope, intercept, and R^2) are also provided for context. Both linear regressions show a slope near unity and a low intercept value (around 4 ppb) with a good fit R^2 value.

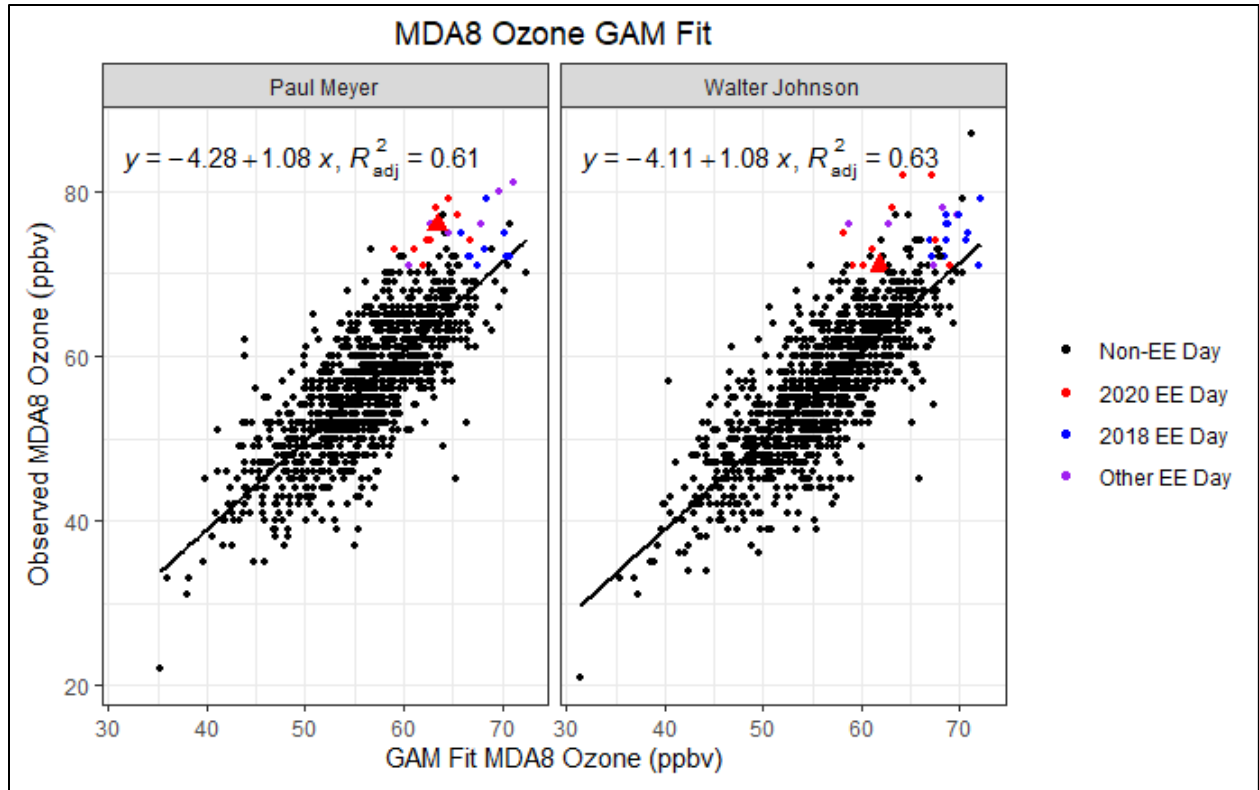


Figure 3-67. GAM MDA8 Fit versus Observed MDA8 ozone for EE affected sites on May 28, 2020. Black circles indicate data not associated with the 2018 or 2020 EE days, red circles indicate 2020 EE days, blue circles indicate 2018 EE days, and purple circles indicate 2014-2016 EE days. May 28 is shown as a red triangle. The black line is linear regression of the data and statistics (equation and R^2 value) are shown in the top of each sub-figure.

Table 3-14 provides the GAM results for May 28, 2020, at each monitoring site affected by the EE. GAM residuals show a modeled wildfire impact of 10-13 ppb for all monitoring sites, with MDA8 GAM prediction values well below the 0.070 ppm standard. These values suggest that there was a significant, non-typical enhancement in MDA8 ozone concentrations at the affected Clark County monitoring sites on May 28, 2020.

Table 3-14. May 28 GAM results and residuals for each site. The GAM residual is the difference between observed MDA8 ozone and the GAM Prediction. We also estimate the minimum predicted fire influence based on the positive 95th quantile and GAM prediction value.

Site Name	MDA8 O ₃ Concentration (ppm)	MDA8 GAM Prediction (ppm)	GAM Residual (ppm)
Paul Meyer	0.076	0.063	0.013
Walter Johnson	0.071	0.061	0.010

Finally, **Figure 3-68** shows a two-week time series of observed MDA8 ozone values across Clark County and GAM prediction values at those sites. May 28, 2020, shows the large gap between observed MDA8 ozone and GAM-predicted values. Outside of the possible EE day, the GAM prediction values are close to the observed values, suggesting that immediately before and after the event, we are able to accurately predict typical fluctuations in ozone on non-event days.

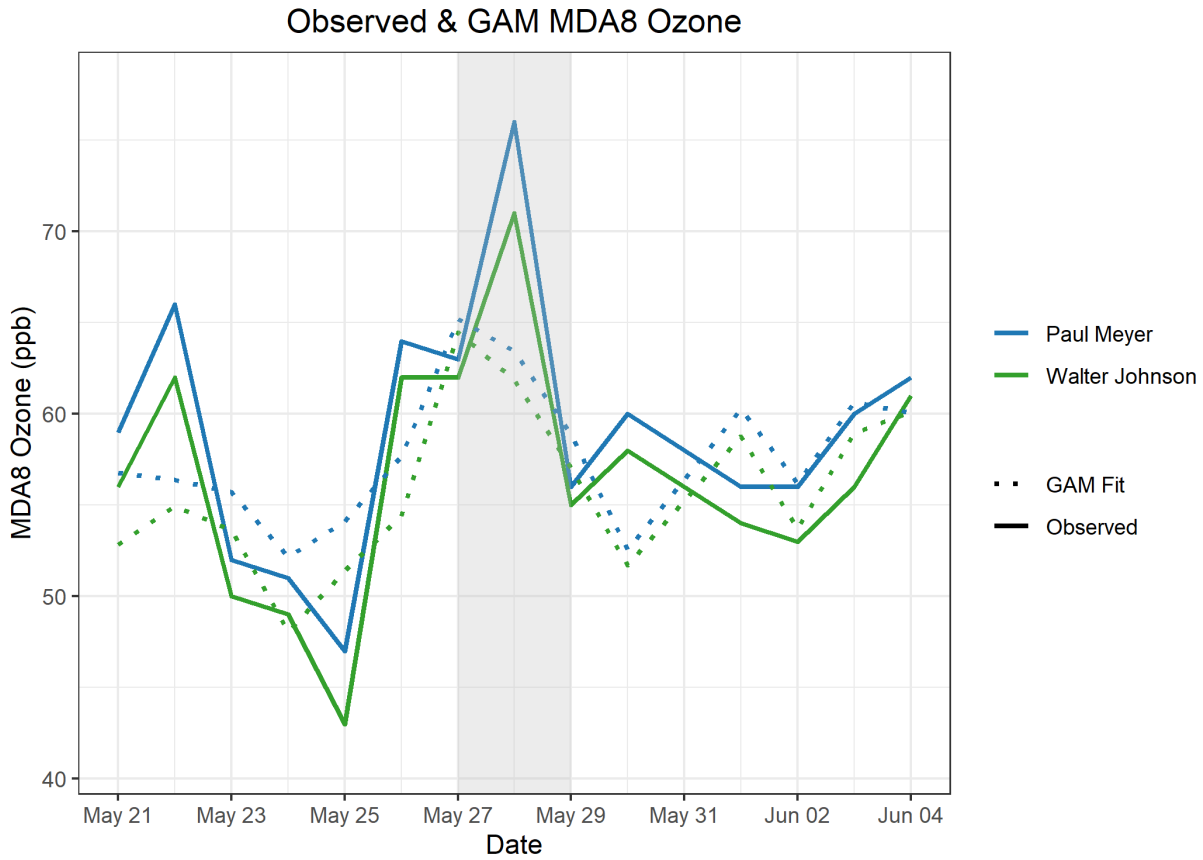


Figure 3-68. GAM time series showing observed MDA8 ozone for two weeks before and after the May 28 EE (solid lines). The GAM MDA8 ozone fit value is also shown for two weeks before and after May 28 (dotted line).

Overall, the GAM evidence clearly demonstrates that a non-typical source of ozone significantly impacted concentrations on May 28, 2020, at both EE-affected Clark County sites. Additionally, based on evidence in Figures 3-63 and 3-64, the high residuals on May 28 are unlikely to be a GAM overprediction based solely on unaccounted influence from the Los Angeles Basin. When the GAM evidence is coupled with stratospheric intrusion evidence from Sections 3.1 through 3.5, we suggest based on the weight of evidence presented, that the enhancement in ozone is due to a stratospheric intrusion over Idaho and Utah that was transported to Clark County, Nevada.

3.6 Clear Causal Relationship Conclusions

The analyses conducted in this report support the impact of a stratospheric intrusion over Idaho and Utah that was transported to Clark County, Nevada, and enhanced ozone concentrations on May 28, 2020. We find that:

1. Visible satellite imagery, model results, tropospheric measurements, and back/forward trajectories support the conclusion of stratospheric-influenced, ozone-rich air being transported from the source region over Idaho and Utah to Clark County between May 24-25 and the EE date.
2. A large mixing layer, supported by (a) skew-T sounding diagrams and boundary layer modeling and (b) meteorological analyses from the source region and Clark County, supports the transport and mixing of ozone-rich air down to the surface in Clark County on the EE date.
3. Comparisons with non-event concentrations, regionally high ozone concentrations on the EE date, meteorologically similar day analysis, and GAM statistical modeling support the conclusion that the ozone concentrations seen in Clark County were well above typical spring concentrations and likely due to outside influences, such as an upwind SOI.

The analyses presented in this report fulfill the requirements for both a Tier 1 and 2 stratospheric intrusion EE demonstration, and all conclusions for each type of analysis are summarized in [Table 3-15](#). The effect of the SOI event in Clark County caused ozone exceedances at the Paul Meyer and Walter Johnson monitoring stations. Even a small enhancement in ozone concentrations from an SOI on May 28—in addition to typical photochemical production and transport of anthropogenic ozone and ozone precursors—can push MDA8 ozone concentrations above the NAAQS threshold. Since stratospheric intrusions are classified as natural events, and we provide a clear causal relationship between the SOI event and the monitored exceedances, we conclude that the ozone exceedance event on May 28, 2020, in Clark County was not reasonably controllable or preventable.

Table 3-15. Results for each tier analysis of the May 28, 2020, EE.

Type of Analysis	Requirement	Finding
Historical comparison	<ul style="list-style-type: none"> • ≥ 5 years of peak daily ozone data with other high event days flagged • Table with percentile ranks of days • Historical diurnal profile comparison (Tier 2) 	<ul style="list-style-type: none"> • The May 28 ozone exceedance occurred during a typical ozone season and event concentrations were significantly higher than non-event concentrations • Percentile ranks for all affected sites were ≥ 97th percentile
Event overview	<ul style="list-style-type: none"> • Spatial and temporal depictions of ozone during the event • Description of surface and upper air meteorological conditions during the event • Begin to establish the complex relationship between the intrusion and eventual impact at surface (Tier 2) 	<ul style="list-style-type: none"> • The SOI source region over Idaho and Utah shows stratospheric-tropospheric exchange on May 25 from 00:00 to 23:00 UTC • Ozone-rich air was transported south to the east and then looped back north before descending into Clark County during the May 28 EE
Establish stratospheric intrusion	<p>Several of following are likely needed:</p> <ul style="list-style-type: none"> • Water vapor imagery • Total column ozone • Meteorological evidence 	<ul style="list-style-type: none"> • Visible water vapor, ozone satellite imagery, and meteorological data were consistent with an SOI event over Idaho and Utah on May 25 • Model results of IPV, ozone, and CO are also consistent with an SOI in the source region on May 25
Establish stratospheric air reached surface	<p>Several of following are likely needed:</p> <ul style="list-style-type: none"> • LIDAR, rawinsonde data • Meteorological evidence • Online AQ model cross sections • Trajectory models 	<ul style="list-style-type: none"> • Trajectory analysis to and from the source region and Clark County show transport of an ozone-rich air mass • Meteorological and LIDAR (from Boulder, CO) analysis show the transport from the source region along with measurements of ozone from the source region • Model cross-sections of ozone and CO data confirm a descending branch of high ozone and low CO from an SOI event
Impacts at the surface	<p>Several of following are likely needed:</p> <ul style="list-style-type: none"> • Coincidence between high ozone and meteorological/AQ conditions characteristic of stratospheric intrusions • Statistical model evidence of impacts 	<ul style="list-style-type: none"> • Surface measurement on May 28 in Clark County show abnormally low water vapor and abnormally high ozone, with typical NO_x levels. This suggests SOI influence, but not unusually high photochemical influence on ozone concentrations. • Meteorologically similar day analysis shows that average MDA8 ozone across similar days was well below the ozone NAAQS and 10 ppb lower than the May 28 exceedance at all affected sites • GAM statistical modeling of May 28 indicates an outside source of ozone enhancing ozone concentrations during the EE

4. Natural Event

The Exceptional Events Rule (81 FR 68216) states that a “[n]atural event, which may recur, is one in which human activity plays little or no direct causal role.” The preamble to the Exceptional Events rule notes that the EPA considers stratospheric ozone intrusions to be natural events, as humans have no direct impact on their occurrence. The Clark County Department of Environment and Sustainability has shown through the analyses provided in Section 3.6 of this demonstration that the hypothesized stratospheric intrusion, which existed simultaneously with local photochemical production of ozone, contributed to identified ozone exceedances at the Paul Meyer and Walter Johnson monitoring sites on May 28. Through these analyses and the fact that stratospheric intrusions are purely natural, the Clark County Department of Environment and Sustainability has satisfied the “human activity that is unlikely to recur at a particular location or a natural event” element of 40 CFR 50.14(c)(3).

5. Not Reasonably Controllable or Preventable

The documentation provided in Section 3.6 of this demonstration shows that the stratospheric intrusion contributed to the identified ozone exceedances at the Paul Meyer and Walter Johnson monitoring sites on May 28. Through these analyses and the fact that stratospheric intrusions are purely natural events that cannot be prevented or controlled, the Clark County Department of Environment and Sustainability has satisfied the “not reasonably controllable or preventable” criterion.

6. Public Comment

This exceptional event demonstration will undergo a 30-day public comment period concurrent with EPA's review beginning on July 1, 2021. A copy of the public notice, along with any comments received and responses to those comments, will be submitted to EPA after the comment period has closed, consistent with the requirements of 40 CFR 50.14(c)(3)(v). [Appendix D](#) contains documentation of the public comment process.

7. Conclusions and Recommendations

The analyses conducted in this report support the conclusion that an SOI event occurred over Idaho and Utah on May 24-25 and ozone-rich air from that event was transported into Clark County, Nevada, on May 28, 2020, affecting ozone concentrations. This EE demonstration has provided the following elements required by the EPA guidance for SOIs (U.S. Environmental Protection Agency, 2018):

1. A narrative conceptual model that describes the SOI event over Idaho and Utah and how the transport of ozone-rich air led to ozone exceedances downwind in Clark County (Section 1.4).
2. A clear causal relationship between the SOI and the May 28 exceedance through ground and satellite-based measurements, trajectories, comparison with non-event concentrations, vertical profile analysis, and statistical modeling (Section 3).
3. Event ozone concentrations at or above the 97th percentile when compared with the last five years of observations (yearly and ozone season-only) at each site and among the four highest ozone days at each site (excluding other 2018 and 2020 EE events—Section 3).
4. Stratospheric intrusions are considered to be natural events, as humans have no direct impact on their occurrence (Section 4).
5. Demonstrated that transport from an SOI event is neither reasonably controllable or preventable (Section 5).
6. This demonstration went through the public comment process via Clark County's Department of Environment and Sustainability (Section 6).

The major conclusions and supporting analyses found in this report are:

1. Visible satellite imagery, model results, tropospheric measurements, and back/forward trajectories support the conclusion of stratospheric-influenced, ozone-rich air being transported from the source region over Idaho and Utah to Clark County between May 24-25 and the EE date.
2. A large mixing layer, supported by (a) skew-T sounding diagrams and boundary layer modeling and (b) meteorological analyses from the source region and Clark County, supports the transport and mixing of ozone-rich air down to the surface in Clark County on the EE date.
3. Comparisons with non-event concentrations, regionally high ozone concentrations on the EE date, meteorologically similar day analysis, and GAM statistical modeling support the conclusion that the ozone concentrations seen in Clark County were well above typical spring concentrations and likely due to outside influences, such as an upwind SOI.

The analyses presented in this report fulfill the requirements for both a Tier 1 and 2 stratospheric intrusion EE demonstration, and all conclusions for each type of analysis are summarized in Table 3-15. The effect of the SOI event in Clark County caused ozone exceedances at the Paul Meyer and Walter Johnson monitoring stations. Since stratospheric intrusions are classified as natural events, and we provide a clear causal relationship between the SOI event and the monitored exceedances, we conclude that the ozone exceedance event on May 28, 2020, in Clark County was not reasonably controllable or preventable.

8. References

- Alvarado M., Lonsdale C., Mountain M., and Hegarty J. (2015) Investigating the impact of meteorology on O₃ and PM_{2.5} trends, background levels, and NAAQS exceedances. Final report prepared for the Texas Commission on Environmental Quality, Austin, TX, by Atmospheric and Environmental Research, Inc., Lexington, MA, August 31.
- Arizona Department of Environmental Quality (2016) State of Arizona exceptional event documentation for wildfire-caused ozone exceedances on June 20, 2015 in the Maricopa nonattainment area. Final report, September. Available at https://static.azdeq.gov/pn/1609_ee_report.pdf.
- Arizona Department of Environmental Quality (2018) State of Arizona exceptional event documentation for wildfire-caused ozone exceedances on July 7, 2017 in the Maricopa Nonattainment Area. Final report, May. Available at https://static.azdeq.gov/pn/Ozone_2017ExceptionalEvent.pdf.
- Camalier L., Cox W., and Dolwick P. (2007) The effects of meteorology on ozone in urban areas and their use in assessing ozone trends. *Atmospheric Environment*, 41, 7127-7137, doi: 10.1016/j.atmosenv.2007.04.061.
- Chouza F., Leblanc T., Brewer M., Wang P., Piazzolla S., Pfister G., Kumar R., Drews C., Tilmes S., and Emmons L. (2020) The impact of Los Angeles basin pollution and stratospheric intrusions on the surrounding San Gabriel Mountains as seen by surface measurements, lidar, and numerical models. *Atmos. Chem. Phys. Discuss.*, 2020, 1-29. Available at <https://acp.copernicus.org/preprints/acp-2020-1208/>.
- Clark County Department of Air Quality (2019) Ozone Advance program progress report update. August.
- Clark County Department of Environment and Sustainability (2020) Revision to the Nevada state implementation plan for the 2015 Ozone NAAQS: emissions inventory and emissions statement requirements. September. Available at https://files.clarkcountynv.gov/clarknv/Environmental%20Sustainability/SIP%20Related%20Documents/O3/20200901_2015_O3%20EI-ES_SIP_FINAL.pdf?t=1617690564073&t=1617690564073.
- Code of Federal Regulations (1997) Title 40, Part 58, Appendix D. Network design for SLAMS, NAMS, and PAMS.
- Gong X., Kaulfus A., Nair U., and Jaffe D.A. (2017) Quantifying O₃ impacts in urban areas due to wildfires using a generalized additive model. *Environ. Sci. Technol.*, 51(22), 13216-13223, doi: 10.1021/acs.est.7b03130.
- Gong X., Hong S., and Jaffe D.A. (2018) Ozone in China: spatial distribution and leading meteorological factors controlling O₃ in 16 Chinese cities. *Aerosol and Air Quality Research*, 18(9), 2287-2300. Available at <http://dx.doi.org/10.4209/aaqr.2017.10.0368>.
- Jaffe D.A., Bertschi I., Jaegle L., Novelli P., Reid J.S., Tanimoto H., Vingarzan R., and Westphal D.L. (2004) Long-range transport of Siberian biomass burning emissions and impact on surface ozone in western North America. *Geophys. Res. Lett.*, 31(L16106).
- Jaffe D.A., Wigder N., Downey N., Pfister G., Boynard A., and Reid S.B. (2013) Impact of wildfires on ozone exceptional events in the western U.S. *Environ. Sci. Technol.*, 47(19), 11065-11072, doi: 10.1021/es402164f, October 1. Available at <http://pubs.acs.org/doi/abs/10.1021/es402164f>.
- Kroll J.H., Heald C.L., Cappa C.D., Farmer D.K., Fry J.L., Murphy J.G., and Steiner A.L. (2020) The complex chemical effects of COVID-19 shutdowns on air quality. *Nature Chemistry*, 12(9), 777-779, doi: 10.1038/s41557-020-0535-z. Available at <https://doi.org/10.1038/s41557-020-0535-z>.
- Langford A.O. (2014) Las Vegas ozone study (LVOS). Final report prepared for the Clark County Department of Air Quality, Las Vegas, NV, by the National Oceanic and Atmospheric Administration Earth System Research Laboratory, Chemical Sciences Division, Boulder, CO, MOU

- #CBE 602948-13, July 25. Available at <https://csl.noaa.gov/projects/lvos/LVOSfinalreportCBE602948-13.pdf>.
- Langford A.O., Senff C.J., Alvarez R.J., Brioude J., Cooper O.R., Holloway J.S., Lin M.Y., Marchbanks R.D., Pierce R.B., Sandberg S.P., Weickmann A.M., and Williams E.J. (2015) An overview of the 2013 Las Vegas Ozone Study (LVOS): impact of stratospheric intrusions and long-range transport on surface air quality. *Atmospheric Environment*, 109, 305-322, doi: 10.1016/j.atmosenv.2014.08.040, 2015/05/01/. Available at <http://www.sciencedirect.com/science/article/pii/S1352231014006426>.
- Langford A.O. and Senff C.J. (2019) Fires, asian, and stratospheric transport-Las Vegas ozone study (FAST-LVOS). Report prepared for the Clark County Department of Air Quality, Las Vegas, NV, by the National Oceanic and Atmospheric Administration Earth System Research Laboratory, Chemical Sciences Division, Boulder, CO, and the Cooperative Institute for Research in Environmental Sciences, University of Colorado, Boulder, CO, CBE 604318-16, December. Available at <https://csl.noaa.gov/projects/fastlvos/FAST-LVOSfinalreport604318-16.pdf>.
- Louisiana Department of Environmental Quality (2018) Louisiana exceptional event of September 14, 2017: analysis of atmospheric processes associated with the ozone exceedance and supporting data. Report submitted to the U.S. EPA Region 6, Dallas, TX, March. Available at https://www.epa.gov/sites/production/files/2018-08/documents/ldeq_ee_demonstration_final_w_appendices.pdf.
- McClure C.D. and Jaffe D.A. (2018) Investigation of high ozone events due to wildfire smoke in an urban area. *Atmospheric Environment*, 194, 146-157, doi: 10.1016/j.atmosenv.2018.09.021, 2018/12/01/. Available at <http://www.sciencedirect.com/science/article/pii/S1352231018306137>.
- McVey A., Pernak R., Hegarty J., and Alvarado M. (2018) El Paso ozone and PM_{2.5} background and totals trend analysis. Final report prepared for the Texas Commission on Environmental Quality, Austin, Texas, by Atmospheric and Environmental Research, Inc., Lexington, MA, June. Available at <https://www.tceq.texas.gov/assets/public/implementation/air/am/contracts/reports/da/582188176307-20180629-aer-ElPasoOzonePMBBackgroundTotalsTrends.pdf>.
- National Weather Service Forecast Office (2020) Las Vegas, NV: general climatic summary. Available at <https://www.wrh.noaa.gov/vef/lasum.php>.
- Parker H.A., Hasheminassab S., Crouse J.D., Roehl C.M., and Wennberg P.O. (2020) Impacts of traffic reductions associated with COVID-19 on Southern California air quality. *Geophysical Research Letters*, 47(23), e2020GL090164. Available at <https://agupubs.onlinelibrary.wiley.com/doi/abs/10.1029/2020GL090164>.
- Pernak R., Alvarado M., Lonsdale C., Mountain M., Hegarty J., and Nehr Korn T. (2019) Forecasting surface O₃ in Texas urban areas using random forest and generalized additive models. *Aerosol and Air Quality Research*, 19, 2815-2826, doi: 10.4209/aaqr.2018.12.0464.
- Sacramento Metropolitan Air Quality Management District (2011) Exceptional events demonstration for 1-hour ozone exceedances in the Sacramento regional nonattainment area due to 2008 wildfires. Report to the U.S. Environmental Protection Agency, March 30.
- Simon H., Baker K.R., and Phillips S. (2012) Compilation and interpretation of photochemical model performance statistics published between 2006 and 2012. *Atmospheric Environment*, 61, 124-139, doi: 10.1016/j.atmosenv.2012.07.012.
- Solberg S., Walker S.-E., Schneider P., Guerreiro C., and Colette A. (2018) Discounting the effect of meteorology on trends in surface ozone: development of statistical tools. Technical paper by the European Topic Centre on Air Pollution and Climate Change Mitigation, Bilthoven, the Netherlands, ETC/ACM Technical Paper 2017/15, August. Available at https://www.eionet.europa.eu/etcs/etc-atni/products/etc-atni-reports/etcacm_tp_2017_15_discount_meteo_on_o3_trends.

- Solberg S., Walker S.-E., Guerreiro C., and Colette A. (2019) Statistical modelling for long-term trends of pollutants: use of a GAM model for the assessment of measurements of O₃, NO₂ and PM. Report by the European Topic Centre on Air pollution, transport, noise and industrial pollution, Kjeller, Norway, ETC/ATNI 2019/14, December. Available at <https://www.eionet.europa.eu/etcs/etc-atni/products/etc-atni-reports/etc-atni-report-14-2019-statistical-modelling-for-long-term-trends-of-pollutants-use-of-a-gam-model-for-the-assessment-of-measurements-of-o3-no2-and-pm-1>.
- Texas Commission on Environmental Quality (2021) Dallas-Fort Worth area exceptional event demonstration for ozone on August 16, 17, and 21, 2020. April. Available at <https://www.tceq.texas.gov/assets/public/airquality/airmod/docs/ozoneExceptionalEvent/2020-DFW-EE-Ozone.pdf>.
- U.S. Census Bureau (2010) State & County QuickFacts. Available at <http://quickfacts.census.gov/qfd/states/.html>.
- U.S. Environmental Protection Agency (2015) 40 CFR Part 50, Appendix U: interpretation of the primary and secondary National Ambient Air Quality Standards for ozone. Available at https://www.ecfr.gov/cgi-bin/text-idx?SID=43eb095cc6751633290941788ab4f3bd&mc=true&node=ap40.2.50_119.u.
- U.S. Environmental Protection Agency (2016) Guidance on the preparation of exceptional events demonstrations for wildfire events that may influence ozone concentrations. Final report, September. Final report, September. Available at www.epa.gov/sites/production/files/2016-09/documents/exceptional_events_guidance_9-16-16_final.pdf.
- U.S. Environmental Protection Agency (2018) Guidance on the preparation of exceptional events demonstrations for stratospheric ozone intrusions. Report by the U.S. Environmental Protection Agency Office of Air Quality Planning and Standards, Air Quality Policy Division, Air Quality Assessment Division, Research Triangle Park, NC, EPA-457/B-18-001, November. Available at https://www.epa.gov/sites/production/files/2018-11/documents/exceptional_events_soi_guidance_11-8-2018.pdf.
- U.S. Environmental Protection Agency (2020) Green Book: 8-hour ozone (2015) area information. Available at <https://www.epa.gov/green-book/green-book-8-hour-ozone-2015-area-information>.
- Venter Z.S., Aunan K., Chowdhury S., and Lelieveld J. (2020) COVID-19 lockdowns cause global air pollution declines. *Proceedings of the National Academy of Sciences*, 117(32), 18984-18990, doi: 10.1073/pnas.2006853117. Available at <https://www.pnas.org/content/pnas/117/32/18984.full.pdf>.
- Wood S. (2020) Mixed GAM computation vehicle with automatic smoothness estimation. Available at <https://cran.r-project.org/web/packages/mgcv/mgcv.pdf>.
- Wood S.N. (2017) *Generalized additive models: an introduction with R*, 2nd edition, CRC Press, Boca Raton, FL.
- Zhang L., Lin M., Langford A.O., Horowitz L.W., Senff C.J., Klovenski E., Wang Y., Alvarez R.J., II, Petropavlovskikh I., Cullis P., Sterling C.W., Peischl J., Ryerson T.B., Brown S.S., Decker Z.C.J., Kirgis G., and Conley S. (2020) Characterizing sources of high surface ozone events in the southwestern US with intensive field measurements and two global models. *Atmospheric Chemistry & Physics*, 20, 10379-10400, doi: 10.5194/acp-20-10379-2020. Available at <https://acp.copernicus.org/articles/20/10379/2020/acp-20-10379-2020.pdf>.